A ROLE FOR THE ENDOSOMAL SNARE COMPLEX AND TETHERS IN AUTOPHAGY

A thesis submitted to the
INSTITUTE OF MOLECULAR, CELL AND SYSTEMS BIOLOGY

For the degree of
DOCTOR OF PHILOSOPHY

by
Marianne Cowan

College of Medical, Veterinary and Life Sciences
Institute of Molecular, Cell and Systems Biology
University of Glasgow
October 2013

Abstract

Autophagy is a major route for lysosomal and vacuolar degradation in mammals and yeast respectively. It is involved in diverse physiological processes and implicated in numerous pathologies. The process of autophagy is initiated at the pre-autophagosomal structure and is characterised by the formation of a double membrane vesicle termed the autophagosome which sequesters cytosolic components and targets them for lysosomal/vacuolar degradation. The molecular mechanisms that regulate autophagosome formation are not fully understood. The conserved oligomeric Golgi (COG) complex is a hetero-octameric tethering factor implicated in autophagosome formation which interacts directly with the target membrane SNARE proteins Syntaxin 6 and Syntaxin 16 via the Cog6 and Cog4 subunits respectively. The work presented in this thesis demonstrates direct interaction of the yeast orthologue of Syntaxin 16, Tlg2, with Cog2 and Cog4. In addition, I investigated binding of the COG complex subunits to Tlg1, Vti1 and Snc2, the partner SNARE proteins of Tlg2. Direct interaction of Tlg1, the yeast orthologue of Syntaxin 6, with Cog1, Cog2 and Cog4 were observed. Given that Tlg2 has previously been shown to regulate autophagy in yeast, these data support a conserved role for the COG complex in mediating autophagosome formation through regulation of SNARE complex formation.

In addition to investigating binding of COG complex subunits to the endosomal SNARE complex, I have also investigated a role for autophagy in regulating Tlg2 levels. The SM protein Vps45 has previously been shown to stabilise Tlg2 cellular levels. Our laboratory has demonstrated a role for both the proteasome and vacuole in the degradation of Tlg2. Here I demonstrated a role for autophagy in the regulation of Tlg2 levels and show that Swf1-mediated palmitoylation may serve to protect Tlg2 from being selectively targeted for autophagy. I also investigated the effects of the yeast T238N mutation on Vps45 function. The analogous mutation in human Vps45 has recently been associated with congenital neutropenia. Vps45 function is best characterised in yeast where it associates with membranes via Tlg2 and is required for membrane traffic from the trans-Golgi network into the endosomal system. Cellular levels of Vps45 T238N were destabilised and a concomitant reduction in Tlg2 levels was also observed. Vacuolar protein sorting remained unaffected in yeast cells harboring Vps45

T238N but was subjected to increased apoptosis under hydrogen peroxide-mediated stress. This identifies a novel role for Vps45 in maintaining cell viability. Finally, I also investigated a role for endosomal trafficking and autophagy in *C.elegans* post-embryonic development and identified a role for these pathways in the clearance of the pre-moult increase in intracellular membranes and cuticular formation.

Table of Contents

List of Tables

List of Figures

Acknowledgements

First and foremost I would like to thank my supervisor Dr Nia Bryant for allowing me to undertake my PhD under her exceptional supervision. Your continuous guidance, support and constructive feedback during this time have greatly contributed to my development as a scientist and for this I am most grateful.

I would also like to thank Dr Iain Johnstone for overseeing my *C.elegans* project and members of my academic panel, Dr Mike Blatt and Dr Joanna Wilson, for your suggestions. I owe my thanks to Martin Werno in the Chamberlain lab (University of Strathclyde) for showing me how to perform acyl-Rac experiments and to Stephanie Evans for your patience and advice with yeast dissections. Other contributions in the form of yeast strains have also been greatly appreciated and I would like to thank Dr Joe Gray (University of Glasgow) and Dr Daniel Klionsky (University of Michigan) for these.

Thanks to all the members of lab 241 for your kind help and advice when needed. In particular, thanks to Dr Scott Shanks for teaching me everything yeast related during my early days in the lab. Also, thanks to my bench buddy Laura Stirrat for your fine company – you have provided me with the necessary laughs to see me through my more challenging days in the lab.

It is fair to say that all of this would not have been possible without the financial assistance received from the University of Glasgow and as such, I would like to say a very big thank you!

Last but not least, a special thanks to my wonderful family for your support and continued interest in my studies. My dear husband, Douglas – I owe you an especially BIG thank you for your never-ending patience, encouragement and love throughout my PhD and beyond.

Author’s Declaration

I declare that the work presented in this thesis has been carried out by me, unless otherwise cited or acknowledged. It is entirely of my own composition and has not, in whole or in part, been submitted for any other degree.

Marianne Cowan

October 2013

Definitions/Abbreviations

°C	degree Celsius
3AT	3-aminotriazole
Acyl-Rac	acyl resin-assisted capture
AD	activation domain
APS	ammonium persulphate
ATG	autophagy related gene
ATP	adenosine triphosphate
BD	binding domain
bp	base pairs
BSA	bovine serum albumin
$CaCl_2$	calcium chloride
C.elegans	*Caenorhabditis elegans*
CEN	centromeric
CGC	*C.elegans* Genetics Centre
COG	conserved oligomeric Golgi
COP	coat protein complex
CPY	carboxypeptidase Y
C-terminal	carboxy-terminal
$CuCl_2$	copper chloride
Cvt	cytoplasm-to-vacuole targeting
dATP	deoxyadenosine triphosphate
dCTP	deoxycytidine triphosphate
DFCP1	double FYVE domain containing protein 1
dGTP	deoxyguanosine triphosphate
dH_2O	distilled water
DMSO	dimethyl sulfoxide
DNA	deoxyribonucleic acid
dNTP	deoxyribonucleotide triphosphate
DslI	dependence on SLY1-20
DTT	ditiothreitol
dTTP	deoxythymidine triphosphate
Dpy	dumpy
E1	ubiquitin activating enzyme
E2	ubiquitin conjugating enzyme
E3	ubiquitin ligase
ECL	enhanced chemiluminescence
E.coli	*Escherichia coli*
EDTA	ethylenediaminetetraacetic acid
ER	endoplasmic reticulum
Fc	fragment crystallisable
g	gravity
GARP	Golgi-associated retrograde protein
GFP	green fluorescent protein
GST	glutathione S-transferase
GTPase	guanosine triphosphatase
H_2O	water
H_2O_2	hydrogen peroxide
HA	hemagglutinin

Habc	helices a, b and c
HCl	hydrogen chloride
HEPES	4-(2-hydroxyethyl)-1-piperazineethanesulfonic acid
HRP	horseradish peroxidise
IgG	immunoglobulin G
IPTG	isopropyl β-D-1-thiogalactopyranoside
KanR	kanamycin resistant
kb	kilobase pair
KCl	potassium chloride
kDa	kilodalton
K_2HPO_4	dipotassium hydrogen orthophosphate
KH_2PO_4	potassium dihydrogen orthophosphate
KOAc	potassium acetate
KPO_4	potassium phosphate buffer
L stage	larval stage
LC3	microtubule-associated protein 1 light chain 3
Lon	long
LSB	Laemmli sample buffer
M	moles
mA	milliAmperes
mM	millimoles
MMTS	methyl methanethiosulfonate
mg	milligrams
$MgCl_2$	magnesium chloride
$MgSO_4$	magnesium sulphate
ml	millilitres
mm	millimetres
mRNA	messenger ribonucleic acid
MVB	multivesicular body
N-terminal	amino-terminal
NaCl	sodium chloride
Na_2HPO_4	disodium hydrogen orthophosphate
NaOH	sodium hydroxide
NEM	N-ethylmalemide
ng	nanograms
NGM	nematode growth media
NH_2OH	hydroxylamine
nM	nanomoles
nm	nanometres
NP-40	nonyl phenoxypolyethoxylethanol
NSF	N-ethylmalemide sensitive factor
OD_{600}	optical density at 600 nanometres
ORF	open reading frame
PAS	pre-autophagosomal structure
PBS	phosphate buffered saline
PBS-T	phosphate buffered saline containing 0.1% Tween-20
PCR	polymerase chain reaction
Pep12	carboxypeptidase Y-deficient protein 12
PIPES	1,4-piperazinediethanesulfonic acid
pmol	picomoles
PrA	protein A
PtdIns(3)K	phosphatidylinositol 3-kinase
PtdIns(3)P	phosphatidylinositol 3-phosphate

Raff	raffinose
Rol	roller
S.cerevisiae	*Saccharomyces cerevisiae*
SD	synthetic defined
SDM	site-directed mutagenesis
SDS	sodium dodecyl sulphate
SDS-PAGE	sodium dodecyl sulphate polyacrylamide gel electrophoresis
Sec	secretory
SH	sulfhydryl
Sly1	suppressor of loss of Ypt1
SM	Sec1/Munc18
Sma	small
SNAP	synaptosomal-associated protein
SNARE	soluble NEM sensitive factor attachment protein receptor
Snc	suppressor of the null allele of CAP
Sorb	sorbitol
Swf1	spore wall formation protein 1
SWLB	single worm lysis buffer
TAE	Tris-acetic acid EDTA
TB	Terrific broth
TBS-T	Tris-buffered saline Tween-20
TE	Tris-EDTA
TEMED	tetramethylethylenediamine
TGN	*trans*-Golgi network
Tlg	target-SNARE of the late Golgi compartment protein
TMD	transmembrane domain
TORC1	target of rapamycin complex 1
t-SNARE	target-SNARE
TST	Tris-saline-Tween-20
Tul1	transmembrane ubiquitin ligase protein 1
Unc	uncoordinated
µg	micrograms
µm	micrometres
UV	ultraviolet
V	volts
VAMP	vesicle-associated membrane protein
Vps	vacuolar protein sorting
v-SNARE	vesicle-SNARE
Vti1	Vps10 (ten) interacting protein 1
v/v	volume per volume
w/v	weight per volume
YPD	yeast extract peptone dextrose
YPG	yeast extract peptone galactose

Chapter 1 – Introduction

Cellular housekeeping and energy homeostasis plays an important role in maintaining eukaryotic cell viability. Macroautophagy, henceforth referred to as autophagy, assists in this function by sequestering cytosolic components into double-membrane vesicles called autophagosomes and targeting them for lysosomal/vacuolar degradation (Mizushima et al., 2008).

Autophagy (Figure 1-1) is initiated by the formation of an isolation membrane which expands sufficiently to accommodate its content. The defining feature of this pathway is the formation of the autophagosome which results from fusion of the two leading edges of the expanding isolation membrane. Delivery of the internal vesicle of the autophagosome, or autophagic body, to the lysosome and vacuole in mammals and yeast, respectively, defines the terminal step of autophagy (Baba et al., 1994; Baba et al., 1995). Mutations in autophagy related genes (*ATG*) have highlighted the importance of this pathway in a number of physiological processes and pathologies (section 1.1.7) (Mizushima et al., 2008).

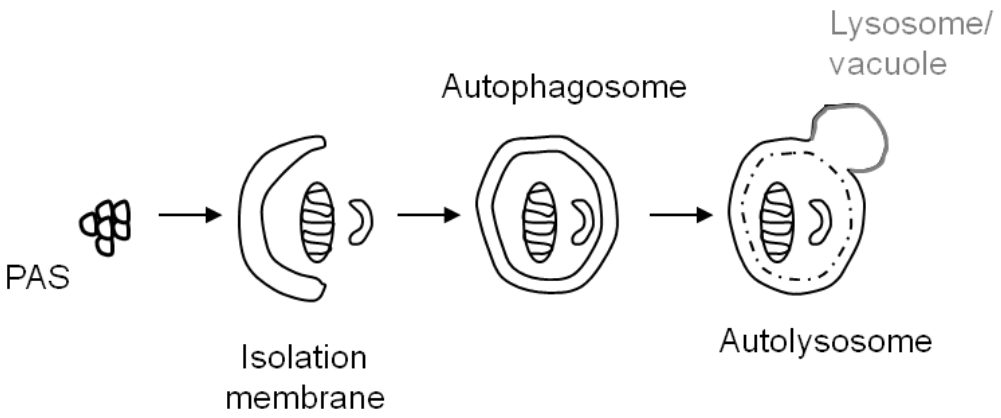

Figure 1-1. The process of autophagy
Autophagy is initiated at a perivacuolar site termed the pre-autophagosomal structure (PAS) by the formation of an isolation membrane which expands and non-selectively engulfs cytosolic components in the process. Fusion of the two leading edges of the isolation membrane results in the formation of a double-membrane vesicle termed the autophagosome. Fusion between the external membrane of the autophagosome and the lysosome results in the formation of the autolysosome. The internal vesicle of the autophagosome, or autophagic body, and its contents are subsequently degraded by the autolysosome and recycled by the cell. Adapted from (Mizushima, 2005).

I am particularly interested in the mechanisms that underlie membrane fusion and during the course of this project I became interested in the generation of the isolation membrane and subsequent formation of the autophagosome. Evidence suggests that expansion of the isolation membrane is followed by fusion of the leading edges to form an autophagosome (Geng & Klionsky, 2010; Geng et al., 2010; van der Vaart & Reggiori, 2010). The molecular fusion machinery involved in the generation and subsequent formation of autophagosomes remain unknown however a number of key players are thought to be involved during these early stages including soluble N-ethylmalemide (NEM) sensitive factor (NSF) attachment protein receptor (SNARE) proteins (section 1.2) and tethering complexes (section 1.4).

1.1 Autophagy

1.1.1 Identification of autophagy

Autophagosomes were initially described in the newborn mouse kidney as being "large bodies that represent vacuoles which have accumulated a high concentration of amorphous material" and "that sometimes contain… altered mitochondria"(Clark, 1957). Cytoplasmic granules were observed to decrease in abundance (within a week postnatally) as cells differentiated. This observation corresponds to recent data describing a homeostatic role for autophagy during the early stages of development (Kuma *et al.*, 2004; Saitoh *et al.*, 2009; Sato & Sato, 2013). In 1962, electron microscopy data obtained by Ashford and Porter demonstrated a glucagon-mediated increase in the lysosomal content of cells examined from perfused rat livers (Ashford & Porter, 1962). It was reported that these so called 'lysosomes' preferentially engulfed mitochondria. Other identifiable content within these lysosomes included small vesicles and endoplasmic reticulum (ER). The term 'autophagy' was subsequently coined in 1963 by de Duve to describe novel double-membrane vesicles related to lysosomes that contain parts of the cytosolic content including organelles in varying degrees of structural decay (Clark, 1957; Ashford & Porter, 1962; De Duve, 1963; De Duve & Wattiaux, 1966). The sequestering vesicles involved were termed autophagosomes; the biogenesis of these structures remain controversial.

Since the term ‘autophagy’ was introduced, the process of autophagy has been shown to be up-regulated in hepatic cells of starved animals (Novikoff et al., 1964) and that the size of hepatic lysosomes increase as a result of glucagon administration (Deter & De Duve, 1967). Using a quantitative morphological approach Deter and colleagues confirmed this observed increase in autophagy to be glucagon-mediated.

1.1.2 Functional significance of autophagy

Autophagy is an evolutionary conserved and adaptive catabolic process that plays a central role in maintaining intracellular homeostasis and thereby cellular health. The term ‘autophagy’ directly translates to ‘self-eating’ and it is a major route for lysosomal/vacuolar degradation in eukaryotes (Reggiori & Klionsky, 2002; Yorimitsu & Klionsky, 2005b; Yang & Klionsky, 2010).

Autophagy is a ubiquitous degradative process that occurs at a basal level and can be rapidly up-regulated in response to cellular stress. For instance, nutrient deprivation is the most common trigger of autophagy induction (section 1.1.6) and in yeast nitrogen starvation represents the most potent stimulus of this pathway (Takeshige et al., 1992). Basal levels of autophagy play an important role in constitutive turnover of cytosolic components. Up-regulation of this process is important in providing amino acids derived from degraded proteins and/or organelles which in turn are utilised to provide cells with the necessary chemical energy that is required for cellular maintenance and growth (Mizushima, 2005).

Although recent evidence suggest a link between autophagy and ubiquitin-mediated degradation via the proteasome (Zhao et al., 2007), these two processes are functionally distinct. Autophagy shares some functional overlap with the yeast biosynthetic pathway known as the cytoplasm-to-vacuole targeting (Cvt) pathway (Klionsky *et al.*, 1992; Scott *et al.*, 1996; Hutchins & Klionsky, 2001). The Cvt pathway is unique to yeast and both autophagy and the Cvt pathway coexist is yeast (section 1.1.3) (Klionsky, 2005).

1.1.3 Autophagy versus the cytosol-to-vacuole targeting pathway

Significant breakthrough in our understanding of autophagy came from genetic screens in yeast, such as *Saccharomyces cerevisiae* (*S.cerevisiae*) (Thumm *et al.*, 1994; Harding *et al.*, 1995). Autophagy and the yeast Cvt pathway are morphologically similar thus the latter is considered to be an autophagy-related pathway (Baba et al., 1997). It was not until the identification of the *ATG* genes in yeast (Matsuura et al., 1997) and subsequent molecular analysis of autophagy in higher eukaryotes (Mizushima et al., 1998) that these two pathways were shown to share some common molecular machinery that is involved in the formation of the autophagosome (Harding *et al.*, 1996; Scott *et al.*, 1996; Baba *et al.*, 1997). This subset of 'core' Atg proteins all function during the early phases of autophagosome formation and include the Atg1-Atg13-Atg17 kinase complex (Scott et al., 2000), the class III phosphatidylinositol 3-kinase (PtdIns3K) complex I (Petiot *et al.*, 2000; Kihara *et al.*, 2001), the Atg8 (Kirisako et al., 1999) and Atg12 (Mizushima et al., 1998) ubiquitin-like conjugation systems and the integral membrane protein Atg9 (Noda et al., 2000). In addition to these core Atg proteins, autophagy- and Cvt-specific proteins have also been identified (Kawamata et al., 2008).

Despite sharing similar morphological features, important differences exist between autophagy and the Cvt pathway. The Cvt pathway is a constitutively active biosynthetic pathway that serves to selectively sequester and deliver specific enzymes, such as aminopeptidase I (Klionsky et al., 1992) and α-mannosidase (Yoshihisa & Anraku, 1990), from the cytosol to the vacuole; in contrast, autophagy is an inducible degradative pathway that terminates in the lysosomal/vacuolar compartment (Yang & Klionsky, 2010). Transport vesicle formation is a key regulatory step of the Cvt and autophagic pathways and the pre-autophagosomal structure (PAS) represents the site for vesicle formation (Suzuki *et al.*, 2001; Kim *et al.*, 2002). However, the diameter of the sequestering vesicles involved differs; in the Cvt pathway, the diameter of the vesicle measures approximately 140-160 nanometers (nm) (Kim et al., 2002) compared to 400-900 nm for the autophagosome (Takeshige et al., 1992). This difference in size reflects the ability of the autophagosome to adjust its size appropriately in order to accommodate its cargo.

1.1.4 The process of autophagy

In yeast, autophagy is initiated by nucleation of the isolation membrane at a perivacuolar site termed the PAS (Figure 1-1) (Noda *et al.*, 2000; Suzuki *et al.*, 2001; Kim *et al.*, 2002). The PAS was originally identified based on observations using fluorescence microscopy that core Atg components, including Atg1, Atg8 and Atg9, exhibit perivacuolar punctate structures that co-localise with aminopeptidase I (section 1.1.3) under autophagy inducing conditions. The PAS therefore defines the focal point for the assembly of Atg proteins which are recruited in a hierarchical fashion during the early stages of autophagy.

The hierarchical relationship between the core Atg proteins has been determined by systematic synthetic disruption of each *ATG* gene followed by morphometric analysis (Suzuki *et al.*, 2007). This analysis revealed that Atg17, which forms a complex with Atg29 and Atg31 (Kabeya *et al.*, 2007; Kawamata *et al.*, 2008; Kabeya *et al.*, 2009), is required for the recruitment of all downstream Atg proteins. Specifically, the PAS localisation of Atg17 is unaffected in core *atg* mutant strains; in contrast, the PAS localisation of the remaining core Atg proteins is impaired in *atg17* (Suzuki *et al.*, 2007). The PAS localisation of the Atg17-Atg29-Atg31 complex and its subsequent binding to Atg11 via Atg17 (Yorimitsu & Klionsky, 2005a) is regulated by phosphorylation of Atg29 (Mao *et al.*, 2013). Binding between Atg11 and the Atg17-Atg29-Atg31 complex is required for recruiting Atg1-Atg13 (refer to section 1.1.6) to the PAS. Yeast two-hybrid analyses and co-immunoprecipitation experiments have demonstrated that the recruitment of Atg1-Atg13 to the PAS is mediated by a direct interaction between Atg17 and Atg13 (Kabeya *et al.*, 2005). Furthermore, complex formation between Atg17-Atg29-Atg31 and Atg1-Atg13 is required for Atg1 kinase activity and thereby autophagy (Kamada *et al.*, 2000; Kabeya *et al.*, 2005). Downstream Atg proteins are subsequently recruited in the following order: the integral membrane protein Atg9 is recruited to the PAS via direct association with Atg11 (He *et al.*, 2006), which plays a role in linking cargo to the vesicle-forming machinery at the PAS, possibly via its coiled-coil tethering actions (Yorimitsu & Klionsky, 2005a; Lipatova *et al.*, 2012). In turn, recruitment of the autophagy-specific PtdIns(3)K complex 1, composed of Vps34, Vps15, Atg6 and At14, to the PAS is mediated by direct association between Atg13 and Atg14 (Jao *et al.*, 2013). The ubiquitin ligase-like system composed of Atg12-Atg5-Atg16 localises to the developing

autophagosome where it facilitates lipidation and correct subcellular localisation of Atg8 (Mizushima *et al.*, 1998; Mizushima *et al.*, 1999; Hanada *et al.*, 2007). Atg8 functions downstream from Atg12-Atg5-Atg16 and the PtdIns(3)K complex 1 and is recruited to the PAS via an Atg9-dependent mechanism (Suzuki *et al.*, 2001; Suzuki *et al.*, 2007). Expression of Atg8 is upregulated in response to autophagy induction and levels of Atg8 directly correlate with autophagosome size (Xie *et al.*, 2008).

To date, 33 *ATG* genes have been identified in the yeast model system *S.cerevisiae,* which is extensively used for studying autophagy (Kanki et al., 2009; Okamoto et al., 2009). Homologs of the yeast *ATG* genes exist in other eukaryotes, including mammals (Reggiori & Klionsky, 2002). The corresponding gene products are often orthologs that perform similar functions and their hierarchical relationship is consistent with that of yeast [reviewed in (Suzuki & Ohsumi, 2010)]. Emerging evidence suggests that the previously unidentified mammalian PAS equivalent may also exist in mammals. The double FYVE domain-containing protein 1 (DFCP1) is a novel phospholipid binding protein that translocates to a sub-domain of the ER, termed the omegaosome, under autophagy-inducing conditions. Omegasomes partially co-localise with the autophagosomal marker green fluorescent protein microtubule-associated protein 1 light chain 3 (GFP-LC3) as well as Vps34-containing vesicles under these same conditions (Axe *et al.*, 2008; Itakura & Mizushima, 2010). Three-dimensional electron tomography has confirmed a physical connection between omegasomes and the isolation membrane complex. This is suggestive of a role for the ER in autophagosome formation in mammalian cells (Yla-Anttila *et al.*, 2009).

Following the organisation of the vesicle-formation complex at the PAS, the isolation membrane sequesters various cytosolic components within its boundaries and expands sufficiently prior to vesicle completion to accommodate its cargo. The source from which the membranes are acquired and which are required for the expansion of the isolation membrane remain controversial. Evidence to date have supported a role for the Golgi (Geng & Klionsky, 2010; van der Vaart & Reggiori, 2010), ER (Young et al., 2006), mitochondria (Hailey et al., 2010) and plasma membrane (Ravikumar et al., 2010) in the expansion of the isolation membrane. Recent progress in this field lean towards a role for post-ER Golgi compartments in the formation of the isolation membrane in yeast. Atg9, which is an integral

membrane protein (Noda *et al.*, 2000), localises to the Golgi apparatus and late endosome (Young et al., 2006). Under nutrient replete conditions, Atg9 cycles between the Golgi apparatus and late endosomes however under nutrient starvation conditions, and when autophagy is induced, Atg9 relocalise to a peripheral punctate compartment that is within close proximity of the vacuole and which is consistent with the PAS (Young *et al.*, 2006; Mari *et al.*, 2010). Based on these observations it has been proposed that Atg9 sources pre-existing membranes from the Golgi apparatus and late endosomes and subsequently transports these membranes to the PAS under autophagy inducing conditions. Acquisition of these Golgi and late endosome derived membranes results in expansion of the isolation membrane. This is a necessary step in the elongation of the isolation membrane and therefore the formation of autophagosomes. Furthermore, autophagosomes exhibit many of the properties which are likely derived from an endocytic compartment including enrichment in phosphatidylinositol 3-phosphate [PtdIns(3)P] (Obara *et al.*, 2008).

The target-SNARE Tlg2 (t-SNARE of the late Golgi compartment protein 2), its SM protein Vps45 and the COG complex regulate membrane traffic within the Golgi and endosomal systems (Abeliovich *et al.*, 1998; Holthuis *et al.*, 1998a; VanRheenen *et al.*, 1998; Whyte & Munro, 2001). Consistent with a role for post-ER Golgi compartments in autophagosome formation, the PAS localisation of Atg9 is reduced and redistributed throughout the cytosol in both *cog* (Yen *et al.*, 2010) and *tlg2* (Ohashi & Munro, 2010; Nair *et al.*, 2011) deficient yeast. Atg9 cycles between peripheral structures and the PAS and its retrieval from the PAS is dependent on Atg1 (Reggiori *et al.*, 2004). An epistasis assay that relies on the *atg1*Δ phenotype has been employed in recent years to investigate anterograde transport of Atg9 to the PAS. Yen and colleagues demonstrated that Atg9-GFP localises to multiple puncta in an *atg1*Δ*cog1*Δ strain under autophagy inducing conditions (Yen *et al.*, 2010). This observation is indicative of impaired anterograde movement of Atg9 to the PAS thereby implicating a role for the COG complex in Atg9 trafficking. Similarly, the *tlg2*Δ*atg24*Δ mutant combination exhibits a strong autophagy deficient phenotype as defined by the GFP-Atg8 processing assay and in combination with *atg1*Δ results in inhibition of Atg9 accumulation at the PAS (Ohashi & Munro, 2010). In a separate study Nair and colleagues demonstrated that the frequency of colocalisation between Atg9-GFP and red fluorescent protein (RFP)-aminopeptidase 1, a marker for the PAS, was reduced

from 55% in wild type cells to 30% in *tlg2*Δ cells (Nair *et al.*, 2011). They confirmed mislocalisation of Atg9 to the PAS was a result of impaired anterograde transport by quantifying the number of *atg1*Δ*tlg2*Δ mutant cells in which Atg9 was localised to multiple puncta as opposed to a single puncta under autophagy inducing conditions. Additionally it was also demonstrated that *tlg2*Δ cells exhibit a significant reduction in Pho8Δ60 activity. *PHO8* encodes the vacuolar alkaline phosphatase which contains an N-terminal transmembrane domain. Pho8 is delivered to the vacuole via the secretory pathway and its transmembrane domain signals translocation into the ER. Pho8Δ60 lacks the transmembrane domain and instead localises to the cytosol. Pho8Δ60 is exclusively delivered to the vacuole via autophagy thus Pho8Δ60 activity can be utilised to quantify the magnitude of autophagy (Noda *et al.*, 1995). Moreover, inhibition of Golgi transport functions severely impair phagophore expansion and thus autophagosome formation (van der Vaart & Reggiori, 2010). Collectively, these observations support a role for Golgi and endosomal systems as well as Tlg2 and the COG complex in the generation of autophagosomes. The closely interlinked relationship between the endosomal system, autophagy and the Cvt pathway is depicted in Figure 1-2. Localisation of the key proteins under investigation in the current study, Tlg2, Vps45 and the COG complex, are indicated (Figure 1-2).

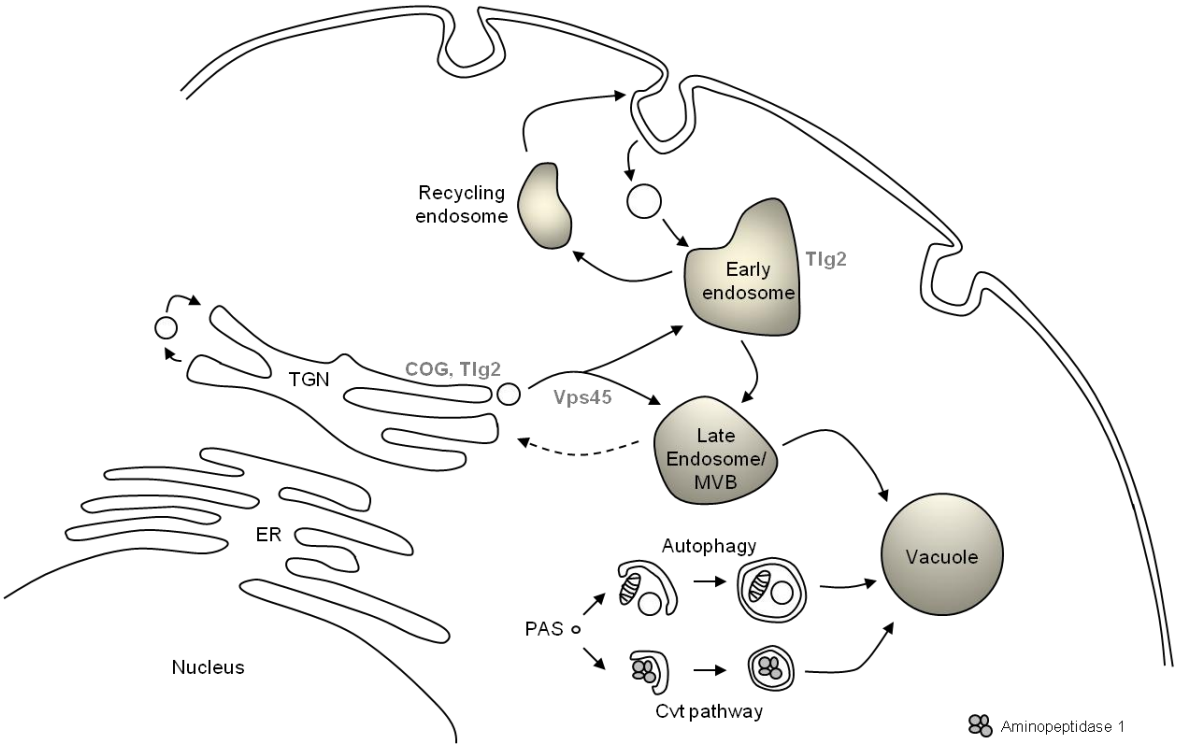

Figure 1-2. Schematic representation of the endosomal system, autophagy and the Cvt pathway in yeast.
Key trafficking pathways within the endosomal system, autophagy and the Cvt pathway are indicated. Tlg2 localises to the trans Golgi network (TGN) and early endosomes; Vps45 is required for the delivery of vesicle-bound proteins from the TGN to the endosomal system; the COG complex localises to the Golgi. Both the degradative autophagy and biosynthetic Cvt pathways terminate at the vacuole. Proteins trafficking through the endosomal system can be targeted to either the vacuole or proteasome (not depicted). ER, endoplasmic reticulum.

Fusion of the two leading edges of the expanding isolation membrane results in the formation of the autophagosome (Mizushima, 2007). The COG complex, a tethering factor that mediates retrograde vesicular trafficking of Golgi resident proteins and control exit from the Golgi (VanRheenen *et al.*, 1999; Suvorova *et al.*, 2002) localizes to the PAS (Yen et al., 2010). Moreover, COG complex subunits interact with Atg proteins and mutants of the COG complex subunits result in a dispersed localization of the Atg8 ubiquitin conjugation system throughout the cytosol. The Atg8 conjugation system is required for autophagosome generation (Ohsumi, 2001; Nakatogawa *et al.*, 2007) and its mislocalisation leads to defective autophagosome formation and completion (Yen et al., 2010). Localization of the COG complex subunits to the PAS combined with its role as a tethering factor implicates a role for this complex during the early phases of autophagy. More recent evidence support a role for SNARE-mediated homotypic fusion reactions in the formation of autophagosomes and thereby autophagy. Atg16 forms a complex

with the Atg12-Atg5 conjugate and associates with autophagosomal precursor membranes. This complex is required for isolation membrane expansion and dissociates from the membrane upon autophagosome completion (Mizushima *et al.*, 2001). Moreau and colleagues recently demonstrated that homotypic fusion between Atg16 precursor membranes is required for autophagosome maturation (Moreau *et al.*, 2011). Specifically, it was demonstrated that the vesicle-associated membrane protein (VAMP) 7, which is required for endosomal to lysosomal vesicle transport (Advani *et al.*, 1998; Bogdanovic *et al.*, 2002), colocalise to the PAS with Atg16, LC3 (mammalian homologue of Atg8) and the autophagic precursor marker Atg5 (Moreau *et al.*, 2011). Atg16 also co-localised with the endogenous partner SNARE proteins of VAMP7: Syntaxin 7, Syntaxin 8 and Vti1. Homotypic fusion between Atg16-associated precursor membranes results in the formation of larger vesicles which mature to form autophagosomes. However, knockdown of VAMP7 and its partner SNARE proteins resulted in an accumulation of smaller Atg16-associated vesicles and an overall decrease in the rate of fusion of Atg16-specific vesicles. This demonstrated the requirement for homotypic fusion in the generation of mature autophagosomes. However, other SNARE proteins are likely to be implicated in homotypic fusion reactions at this early stage of autophagy as the addition of tetanus neurotoxin, which specifically cleaves VAMP1, VAMP2 and VAMP3, but not VAMP7, also resulted in the accumulation of small Atg16 vesicles compared to control cells. Tlg2 has been shown to regulate autophagy in yeast and has a well-established role in homotypic fusion reactions in both the endocytic and autophagy-related Cvt pathways (Abeliovich *et al.*, 1999; Brickner *et al.*, 2001; Ohashi & Munro, 2010; Nair *et al.*, 2011). However, the molecular mechanisms by which Tlg2 regulates autophagy remain unknown.

Maturation of the autophagosome defines the terminal step of autophagy and it involves homo- and heterotypic fusion with other autophagosomes and lysosomes/vacuoles, respectively (Tooze & Yoshimori, 2010). Fusion of the autophagosome with the lysosome is mediated by Syntaxin 17 and its partner SNARE proteins SNAP29 (synaptosomal-associated protein 29) and VAMP8 (Itakura *et al.*, 2012). This results in delivery of the internal vesicle of the autophagosome, the autophagic body, to the lysosome/vacuole. The product of this fusion is known as the autolysosome and it is here that the autophagic body and its content is degraded with constituent components being recycled for subsequent use by the cell.

Autophagy was originally thought of as a non-selective pathway (Baba et al., 1994) however growing evidence support a role for ubiquitin-mediated selection in this process (section 1.1.5).

1.1.5 Ubiquitination and selective autophagy

Ubiquitin is a small 76 residue [8.5 kilodalton (kDa)] protein that is ubiquitously expressed and highly conserved across eukaryotes (Goldstein *et al.*, 1975; Ciechanover *et al.*, 1980). Attachment of ubiquitin to proteins, or ubiquitination, is a reversible post-translational modification which can selectively target substrates for proteasome-mediated degradation. Ubiquitination can also signal substrate proteins for lysosome-mediated degradation and coordinate protein localisation and protein activation status (Katzmann *et al.*, 2002; Gregory *et al.*, 2003; Muratani & Tansey, 2003). The process of ubiquitination is achieved through the addition of one (mono-ubiquitination) or several (poly-ubiquitination) ubiquitin molecules to the substrate protein and is mediated by the sequential action of three enzymes: E1, E2 and E3 [reviewed in (Pickart, 2001)] . Together these enzymes mediate the three main steps involved in ubiquitination: activation, conjugation and ligation of ubiquitin to its substrate protein (Figure 1-3). The ubiquitin-activating enzyme E1 activates ubiquitin via an adenosine triphosphate (ATP)-dependent process. The activated ubiquitin molecule is then transferred to the ubiquitin-conjugating enzyme, E2, prior to reaching the third and final step in the ubiquitination cascade, E3. E3 is a ubiquitin protein ligase that recognises and bind specific target substrates and subsequently labels the substrate with ubiquitin. More specifically, ubiquitin associates with free amino groups usually via lysine residues within substrate proteins via a N-terminal glycine residue. Ubiquitin itself contains seven lysine (K) residues (K6, K11, K27, K29, K33, K48 and K63), which in turn can serve as ubiquitin-acceptor sites to form polyubiquitin chains.

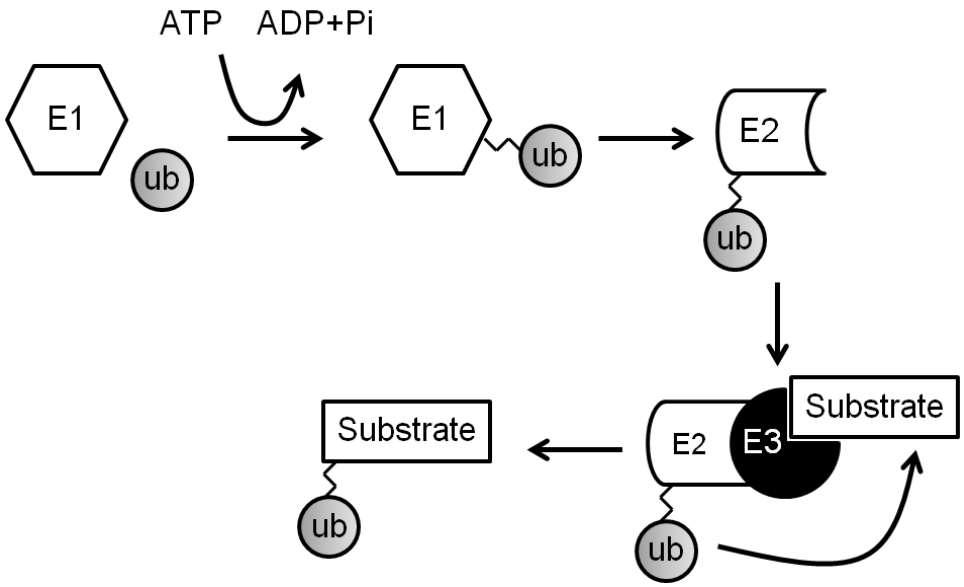

Figure 1-3. Schematic overview of ubiquitination
Ubiquitination of substrate proteins is achieved by the sequential actions of three different types of enzymes: E1, E2 and E3. Ubiquitin is activated by the ubiquitin-activating enzyme E1 in an ATP dependent manner and is subsequently transferred to the ubiquitin-conjugating enzyme E2.The E3 ubiquitin protein ligase mediates substrate specificity and transfers the activated ubiquitin moiety onto target substrates.

Identification of the yeast and mammalian autophagy receptors Atg19 and p62, which have the ability to simultaneously bind ubiquitin and the autophagosome-associated ubiquitin-like proteins Atg8 and LC3, respectively, provided insight into how protein cargo can be selectively targeted to the vacuole and lysosome via autophagy (Pankiv *et al.*, 2007; Noda *et al.*, 2008). The ubiquitin binding protein p62 contains a N-terminal LC3-interacting region (LIR) and a carboxy (C)-terminal ubiquitin-associated (UBA) domain (Pankiv *et al.*, 2007; Isogai *et al.*, 2011). The p62 UBA domain mediates binding to ubiquitinated cargo and leads to aggregate formation which is recruited to the autophagosomes via direct interaction with LC3. Consistent with this model, selective degradation by autophagy requires the presence of p62 and its ability to associate with LC3 and ubiquitin (Bjorkoy *et al.*, 2005; Komatsu *et al.*, 2007; Pankiv *et al.*, 2007). The yeast Atg8-Atg19 system is thought to operate in a similar manner to its mammalian homologs, LC3-p62 (Chang & Huang, 2007; Noda *et al.*, 2008).

1.1.6 Regulation of autophagy by signalling pathways

Target of rapamycin complex 1 (TORC1) is a nutrient-sensitive serine/threonine kinase that has been shown to inhibit autophagy under nutrient replete conditions and may provide the link between nutrient limitation and induction of autophagy (Noda & Ohsumi, 1998; Scott *et al.*, 2004). TORC1-mediated regulation of autophagy is mediated by a series of events. Under nutrient replete conditions, TORC1 is incorporated into an Atg13 containing complex and subsequently phosphorylates Atg13 (Hosokawa et al., 2009) (Figure 1-4). Phosphorylated Atg13 is unable to associate with Atg1 (Kamada et al., 2000), the only serine/threonine protein kinase that has been identified among the Atg proteins (Matsuura et al., 1997). Failure of an interaction between Atg13 and Atg1 results in inhibition of autophagy. Nutrient limitation or rapamycin treatment inhibits the activity of TORC1 (Noda & Ohsumi, 1998). This leads to dephosphorylation of Atg13 which exhibits a high affinity for binding to Atg1. Upon binding, dephosphorylated Atg13 activates Atg1 kinase activity (Kijanska *et al.*, 2010). Association between Atg1 and Atg13 is required for the initiation of autophagy (Kamada et al., 2000). These events implicate an important regulatory role for TORC1 kinase activity in autophagy.

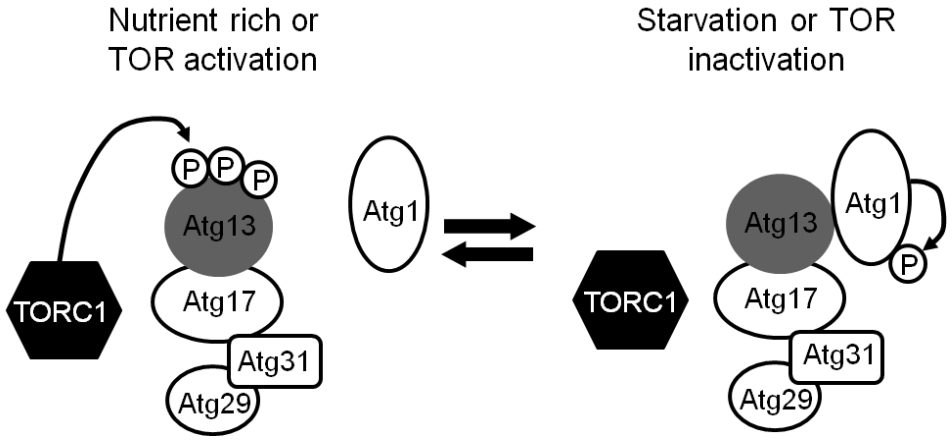

Figure 1-4. Regulation of autophagy by TORC1
Target of rapamycin complex 1 (TORC1) activity negatively regulates autophagy. Atg13 is phosphorylated in a TORC1-dependent manner under nutrient rich conditions and forms part of the core complex required for the initiation of autophagy. Phosphorylation of Atg13 prevents its association with Atg1 and thereby inhibits autophagy. Nutrient limitation inhibits TORC1 activity and as result dephosphorylation of Atg13. Under these conditions, Atg13 is able to associate with Atg1. This interaction is required for Atg1 kinase activity which leads to the induction of autophagy.

1.1.7 Autophagy in disease and development

Although autophagy was originally identified as a starvation-induced survival response (section 1.1.1) (Novikoff *et al.*, 1964; Deter & De Duve, 1967), a role for this pathway in a number of human pathologies, aging and development has been addressed in recent years (Choi *et al.*, 2013).

Reduced autophagic activity is associated with cancer and neurodegenerative conditions. For instance, inhibition of TORC1 by rapamycin, which leads to induction of autophagy, has been demonstrated to reduce huntington aggregate accumulation in cell models of Huntington's disease (Ravikumar et al., 2004). Inhibition of autophagy in these same cell models produced the opposite effect. Autophagic activity is also important in suppressing tumour development (Edinger & Thompson, 2003). Mutations in *beclin-1* (the mammalian homolog of the yeast *Atg6/Vps30* gene) lead to defects in autophagy and intriguingly monoallelic deletion of *beclin-1* occur in 40-75% of sporadic human breast, ovarian and prostate cancers (Liang et al., 1999; Qu et al., 2003; Yue et al., 2003). A reduction in the efficiency of proteolysis of long-lived organelles and misfolded proteins is associated with ageing therefore a role for autophagy in this process has been suggested (Donati *et al.*, 2001; Del Roso *et al.*, 2003; Martinez-Vicente *et al.*, 2005). This can be partly attributed to an accumulation of lipofuscin, which are highly oxidised, insoluble cross-linked protein aggregates, in lysosomes that occur with ageing. This impairs the proteolytic activity of lysosomes as well as the ability of lysosomes to fuse with autophagic structures and in effect lead to progressive accumulation of damaged or long-lived proteins and organelles (Terman et al., 1999; Terman et al., 2007). This reduction in the efficiency of autophagy may also contribute to the pathogenesis of some age-related diseases. Furthermore, defects in autophagy lead to various abnormalities in cellular differentiation and development (Kuma *et al.*, 2004; Mizushima & Levine, 2010).

As discussed above, autophagy is involved in multiple biological processes and it is therefore of great interest to further investigate the mechanisms involved in ensuring proper function of autophagy. A thorough understanding of autophagy could potentially lead to the development of novel treatment strategies and improved management of the pathologies and conditions mentioned above.

1.2 SNARE proteins

1.2.1 Structure and function of SNARE proteins

The SNARE family of proteins is highly conserved throughout evolution and plays a central role in intracellular membrane fusion (Jahn & Sudhof, 1999; Lin & Scheller, 2000). The defining feature of this family of proteins is the cytosolic SNARE motif: a repeated heptad pattern of hydrophobic amino acids that spans approximately 60-70 residues in length (Figure 1-5) (Weimbs et al., 1997). The SNARE motif mediates core complex formation that exhibits a parallel four-helical structure (Hanson *et al.*, 1997; Sutton *et al.*, 1998; Antonin *et al.*, 2002). This molecular arrangement requires one arginine (R)-SNARE (such as VAMP2) and three glutamine (Q)-SNAREs (labelled either Qa, Qb or Qc) (Fasshauer et al., 1998). These SNAREs, which are associated with their respective membranes via their carboxy (C)-termini, are contributed by the vesicle (v-SNARE) and target membrane (t-SNARE), respectively, and act to bring opposing membranes within close proximity for subsequent fusion. For the purpose of this review, the v- and t-SNARE nomenclature will be used from here on.

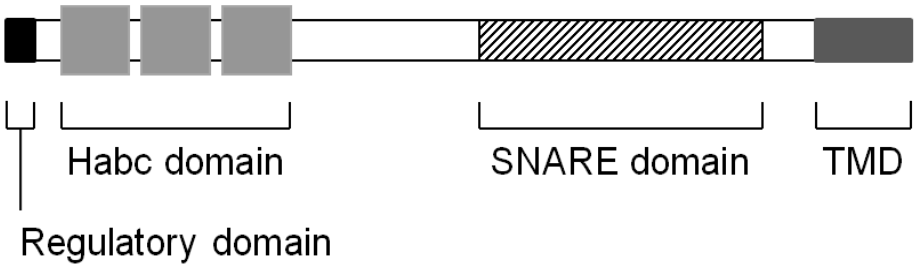

Figure 1-5. Domain structure of the syntaxin proteins
The syntaxin family of SNARE proteins contain an N-terminal residue regulatory domain (solid black rectangle) that is followed by the Habc domain (for helices Ha, Hb and Hc; represented as three solid grey squares). The SNARE domain is the defining feature of syntaxin proteins (represented by a diagonally striped rectangle) and is followed by the C-terminal transmembrane domain (TMD; represented by a solid dark grey rectangle). Adapted from (Fernandez *et al.*, 1998).

In addition to the SNARE domain, the syntaxin SNARE proteins possess an autonomously folded amino (N)-terminal domain that forms a three-helix bundle structure (Fernandez *et al.*, 1998; Dulubova *et al.*, 2001; Gonzalez *et al.*, 2001). This domain is called the Habc domain (for helices Ha, Hb and Hc) (Figure 1-5).

The neuronal Syntaxin 1a Habc domain binds intramolecularly to the C-terminal SNARE motif to regulate core complex formation (Hanson *et al.*, 1995; Nicholson *et al.*, 1998; Burkhardt *et al.*, 2008). In this closed conformation (Figure 1-6, A), neuronal Syntaxin 1a is unable to interact with its partner SNARE proteins therefore core complex formation is prevented (Pevsner *et al.*, 1994; Dulubova *et al.*, 1999). Inhibition of the SNARE motif by the Habc domain is released in the open conformation (Figure 1-6, B) by the actions of its regulatory SM protein, Munc18a (Dulubova *et al.*, 1999; Verhage *et al.*, 2000; Gerber *et al.*, 2008). Binding of Munc18a to the closed conformation of neuronal Syntaxin 1a leads to core complex assembly and thereby membrane fusion and subsequent exocytosis. Loss of Munc18a function leads to a complete block in neurotransmitter release thereby supporting a regulatory role for Munc18a in neuronal Syntaxin 1a activity (Verhage *et al.*, 2000; Weimer & Richmond, 2005). This mode of regulation (section 1.3.2) extends to other SNARE protein complexes and their respective SM proteins including Vps45 (vacuolar protein sorting protein 45) (section 1.3) and its cognate syntaxin Tlg2 (section 1.2.3) (Bryant & James, 2001; Dulubova *et al.*, 2002).

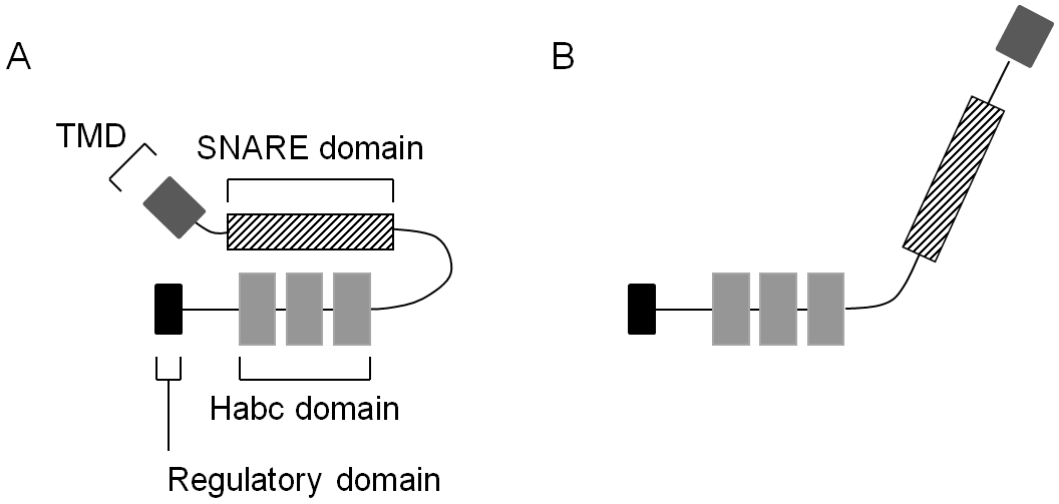

Figure 1-6. Closed and open conformations of the SNARE proteins
A. In the closed conformation the Habc domain (represented by three grey rectangles) inhibits SNARE complex formation by binding to the SNARE domain (diagonally striped rectangle). **B.** SNARE complex formation is able to proceed in the open conformation.

Assembled core complexes that bridge the vesicle and target membranes are referred to as *trans*-SNARE complexes. Following membrane fusion the core complex subunits all reside on the same membrane in a *cis*-SNARE complex that exhibits great stability (Ungar & Hughson, 2003). The NSF chaperone and SNAP co-chaperone disassemble *cis*-SNARE complexes in an ATP dependent manner and render the SNARE complex subunits available for subsequent rounds of core complex formation (Sollner *et al.*, 1993a).

1.2.2 Expression and localisation of SNARE proteins

SNARE proteins were originally identified as binding partners of NSF and SNAPs by affinity purification and were localised to vesicle or target membranes (Bennett et al., 1992; Sollner et al., 1993b). SNARE proteins exhibit a differential pattern of expression. For example, Syntaxins 1a and 1b mediate neurotransmission and are therefore highly expressed in neurons (Bock et al., 2001). Additionally, SNARE proteins localise to distinct compartments within the cell (Pelham, 2001). For example, Snc1/2 proteins localise to endocytic vesicles in yeast and fuse with endosomal compartments in a Tlg2-dependent manner (Seron *et al.*, 1998; Gurunathan *et al.*, 2000; Lewis *et al.*, 2000).

1.2.3 The endosomal SNARE complex

Much of our understanding regarding membrane fusion has stemmed from research that has used the yeast model system *S.cerevisiae.* In particular, the yeast endosomal SNARE complex, which includes the syntaxin t-SNARE Tlg2, has been extensively studied. Tlg2 is a 396 amino acid protein that exhibits a domain structure typical of syntaxins (Dulubova et al., 2002) (Figure 1-5; section 1.2.1). Tlg2 localises to the trans-Golgi network (TGN) and early endosomes where it plays an important role in membrane traffic (Abeliovich *et al.*, 1998; Holthuis *et al.*, 1998b; Seron *et al.*, 1998; Abeliovich *et al.*, 1999). More specifically, Tlg2 was identified as a nonessential protein that is required for the efficient trafficking of the yeast vacuolar protease carboxypeptidase Y (CPY) (Abeliovich *et al.*, 1998). Tlg2 interacts with the t-SNAREs Tlg1 and Vti1 and the v-SNARE Snc2 to form a functional core complex (Holthuis *et al.*, 1998b; Paumet *et al.*, 2001). The *S.cerevisiae* SM protein Vps45 (section 1.3) regulates core complex assembly involving Tlg2 by binding to a short N-terminal 36 residue peptide motif on Tlg2 or a C-terminal binding site that includes that Habc, linker

and SNARE motif regions (Figure 1-5) (Dulubova *et al.*, 2002; Carpp *et al.*, 2006; Furgason *et al.*, 2009). These interactions are consistent with modes 1 and 2 binding, respectively. Competition assays performed between full length Tlg2 and Tlg2 lacking the N-terminal peptide motif, or the latter construct with the first 36 N-terminal residues of Tlg2, indicates that the Tlg2 N-peptide modulates the binding affinity of Vps45 to the closed Tlg2 conformation. Thus, the Tlg2 N-peptide regulates incorporation of Tlg2 into a functional SNARE complex (Furgason *et al.*, 2009). Simultaneous mutation of the N-peptide and C-terminal binding regions abrogates Tlg2 function. However, the presence of at least one of the two Vps45 binding sites is sufficient for Tlg2 function as assessed by the CPY-secretion assay. Additionally, Vps45 has also been shown to associate with Tlg2 preassembled in a SNARE complex (Carpp *et al.*, 2006). This mode 3 binding is required to prime vesicle fusion and implicates a role for Vps45 at different stages during the SNARE complex assembly/disassembly cycle. In addition to modulating Tlg2 function, Vps45 also stabilises Tlg2 with Vps45 deficient cells containing reduced cellular levels of Tlg2 (Nichols *et al.*, 1998; Bryant & James, 2001). This effect is due to an increase in Tlg2 protein turnover, which in turn is mediated by both the vacuole and proteasome (Bryant & James, 2001; Struthers, 2009).

Tlg2 and its SM proteinVps45 play a role in homotypic fusion reactions in the endosomal pathway (Brickner et al., 2001) as well as homotypic fusion reactions that sequester aminopeptidase I into Cvt vesicles (Abeliovich et al., 1999). These findings combined with the endosomal localisation of Tlg2 support a likely role for Tlg2 and its SM proteins Vps45 in autophagosome formation.

1.2.4 Syntaxin 16 is the mammalian orthologue of Tlg2

The domain structure and N-terminal peptide motif is highly conserved between Tlg2 and the mammalian Syntaxin 16 (Dulubova et al., 2002). Both of these SNAREs bind to their respective SM proteins, Vps45 and mVps45, via their conserved short N-terminal peptide motifs (Tellam *et al.*, 1997; Dulubova *et al.*, 2002; Burkhardt *et al.*, 2008). These observations, combined with the ability of Syntaxin 16 to functionally complement mutant phenotypes of *TLG2* deficient yeast cells (Struthers et al., 2009) confirms that Syntaxin 16 is the mammalian orthologue of Tlg2 (Tellam *et al.*, 1997; Simonsen *et al.*, 1998; Tang *et al.*, 1998).

1.2.5 Regulation of Tlg2 cellular levels

Tlg2 mediates membrane traffic within the yeast endosomal system together with its partner SNARE proteins Tlg1, Vti1 and Snc2 (Abeliovich *et al.*, 1998; Holthuis *et al.*, 1998a; Seron *et al.*, 1998; Paumet *et al.*, 2001). The SM protein Vps45 associates with intracellular membranes predominantly in a Tlg2-dependent manner and positively regulates SNARE complex formation (Nichols *et al.*, 1998; Bryant & James, 2001). Tlg2 cellular levels are reduced in cells lacking Vps45 despite being synthesised to similar levels in both wild type and *vps45* cells. This reduction in Tlg2 steady-state levels is mediated by both the proteasome and vacuole in yeast (Bryant & James, 2001; Struthers, 2009). Specifically, loss of proteasome activity in a *vps45* background restores Tlg2 to near wild type levels (Bryant & James, 2001). In contrast, loss of vacuolar protease activity by the *pep4-3* mutation has no observable effect on Tlg2 levels in a *vps45* background. However, further investigations revealed that cells harboring the *pep4-3* mutation exhibit increased levels (approximately 2-fold) of Tlg2 when compared with congenic wild type cells containing active vacuolar proteases (Struthers, 2009). This observation highlights the requirement for Vps45 in the efficient delivery of proteins, including Tlg2, into the vacuolar pathway (Piper *et al.*, 1994; Bryant *et al.*, 1998). Collectively these data suggest a model by which Tlg2 is degraded by both the proteasome and vacuole under wild type conditions whereas the proteasome is the principal site for Tlg2 degradation in cells lacking Vps45.

Ubiquitin is the classic signal for proteasomal-mediated degradation of proteins (Glickman & Ciechanover, 2002) however it can also signal the entry of proteins, including Tlg1, into the multivesicular body (MVB) pathway, which terminates in the vacuole (Reggiori & Pelham, 2001; Reggiori & Pelham, 2002). Tlg1 is protected from trans-membrane ubiquitination ligase 1 (Tul1)-mediated ubiquitination by palmitoylation, a reversible post-translational modification which may also be implicated in the regulation of Tlg2 (Valdez-Taubas & Pelham, 2005). Both the proteasome and vacuole are involved in the regulation of Tlg2 cellular levels (Bryant & James, 2001; Struthers, 2009). However, a role for autophagy in the vacuolar-mediated regulation of Tlg2 remains to be investigated. Our laboratory has generated preliminary evidence to show that Tlg2 is ubiquitinated in both wild type and Vps45 deficient cells (Struthers *et al.*, 2009).

1.2.5.1 Protein palmitoylation

Palmitoylation is a reversible post-translation modification involving the addition of a palmitate molecule to a cysteine residue via a thioester bond [reviewed in (Salaun *et al.*, 2010)]. This reaction is mediated by substrate specific palmitoyltransferases (Lobo *et al.*, 2002; Roth *et al.*, 2002) and is implicated in diverse cellular processes including regulation of protein function (Veit *et al.*, 1996), localisation (He & Linder, 2009) and stability (Couve *et al.*, 1995). Seven members of the yeast DHHC (aspartate-histidine-histidine-cysteine) family of palmitoyltransferases have been identified in *S.cerevisiae*, including Swf1 (spore wall formation protein 1). The DHHC domain is responsible for the catalytic activity whereas the highly variable N- and C-terminal regions confer substrate specificity (Mitchell *et al.*, 2006; Gonzalez Montoro *et al.*, 2009).

A number of SNARE proteins have been identified as substrates for palmitoylation including the partner SNARE proteins of Tlg2, Tlg1 and Snc2 (Couve *et al.*, 1995; Valdez-Taubas & Pelham, 2005). Both Tlg1 and Snc2 are palmitoylated in a Swf1-dependent manner (Valdez-Taubas & Pelham, 2005). Swf1 appears to preferentially bind substrates containing cysteine residues adjacent to or within transmembrane domains (TMD) (Couve *et al.*, 1995; Yik & Weigel, 2002; Valdez-Taubas & Pelham, 2005). It has been observed that unpalmitoylated proteins that normally undergo palmitoylation are less stable than their modified counterparts (Couve *et al.*, 1995). Consistent with this observation, Tlg1 cellular levels are reduced in *swf1* deficient cells. This effect is mediated by Tul1-dependent ubiquitination of Tlg1 which signals entry into MVB and ultimate degradation in the vacuole (Valdez-Taubas & Pelham, 2005). This observation supports a role for palmitoylation in the regulation of Tlg1 cellular levels. As for Tlg1 and Snc2, Tlg2 contains two potential sites of palmitoylation (Figure 1-7) (Valdez-Taubas & Pelham, 2005). However, a role for palmitoylation in the regulation of Tlg2 steady-state levels remains to be investigated.

```
Tlg2     VELKSADKELNKATH--YQKRTQKCKVILLLTLCVIALFFFVMLKPH
Tlg1     GVVNKLARGRRQLEWVYEKNKEKYDDCCIGLLIVVLIVLLVLAFIA-
Snc2     GFKRGANRVRKQMWWKDLK----M-RMCLFLVVIILLVVIIVPIVVH
```

Figure 1-7. Transmembrane domain protein sequence alignment of yeast SNARE proteins
Cysteine (C) residues located near and/or within the transmembrane domains (TMD) of yeast Tlg2, Tlg1 and Snc2 are highlighted in grey. The hydrophobic TMD is underlined [taken from (Valdez-Taubas & Pelham, 2005)]. Protein sequences were aligned using the European Bioinformatics Institute multiple sequence alignment tool (available at http://www.ebi.ac.uk)

1.3 The SM family of proteins

The SM family of proteins was originally identified in genetic screens in yeast and *C.elegans* (Novick *et al.*, 1980; Gengyo-Ando *et al.*, 1993). Mutations in *C.elegans* UNC-18 (uncoordinated protein 18) are associated with severe uncoordinated phenotypes which reflect its role in the regulation of neurotransmitter release and thereby membrane fusion (Gengyo-Ando *et al.*, 1993). Similarly, Munc18a, a homolog of *C.elegans* UNC-18 and *S.cerevisiae* Sec1 (secretory protein 1), is required for regulating neurotransmitter release via a syntaxin-dependent mechanism (Harrison *et al.*, 1994; Schulze *et al.*, 1994; Misura *et al.*, 2000; Verhage *et al.*, 2000). Subsequent work in this field has contributed to the well established role for SM proteins in the regulation of SNARE protein function and thereby membrane fusion (section 1.3.2) [reviewed in (Jahn, 2000)] although the precise role for this family of proteins remains unclear.

1.3.1 SM protein structure

SM proteins are evolutionarily conserved hydrophilic proteins ranging between 60-70 kDa (Halachmi & Lev, 1996). Four members belonging to the SM family of proteins have been identified in yeast: Sec1, Sly1 (suppressor of loss of Ypt1), Vps33 and Vps45. SM proteins regulate membrane fusion by direct association with distinct subsets of SNARE proteins and share a high degree of homology across the entire length of their primary sequence. Crystal structures of nSec1/Munc18a, Sly1 and more recently Vps33 have been solved and demonstrate overall conservation in SM protein structure (Bracher *et al.*, 2000; Misura *et al.*, 2000; Bracher & Weissenhorn, 2002; Baker *et al.*, 2013). More

specifically, SM proteins adopt an arch-shaped structure composed of domains 1, 2 and 3. The latter is further subdivided into domains 3a and 3b. The central arch is formed between domains 1 and 3a. Mutations in domain 3a result in defective SNARE complex assembly and inhibition of membrane fusion at the stage of vesicle docking, which coincides with binding pre-assembled SNARE complexes (Boyd *et al.*, 2008; Hashizume *et al.*, 2009; Pieren *et al.*, 2010).

1.3.2 Regulation of membrane fusion by SM proteins

Three distinct modes of interaction between SM and SNARE proteins have been identified (Figure 1-8). Mode 1 binding was first described between neuronal Munc18a and its cognate SNARE protein Syntaxin 1a (Misura *et al.*, 2000). Mode 1 binding is characterised by the SM protein binding to its cognate SNARE protein in the closed conformation via an arched shaped cavity. This interaction is mediated by both the Habc and SNARE domains and was initially thought to be inhibitory. The interaction between Munc18a and Syntaxin1a was later demonstrated to be required for neurotransmitter release (Verhage *et al.*, 2000), supporting a role for SM-SNARE pairing in regulation of SNARE complex assembly and thereby membrane fusion. In contrast to mode 1 binding, the SM protein Sly1, which is required for Golgi and ER fusion, regulates its cognate SNARE protein Sed5 via a direct interaction with a short N-terminal peptide preceding the Habc domain referred to as mode 2 binding (Yamaguchi *et al.*, 2002). Crystal structure analysis of Sly1 in complex with Sed5 revealed that this interaction is mediated by a hydrophobic pocket located on the outer surface of Sly1 (Bracher & Weissenhorn, 2002). The Munc18c -Syntaxin 4 interaction also conforms to mode 2 binding (Latham *et al.*, 2006). The third mode of interaction (mode 3) is purely based on experimental data available and lacks structural evidence. The localisation of the SM protein Sec1 coincides with sites of vesicle secretion where SNARE proteins are known to function. However, mutants defective in SNARE complex assembly mislocalise Sec1; mutants defective in SNARE complex disassembly display robust localisation of Sec1 (Carr *et al.*, 1999). Thus, mode 3 binding is characterised by SM proteins binding to assembled SNARE complexes.

The SM proteins Munc18a and Vps45 can associate with their respective cognate SNARE proteins Syntaxin 1a and Tlg2 using multiple modes of binding (Dulubova

et al., 2002; Bryant & James, 2003; Carpp *et al.*, 2006; Dulubova *et al.*, 2007; Burkhardt *et al.*, 2008; Furgason *et al.*, 2009). Distinct modes of interaction between SM and SNARE proteins implicate a role for SM proteins at different stages in the SNARE complex assembly and disassembly process. This supports a chaperone-like function for SM proteins in SNARE complex formation which may serve to protect assembly intermediates from premature NSF-mediated disassembly (Xu *et al.*, 2010).

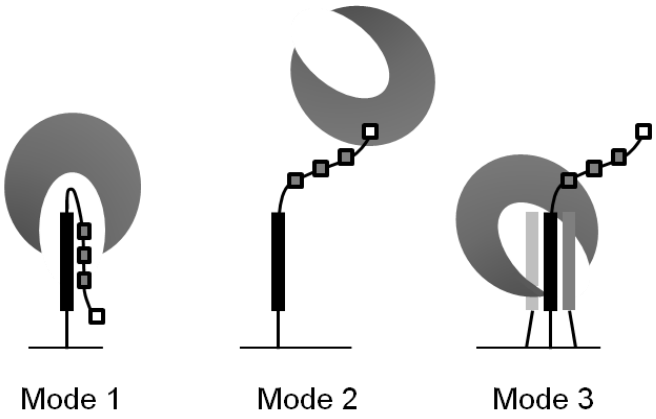

Figure 1-8. Modes of SM protein binding to SNARE proteins
SM proteins associate with their cognate SNARE proteins via three distinct modes of interaction: modes 1, 2 and 3. Mode 1 binding involves SM proteins binding their cognate SNARE proteins via an arch-shaped cavity in the closed conformation. A hydrophobic pocket present on the outer surface of SM proteins mediates binding to a short regulatory N-terminal domain on their cognate SNARE proteins during mode 2 binding. Mode 3 binding involves the SM protein binding to preassembled SNARE complexes.

1.3.3 Other SM protein interactions

Both the COG and Dsl1 (dependence on Sly1-20) tethering complexes contain the evolutionarily conserved MUN domain (Pei *et al.*, 2009) which was originally identified in Munc13 as a minimal sequence required for vesicle priming (Augustin *et al.*, 1999; Basu *et al.*, 2005). Basu and colleagues demonstrated that the MUN domain of Munc13a was sufficient to rescue a complete block in neurotransmitter release in hippocampal neurons deficient for Munc13a/b. The MUN domain of Munc13a has since been shown to directly interact with the SNARE domain of Syntaxin 1a to facilitate transition from a closed Syntaxin 1a-Munc18a complex to the SNARE complex (Guan *et al.*, 2008; Ma *et al.*, 2011). Remote homology and structural conservation between the Munc13 MUN domain and the COG complex tethering subunits is indicative of a conserved functional role (Pei *et al.*, 2009; Li *et*

al., 2011). Indeed, a number of COG:SNARE interactions have been identified in yeast and mammals and increasing evidence supports a role for the COG complex in promoting SNARE complex assembly via direct association with the SNARE domain (Suvorova *et al.*, 2002; Shestakova *et al.*, 2007; Laufman *et al.*, 2011; Laufman *et al.*, 2013). It is likely that SM proteins may also directly associate with tethering factors to assist in regulated core complex formation. Interaction between the SM protein Sly1, which is required for membrane fusion at the ER-Golgi interface, and subunits of the COG and Dsl1 tethering complexes have been shown to be required for efficient colocalisation of partner SNARE proteins and thereby SNARE complex formation (Vanrheenen *et al.*, 2001; Laufman *et al.*, 2009). Consistent with a role for MUN domain containing tethers in regulating membrane fusion in association with SM protein, biochemical analysis has revealed a direct interaction between the Cog4 and the SM protein mVps45 (Laufman *et al.*, 2013). Cog4 was also shown to associate with Syntaxin 16 and Vti1, the cognate syntaxins of Vps45. Collectively these data implicate an additional level of regulation in membrane fusion and resonates the idea that multivalent interactions are an increasingly common feature of the fusion machinery which serves to improve the fidelity of vesicle trafficking.

1.3.4 Identification of the SM protein Vps45

Two distinct routes operate in the delivery of newly synthesised vacuolar proteins: the CPY and alkaline phosphatase pathways (Conibear & Stevens, 1998). The former constitutes the principal route for the delivery of newly synthesised proteins, including CPY, to the vacuole. CPY is a soluble hydrolase that normally resides within the vacuole. CPY is synthesised as a pro-protein containing a sorting signal directing its sequential transport to the vacuole via the ER, Golgi and pre-vacuolar compartment (Stevens *et al.*, 1982; Valls *et al.*, 1987). CPY is proteolytically processed to its mature form within the vacuole (Rothman *et al.*, 1989). Yeast genetic screens have identified over 45 genes required for the efficient delivery and sorting of vacuolar resident hydrolases; these are collectively referred to as vacuolar protein sorting (*VPS*) genes (Robinson *et al.*, 1988; Rothman *et al.*, 1989). *VPS* genes are further categorised into six distinct classes (A to F) based on the vacuolar morphology they exhibit under mutant conditions (Raymond *et al.*, 1992).

Vps45 belongs to the class D *vps* mutants and is required for the delivery of newly synthesised proteins from the TGN into the endosomal system (Raymond *et al.*, 1992; Cowles *et al.*, 1994; Piper *et al.*, 1994; Bryant *et al.*, 1998). *VPS45* encodes a 67 kDa SM protein homolog that is peripherally associated with intracellular membranes predominantly in a Tlg2-dependent manner (Cowles *et al.*, 1994; Nichols *et al.*, 1998). Yeast deficient in Vps45 accumulate small intracellular vesicles, missort and subsequently secrete a portion of the vacuolar hydrolase CPY and are temperature sensitive for growth. These phenotypes highlight the role for Vps45 in endosomal trafficking. Furthermore, Vps45 is required for stable expression and function of its cognate SNARE protein Tlg2 (Nichols *et al.*, 1998; Bryant & James, 2001). This regulatory feature is conserved amongst several SM proteins functioning at various membrane trafficking steps (Toonen *et al.*, 2005; Latham *et al.*, 2006).

1.4 Tethering proteins

Tethering proteins are a diverse group of peripherally associated membrane proteins that facilitate the initial physical contact between vesicle and acceptor membranes prior to fusion [reviewed in (Pfeffer, 1999)]. Tethering proteins localise to and operate within distinct compartments of the secretory and endocytic pathways. For example, the Dsl1 complex is required for recycling traffic from the Golgi to the ER (Zink *et al.*, 2009) whereas the COG complex is required for retrograde traffic to and within the Golgi (Suvorova *et al.*, 2002). Tethering proteins are categorised into three distinct groups based on structural and functional similarities: 1) oligomeric complexes that associate with SNARE proteins and typically act as Rab effectors, 2) oligomeric complexes that function as Rab protein activators and 3) coiled-coil tethers. The COG complex, together with the Dsl1, GARP (Golgi-associated retrograde protein) and exocyst complexes belong to the first group of tethering proteins and are collectively referred to as the DCGE group. The DCGE group of tethers contain evolutionarily conserved sequence MUN domains which are discussed in more detail in section 1.3.3.

1.4.1 Function of the COG tethering complex

The COG complex, which was initially isolated based on its ability to stimulate Golgi transport *in vitro* (Walter et al., 1998), plays an important role in retrograde vesicular transport of Golgi resident proteins as well as ER-to-Golgi and endosome-to-Golgi vesicular transport (VanRheenen *et al.*, 1998; Whyte & Munro, 2001; Zolov & Lupashin, 2005). The importance of the COG complex in these roles is highlighted by conditions in which COG complex subunits have been mutated, deleted or experimentally knocked down. For instance, mutations in a number of the COG complex subunits are associated with human congenital disorders of glycosylation (Shestakova et al., 2006; Zeevaert et al., 2008). The phenotypes exhibited by mutant COG complex subunits include abnormal Golgi morphology (Ungar et al., 2002), accumulation of vesicles (Wuestehube *et al.*, 1996; Zolov & Lupashin, 2005) and abnormal glycosylation of proteins (Shestakova *et al.*, 2006; Smith & Lupashin, 2008).

The COG complex can be functionally classified as a multisubunit tethering complex that binds to SNARE proteins and typically act as Rab effectors (section 1.4) (Sztul & Lupashin, 2009). Rab proteins have previously been shown to be required for vesicle docking and regulation of SNARE complex formation *in vivo*, possibly via interaction with tethering factors (Lian *et al.*, 1994; Sogaard *et al.*, 1994). Direct interactions between the COG complex and various Golgi t- and v-SNAREs including Syntaxin 16 and Vti1 have been identified (Suvorova *et al.*, 2002; Shestakova *et al.*, 2007; Laufman *et al.*, 2013). It is suggested that the COG complex, which is an effector of the Rab protein Ypt1 (Suvorova *et al.*, 2002), is involved in regulating the formation and stability of the SNARE complex as well as providing a platform for recruiting additional fusion machinery. It is proposed that the COG complex mediates the initial physical contact between transport vesicles and their target membranes (Figure 1-9) based on its ability to directly interact with subunits of the COPI coat. Furthermore, the COG complex has been shown to localise to the PAS under autophagy inducing conditions in yeast and as discussed previously (section 1.1.4), it is also able to bind to a number of Atg (Yen et al., 2010) and SNARE proteins (Suvorova *et al.*, 2002; Shestakova *et al.*, 2007). Collectively, these data implicate a role for the COG complex and the Golgi SNARE proteins and their respective cognate SM proteins in the biogenesis and formation of autophagosomes.

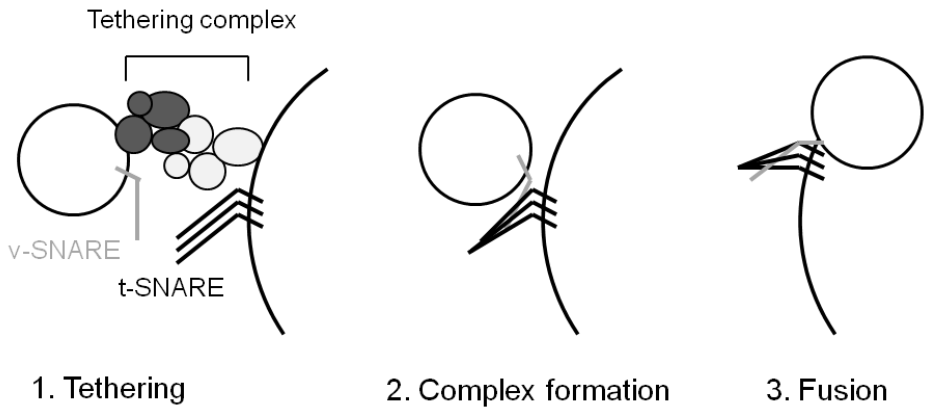

Figure 1-9. Schematic diagram of membrane fusion
Membrane fusion requires initial physical interaction between a vesicle (v) and target (t) membrane (tethering). This is followed by a closer interaction between opposing v- and t-SNARE proteins (*tans*-SNARE complex formation) that ultimately leads to the formation of a *cis*-SNARE complex (fusion). Adapted from (Whyte & Munro, 2002)

1.4.2 Molecular structure of the COG complex

The COG complex is a large octameric structure with a combined mass of approximately 700 kDa (VanRheenen *et al.*, 1999; Whyte & Munro, 2001; Ungar *et al.*, 2002). The eight COG subunits (Cog 1 to 8) are organized into two heterotrimetric complexes composed of Cog2, -3, -4 and Cog5, -6 -7 linked by a Cog1/Cog8 heterodimer (Figure 1-10) (Ungar *et al.*, 2002; Fotso *et al.*, 2005; Oka *et al.*, 2005; Ungar *et al.*, 2005). Binary interactions between the different Cog subunits are mediated by their N-termini whereas the Cog1 C-terminal domain plays an important role in bridging the Cog5-8 subunits to the complex (Lees et al., 2010). The Cog1-4 and Cog5-8 sub-complexes are referred to as lobes A and B, respectively. In yeast, deletion of any of the lobe A subunits result in severe growth defects and are required for maintenance of overall Golgi structure (Whyte & Munro, 2001; Peanne *et al.*, 2011). In contrast, deletion of the lobe B subunits induces mild growth defects and is required for organising and stabilising Golgi glycosylation enzymes. The differential effects of lobe A and B of the COG complex indicates that the different Cog subunits mediate different functional roles within the complex (Whyte & Munro, 2001; Bruinsma *et al.*, 2004; Oka *et al.*, 2004; Oka *et al.*, 2005). COG genes are ubiquitously expressed however their level of expression appears to be differentially regulated across tissue types (Quental et al., 2010). Localisation of the COG complex to the cytosolic surface of the Golgi

apparatus provides evidence in support of its role as a tethering complex (Podos et al., 1994; Suvorova et al., 2001).

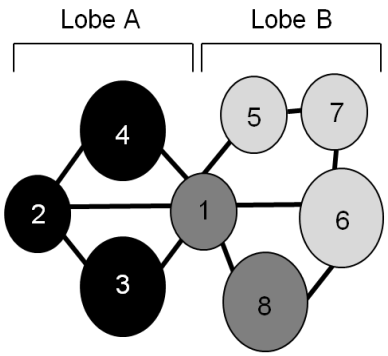

Figure 1-10. Architecture of the COG complex
The COG complex is an octameric structure that is arranged in two lobes: lobe A consists of Cog1 to Cog4; lobe B consists of Cog5 to Cog8. Lobes A and B are linked via a heterodimer consisting of Cog1 and Cog8. The numbers 1 to 8 represent Cog subunits 1 to 8, respectively. Adapted from (Quental *et al.*, 2010)

1.5 *C.elegans*: An introduction

Caenorhabditis elegans (*C.elegans*) are small, free-living transparent nematodes measuring approximately 1.2 millimetres (mm) in length (Brenner, 1974). They were originally employed as a model organism for studying aspects of development and genetics. As such, a large number of *C.elegans* mutants have been described (Brenner, 1974). The vast majority of *C.elegans* mutants are recessive and are broadly categorised based on phenotype including uncoordinated (Unc), roller (Rol), dumpy (Dpy), small (Sma) and long (Lon). Uncoordinated phenotypes range in severity from paralysis to small deviations in normal body movement. Roller mutants rotate around their long axis during motion whereas dumpy and small mutants are typically shorter and wider than their wild type counterparts, respectively. In contrast, long mutants are longer and thinner than wild type nematodes.

C.elegans are sexually dimorphic and can exist as either hermaphrodites or males (Wood, 1988). The former is the predominant sexual form. Self-fertilizing hermaphrodites lead to homozygosity of alleles and their clones are considered to be genetically identical. In the laboratory environment males are typically utilised to transfer genetic markers from one hermaphrodite to another in order to produce new genetic combinations.

1.5.1 *C.elegans* post-embryonic development

C.elegans are eutelic in nature: wild type N2 adult hermaphrodites contain a constant 959 somatic cells once cell division is complete (Sulston *et al.*, 1983). Thereafter, both the position and number of these cells remain constant and *C.elegans* growth is purely achieved via cell enlargement. Collectively these characteristic features lend *C.elegans* to the study of the biology of a single cell within an intact, multicellular organism.

Following embryonic development, *C.elegans* proceed through four larval (L) stages, referred to as L1 to L4, prior to reaching adulthood (Figure 1-11) (Singh & Sulston, 1978). Under standard laboratory conditions (20°C), egg-to-egg duration for the wild type N2 strain is 3 days. The end of each of the four larval stages is defined by moulting of the old cuticle which is synthesised five times during development: once in the embryo and subsequently at the end of each of the four larval stages prior to moulting [reviewed in (Page & Johnstone, 2007). Moulting is accompanied by the synthesis and secretion of a new stage-specific cuticle which is predominantly composed of cuticle collagen proteins (section 1.5.2) (Cox *et al.*, 1981b). Cuticle protein synthesis peaks during each moult and is much reduced during the inter-moult period (section 1.5.3) (Cox *et al.*, 1981a).

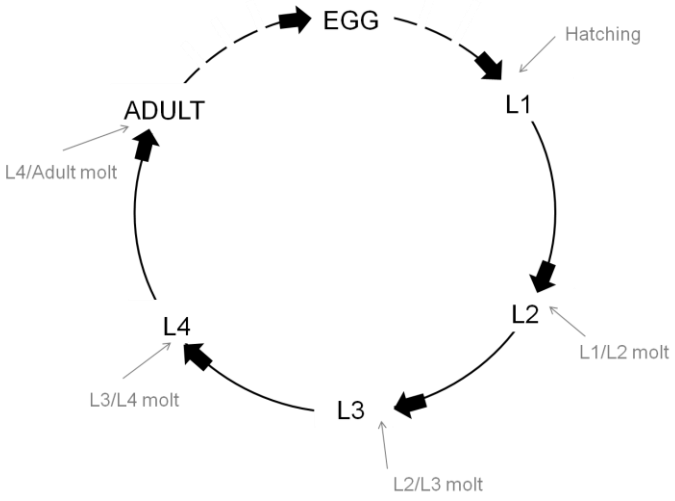

Figure 1-11. *C.elegans* development
C.elegans proceed through four larval stages (L1 to L4) prior to reaching adulthood. The cuticle is synthesised five times during development and is shed four times during this time. Egg-to-egg duration in wild type N2 nematodes grown at 20°C is approximately 3 days.

1.5.2 *C.elegans* cuticle

Cuticular components, including collagen proteins, are synthesised by an underlying hypodermal cell layer surrounding the body of the animal. The cytoplasm of the hypodermal cells are characterised by a relatively smooth appearance during the inter-moult period (Singh & Sulston, 1978). This contrasts with a granular appearance caused by densely packed Golgi bodies preceding each moult. This cyclical appearance of Golgi bodies, as well as intracellular membranes and vesicles, reflects an increase in synthetic activity. The pre-moult increase in intracellular membranes and vesicles is rapidly cleared following each moult. However, the molecular mechanisms underlying this clearance process remains to be investigated.

Newly synthesised cuticular components are secreted via the apical membrane of the hypodermal cells. During the synthetic period, actin filaments are organised circumferentially around the body of the nematode and disperse between each moult (Costa *et al.*, 1997). This actin localisation corresponds with grooves forming on the apical membrane of the hypodermal cells and subsequently forms the annular pattern present on the surface of the outer cuticle layer (Figure 1-12). Cuticular annular furrows are present during all stages of *C.elegans* development. Both the DPY-7 and DPY-10 cuticle collagen proteins localise within or just beneath the annular furrows and are required for their continued persistence (McMahon *et al.*, 2003).

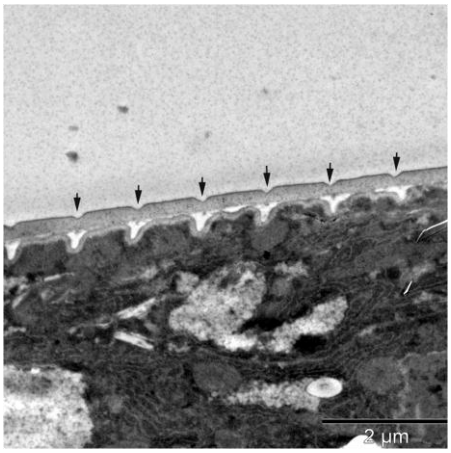

Figure 1-12. Structural organisation of the *C.elegans* cuticle
Transmission electron microscopy image showing the structural organisation of the *C.elegans* cuticle. Invaginations, or furrows, present within the outer layer of the cuticle (indicated by black arrows) are established during the early stages of the cuticular synthetic period. Scale bar represents 2 µm. Figure provided by Dr Iain Johnstone, University of Glasgow.

The cuticle of *C.elegans* is highly resistant to solubilisation (Cox *et al.*, 1981b). The ultrastructure of the cuticle is well preserved following treatment with reducing agents. This reflects the extensive network of covalent cross-links that occur between cuticle proteins, including polymerised cuticle collagens (section 1.5.4). Thus, soluble proteins reflect the intracellular portion.

1.5.3 Temporal expression of cuticle collagen genes

Cuticle collagen genes exhibit distinct temporal patterns of expression repeated during each synthetic period of *C.elegans* post-embryonic development (Johnstone & Barry, 1996). Cuticle collagen genes can be classified into early, intermediate or late expression genes based on the time of peak mRNA (messenger ribonucleic acid) abundance during each synthetic period. The significance underlying the temporal pattern in cuticle collagen gene expression may be related to a limiting mechanism. More specifically, restricting the abundance of collagen gene expression at any point in time may facilitate the specificity required for interchain formation between collagen monomers (section 1.5.4)

The distinct and known temporal patterns of collagen protein expression observed during *C.elegans* development can be employed to decipher the molecular mechanisms involved in the appearance and clearance of collagen proteins. For this project, this approach was employed as an initial investigation to elucidate the role of endosomal trafficking and autophagy in the regulation of *C.elegans* development.

1.5.4 Collagen protein structure

The cuticle is predominantly composed of collagen proteins which have a characteristic Glycine-X-Y tripeptide repeat interrupted by conserved cysteine residues (Cox *et al.*, 1981b; Kramer *et al.*, 1982; Kramer *et al.*, 1990). The length and organisation of each Glycine-X-Y block repeat defines each collagen, which is subsequently divided into collagen subfamilies based on sequence homology [reviewed in (Johnstone, 2000)]. Monomeric cuticle collagens are synthesised as pro-collagens and are subjected to post-translational modification and trimerisation within the ER [reviewed in (Page & Johnstone, 2007)]. Upon secretion, cuticle collagens polymerise and remain intact as the mature cuticle. Monomeric collagen

peptides form a helical secondary structure with each turn composed of three residues [reviewed in (Shoulders & Raines, 2009)]. The glycine residues in the Glycine-X-Y tripeptide repeat typically occupy positions 1, 4, 7, etc. This arrangement results in the glycine residues being stacked along one side of the monomeric peptide. Trimerisation results in glycine residues being arranged within the core of each triple helix. Thus, glycine residues are important structural features of collagens and steric hindrance in this arrangement can lead to defects in the triple helical structure and thereby morphology. For example, the *dpy-7* and *dpy-10* collagen genes are co-ordinately expressed during *C.elegans* post-embryonic development (section 1.5.3) (McMahon 2003). This is consistent with the biochemical properties of their encoded proteins, DPY-7 and DPY-10, as obligate interacting collagen proteins that co-localise within the cuticle annular furrows (section 1.5.2). Glycine substitution mutations in either *dpy-7* or *dpy-10* accumulate not only more soluble protein than their respective wild type counterparts, but also accumulate more of their obligate DPY-10 or DPY-7 wild type partner protein, respectively. The accumulation of DPY-7 in the *dpy-10(sc48)* genetic background may reflect defective trimerisation (McMahon *et al.*, 2003). The portion of DPY-7 present in the cuticle of *dpy-10(sc48)* nematodes appears fragmented and results in aberrant cuticle morphology (i.e. Dpy phenotype). Glycine substitution mutations in a number of other collagen genes also result in Dpy phenotypes (Levy *et al.*, 1993). The role of protein structure and function is further highlighted by the observation that *dpy-7* and *dpy-10* null mutants result in the absence of any detectable DPY-7 and DPY-10, respectively, as well as their corresponding wild type or glycine substitution obligate DPY-10 or DPY-7 partners (personal communication with Dr Iain Johnstone). This suggests that DPY-7 and DPY-10 are components of the same cuticular structure, possibly existing as a heterotrimetric cuticle collagen. Collectively, these observations highlight the contribution of collagen proteins to the formation of the cuticle and thereby nematode morphology.

1.5.5 UNC-51 is the *C.elegans* ortholog of yeast Atg1

The molecular understanding of autophagy is best characterised in yeast (section 1.1). However, functional conservation of yeast Atg proteins in higher eukaryotes have greatly assisted our understanding of autophagy in more complex organisms, including *C.elegans*. UNC-51 is the *C.elegans* ortholog of yeast Atg1, a key

regulator of autophagy (Matsuura *et al.*, 1997). Similar to its yeast ortholog, UNC-51 is implicated in autophagy induction based on the observation that *unc-51* mutants mislocalise the autophagy marker GFP (green fluorescent protein)-LGG1 (orthologue of yeast Atg8/mammalian LC3) (McMahon *et al.*, 2003; Melendez *et al.*, 2003). UNC-51 also contributes additional functions not previously described for yeast Atg1 and likely reflects functional divergence between yeast and *C.elegans*. For instance, mutations in *unc-51* result in reduced body size due to a decrease in cell size (Aladzsity *et al.*, 2007). This implicates a role for UNC-51 in the regulation of normal cell growth. Furthermore, UNC-51 and its binding partner UNC-14 are required for axonal elongation and guidance in *C.elegans* (Hedgecock *et al.*, 1985; Ogura *et al.*, 1994; Ogura & Goshima, 2006). Consistent with this neuronal specific function, mutations in *unc-51* result in an uncoordinated phenotype (Brenner, 1974).

Other autophagy specific genes in *C.elegans* have implicated a role for this process in *C.elegans* pre- and post-embryonic development, survival during starvation and lifespan extension (refer to section 1.1.7) (Melendez *et al.*, 2003; Kang *et al.*, 2007; Zhang *et al.*, 2009).

1.5.6 VPS-45 function in *C.elegans*

Endocytosis plays an important role in the uptake of extracellular molecules, internalisation of plasma membrane resident proteins, protein recycling and lysosome-mediated degradation in eukaryotic cells. The yeast SM protein Vps45 (section 1.3.4) has previously been shown to be required for membrane traffic between the TGN and endosomal system (Cowles *et al.*, 1994; Piper *et al.*, 1994). Increasing evidence supports a role for Vps45 in endocytic transport in multicellular organisms (Nielsen *et al.*, 2000; Gengyo-Ando *et al.*, 2007). More specifically, the *C.elegans* ortholog of yeast Vps45, referred to as VPS-45, has been implicated in receptor-mediated endocytosis required for the uptake of yolk and cholesterol during early embryonic development (Matyash *et al.*, 2001; Gengyo-Ando *et al.*, 2007). Cholesterol is required for the successful completion of moulting, reproductive growth and development in *C.elegans* (Yochem *et al.*, 1999; Matyash *et al.*, 2004). Collectively, these observations implicate a role for VPS-45 and thereby endocytosis in *C.elegans* pre- and post-embryonic development.

1.6 Project aims

Multivalent interactions are becoming an increasingly common feature of the molecular fusion machinery operating at multiple membrane trafficking steps. These interactions are likely to encode the regulation and specificity of intracellular membrane fusion events across multiple pathways, including autophagy. Autophagy is implicated in a number of physiological processes and pathologies (Choi *et al.*, 2013) and as such it is of great scientific importance to decipher the molecular mechanisms involved in this process.

The t-SNARE Tlg2 and the COG tethering complex have previously been shown to regulate autophagy in yeast (Abeliovich *et al.*, 1999; Yen *et al.*, 2010) possibly by assisting in the recruitment and delivery of membrane from the endosomal pathway to the growing autophagosomal precursor at the PAS. Both *tlg2* and *cog* mutant strains display similar phenotypes: mislocalisation of the membrane associated Atg9 protein (Ohashi & Munro, 2010; Yen *et al.*, 2010; Nair *et al.*, 2011), which has been shown to associate with Golgi and endosomal acquired membrane destined for the PAS (Young *et al.*, 2006; Ohashi & Munro, 2010). Direct associations between subunits of the COG complex and SNARE proteins have previously been identified (Suvorova *et al.*, 2002; Laufman *et al.*, 2011; Laufman *et al.*, 2013). However, it remains to be investigated if Tlg2 and its partner SNARE proteins Tlg1, Vti1 and Snc2 associate with subunits of the COG complex. These investigations form the basis of my first project aim: to determine if Tlg2 and its partner SNARE proteins directly associate with subunits of the COG complex.

In order to achieve regulated membrane fusion, it is important to regulate levels of the proteins participating in this event. Vps45 have previously been shown to be required for stabilising Tlg2 cellular levels (section 1.2.5) (Nichols *et al.*, 1998; Bryant & James, 2001). Vps45 deficient cells exhibit reduced levels of its cognate SNARE protein Tlg2. This effect is due to an increase in turnover of Tlg2 and is mediated by both the proteasome and vacuole (Bryant & James, 2001; Struthers, 2009). The latter defines the terminal step of autophagy. Thus, the second aim of my study was to investigate a role for autophagy and associated post-translational modifications in the regulation of Tlg2 steady-state levels.

Vps45 can associate with its cognate syntaxin Tlg2 via modes 1, 2 and 3 binding (section 1.3.2) (Dulubova *et al.*, 2002; Carpp *et al.*, 2006; Furgason *et al.*, 2009). Binding via modes 1 and 3 involves the arch-shaped cavity of Vps45, which is composed of domains 1 and 3a, to bind Tlg2 in the closed conformation or Tlg2-containing SNARE complex, respectively (section 1.2.1). Mutations in residues contained within these domain regions can sterically hinder this association and as a result interfere with SNARE complex formation (section 1.3.1) (Boyd *et al.*, 2008; Hashizume *et al.*, 2009). An association between congenital neutropenia and Vps45 has been made and involve a single amino acid change in human Vps45 at position 224 (Thr224Asn, T224N), which corresponds to domain 3a (Stepensky *et al.*, 2013; Vilboux *et al.*, 2013). The third chapter of my thesis investigates the effects of the analogous mutation in yeast, Vps45 T238N, on Vps45 function.

Moulting in *C.elegans* is accompanied by synthesis and secretion of a new stage-specific cuticle (section 1.5.1) [reviewed in (Page & Johnstone, 2007)]. Cuticle components are synthesised by an underlying hypodermal cell layer (section 1.5.2) (Singh & Sulston, 1978). Cuticle protein synthesis peaks during each moult and is much reduced during the inter-moult period (Cox *et al.*, 1981a; Johnstone & Barry, 1996). This corresponds with the cyclical appearance of Golgi bodies, as well as intracellular membranes and vesicles that have been observed by Nomarksi microscopy during *C.elegans* post-embryonic development (Singh & Sulston, 1978). This observation reflects the increase in synthetic activity which is rapidly cleared following each moult. The aim of my fourth chapter was to investigate a role for endosomal trafficking and autophagy in the clearance of this observed increase in intracellular content during *C.elegans* post-embryonic development.

Chapter 2 – Materials and Methods

2.1 Materials

Unless stated otherwise, all chemicals and reagents used in this study were purchased from BioRad Laboratories Ltd. (Hemel Hempstead, UK), Clontech Laboratories Inc. (California, USA), Fisher Scientific Ltd. (Loughborough, UK), GE Healthcare (Chalfont St Giles, UK), Invitrogen Ltd. (Paisley, UK), Qiagen Ltd. (Crawley, UK), Sigma-Aldrich Ltd. (Poole, UK) and VWR Prolabo (Lutterworth, UK).

Enzymes and reagents used for molecular biology were purchased from New England Biolabs Ltd. (Hitchin, UK), Promega Ltd. (Southampton, UK), Roche Diagnostics Ltd. (Burgess Hill, UK), Stratagene/Agilent Technologies Ltd. (Stockport, UK) and Yorkshire Bioscience Ltd. (York, UK).

Bacterial [*Escherichia coli* (*E.coli*)], yeast [*S.cerevisiae*] and nematode [*C.elegans*] growth media components were purchased from ForMedium™ (Norfolk, UK) and Melford Laboratories Ltd. (Suffolk, UK). Antibiotics used in this study are listed in Table 2-1 and were purchased from Sigma-Aldrich Ltd. (Poole, UK). All antibiotics were prepared as stock solutions and stored at -20°C.

Table 2-1 Antibiotics used in this study

Antibiotic	[Stock]	[Final]	Source
Ampicillin sodium salt	100 mg/ml in dH_2O	100 µg/ml	Sigma-Aldrich Ltd.
Kanamycin disulfate salt	100 mg/ml in dH_2O	100 or 25 µg/ml	Sigma-Aldrich Ltd.
Streptomycin sulfate salt	12.5 mg/ml in dH_2O	12.5 µg/ml	Sigma-Aldrich Ltd.
G418 disulfide salt	200 mg/ml in dH_2O	100 µg/ml	Sigma-Aldrich Ltd.

2.1.1 Antibodies

Primary and secondary antibodies used in this study are listed in Table 2-2. Polyclonal antibodies against Tlg2, Tlg1, Snc2 and Vps45 that were generated by Eurogentec (Southampton, UK) were raised in rabbits immunised with peptides consisting of the indicated amino acid residues (Table 2-2).

Table 2-2 Antibodies used in this study

Antibody	Description	Dilution	Reference/Source
Primary[a]			
anti-HA	Mouse monoclonal antibody against residues 98-106 (YPYDVPDYA) of the human influenza virus haemagglutinin	1:1000	Cambridge Bioscience Ltd.
anti-cMyc	Mouse monoclonal antibody against residues 408-439 (EQKLISEEDL) of the human $p62^{c\text{-}Myc}$ protein	1:1000	Sigma-Aldrich Ltd.
anti-Vps45	Affinity purified rabbit polyclonal antisera against residues 563-577 (ILSTKEYMDSIRSAK) of the *S.cerevisiae* Vps45 protein	1:100	Eurogentec
anti-Tlg2	IgG purified from rabbit polyclonal antisera against residues 272-287 (QDLVVDQGTIVDRIDY) and 387-396 (ESENDALDDLL) of the *S.cerevisiae* Tlg2 protein	1:100	Eurogentec
anti-Tlg1	Rabbit polyclonal antisera against *S.cerevisiae* Tlg1 protein	1:500	Eurogentec
anti- Snc2	Rabbit polyclonal antisera against residues 72-86 (GFKRGANRVRKQMWW) of the *S.cerevisiae* Snc2 protein	1:500	Eurogentec
anti-Vti1	Rabbit polyclonal antisera against residues 1-105 (MSSLLISYESDFKTTLEQAKASLAEA PSQPLSQRNTTLKHVEQQQDELFDLLDQM DVEVNNSIGDASERATYKAKLREWKKTIQS DIKRPLQSLVDSGDRDRLFG) of the *S.cerevisiae* Vti1 protein	1:500	(Coe *et al.*, 1999)
anti-CPY[b]	Mouse monoclonal antibody (clone 10A5B5)	1:1000	Invitrogen Ltd.
anti-Pgk1	Rabbit polyclonal antisera against the *S.cerevisiae* Pgk1 protein	1:1000	(Piper *et al.*, 1994)
anti-DPY-7	Mouse monoclonal antibody	1:100	(McMahon *et al.*, 2003)
anti-β-actin	Mouse monoclonal antibody (clone AC-15)	1:1000	Sigma-Aldrich Ltd.

Secondary[c]			
anti-mouse	HRP conjugated whole IgG from sheep	1:2000	GE Healthcare
anti-rabbit	HRP conjugated whole IgG from donkey	1:5000	GE Healthcare
Alexa Fluor® 488 anti-rabbit	Fluorophore conjugated whole IgG from goat	1:200	Invitrogen Ltd.

[a] Primary antibodies diluted in 1% (w/v) non-fat dried milk in PBS-T

[b] Primary antibody diluted in 1.5% (w/v) non-fat dried milk in TBS-T

[b] Secondary antibodies were diluted in 5% (w/v) non-fat dried milk in PBS-T or TBS-T

2.1.2 Bacterial, yeast and nematode strains

Bacterial (*E.coli*), yeast (*S.cerevisiae*) and nematode (*C.elegans*) strains used in this study are listed in Table 2-3, Table 2-4 and Table 2-5, respectively. Plasmids were propagated in either One Shot® TOP10 or XL1-Blue *E.coli*. BL21 Star™ (DE3) *E.coli* was routinely used for the production of recombinant fusion proteins. *C.elegans* Bristol strain N2 was used as the wild-type strain. All *C.elegans* mutant strains used in this study were derived from the N2 wild-type background.

Table 2-3 *E.coli* strains used in this study

Strain	Genotype	Source
BL21 Star™ (DE3)	F^- *ompT hsdS*$_B$ (*r*$_B^-$*m*$_B^-$) *gal dcm rne 131* (DE3)	Invitrogen Ltd.
One Shot® TOP10	F^- *mcr*A Δ(*mrr-hsd*RMS-*mcr*BC) φ80*lac*ZΔM15 Δ*lac*X74 *rec*A1 *ara*D139 Δ(*ara-leu*)7697 *gal*U *gal*K *rps*L (StrR) *end*A1 *nup*G	Invitrogen Ltd.
XL1-Blue	*recA1 endA1 gyrA96 thi-1 hsdR17 supE44 relA1 lac* [F´ *proAB lacI*^{q}*ZΔM15* Tn*10* (Tet^r)]	Stratagene
OP50-1	uncharacterised	CGC[a]

[a] Caenorhabditis Genetics Centre

Table 2-4 *S.cerevisiae* strains used in this study

Stock ID	Strain	Genotype	Reference/Source
75	AH109	*MATa trp1-901 leu2-3 112 ura3-52 his3-200 gal4Δ gal80Δ LYS2::GAL1$_{UAS}$-GAL1$_{TATA}$-HIS3 GAL2$_{UAS}$-GAL2$_{TATA}$-ADE-2 URA3::MEL1$_{UAS}$-MEL1$_{TATA}$-lacZ*	Clontech Laboratories
10	SEY6210	*MATα leu2-3, 112 ura3-52 his3-Δ200 trpI-Δ901 lys2-801 suc2-Δ9 GAL*	(Robinson *et al.*, 1988)
91	MSY001	SEY6210 *tlg2*Δ::KAN	(Struthers, 2009)
42	LCY007	SEY6210 vps45Δ::KAN	Constructed by Dr L Carpp
94	RMY8	SEY6210 *pep4-3*	(Shanks *et al.*, 2012)
95	MSY002	SEY6210 *pep4-3 vps45*Δ	(Shanks *et al.*, 2012)
116	WLY206[a]	SEY6210 *KAN::pGAL1-3HA-COG1*	(Yen *et al.*, 2010)
117	WLY207[a]	SEY6210 *KAN::pGAL1-3HA-COG3*	(Yen *et al.*, 2010)
118	WLY208[a]	SEY6210 *KAN::pGAL1-3HA-COG4*	(Yen *et al.*, 2010)
119	WLY209[a]	SEY6210 *KAN::pGAL1-3HA-COG2*	(Yen *et al.*, 2010)
122	WLY218[a]	SEY6210 *KAN::pGAL1-3HA-COG6*	(Yen *et al.*, 2010)
2	RPY10	*MATα ura3-52 leu2-3 112 his4-519 ade6 gal2*	(Piper *et al.*, 1994)
6	NOzY2	RPY10 *vps45*Δ::KAN	(Bryant & James, 2001)
124	YMC001	RPY10 *cog1*Δ::*KAN*	This study
131	YMC002	RPY10 *atg1*Δ::*KAN*	This study
4	NOzY4	RPY10 *tlg2*Δ::KAN	(Bryant & James, 2001)
1	SF838-9D	RPY10 *pep4-3*	(Rothman & Stevens, 1986)
56	RMY3	RPY10 *pep4-3 end3*Δ	Constructed by Dr R McCann
30	LCY004b	RPY10 *vps21*Δ::KAN	Constructed by Dr L Carpp
96	AACY5	RPY10 *vps27*Δ::LEU	(Piper *et al.*, 1995)
132	BY4742[b]	*MATα his3Δ1 leu2Δ0 ura3Δ0 lys2Δ0*	ResGen
141	*vps45*Δ[b]	BY4742 *vps45*Δ*::KAN*	ResGen
107	*cog1*Δ[a]	BY4742 *cog1*Δ::*KAN*	ResGen
108	*cog6*Δ[a]	BY4742 *cog6*Δ::*KAN*	ResGen
111	*atg1*Δ[a]	BY4742 *atg1Δ*::*KAN*	ResGen
143	YMC006	BY4742 *vps45*Δ::KAN *atg1*Δ::NAT1	This study
140	*swf1*Δ[b]	BY4742 *swf1*Δ::KAN	ResGen

[a] Gift from Dr D Klionsky, University of Michigan, USA

[b] Gift from Dr J Gray, University of Glasgow, UK

Table 2-5 *C.elegans* strains used in this study

Strain	Genotype	Phenotype	Reference/Source
N2	Wild type	Wild-type	(Brenner, 1974), CGC
IA757	*vps-45 (tm246)*	Moulting defect, *ts* larval lethality	(Gengyo-Ando *et al.*, 2007)
IA337	*dpy-10 (sc48)*	Dumpy, left roller	Dr C. Clucas
CB128	*dpy-10 (e128)*	Dumpy, non–roller	(Brenner, 1974)
IA823	*vps-45 (tm246); dpy-10 (e128)*	Dumpy	This study
IA779	*vps- 45 (tm246); dpy-10 (sc48)*	Mild dumpy	This study
CB369	*unc-51 (e369)*	Mostly paralyzed, egg-laying defective and dumpy	(Brenner, 1974), CGC
IA835	*dpy-10(sc48); unc-51(e369)*	Severely paralysed, egg-laying defective, dumpy	This study
IA836	*dpy-10(e128); unc-51(e369)*	Severely paralysed, egg-laying defective, dumpy	This study

2.1.3 Growth media

With the exception of OP50-1 (refer to section 2.13.2) bacterial cells were routinely grown in liquid 2YT media [1.6% (w/v) tryptone, 1% (w/v) yeast extract, 0.5% (w/v) NaCl] containing the appropriate antibiotic if required. Solid media was prepared by the addition of 2% (w/v) agar prior to autoclaving. For the purpose of recombinant fusion protein production (section 2.11), transformed BL21 Star™ (DE3) cells were grown in Terrific Broth (TB) [1.2% (w/v) tryptone, 2.4% (w/v) yeast extract, 0.4% (v/v) glycerol, 17 mM KH_2PO_4, 72 mM K_2HPO_4] containing the appropriate antibiotic (refer to Table 2-1).

Yeast cells were grown non-selectively in YPD [1% (w/v) yeast extract, 2% (w/v) peptone, 2% (w/v) glucose] or YPG Raff [1% (w/v) yeast extract, 2% (w/v) peptone, 2% (w/v) galactose, 2% (w/v) raffinose] media, or selectively on minimal synthetic defined (SD) media [0.675% (w/v) yeast nitrogen base without amino acids, 2% (w/v) glucose] lacking the appropriate amino acids. As before, solid media was prepared by the addition of 2% (w/v) agar prior to autoclaving. Bacterial

and yeast agar plates were poured in a sterile environment and routinely stored at 4°C.

C.elegans strains were cultured on Nematode Growth Medium (NGM) agar seeded with *E.coli* strain OP50-1 as a food source as described (Brenner, 1974). NGM agar was prepared by autoclaving 3% (w/v) NaCl, 2.5% (w/v) peptone, 1.7% (w/v) agar and 5 µg/ml cholesterol in 390 ml H_2O. The agar was allowed to cool to approximately 55°C prior to aseptically adding both $CaCl_2$ and $MgSO_4$ to a final concentration of 1 mM and potassium phosphate buffer (KPO_4, pH 6.0) to a final concentration of 25 mM. Agar plates were poured in a sterile environment and allowed to solidify. NGM agar was seeded with 0.1 ml OP50-1 liquid culture (refer to section 2.13.2) and incubated overnight at 37°C to allow growth. NGM agar plates seeded with OP50-1 were stored at room temperature for up to 2 weeks.

2.2 Molecular Biology

2.2.1 Purification of plasmid DNA from *E.coli*

Plasmids used in this study are listed in Table 2-6. Plasmid deoxyribonucleic acid (DNA) that was used as a template for polymerase chain reaction (PCR) (refer to section 2.2.4) or bacterial and yeast cell transformations (described in sections 2.11.2 and 2.5.3, respectively) was purified using the microcentrifugation protocol provided with the Promega Wizard® Plus SV Miniprep kit. This protocol is based on a modified alkaline lysis procedure initially described by Birnboim and colleague (Birnboim & Doly, 1979). 10 ml 2YT containing appropriate antibiotic was inoculated with the desired *E.coli* strain and incubated overnight in a 37°C shaking incubator. Cells from 1 ml of the overnight bacterial culture were harvested in a 1.5 ml eppendorf tube by centrifugation for 5 minutes at 3000 *g*. All subsequent steps were performed as outlined in the manufacturer's instruction manual. Purified plasmid DNA was routinely stored at -20°C.

Table 2-6 List of plasmids used in this study

Stock	Plasmid[a]	Description	Source
365	pGBKT7-53	Yeast expression plasmid (2μ, TRP1) encoding GAL4 BD-cMyc -murine p53	Clontech
368	pTD1-1	Yeast expression plasmid (2μ, LEU2) encoding GAL4 AD-HA-SV40 large T-antigen	Clontech
607	pGBDU-Cog1	Yeast expression plasmid (2μ, URA3) encoding GAL4 BD-Cog1	(Yen *et al.*, 2010)
608	pGBDU-Cog2	Yeast expression plasmid (2μ, URA3) encoding GAL4 BD-Cog2	(Yen *et al.*, 2010)
609	pGBDU-Cog3	Yeast expression plasmid (2μ, URA3) encoding GAL4 BD-Cog3	(Yen *et al.*, 2010)
610	pGBDU-Cog4	Yeast expression plasmid (2μ, URA3) encoding GAL4 BD-Cog4	(Yen *et al.*, 2010)
615	pGBDU-53	Yeast expression plasmid (2μ, URA3) encoding GAL4 BD-p53	This study
611	pGAD-Cog1	Yeast expression plasmid (2μ, LEU2) encoding GAL4 AD-Cog1	(Yen *et al.*, 2010)
612	pGAD-Cog2	Yeast expression plasmid (2μ, LEU2) encoding GAL4 AD-Cog2	(Yen *et al.*, 2010)
613	pGAD-Cog3	Yeast expression plasmid (2μ, LEU2) encoding GAL4 AD-Cog3	(Yen *et al.*, 2010)
614	pGAD-Cog4	Yeast expression plasmid (2μ, LEU2) encoding GAL4 AD-Cog4	(Yen *et al.*, 2010)
562	pCMD041	Yeast expression plasmid (2μ, TRP1) encoding GAL4 BD-cMyc-Tlg2, residues 1-309	(MacDonald, 2009)
563	pCMD042	Yeast expression plasmid (2μ, TRP1) encoding GAL4 BD-cMyc-Tlg2, residues 37-309	(MacDonald, 2009)
564	pCMD043	Yeast expression plasmid (2μ, TRP1) encoding GAL4 BD-cMyc-Tlg2, residues 231-309	(MacDonald, 2009)
575	pCMD054	Yeast expression plasmid (2μ, LEU2) encoding GAL4 AD-HA-Tlg2, residues 1-309	(MacDonald, 2009)
576	pCMD055	Yeast expression plasmid (2μ, LEU2) encoding GAL4 AD-HA-Tlg2, residues 37-309	(MacDonald, 2009)
577	pCMD056	Yeast expression plasmid (2μ, LEU2) encoding GAL4 AD-HA-Tlg2, residues 231-309	(MacDonald, 2009)
478	pETDuet-1 GST	*E.coli* expression vector encoding GST	Constructed by Dr F Brandie

467	pCMD007	*E.coli* expression vector encoding a C-terminal GST-tagged version of the cytosolic domain of Tlg2, residues 221-309	(Struthers *et al.*, 2009)
480	pCMD008	*E.coli* expression vector encoding a C-terminal GST-tagged version of the cytosolic domain of Tlg2, residues 1-309	(Struthers *et al.*, 2009)
546	pCMD032	*E.coli* expression vector encoding a C-terminal GST-tagged version of the cytosolic domain of Tlg2, residues 37-309	(MacDonald, 2009)
112	pCOG022	*E.coli* expression vector encoding two tandem repeats of the IgG binding domains of *S.aureus* PrA	(Carpp *et al.*, 2006)
87	pCOG025	*E.coli* expression vector encoding a C-terminal PrA-tagged version of the cytosolic domain of Tlg2, residues 1-318	(Carpp *et al.*, 2006)
89	pCOG026	*E.coli* expression vector encoding a C-terminal PrA-tagged version of the cytosolic domain of Tlg2, residues 37-309	(Carpp *et al.*, 2006)
90	pCOG027	*E.coli* expression vector encoding a C-terminal PrA-tagged version of the cytosolic domain of Tlg2, residues 231-309	Constructed by Dr L Carpp
201	pCOG045	*E.coli* expression vector encoding a C-terminal PrA-tagged version of the cytosolic domain of Snc2, residues 1-88	(Carpp *et al.*, 2006)
209	pCOG048	*E.coli* expression vector encoding a C-terminal PrA-tagged version of the cytosolic domain of Vti1, residues 1-187	(Carpp *et al.*, 2006)
242	GST-Tlg1	E.coli expression vector encoding a N-terminal GST-tagged version of Tlg1, residues 1-224	(Coe *et al.*, 1999)
NA	pETDuet-Sx4 GST	E.coli expression vector encoding a C-terminal GST-tagged version of the cytosolic portion of Syntaxin 4, residues 1-273	(Aran *et al.*, 2009)
50	pHA-TLG2	Yeast expression plasmid (2µ URA) encoding a N-terminal HA-tagged version of Tlg2	(Seron *et al.*, 1998)
349	pYORC-YCO18C	*TLG2* kanMX4 drug resistant disruption cassette cloned in the *Eco*RV site of pUG7	(Seron *et al.*, 1998)
13	pNB701	Yeast expression plasmid (*CEN*, *URA3*) encoding Pho8 from the *CUP1* promoter	(Struthers *et al.*, 2009)
354	pMAZ006	Yeast expression plasmid (*CEN*, *URA3*) encoding a C-terminal HA-tagged version of yeast Tlg2 from the *CUP1* promoter	(Struthers *et al.*, 2009)

135	pCOG070	Yeast expression plasmid (*2µ*, *URA3*) encoding a C-terminal HA-tagged version of yeast full-length Vps45 from the *VPS45* promoter	(Carpp *et al.*, 2006)
636	pMC007	As pCOG070 encoding HA-Vps45T238N	This study, (Stepensky *et al.*, 2013)
135	YEp352	Yeast expression plasmid (*2µ*, *URA3*), parent of pCOG070	(Hill *et al.*, 1986)
280	pNB706	Yeast expression plasmid (*CEN*, *LEU2*) encoding a C-terminal HA-tagged version of yeast full-length Vps45	(Carpp *et al.*, 2006)
637	pMC004	As pNB706 encoding HA-Vps45T238N	This study
433	pRS415	Yeast expression plasmid (*CEN*, *LEU2*), parent of pNB706	Stratagene

[a] Unless stated otherwise, plasmid bacterial selection used was Amp

2.2.2 Agarose gel electrophoresis

DNA samples were analysed by agarose gel electrophoresis. Agarose powder [0.5-2% (w/v]) was dissolved in TAE buffer (40 mM Tris-acetate, 1 mM EDTA, pH 8.0) by heating in a microwave. The gel solution was allowed to cool to approximately 55°C prior to the addition of ethidium bromide to a final concentration of 0.5 µg/ml. The gel was cast into an ultraviolet (UV)-transparent plastic tray positioned directly on top of the BioRad Sub-Cell® GT agarose gel electrophoresis unit stage. An 8- or 15-well comb was positioned near the cathode and the gel was left to solidify (approximately 30 minutes). The gel was submerged in TAE buffer and the DNA samples were prepared by adding 6X DNA loading dye [0.25% (w/v) bromophenol blue, 0.25% (w/v) xylene cyanol FF, 30% (v/v) glycerol]. Loading dye was omitted for all PCR reactions (refer to section 2.2.4) containing 5X Green GoTaq® reaction buffer. The DNA samples were loaded into the wells contained within the gel and a constant electric potential of 90 volts (V) was applied for 20-40 minutes. 5 µl of either a 100 base pair (bp) or 1 kilobase pair (kb) DNA marker was routinely included as a DNA standard. Resolved DNA samples were visualised with an UV transilluminator (Ultra-Violet Products Inc., Cambridge, UK) and digital images were acquired using a ChemiDoc™ XRS+ system equipped with BioRad Quantity One® 4.6.5 1-D analysis software.

2.2.3 Gel extraction and purification of DNA

DNA fragments that were resolved by agarose gel electrophoresis (described in section 2.2.2) that were to be used for subsequent procedures were excised from the gel with a clean scalpel and transferred to a 1.5 ml eppendorf tube. DNA was then extracted and purified from the agarose gel matrix using the QIAGEN QIAquick gel extraction kit as outlined in the manufacturer's instruction manual. This kit employs a simple bind-wash-elute procedure that recovers up to 95% of a sample containing up to 10 µg of DNA. Purified DNA was routinely stored at -20°C.

2.2.4 Polymerase Chain Reaction

Oligonucleotide primer pairs were designed to amplify desired DNA sequences by PCR. All primers used in this study are listed in Table 2-7. Primers were synthesised by Yorkshire Bioscience Ltd. and were routinely diluted to 50 picomoles (pmol) in dH_2O prior to storage at -20°C. The PCR reaction mix was typically made up to a total volume of 50 µl in a 0.2 ml thin-walled PCR tube. Either GoTaq® Flexi or *Pfu* DNA polymerase combined with their respective buffers were used. All PCR products were analysed by agarose gel electrophoresis (described in section 2.2.2). An example of a standard PCR mix used in this study is shown in Table 2-8. Standard PCR conditions were employed as outlined in Table 2-9.

Table 2-7 Oligonucleotides used in this study

Oligo	Identity	Sequence
572	COG1 5’	5’ CTAAAAAAAACCAATACGATAGAAA 3’
573	COG1 3’	5’ GTACCCTCCCTCGTGCTATTATA 3’
574	COG1 *KAN* 5’	5’ ATTCGTACAACAAATCTTGTGGTAGAAAACCTAAAAAAAAC CAATACGATAGAAA*CGGATCCCCGGGTTAATTAA* 3’
575	COG1 *KAN* 3’	5’ ATTATCATTATCAATAAGTTTGCGAGGCGGGTACCCTCCCT CGTGCTATTATA*GAATTCGAGCTCGTTTAAAC* 3’
576	ATG1 5’	5’ CAAATCTCTTTTACAACACCAGA 3’
577	ATG1 3’	5’ TAAGAAAACCATATTATGCATCAC 3’
578	ATG1 *KAN* 5’	5’ GAAGCTACCCCATATTTTCAAATCTCTTTTACAACACCAGA *CGGATCCCCGGGTTAATTAA* 3’
579	ATG1 *KAN* 3’	5’ AAAATATAGCAGGTCATTTGTACTTAATAAGAAAACCATAT TATGCATCAC*GAATTCGAGCTCGTTTAAAC* 3’
586	VPS-45 TM246 sense2	5’ ATAGGGACAGAAGGACACGC 3’
587	VPS-45 TM246 anti2	5’ AAGCTGCGAACACTCTCTA 3’
588	VPS-45 WT sense	5’ GAGCCAAGATTCAGCCAGT 3’
620	VPS45 T238N For	5' CTGATCCTATAAATCCTTTACTTCAACCTTGGACC 3'
621	VPS45 T238N Rev	5' GGTCCAAGGTTGAAGTAAAGGATTTATAGGATCAG 3'

Table 2-8 Standard PCR reaction mix

Component	Volume (µl)
5X Buffer	10
$MgCl_2$ (25 mM)[a]	2
dNTPs (10 mM)[b]	2
Forward primer (5 pmol)[c]	1
Reverse primer (5 pmol)[d]	1
dH_2O	33
GoTaq® Flexi DNA polymerase	0.25
DNA template (50-100 ng)	1
Total	~50

[a] $MgCl_2$ was excluded for all PCR reactions where *Pfu* DNA polymerase 10X Buffer was used.

[b] dNTP mix contained 10 mM of each of dATP, dCTP, dGTP and dTTP.

[c] Two different forward primers were included in the PCR reaction mix for genotyping *C.elegans*.

[d] The volume of reverse primer used was doubled in all *C.elegans* genotyping reactions.

Table 2-9 Standard PCR conditions

Step	Temperature	Time	Number of cycles
1. Initial denaturation	94°C	2 minutes	1
2. Denaturation	94°C	30 seconds	
3. Anneal	44°C-55°C[a]	30 seconds	Repeat steps 2-4 for 30-35 cycles
4. Extension	72°C	2 minutes[b]	
5. Final extension	72°C	5 minutes	1
6. Hold	6°C	Indefinite	

[a] Annealing temperatures varied based on primer length.

[b] The size of amplified DNA determined extension time. This was calculated as 1 minute per kb (using Go*Taq* polymerase).

2.2.5 Site-directed mutagenesis

Site-directed mutagenesis (SDM) was performed using a PCR-based approach with double-stranded plasmid DNA templates isolated from *E.coli* (section 2.2.1). Two complimentary oligonucleotide primers were used in each reaction. The primers were designed to incorporate the desired mismatched base(s) in the centre but were otherwise complementary to the target DNA. The PCR mix was prepared as outlined in Table 2-8 using the high fidelity polymerase *Pfu*. The PCR conditions employed are outlined in Table 2-10. Following amplification the PCR mix was treated with 1 µl of the restriction endonuclease *DpnI* for 1 hour at 37°C to selectively digest methylated template DNA isolated from *E.coli* (Lacks & Greenberg, 1975). DNA synthesised *in vitro* by PCR is unmethylated and therefore resistant to cleavage by *DpnI*. The *DpnI*-resistant molecules were subsequently recovered by transforming XL1- Blue *E.coli* to antibiotic resistance as outlined under section 2.11.2. Plasmid DNA was isolated from candidate antibiotic resistant colonies (section 2.2.1). Plasmid DNA concentration was determined using a NanoDrop 2000 micro-volume spectrophotometer set at an absorbance reading of 280 nm. Sequencing of plasmid DNA [600 nanogram (ng) per sample] was carried out by the University of Dundee sequencing service to confirm successful SDM.

Table 2-10 SDM PCR conditions

Step	Temperature	Time	Number of cycles
1. Initial denaturation	95°C	1 minute	1
2. Denaturation	95°C	1 minute	
3. Anneal	55°C	1 minute	Repeat steps 2-4 for 16 cycles
4. Extension	68°C	17 minutes[a]	
5. Denaturation	94°C	1 minute	1
6. Anneal	55°C	1 minute	1
7. Final extension	72°C	10 minutes	1
7. Hold	6°C	Indefinite	

[a] The size of the amplified DNA determined extension time. This was calculated as 2 minute per kb (using *Pfu* polymarase)

2.2.6 Restriction endonuclease digestion of DNA

Plasmid DNA was digested using either a single restriction endonuclease or two simultaneously. The latter was only performed where both enzymes exhibited maximum activity in the same buffer. Sequential digestions were performed in the case where two different buffers were required for maximum enzyme activity. DNA from the first digest was recovered by gel extraction (described in section 2.2.3). Agarose gel electrophoresis (described in section 2.2.2) was employed to analyse recovered DNA prior to use in subsequent reactions. Digestion reactions were prepared in 1.5 ml eppendorf tubes and in a total volume of 50 µl. These were routinely incubated for 2-4 hours at 37°C. Linearised DNA fragments were analysed by agarose gel electrophoresis (refer to section 2.2.2). An example of all the components included in a standard single restriction endonuclease digest is shown in Table 2-11.

Table 2-11 Standard restriction enzyme digest

Component	Volume (µl)
Plasmid DNA (1 µg/µl)	10
10X Buffer	5
Restriction enzyme	1.5
10X Bovine serum albumin (BSA)	5
dH_2O	28.5
Total	50

2.2.7 Ligation of DNA

DNA fragments that were either amplified using PCR (described in section 2.2.4) or excised from existing vectors by restriction endonuclease digestion (described in section 2.2.6) were ligated into plasmids that had also been digested with the appropriate restriction endonuclease(s) to produce compatible ends for ligation. Linearised plasmid and insert DNA was resolved by agarose gel electrophoresis (refer to section 2.2.2) following digestion, excised and isolated by gel extraction (described in section 2.2.3). Purified insert and plasmid DNA were subsequently used at a 3:1 molar ratio for ligation reactions as outlined in Table 2-12. Negative controls containing either DNA insert or plasmid DNA alone, or no DNA were routinely included. Ligation reactions were carried out for at least 2 hours or up to overnight at room temperature prior to transformation into XL1-Blue competent bacterial cells (described in section 2.11.2). Transformations were selected on solid 2YT media containing the appropriate antibiotic. Plasmid DNA was subsequently purified from resultant colonies (described in section 2.2.1) and analysed by either restriction endonuclease digestion (section 2.2.6) or PCR (section 2.2.4). The resulting products were resolved alongside appropriate controls by agarose gel electrophoresis (described in section 2.2.2).

Table 2-12 DNA ligation reaction

Component	Volume (µl)
DNA insert (~0.5 µg/µl)	6
Plasmid DNA (~0.5 µg/µl)	2
10X T4 DNA ligase buffer	1
T4 DNA ligase	1
Total	10

2.3 Protein analysis

2.3.1 SDS-polyacrylamide gel electrophoresis

Proteins were resolved according to their electrophoretic mobility using discontinuous sodium dodecyl sulphate polyacrylamide gel electrophoresis (SDS-PAGE) as described previously (Laemmli, 1970). Gels were prepared in a vertical mould with a thickness of 0.75, 1.0 or 1.5 cm and were composed of a lower resolving region [7.5%-15% (v/v) acrylamide, 750 mM Tris-HCl (pH 8.8), 0.2% (w/v) SDS] and an upper stacking region [5% (v/v) acrylamide, 250 mM Tris-HCl (pH 6.8), 0.2% (w/v) SDS]. Polymerisation was catalysed by the addition of ammonium persulfate (APS) and tetramethylenediamine (TEMED) to a final concentration of 8 mM and 200 nM, respectively. The gels were transferred to a BioRad mini-PROTEAN® 3 electrophoresis unit and submerged in running buffer [25 mM Tris base, 190 mM glycine, 0.1% (w/v) SDS]. Samples containing the proteins to be analysed were loaded into wells contained within the stacking region and a constant electric potential of 150-180 V was applied for the duration of the gel run. BioRad all blue precision plus protein standard was routinely included in the analysis. Resolved proteins contained within the gel were subjected to either Coomassie™ blue staining (described in section 2.3.2) or immunoblot analysis (described in sections 2.3.3 and 2.3.4).

2.3.2 Coomassie™ blue staining

Proteins resolved using SDS-PAGE (described in section 2.3.1) were visualised by submerging the gel in Coomassie™ blue staining solution [0.25% (w/v) Brilliant Blue R-250, 40% (v/v) methanol, 10% (v/v) acetic acid] for 1 hour on a shaking platform. The resolved proteins were subsequently visualised by de-staining the gel under constant motion in a solution of 15% (v/v) methanol, 15% (v/v) acetic acid.

2.3.3 Western blot transfer

Resolved proteins (refer to section 2.3.1) were made accessible to antibody detection by transferring and immobilising protein bands contained within the acrylamide gel onto Protran nitrocellulose membranes (0.45 µm pore size) (Whatman, Kent, UK). The protein gel and membrane was sandwiched between three layers of Whatman 3 mm filter paper pre-soaked in semi-dry transfer buffer [50 mM Tris base, 40 mM glycine, 0.1% (w/v) SDS, 10% (v/v) methanol]. The sandwich was compiled on top of the anode of a BioRad Trans-Blot® SD semi-dry electrophoretic transfer cell. Air bubbles were carefully removed by gently rolling a pipette over the completed sandwich. The cathode was carefully positioned in place and a constant current of 180 milliamperes (mA) was applied for 40 minutes for one transfer but no more than 80 minutes for up to four transfers. The transfer efficiency was visualised by staining the nitrocellulose membrane with Ponceau S solution [0.1% (w/v) Ponceau S, 5% (v/v) acetic acid] followed by rinsing in dH_2O.

2.3.4 Immunological detection of proteins

Nitrocellulose membranes were blocked in 5% non-fat dried milk (w/v) in PBS-T [140 mM NaCl, 3 mM KCl, 1.5 mM KH_2PO_4, 8 mM Na_2HPO_4, 0.1% (v/v) Tween-20] for at least 20 minutes to prevent non-specific antibody binding to the membrane in subsequent steps. Membranes were rinsed in PBS-T prior to incubating with primary antibody (listed in Table 2-2) diluted in 1% (w/v) non-fat dried milk in PBS-T for 2 hours at room temperature or overnight at 4°C. Primary antibody solutions were poured off and non-specifically bound primary antibody was washed off with PBS-T six times, with each washing interval lasting 5 minutes. The appropriate secondary antibody conjugated to horseradish peroxidase (HRP) (listed in Table 2-2) was diluted in 5% (w/v) non-fat dried milk in PBS-T and incubated with gentle mixing for 1 hour at room temperature. Excess secondary antibody was washed from the membrane as before and proteins were visualised using enhanced chemiluminescence (ECL). Membranes were exposed on Kodak general purpose blue medical X–ray film (Kodak, USA) and developed using a Kodak X–OMAT 2000 processor (Kodak, USA).

2.4 IgG affinity purification

Staphylococcal protein A (PrA) binds differentially to the fragment crystallisable (Fc) region of mammalian immunoglobulin G (IgG) (Langone, 1982). This property was utilised to enrich IgG from crude rabbit antiserum. 2 ml of 50% PrA-agarose was washed three times with 10 ml of PBS and transferred to a 1.5 ml eppendorf tube. Equal volumes of PBS and antiserum were prepared to a total volume of 1 ml and filtered directly into the agarose through a 0.2 µm filter. IgG contained within the antiserum was allowed to bind to the PrA-agarose slurry for 1 hour at 4°C under constant rotation. Bound IgG was eluted from the immobilised PrA using a low pH elution buffer (50 mM glycine-HCl, pH 2.5). The elution step was repeated six times and was performed as follows. For every elution, 1 ml of elution buffer was added to the agarose mix and the content of the tube was inverted several times to ensure thorough mixing. The tube was then kept on ice to allow the beads to settle. The supernatant (eluate) was carefully removed without disturbing the beads and transferred into a fresh 1.5 ml eppendorf tube. 1 M Tris-HCl (pH 10.0) was added to $1/10^{th}$ the total volume of the eluate to neutralise the buffer. The protein concentrations of the six elution fractions were obtained by measuring their absorbance at 280 nm. The fractions with the highest protein concentrations were pooled and subsequently dialysed overnight at 4°C in a 8-10 kDa molecular weight cut off Float-A-Lyzer® G2 dialysis device (Spectrum Laboratories, Inc., USA) against 5 litres of PBS. The dialysed sample was aliquoted the following day and stored at -80°C.

2.5 General yeast methods

2.5.1 Cryopreservation and maintenance of yeast cell stock

Yeast strains were prepared for long-term storage as follows. 5 ml of YPD or the appropriate selective SD media was inoculated with a single colony of the desired yeast strain and incubated overnight in a 30°C shaking incubator. The next day 1.5 ml of the overnight culture was transferred into a 2 ml cryovial and 8% (v/v) DMSO (dimethyl sulfoxide) was added. The content of the vial was thoroughly mixed, the vial labelled and stored at -80°C. Yeast strains were recovered by streaking a small amount of the frozen stock out onto YPD or selective agar plates. The plates were sealed with Parafilm (Pechiney Plastic Packaging Company, Chicago, USA) and incubated at 30°C for 3 days to allow colonies to develop. Stock plates were subsequently kept at 4°C for up to 2 weeks.

2.5.2 Preparation of competent yeast cells

Chemically competent yeast cells were prepared as follows. A single colony of the desired yeast strain was used to inoculate a 50 ml culture of YPD media and grown overnight in a shaking incubator at 30°C. The overnight culture was diluted to an optical density at 600 nanometres (OD_{600}) of 0.2 the following day and was further incubated at 30°C until an OD_{600} of 0.8-1.0. The cells were harvested by centrifugation at 1000 *g* for 2 minutes. The supernatant was discarded and the cell pellet was washed by resuspension in 10 ml LiTE-Sorb [10 mM Tris-HCl (pH 7.6), 0.1 M lithium acetate, 1 mM EDTA, 1.2 M sorbitol] before pelleting again. The cells were resuspended in 1 ml of LiTE-Sorb and incubated in a 30°C shaking incubator for 1 hour. This was followed by an incubation period of at least 20 minutes on ice. The cells could then be used directly for transformation (section 2.5.3) or alternatively, prepared for storage at -80°C by adding an equivalent volume of ice-cold storage buffer [40% (v/v) glycerol, 0.5% (w/v) NaCl] followed by aliquoting and subsequent snap freezing in liquid nitrogen.

2.5.3 Transformation of competent yeast cells

Competent yeast cells (refer to section 2.5.2) were transformed using a modified rapid lithium acetate/single-stranded carrier DNA/polyethylene glycol protocol (Gietz & Woods, 2002). 100 µl of competent cells were thawed on ice for each transformation. An equivalent volume of 70% (w/v) polyethylene glycol-3350 and 10 µg of plasmid DNA (section 2.2.1) was added per transformation. The contents of the tubes were mixed by gentle inversion. The transformation mix was incubated in a 30°C shaking incubator for 45 minutes. This was followed by a 20 minute heat shock incubation period at 42°C before pelleting the cells by centrifugation at 1000 *g* for 2 minutes. The supernatant was discarded and the cell pellet was resuspended in 200 µl sterile dH_20. 50 µl of each resuspended transformation mix was spread onto solid selective minimal SD media lacking the appropriate amino acids to allow for the selection of successfully transformed cells. The agar plates were incubated at 30°C for 3-5 days to allow colonies to develop.

2.5.4 Preparation of yeast whole cell lysates

Yeast whole cell lysates were prepared using one of two protocols. For the purpose of direct immunoblot analysis (sections 2.3.1, 2.3.3 and 2.3.4) to assess steady-state protein levels, yeast cell lysates were prepared using a rapid Twirl Buffer lysis procedure (section 2.5.4.1). Yeast cell lysates that were subsequently used for pull-down assays were prepared using glass beads (section 2.5.4.2). Details regarding these two protocols are outlined below.

A single yeast cell colony was used to inoculate 10 ml of YPD, YPG Raff or the appropriate selective media. The culture was incubated overnight in a 30°C shaking incubator and diluted to an OD_{600} of 0.2 in the appropriate volume of fresh media the next day (this ranged from 10 ml for Twirl lysate preparation to 100 ml for each pull-down combination). The culture was further incubated at 30°C until it reached an OD_{600} of 0.8-1.0. The cells were harvested by centrifugation at 3000 *g* for 5 minutes. Twirl Buffer and glass bead lysates were then prepared as outlined under sections 2.5.4.1 and 2.5.4.2, respectively.

2.5.4.1 Rapid Twirl buffer lysis procedure

Twirl Buffer lysates were then prepared as follows. Cell pellets were resuspended in 1 ml dH_2O and re-pelleted by centrifugation as before. The resultant cell pellets were resuspended in 100 µl of Twirl Buffer [50 mM Tris-HCl (pH 6.8), 5% (w/v) SDS, 8 M urea, 10% (v/v) glycerol, 0.2% (w/v) bromophenol blue, 10% (v/v) β-mercaptoethanol] per OD_{600} and incubated at 65°C for 10 minutes. The cells were briefly vortexed and stored at -20°C. Whole cell lysates were analysed for steady-state protein levels by loading equal volumes onto an SDS-PAGE gel (section 2.3.1) followed by immunoblot analysis (sections 2.3.3 and 2.3.4).

2.5.4.2 Glass bead lysis procedure

Following the initial centrifugation step, glass bead lysates were prepared by resuspending the cell pellet in 1 ml of binding buffer [40 mM HEPES (pH 7.4), 150 mM KCl, 1 mM dithiothreitol (DTT), 1 mM EDTA, 0.5% (v/v) NP-40]. This was followed by harvesting the cells as before and resuspending the cell pellet in 100 µl of binding buffer per OD_{600}. The cells were transferred to 2 ml screw-capped tubes and 425-600 µm glass beads (Sigma-Aldrich Ltd., Poole, UK) were added to approximately 1/3 the volume. Lysates were then prepared by vortexing 4 x 30 seconds with a 1 minute rest interval on ice in between each vortex. Unlysed cells and glass beads were pelleted by centrifugation at 3000 *g* for 2 minutes and a sample of the supernatant (or yeast whole cell lysate) was saved prior to adding the remaining lysate to the pull-down samples (section 2.12.1). An equal volume of 2X Laemmli sample buffer (LSB) [100 mM Tris-HCl (pH 6.8), 4% (w/v) SDS, 20% (v/v) glycerol, 0.2% (w/v) bromophenol blue, 10% (v/v) β-mercaptoethanol] was added to the lysate sample, heated to 95°C for 5 minutes and stored at -20°C for later immunoblot analysis (sections 2.3.1, 2.3.3 and 2.3.4).

2.5.5 Isolation of yeast genomic DNA

Genomic DNA from *S.cerevisiae* was isolated using a single phenol extraction procedure previously described by Hoffman & Winston (Hoffman & Winston, 1987). A single yeast colony was used to inoculate a 10 ml culture of YPD media. This was grown overnight in a shaking incubator at 30°C. The cells were harvested by centrifugation at 3000 *g* for 2 minutes and resuspended in 0.5 ml sterile H_20, transferred to a 1.5 ml eppendorf tube and collected by centrifugation at 3000 *g* for 1 minute. The resultant supernatant was discarded and the remaining cell pellet resuspended in the residual (~50 µl) liquid by vortexing. 0.2 ml of 2% (v/v) Triton X-100, 1% (w/v) SDS, 100 mM NaCl, 10 mM Tris (pH 8.0) and 1 mM EDTA was added to the resuspended cells in addition to 0.2 ml of phenol:chloroform:isoamyl (25:24:1) alcohol. Cells were lysed by the addition of 0.3 g of glass beads and constant vortexing for 4 minutes. 0.2 ml of TE buffer [10 mM Tris-HCl (pH 8.0), 1 mM EDTA] was added before incubating the lysed mix at 65°C for 3 minutes. Cell debris and unlysed cells were removed by centrifugation at 3000 *g* for 5 minutes. The aqueous layer was transferred to a fresh 1.5 ml eppendorf tube and 1 ml of 100% ethanol was added and mixed by inversion. This was followed by centrifugation at 3000 *g* for 2 minutes. The supernatant was discarded and the pellet was resuspended in 0.4 ml of TE buffer containing 30 µg RNase A. This was incubated for 5 minutes at 37°C. Ten µl of a 4 M solution of ammonium acetate and 1 ml of 100% ethanol was added and mixed by inversion. This was followed by centrifugation at 3000 *g* for 2 minutes. The supernatant was discarded and the remaining pellet was air dried prior to resuspension in 50 µl TE buffer. Isolated yeast genomic DNA was stored at -20°C. This protocol yields approximately 2-4 µg of DNA, which is comparable to other ‘rapid’ DNA preparations previously described (Winston *et al.*, 1983; Holm *et al.*, 1986; Harju *et al.*, 2004).

2.6 Production of mutant yeast strains by homologous recombination

Yeast strains YMC001 (*cog1*∆::*KAN*) and YMC002 (*atg1*∆::*KAN*) were derived from the strain RPY10 (Table 2-4) using a one-step gene disruption procedure. Primer pairs used for the purpose of one-step gene disruption were designed as previously described (Longtine *et al.*, 1998). Briefly, forward and reverse primers (Figure 2-1) contain approximately 40 nucleotides identical to the flanking regions of the desired target gene's open reading frame (ORF). Directly linked to this, the 3' ends of the forward and reverse primers consisted of approximately 20 nucleotides that corresponded to the selectable *E.coli KanR* gene which confers resistance to geneticin (G418) (Wach *et al.*, 1994).

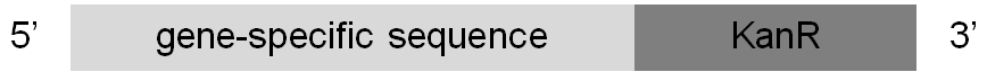

Figure 2-1. One-step gene replacement primers
Forward and reverse primers contained approximately 40 nucleotides of the target gene-specific sequence at the 5' end and were chosen to end just upstream or downstream of the start and stop codons, respectively. Directly linked to this the 3' ends of the forward and reverse primers contained 20 nucleotides that annealed to and allow amplification of the *KanR* selectable marker gene.

PCR was performed using plasmid pYORC–YC018C (Seron *et al.*, 1998) as a template and the appropriate primer pairs. Plasmid pYORC–YC018C contains a KanR module flanked by regions of homology to the *TLG2* ORF cloned in *Eco*RV-cut pUG7. Using plasmid pYORC–YC018C as a template and the gene-specific primers described above, the product of the PCR generated a linear KanR module flanked by homologous regions to the target gene sequence (Figure 2-2). PCR products were analysed by agarose gel electrophoresis (section 2.2.2) and the remaining amplified DNA was directly transformed (section 2.5.3) into competent yeast cells (section 2.5.2). Cells that exhibited resistance to G418 were selected for on YPD-G418 agar plates and incubated at 30°C for 3-5 days to allow colonies to develop. G418-resistant colonies were replica-plated onto solid YPD. Integration of the selectable KanR marker into the correct ORF was identified by whole-cell PCR analysis using either *ATG1*- or *COG1*- specific primer pairs (refer to results section 4.2.3).

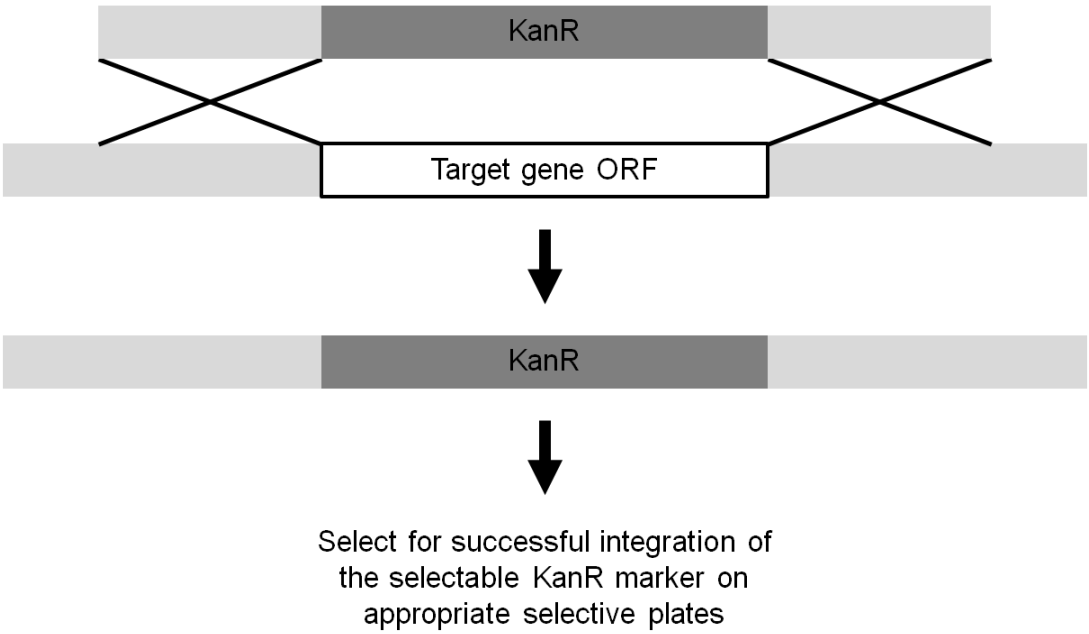

Figure 2-2. One-step gene replacement by homologous recombination
A selectable KanR module (depicted in dark grey) flanked by regions of homology to the target gene sequence (white box) was generated by PCR and transformed into competent yeast cells using a lithium acetate procedure (section 2.5.3). Transformants were selected for on the appropriate selective solid media and successful integration of the selectable marker into the open reading frame (ORF) of the gene of interest was confirmed by PCR analysis.

2.7 Carboxypeptidase Y overlay assay

Yeast cells transformed with the appropriate plasmid (refer to section 2.5.3) were streaked out on selective agar and incubated overnight at 30°C. The freshly grown colonies were replica plated onto fresh selective agar using a sterilised velvet cloth mounted on a replica plating block. Nitrocellulose membrane was overlaid on the replica plated colonies and incubated for 18 hours at 30°C. The membrane was carefully lifted and washed under running tap water to remove all the cells. The membrane was subsequently blocked with 1.5% non-fat dried milk in Tris-Buffered saline Tween-20 (TBST) [20 mM Tris (pH7.5), 137 mM NaCl, 0.1% (v/v) Tween-20] for 1 hour at room temperature prior to assessing secretion of CPY by immunoblot analysis (sections 2.3.3 and 2.3.4).

2.8 Palmitoylation assays

2.8.1 Hydroxylamine treatment

The method employed here was adapted from (Valdez-Taubas & Pelham, 2005) and is summarised in Figure 2-3. 10 ml of the appropriate selective media was inoculated with yeast transformed with the appropriate plasmids (containing the copper inducible *CUP1* promoter) and incubated overnight at 30°C. The overnight cultures were diluted to an OD_{600} of 0.2 the next day in 50 ml fresh selective media containing 100 µM $CuCl_2$ and incubated further at 30°C until an OD_{600} of 0.8-1.0. Cells were harvested by centrifugation at 1000 *g* for 2 minutes and resuspended in 5 ml YPD-Sorb [50%(v/v) YPD, 50% (v/v) 2.5 M sorbitol) containing 15 µl β-mercaptoethanol and 50 µl yeast lytic enzyme (0.3 mg/ml). Cells were then converted to spheroplasts by further incubating the mix for 1 hour at 30°C. The resultant spheroplasts were harvested by centrifugation at 2000 *g* for 5 minutes and were subsequently lysed by resuspension in 250 µl lysis buffer [200 mM sorbitol, 100 mM KoAc, 1% (v/v) Triton X-100, 50 mM KCl, 20 mM PIPES pH 6.8, 3 mM N-ethylmaleimide (NEM), 1 tablet of complete protease inhibitors/50 ml PBS). The sample was incubated under constant rotation for 1 hour at 4°C. Cell lysates were cleared by centrifugation at 12400 *g* for 15 minutes. 100 µg of protein extract (estimated by the Bradford protein assay in section 2.9), in no more than 50 µl, was transferred to a clean 1.5 ml eppendorf tube containing 600 µl of either 1 M hydroxylamine, pH 7.4, or 1 M Tris, pH 7.4, as a control. This was followed by a 1 hour incubation at room temperature under constant rotation. Proteins were precipitated by adding a mixture of chloroform-methanol (600-150 µl, respectively). The samples were briefly vortexed prior to centrifugation at 16000 *g* for 2 minutes. The upper phase was carefully removed without disturbing the interphase. 450 µl of methanol (100% v/v) was added and the samples were again briefly vortexed prior to being centrifuged at 16100 *g* for 2 minutes. The supernatant was discarded and the remaining pellet was thoroughly air-dried and resuspended in 100 µl 1X LSB in the absence of β-mercaptoethanol. Samples were heated at 65°C for 15 minutes. 20 µl per sample was analysed by SDS-PAGE (section 2.3.1) followed by immunoblot analysis (sections 2.3.3 and 2.3.4).

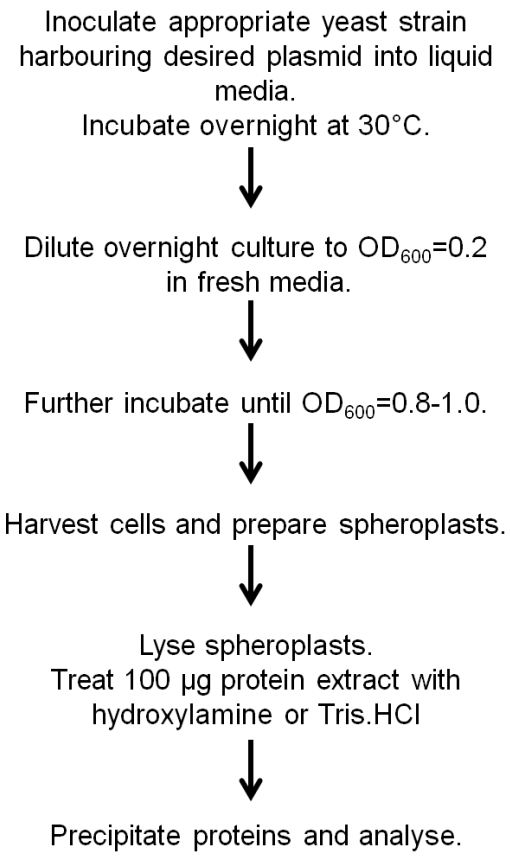

Figure 2-3. Summary flow chart of hydroxylamine treatment protocol
Hydroxylamine treatment of yeast cell extracts was performed as follows. The appropriate yeast strain was inoculated into liquid culture and incubated overnight at 30°C. The culture was diluted to an OD_{600} of 0.2 the following day and further incubated until an OD_{600} of 0.8. The cells were harvested and spheroplasts were prepared. The spheroplasts were lysed and 100 µg of protein extract was treated with hydroxylamine or Tris. Proteins were subsequently precipitated and equal volumes were subjected to SDS-PAGE followed by immunoblot analysis.

2.8.2 Acyl resin-assisted capture

Acyl resin-assisted capture (Acyl-Rac) allows for the identification of novel S-acylated proteins and was employed to investigate palmitoylation of Tlg2 in *S.cerevisiae*. The protocol used during this study was adapted from (Forrester *et al.*, 2011).

The appropriate yeast strains were inoculated into 10 ml YPD and incubated overnight at 30°C with constant shaking. The overnight culture was diluted to an $0D_{600}$ of 0.2 in 100 ml fresh YPD. This was further incubated at 30°C until an $0D_{600}$ of 0.6-1.0. Cells were harvested by centrifugation at 2000 *g* for 3 minutes and the resultant cell pellets were resuspended in 1 ml lysis buffer (25 mM HEPES, 25 mM NaCl, 1 mM EDTA, pH 7.5) containing protease inhibitor cocktail. Cell disruption was achieved by passing resuspended cells through a 25G needle five to ten

times. Cell nuclei were removed by centrifugation at 100 *g* for 2 minutes at 4°C. The remaining supernatant was subjected to further centrifugation at 16100 *g* for 30 minutes at 4°C. The supernatant containing the cytosolic fraction was discarded and the pellet containing the membrane fraction was resuspended in 100 µl lysis buffer containing 0.5% (v/v) Triton X-100. Unmodified cysteine residues containing free sulfhydryl (SH) groups were blocked by treatment with methyl methanethiosulfonate (MMTS). This was performed by adding 200 µl of blocking buffer (100 mM HEPES, 1 mM EDTA, 2.5% (w/v) SDS, 0.1% (v/v) MMTS, pH 7.5) to the previously resuspended proteins and incubating for 3 hours at 40°C with brief vortexing every 30 minutes. Proteins were subsequently precipitated by the addition of three volumes of cold 100% acetone to the protein mixture followed by an incubation at -20°C for 20 minutes. Precipitated proteins were sedimented by centrifugation at 5000 g for 10 minutes. The supernatant was discarded and the pellet was allowed to air dry at room temperature. This was followed by washing the pellet five times by resuspending in 1 ml 70% (v/v) acetone and centrifugation at 5000 *g* for 10 minutes.

For the hydroxylamine treatment and resin capture, freeze-dried Thiopropyl Sepharose® was rehydrated by the addition of dH_2O and rotating for 15 minutes at room temperature. The swollen beads were harvested by centrifugation at 1000 *g* for 5 minutes and any excess water was removed. The beads were resuspended in the appropriate volume of binding buffer [100 mM HEPES, 1 mM EDTA, 1% (w/v) SDS, pH 7.5] (0.1 g of beads in 1 ml binding buffer). 200 µl of beads-binding buffer slurry was transferred into a fresh 1.5 ml eppendorf tube per binding reaction. The beads were allowed to settle by gravity and excess binding buffer was removed. The previously precipitated proteins were resuspended in 400 µl binding buffer and 160 µl was added into two separate tubes each with pre-prepared Thiopropyl Sepharose® beads. The remaining 80 µl was kept as the total input and 20 µl 4X LSB containing 10% beta-mercaptoethanol was added prior to heating at 95ºC for 5 minutes. For treatment with hydroxylamine, a final concentration of 0.5 M freshly prepared hydroxylamine (pH 7.5) was added to the beads-protein-binding buffer solution. As a negative control, 0.5 M Tris (pH 7.5) was added. Samples were then incubated overnight at room temperature with constant rotation. Beads were separated from the unbound fraction by centrifugation at 500 *g* for 3 minutes. The supernatant (i.e. the unbound fraction) was carefully transferred into a fresh 1.5 ml eppendorf tube and 63 µl of 4X LSB

containing 50 mM DTT was added and heated at 95ºC for 5 minutes. The remaining beads were washed five times with 1 ml binding buffer. Bound proteins were eluted from the beads by the addition of 63 µl of 4X LSB containing 50 mM DTT for 15 minutes at room temperature followed by heating at 95ºC for 5 minutes. 15 µl of each sample was subsequently separated by SDS-PAGE (section 2.3.1) and analysed by immunoblot analysis using appropriate antibodies (refer to sections 2.3.3 and 2.3.4).

2.9 Bradford protein assay

Total protein concentration contained within whole cell lysates were estimated using the Bradford protein assay (Bradford, 1976). Bovine serum albumin (BSA) protein standards of known concentrations were prepared using a 0.1 mg/ml BSA stock solution. BSA standards were prepared using dH_2O and concentrations ranged from 0 (dH_2O only), 0.25, 0.5, 0.75, 1, 2, 3, 5 and 6 µg/ml. A 1:300 dilution of each of the samples of unknown concentration was prepared in a total volume of 600 µl. All standards and samples of unknown concentration were prepared in triplicate in a 96-well plate as follows. 150 µl of Quick Start™ Bradford Dye Reagent was pipetted into each well. To this, 150 µl of each BSA standard or sample of unknown protein concentration (pre-diluted to 1:300) was added and triturated. The absorbance of each solution was measured at 595 nm in a FLUOstar OPTIMA microplate reader (BMG Labtech, UK). A standard curve was constructed using the mean measurements obtained from the BSA protein standards. The equation of the linear range of this graph was subsequently used to calculate the concentration of proteins contained in the samples of unknown concentration.

2.10 Hydrogen peroxide halo assay

10 ml YPD or appropriate selective media was inoculated with a colony of the desired yeast strain and incubated at 30°C overnight. The overnight culture was diluted to an OD_{600} of 0.1 in 5 ml sterilised dH_2O. 1 ml of the diluted culture was pipetted onto the desired agar (YPD or selective) and gently swirled in order to cover the entire surface of the plate. Excess culture was carefully removed and plates were dried for 1 hour at room temperature. Sterile discs containing 10 µl hydrogen peroxide (H_2O_2) at concentrations of 0.3 mM, 0.6 mM and 1.5 mM or solvent blank were placed onto each plate. Each plate was performed in triplicate for each strain. Plates were incubated for 2-3 days at 30°C until a lawn of cells appeared. Halos, or regions of no cell growth, were measured in arbitrary units using ImageJ freeware. The relative sensitivity to H_2O_2 for a given strain was determined as previously described (Gourlay & Ayscough, 2005). The logarithm of the H_2O_2 concentration was plotted as a function of halo area (arbitrary units). The H_2O_2 concentration required to give a halo area of 0.3 arbitrary units was calculated by using the line equation for each strain and subsequently determining the inverse of this value. The relative sensitivity for a given strain to H_2O_2 was calculated by dividing the H_2O_2 concentration to produce a halo area of 0.3 on an experimental plate by the H_2O_2 concentration required to produce a halo of the same area on a wild type plate.

2.11 Purification of recombinant fusion proteins from *E.coli*

2.11.1 Preparation of competent bacterial cells

Chemically competent bacterial cells were either purchased from Invitrogen or prepared in–house as follows. 10 ml of 2YT containing relevant antibiotic was inoculated with the desired bacterial strain and incubated in a 37°C shaking incubator overnight. The cells were diluted 1:100 in a total volume of 300 ml 2YT the next day. This culture was further incubated at 37°C until an OD_{600} of 0.6. Cells were harvested by centrifugation at 1000 *g* for 10 minutes and subsequently resuspended in 150 ml ice-cold 0.1 M $CaCl_2$ before being incubated on ice for 30 minutes. The cells were harvested as before and resuspended in 40 ml of ice-cold 0.1 M $CaCl_2$ containing 15% (v/v) glycerol. 200 µl aliquots of competent cells were prepared and stored at -80°C.

2.11.2 Transformation of competent bacterial cells

Chemically competent bacterial cells (section 2.11.1) were transformed according to Invitrogen's protocol described for transforming One Shot® TOP10 chemically competent cells. Briefly, cells were thawed on ice for 15 minutes. 5 µl of purified plasmid DNA (section 2.2.1) or DNA ligation reaction (section 2.2.7) was added to 50 µl of competent *E.coli* cells in 1.5 ml eppendorf tubes. The transformation mix was gently mixed by inversion and incubated on ice for 30 minutes. To facilitate the uptake of DNA into the competent cells, the cells were heat shocked for 30 seconds at 42°C before asceptically adding 250 µl of 2YT media. The cells were incubated for 1 hour at 37°C to allow recovery and were then plated out onto solid 2YT containing the appropriate antibiotic. The plates were incubated overnight at 37°C to allow for the selection of successfully transformed cells.

2.11.3 Cryopreservation and maintenance of plasmid DNA

E.coli harboring plasmid constructs were prepared for long-term storage as follows. A single colony of cells containing the desired transformed plasmid was inoculated into 10 ml 2YT supplemented with the appropriate antibiotic and incubated overnight in a 37°C shaking incubator. 1.38 ml of the overnight culture was transferred into a 2 ml cryovial and DMSO was added to a final concentration of 1 mM, thoroughly mixed and transferred to -80°C for storage. Frozen stocks could be used directly for subsequent inoculations to purify plasmid DNA (section 2.2.1) or for expressing and purifying recombinant fusion proteins (sections 2.11.4, 2.11.5 and 2.11.6)

2.11.4 Expression of recombinant fusion proteins

The following protocol is summarised in Figure 2-4. A single colony of BL21 Star™ (DE3) cells transformed with the desired plasmid was used to inoculate 10 ml 2YT containing the appropriate antibiotic and incubated overnight in a 37˚C shaking incubator. Cells were harvested by centrifugation at 3000 *g* for 5 minutes and resuspended in 9 ml Terrific Broth containing appropriate antibiotic. 3ml of the resuspended cells was added to each pre–prepared and autoclaved 1 litre flask of Terrific Broth containing the appropriate antibiotic. This was then incubated in a 37˚C shaking incubator until an OD_{600} of 0.6–0.8. Isopropyl-β-D-1-thiogalactopyranoside (IPTG) was added to a final concentration of 0.5 mM and

expression of the recombinant fusion proteins was induced by further incubating the cultures overnight in a 22˚C shaking incubator. Cells were harvested by centrifugation at 3000 *g* for 30 minutes and either resuspended in 100 ml PBS containing 5 mM β-mercaptoethanol and EDTA-free protease inhibitor cocktail (for PrA fusion protein production) or GST lysis buffer (100 mM HEPES, 500 mM NaCl, 5 mM $MgCl_2$) containing 5 mM β-mercaptoethanol and complete protease inhibitor cocktail for every 3 litre culture. Cells were disrupted with a M-11OP Microfluidizer® bench-top processor (Microfluidics Ltd, Massachusetts, USA) and incubated with DNAse I for 30 minutes at 4°C. Resultant lysates were clarified by centrifugation at 48400 *g* for 40 minutes at 4°C in a Beckman J2-21 centrifuge (Beckman Instruments Ltd., Glenrothes, UK). 50 µl of the resultant supernatant (or whole cell lysate) was saved for later analysis by adding an equal volume of 2X LSB containing 10% (v/v) β-mercaptoethanol, heating at 95°C for 5 minutes and storing the sample at -20°C.

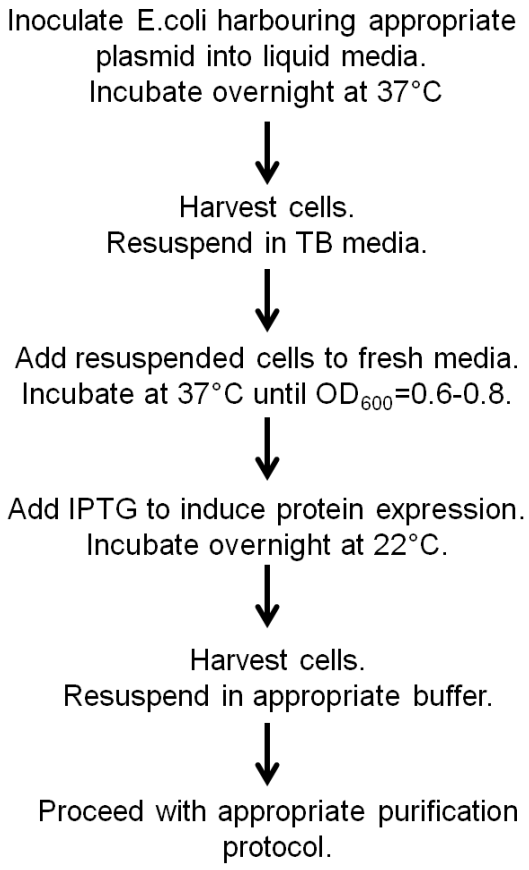

Figure 2-4. Recombinant fusion protein expression summarised
BL21 *E.coli* harboring the desired plasmid was inoculated into 2YT containing the appropriate antibiotic and incubated overnight at 37°C. The overnight culture was harvested and resuspended in Terrific Broth. The resuspended cells were added to fresh Terrific Broth and further incubated at 37°C until an OD_{600} of 0.8. Recombinant fusion protein expression was induced by the addition of IPTG and subsequent overnight incubation at 22°C. Cells were harvested the next day and resuspended in the appropriate buffer. This was followed by cell lysis and subsequent purification of the recombinant fusion proteins.

2.11.5 Purification of GST fusion proteins

Glutathione S-transferase (GST) isoenzymes are present at a high concentration in the cytosol where they catalyse a wide spectrum of reactions including the conjugation of reduced glutathione to a wide variety of substrates containing electrophilic centres via a thioether bond (Chasseaud, 1979; Mannervik, 1985). GST binds to glutathione with high affinity and it is this property that is widely utilised to purify recombinant GST fusion proteins produced in *E.coli* using glutathione coated beads as described below.

Glutathione Sepharose beads were prepared by washing 1 ml of pure beads for every 3 litres of culture three times in 10 ml PBS. Following removal of the last washing solution from the glutathione beads, cleared lysate (section 2.11.4) was added to the beads and incubated for 2 hours or overnight at 4°C under constant rotation. Glutathione beads and bound recombinant GST fusion proteins were pelleted by centrifugation at 1000 *g* for 1 minute. 100 µl of the resultant supernatant (unbound sample) was saved and prepared for later analysis by adding 2X LSB containing 10% (v/v) β-mercaptoethanol, heating for 5 minutes at 95°C and storing the sample at -20°C. The remaining supernatant was discarded and the glutathione beads were washed three times with 10 ml PBS. Following the third wash, 100 µl of the supernatant was saved and prepared for later analysis as before (wash 1 sample). The beads were washed twice more with PBS containing 0.5 mM NaCl. As before, 100 µl of the supernatant was saved following the last wash (wash 2 sample). The remaining supernatant was discarded and the glutathione beads were resuspended in an equal volume of PBS. 50 µl of the resuspended beads were collected and prepared for later analysis as before (beads before sample). The remaining beads were pelleted by centrifugation at 1000 *g* for 1 minute and the supernatant was discarded. Recombinant GST fusion proteins were then eluted from the glutathione beads by adding 1.5 ml of elution buffer (50 mM Tris, 25 mM reduced glutathione, pH 8.0) to the beads followed by a 15 minute incubation at 4°C with constant rotation. The glutathione beads were pelleted by centrifugation at 1000 *g* for 1 minute and the eluted proteins were transferred into a fresh 1.5 ml eppendorf tube. 100 µl of the eluate was saved for analysis as before (elution 1 sample). This elution step was repeated twice more (elution 2 and 3 samples). Following removal of the last eluate, the remaining beads were washed once with PBS and the beads were pelleted by centrifugation

as before. The PBS was discarded and the remaining beads were then resuspended in an equal volume of PBS. The final 100 µl sample was collected from this resuspension and prepared for later analysis as before (beads after sample). The eluted samples were pooled and dialysed overnight at 4°C in the appropriate molecular weight cut off Float-A-Lyzer® G2 device (Spectrum Laboratories, Inc., USA) against 5 litres of PBS containing 10% (w/v) glycerol. The dialysed proteins were aliquoted the following day, snap frozen in liquid nitrogen and stored at -80°C. The samples collected during the purification protocol were analysed by SDS-PAGE (section 2.3.1) followed by immunoblot analysis (sections 2.3.3 and 2.3.4) and Coomassie™ blue staining (section 2.3.2) to analyse the purity of the purified protein.

2.11.6 Purification of Protein A fusion proteins

Staphylococcal PrA is a mammalian immunoglobulin-binding protein present on the cell wall of the bacterium *S.aureus* and exhibits tight binding to the Fc region of immunoglobulins (Langone, 1982). This well characterised interaction was employed to purify recombinant *Staphylococcal* PrA fusion proteins produced in *E.coli* using IgG coated sepharose beads as described below.

IgG Sepharose beads were prepared by washing 1 ml of pure beads for every 3 litres of culture as follows: four times in Tris-Saline-Tween-20 (TST) [50 mM Tris (pH 7.6), 150 mM NaCl, 0.05% Tween-20], twice in 0.5 M acetic acid (pH 3.4) followed by another two washes in TST. Following removal of the last wash solution from the IgG Sepharose beads, cleared lysates containing recombinant PrA-tagged fusion proteins (section 2.6.4) were prepared as outlined for recombinant GST-tagged fusion proteins (section 2.6.5) with the exception of the washing and elution steps. These were performed as follows. Mobilised/recovered PrA fusion proteins were washed ten times with TST followed by an additional two washes with 5 mM ammonium acetate (pH 5.0). As for GST fusion protein purification, two wash samples were collected and prepared for later analysis. Elution of the recovered PrA fusion proteins were performed as described for GST fusion proteins except that the elution buffer used was 0.5 M acetic acid (pH 3.4). All subsequent steps were performed as outlined for GST fusion protein purification.

2.12 Protein interaction assays

2.12.1 GST and Protein A pull-down assays

Equivalent amounts (as determined by Coomassie™ blue staining) of the appropriate dialysed recombinant fusion protein (sections 2.11.5 and 2.11.6) were immobilised to 500 µl prewashed beads (either Glutathione or IgG Sepharose beads as required) in 3 ml PBS overnight at 4°C under constant rotation. Immobilised proteins were washed thoroughly in PBS (for GST fusion proteins) or TST and 5 mM ammonium acetate (pH 5.0) (for PrA fusion proteins) and resuspended in an equal volume of PBS. 30 µl of the agarose slurry was prepared for analysis by adding an equal volume of 2X LSB containing 10% (v/v) β-mercaptoethanol and heating the sample for 5 minutes at 95°C. SDS-PAGE (section 2.3.1) followed by Coomassie™ blue staining (section 2.3.2) was employed to analyse binding of the proteins to the beads. Agarose slurries could be kept at 4°C for up to 2 weeks. Yeast whole cell lysates were then prepared as follows.100 ml of the appropriate yeast strain expressing the desired HA-tagged Cog protein (either yeast strain SEY6210, WLY206, WLY207, WLY208, WLY209, WLY218; refer to Table 2-4) was cultured and lysed using glass beads as outlined under section 2.5.4.2 for each pull-down combination. Pull-down assays were set up as follows. Yeast whole cell lysates (ranging from 500 µl-700 µl) were added to 200 µl of immobilised GST- or PrA-tagged fusion protein slurry in a 1.5 ml eppendorf tube and incubated for 1-2 hours at 4°C under constant rotation. Sepharose beads and associated proteins were recovered by centrifugation at 3000 *g* for 1 minute and thoroughly washed as before. Following removal of the last washing solution the sample was prepared for SDS-PAGE (section 2.3.1) by the addition of an equal volume of 2X LSB containing 10%(v/v) β-mercaptoethanol. This was followed by immunoblot analysis (sections 2.3.3 and 2.3.4) for the presence of bound HA-tagged Cog proteins.

2.12.2 Yeast two-hybrid assay

The yeast two-hybrid assay is a technique to detect protein-protein interactions (Fields & Song, 1989). It relies on the ability of two interacting proteins fused to either a Gal4 DNA binding domain (BD) or activation domain (AD) to activate transcription of a Gal4-responsive reporter gene (refer to section 3.2.1 for more details). For this study, the appropriate yeast two-hybrid plasmid pairs were co-transformed into *S.cerevisiae* strain AH109 as outline under section 2.5.3. Co-transformed yeast auxotrophs were subsequently selected for on solid media lacking the appropriate combination of amino acids. Colonies from successfully co-transformed AH109 yeast cells were replica plated onto the appropriate fresh solid double amino acid drop-out media. Overnight cultures from these stock plates were prepared in the appropriate selective media and were incubated at 30°C overnight and diluted to an OD_{600} of 0.2 in fresh selective media the next day. This was further incubated until an OD_{600} of 0.6-0.8. The cultures were then divided in half and the cells were equilibrated to the same optical density using water and Twirl lysis buffer (refer to section 2.5.4.1), respectively (summarised in Figure 2-5).

For the yeast two-hybrid interaction assay a series of four dilution factors (ranging from 0.1, 0.01, 0.001 and 0.0001) were prepared using the cells that were equilibrated in water. This was followed by spotting 5 µl of the different diluted samples out in triplicate onto the appropriate double (+his) and triple amino acid drop-out (-his) selective agar. Agar plates containing the diluted samples were allowed to dry at room temperature prior to incubation at 30°C for 3 to 5 days to allow growth.

To confirm expression of Gal4 BD and AD fusion proteins Twirl lysates were prepared as outlined under section 2.5.4.1 and subjected to SDS-PAGE (section 2.3.1) followed by immunoblot analysis (sections 2.3.3 and 2.3.4) using antibodies against cMyc and HA epitope tags.

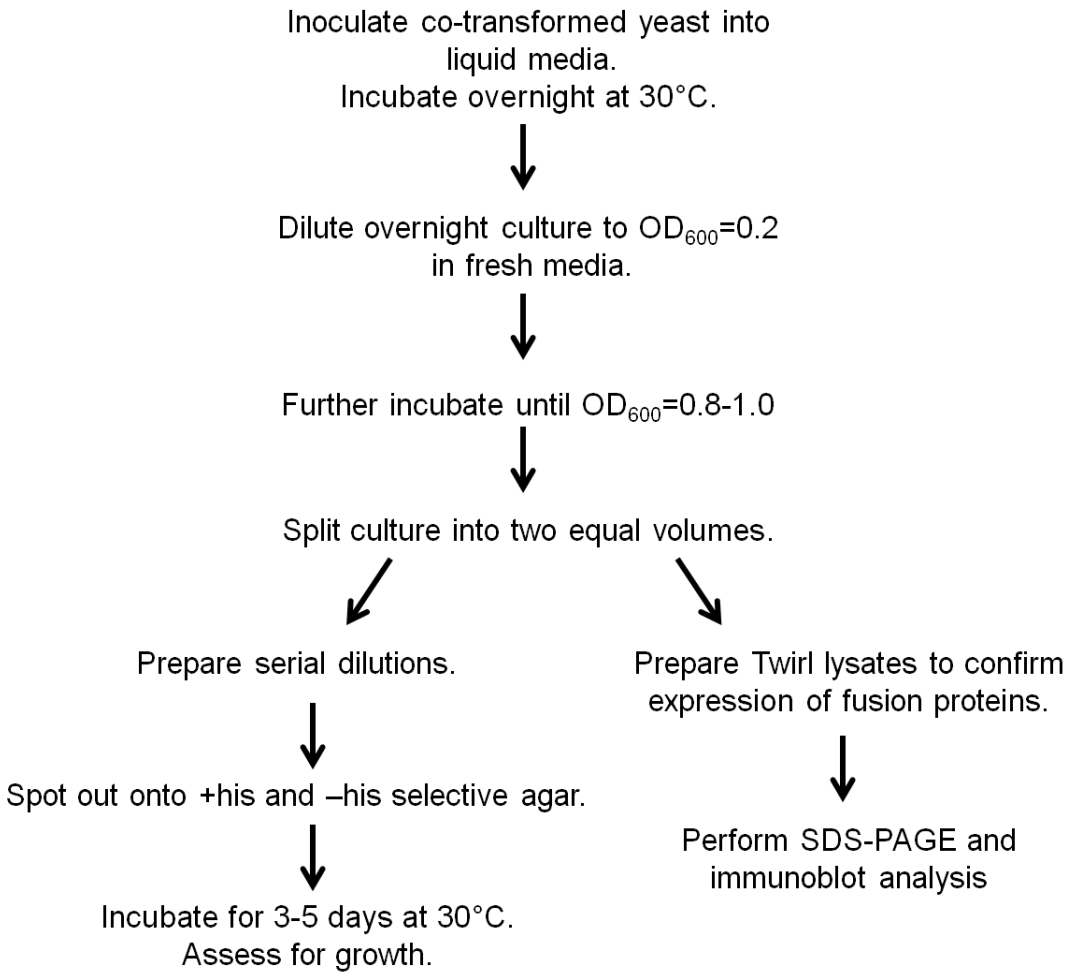

Figure 2-5. Summary flow chart of yeast two-hybrid protocol
The appropriate yeast strain was inoculated in liquid media and cultured overnight at 30°C. The culture was diluted to an OD_{600} of 0.2 the following day and further incubated until an OD_{600} of 0.8. The culture was divided in two at this stage. Serial dilutions were prepared using one half of the total culture and spotted onto +his and –his selective agar. Growth was assessed following incubated for 3-5 days at 30°C. Yeast cell lysates were prepared using the other half culture. Lysates were subjected to SDS-PAGE followed by immunoblot analysis to confirm expression of the activating domain (AD) and binding domain (BD) fusion proteins.

2.13 *C.elegans* methods

2.13.1 Maintenance of *C.elegans* in culture

C.elegans were visualised using a Zeiss Stemi SV6 Stereo 0.8-5.0 zoom microscope (Carl Zeiss, Germany) equipped with a 150 Watt Zeiss KL1500 LCD cold light source. C*.elegans* strains were transferred approximately every 1-3 generations to fresh NGM agar seeded with OP50-1 (section 2.1.3) or alternatively, stock plates could be starved for up to 6 weeks between transfers. *C.elegans* strains were transferred by either 'chunking' or picking individual or several nematodes at any one time with a worm picker and transferring them onto fresh OP50-1 seeded NGM agar. Chunking was routinely used for transferring homozygous or starved stocks to a fresh plate. Briefly, this involved sectioning agar from the old stock plate with a sterilised scalpel and transferring it facing upside-down onto a fresh plate. Heterozygous and wild-type male mating stocks (i.e. containing both wild-type males and hermaphrodites) were transferred with a worm picker composed of platinum wire. The tip of the wire, which was used for picking the nematodes, was flattened, flamed and gently touched to a lawn of OP50-1 before gently touching the top of the chosen nematode. Several nematodes could be transferred using this method at any one time. The tip of the worm picker was then gently lowered to touch the surface of the fresh agar and the nematode(s) were allowed to crawl off the picker. Wild-type male stocks were typically transferred using a 3:5 hermaphrodite to male ratio and using young adults of both sexes.

2.13.2 Preparation of *E.coli* OP50-1 liquid culture

OP50-1 is a variant strain of the original OP50 E*.coli* B strain (Brenner, 1974). Similar to OP50, the OP50-1 strain is an uracil auxotroph however it has been further selected for streptomycin resistance thus making it less prone to contamination. OP50-1 was selected on solid Luria Bertani (LB) media [1% (w/v) tryptone, 0.5% (w/v) yeast extract, 0.5% (w/v) NaCl] containing 12.5 µg/ml streptomycin. Solid media was prepared by the addition of 2% (w/v) agar to the media prior to autoclaving. OP50-1 liquid culture was prepared by inoculating 100 ml LB media containing 12.5 µg/ml streptomycin with a single colony of OP50-1 followed by an overnight incubation at 37°C in a shaking incubator. The liquid culture was ready for use the next day and stored at 4°C.

2.13.3 Cryopreservation and recovery of *C.elegans*

Stocks of *C.elegans* strains were stored in liquid nitrogen (-196°C) as previously described (Brenner, 1974). Briefly, one large NGM agar plate containing freshly starved L1-L2 animals was washed with 1 ml M9 buffer (22 mM KH_2PO_4, 42 mM Na_2HPO_4, 85 mM NaCl, 1 mM $MgSO_4$) and transferred to a 1.5 ml eppendorf tube. An equal volume of *C.elegans* freezing solution [100 mM NaCl, 50 mM KH_2PO_4, 30% (w/v) glycerol, 140 mM NaOH, 0.3 mM $MgSO_4$] was added and thoroughly mixed by inversion. 0.5 ml aliquots were prepared in 2 ml cryovials, transferred to a Styrofoam box and stored at -80°C for approximately 12 hours. The cryovials were transferred to liquid nitrogen the next day for long-term storage. *C.elegans* were recovered by thawing liquid nitrogen stocks at room temperature and transferring the contents to an NGM agar plate seeded with OP50-1. The animals were allowed to recover for 2-3 days at the appropriate temperature. Approximately 10-15 hermaphrodites were individually transferred to separate NGM agar plates and allowed to reproduce for one generation. Progeny were scored for the correct phenotype and were further maintained as outlined under section 2.13.1.

2.13.4 Isolation of *C.elegans* genomic DNA

Genomic DNA from *C.elegans* was isolated using a modified single worm lysis genomic DNA preparation protocol (Wood, 1988). Nematodes from each particular strain were individually lysed in 12.5 µl of single worm lysis buffer (SWLB) [50 mM KCl, 10 mM Tris-HCl (pH 8.3), 2.5 mM $MgCl_2$, 0.45% (v/v) Tween-20, 0.01% (w/v) gelatin, 1% (v/v) β - mercaptoethanol, 60 µg/ml proteinase K]. The nematodes were incubated at 60°C for 1 hour followed by 15 minutes at 95°C to inactivate proteinase K. These samples could be used directly for PCR reactions (refer to section 2.2.4) or stored at -20°C for future use.

2.13.5 Preparation of *C.elegans* whole animal lysates

C.elegans whole animal lysates were prepared for SDS-PAGE (section 2.3.1) and immunoblot analysis (sections 2.3.3and 2.3.4) as follows. Nematodes of mixed developmental stage were washed from culture plates with 1 ml M9 buffer and transferred into a 1.5 ml eppendorf tube. The nematodes were allowed to settle by gravity after which excess buffer was removed. An equal volume of 2X LSB containing 10% beta-mercaptoethanol was added to the nematodes. The sample was vortexed for 10 seconds followed by heating at 95°C for 5 minutes. The sample was once again vortexed for 10 seconds followed by SDS-PAGE (section 2.3.1) and immunoblot analysis (sections 2.3.3 and 2.3.4). *C.elegans* whole animal lysates were stored at -20°C.

2.13.6 *C.elegans* genetic crosses

C.elegans genetic crosses were performed using standard techniques (Wood, 1988). Mutant alleles were identified by PCR amplification (refer to section 2.2.4) with the appropriate primer pairs (Table 2-7) and using single worm genomic DNA (section 2.13.4) as a template or alternatively, visual observation based on phenotype.

2.13.7 Nomarski microscopy

Live *C.elegans* were prepared for visualisation by Nomarski microscopy as follows. Agar pads (0.2 mm thick) consisting of 2% (w/v) agarose dissolved and melted in M9 buffer were prepared onto glass slides (75 mm x 25 mm). A 5-10 µl drop of M9 buffer was placed onto the centre of the agar pad and live *C.elegans* to be observed were transferred into the drop using a worm picker. A glass coverslip was gently laid over the animals prior to being visualised using a Zeiss Axioskop 2 MOT microscope (Carl Zeiss, Germany). Images were acquired using a Hamamatsu camera (Hamamatsu Photonics, Japan) in combination with Openlab 4.0.2 software (Improvision Ltd.). Images were processed for presentation using Microsoft PowerPoint.

2.13.8 Immunofluorescence of *C.elegans*

C.elegans embryos, larvae or adults of similar developmental age were transferred into a 15 µl drop of M9 buffer on a poly-L lysine treated glass slide (75 mm x 25 mm). A glass coverslip (18 mm x 18 mm, 1 mm thickness) was carefully lowered over the buffer using a scalpel blade and excess buffer was removed from the edge of the coverslip. Slides containing the *C.elegans* embryos, larvae or adults were placed onto a pre-cooled aluminium block surrounded by dry ice for 10 minutes. The samples were permeabilised using a freeze-crack method previously described (Siddiqui *et al.*, 1989). The slides containing the permeabilised specimen were immediately transferred into a copelin jar containing 100% methanol pre-chilled to -20°C and incubated at -20°C for 10 minutes. The slides were then transferred into a copelin jar containing 100% acetone pre-chilled to -20°C and further incubated at -20°C for 10 minutes. The specimens were air dried at room temperature prior to being rehydrated with 200 µl of PBS-T for 5 minutes. The specimens were then blocked for 1 hour at 4°C with 1% (w/v) non-fat dried milk in PBS-T. The blocking solution was removed by tilting the slide at a 45° angle and removing excess solution with a tissue. 100 µl of primary antibody (listed in Table 2-2) diluted in blocking solution was applied and incubated overnight at 4°C in a humid chamber. Primary antibody was removed as described for the blocking solution. Non-specifically bound primary antibody was washed off with PBS-T three times, with each washing interval lasting 10 minutes. The appropriate fluorophore-conjugated secondary antibody (listed in Table 2-2) diluted in blocking solution was applied and incubated at 37°C for 1 hour in the dark. Excess secondary antibody was washed off from the specimen as before. 15 µl mounting solution (50% (v/v) glycerol in PBS) was placed on the sample and an 18 mm x 18 mm coverslip was gently lowered over the sample with a scalpel blade to prevent the formation of air bubbles. Excess mounting solution was carefully removed from around the coverslip edge and sealed with clear nail varnish. Specimens were visualised using a Zeiss Axioskop 2 MOT microscope equipped with a HBO100 illuminator (Carl Zeiss, Germany). Images were captured and processed for presentation as described in section 2.13.7.

Chapter 3 – Endosomal SNAREs and autophagy

3.1 Overview and aims

Tlg2, which forms part of the yeast endosomal SNARE complex together with Tlg1, Vti1 and Snc2 (Abeliovich *et al.*, 1998; Paumet *et al.*, 2001), has previously been shown to regulate autophagy in yeast (Abeliovich *et al.*, 1999; Ohashi & Munro, 2010; Nair *et al.*, 2011). It is becoming increasingly apparent that distinct subsets of SNARE proteins are implicated at various stages during the process of autophagy. For example, mammalian Syntaxin 17 localises to the outer membranes of completed autophagosomes (Itakura *et al.*, 2012). Here Syntaxin 17 interacts with its partner SNARE proteins SNAP29 and VAMP8 to facilitate fusion of the autophagosome with the endosome/lysosome. More recent evidence support a role for SNARE-mediated homotypic fusion reactions in the formation of autophagosomes and thereby autophagy (Moreau *et al.*, 2011; Nair *et al.*, 2011). Tlg2 has a well established role in homotypic fusion reactions in both the endocytic and autophagy-related CVT pathways (Brickner *et al.*, 2001). In support of a role for Tlg2 in autophagy, a link between autophagy and SNARE proteins has been provided by the COG complex, a hetero-octameric tethering factor that has been shown to localize to the PAS (Yen *et al.*, 2010). Subunits of the COG complex have been shown to directly interact with SNARE proteins including yeast Vti1 and mammalian Syntaxin 6, which forms part of the core complexes involving Tlg2 and its mammalian ortholog Syntaxin 16, respectively (Suvorova *et al.*, 2002; Shestakova *et al.*, 2007; Laufman *et al.*, 2011). Mutations in a number of COG complex subunits have indicated that this complex is required for efficient autophagosome formation (Yen *et al.*, 2010) possibly by facilitating assembly of SNARE complexes (Shestakova *et al.*, 2007). Interestingly, cycling of Atg9, which is thought to direct recruitment of membranes to autophagosomes, is affected in a similar manner in both *cog* (Yen *et al.*, 2010) and *tlg2* (Ohashi & Munro, 2010; Nair *et al.*, 2011) mutant yeast strains. As a result, mislocalization of Atg9 leads to inefficient and/or incomplete autophagosome formation. Moreover, the COG complex interacts directly with SNARE domain of Syntaxin 6, the mammalian homologue of yeast Tlg1, via the Cog6 subunit (Laufman *et al.*, 2011). This interaction was demonstrated to stabilise steady-state levels of Syntaxin 6 and its partner SNARE proteins, as well as positively regulating SNARE complex assembly. These data lead us to hypothesise that, similar to its role in the Cvt

pathway, Tlg2, which in turn is regulated by the SM protein Vps45 (Bryant & James, 2001), is by association with subunits of the COG complex involved in (homotypic) membrane fusion events regulating autophagosome formation.

This chapter documents a series of yeast two-hybrid and pull down assays that were systematically performed in order to determine if Tlg2 and its partner SNARE proteins Tlg1, Vti1 and Snc2 directly associate with subunits of the COG complex.

3.2 Results

3.2.1 Yeast two-hybrid assays

The yeast two-hybrid assay is a technique to detect protein-protein interactions (Fields & Song, 1989). This system utilises the properties of the *S.cerevisiae* Gal4 protein, a transcriptional activator that is required for gene expression encoding galactose utilising enzymes (Johnston, 1987). The Gal4 protein consists of two functionally essential domains: an N-terminal domain that binds to specific upstream activation DNA sequences (Keegan *et al.*, 1986) and a C-terminal domain containing the activating regions required to initiate transcription (Ma & Ptashne, 1987). These domains are referred to as the DNA binding domain (BD) and activation domain (AD), respectively. The yeast two-hybrid system (Figure 3-1) relies on the ability of two interacting proteins fused to either a Gal4 DNA BD or AD, both of which are required to form a functional Gal4 transcription factor, to activate transcription of a Gal4-responsive reporter gene (Keegan *et al.*, 1986). The protein product of the reporter gene allows growth of the auxotrophic yeast transformants on appropriate solid selective media. This provides a means by which protein-protein interactions can be visualised. Yeast two-hybrid assays were performed as outlined under section 2.12.2. Briefly, the appropriate yeast two-hybrid plasmid pairs (Figure 3-2) were co-transformed into *S.cerevisiae* strain AH109 (Table 2-4) as outlined under section 2.5.3. AH109 is auxotrophic for tryptophan, leucine, uracil and histidine and contains four Gal4-responsive reporter genes: *HIS3*, *ADE2*, *lacZ* and *MEL1* (James *et al.*, 1996). Yeast two-hybrid plasmids are engineered to carry either tryptophan, leucine or uracil nutritional genes, which allow for co-transformed yeast auxotrophs to be selected for on solid SD media lacking the appropriate dual combination of amino acids (denoted control). The reporter gene used in this study, *HIS3*, encodes the enzyme

imidazoleglycerol-phosphate dehydratase and catalyzes the sixth step in the biosynthesis of histidine (Struhl & Davis, 1977). A positive protein-protein interaction between the Gal4 DNA BD and AD fusion proteins results in the reconstitution of the BD and AD of the Gal4 transcription factor. This translates to successful activation of the Gal4-responsive reporter gene (*HIS3* in this case) which was detected by monitoring the ability of the co-transformed AH109 yeast strain to grow on solid SD media lacking the appropriate triple combination of amino acids (denoted -his).

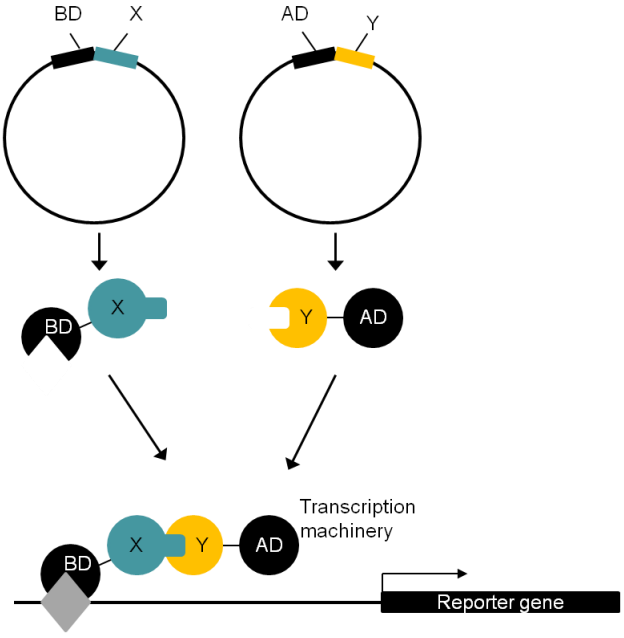

Figure 3-1. Yeast two-hybrid schematic
Protein-protein interaction between proteins X and Y, which are expressed as DNA BD and AD fusion proteins, respectively, brings the Gal4 BD and AD into close physical contact. This results in the reconstitution of the Gal4 transcription factor and subsequent activation of the Gal4-responsive reporter gene. Figure adapted from the Promega yeast two-hybrid system protein interaction guide.

The yeast two-hybrid parent vectors used in this study are depicted in Figure 3-2. Yeast two-hybrid plasmids used in this study are listed in Table 2-6. The Clontech Matchmaker Gal4 two-hybrid vectors pACT2 (Figure 3-2, A) and pGBKT7 (Figure 3-2, B) were used to generate fusion proteins of the Gal4 DNA AD and BD, respectively, of the following truncated versions of Tlg2: the cytosolic portion of Tlg2 (residues 1-309; $Tlg2_{cyto}$), the cytosolic portion of Tlg2 with the first 36 N-terminal amino acids truncated (residues 37-309; $Tlg2_{cyto}\Delta N36$) and the cytosolic portion of Tlg2 with the Habc domain truncated (residues 231-309; $Tlg2_{cyto}\Delta Habc$) (Figure 1-5). These vectors are also engineered to contain the human influenza

virus hemagglutinin (HA) (pACT2) and human p62 cMyc protein (pGBKT7) epitope tags which were utilised to confirm successful expression of the encoded Gal4 DNA BD and AD fusion proteins by immunoblot analysis using the appropriate antibody as described under section 2.12.2. Full-length Cog1, Cog2, Cog3 and Cog4 were expressed as Gal4 DNA AD and BD fusion proteins using vectors pGAD-C1 (Figure 3-2, C) and pGBDU-C1 (Figure 3-2, D), respectively (James *et al.*, 1996; Yen *et al.*, 2010). Vectors pGBDU-C1 and pGAD-C1 do not encode epitope tags. Therefore, successful expression of Cog1 to Cog4 AD and BD fusion proteins was confirmed by known positive interactions between the different Cog subunits (Fotso *et al.*, 2005; Ungar *et al.*, 2005).

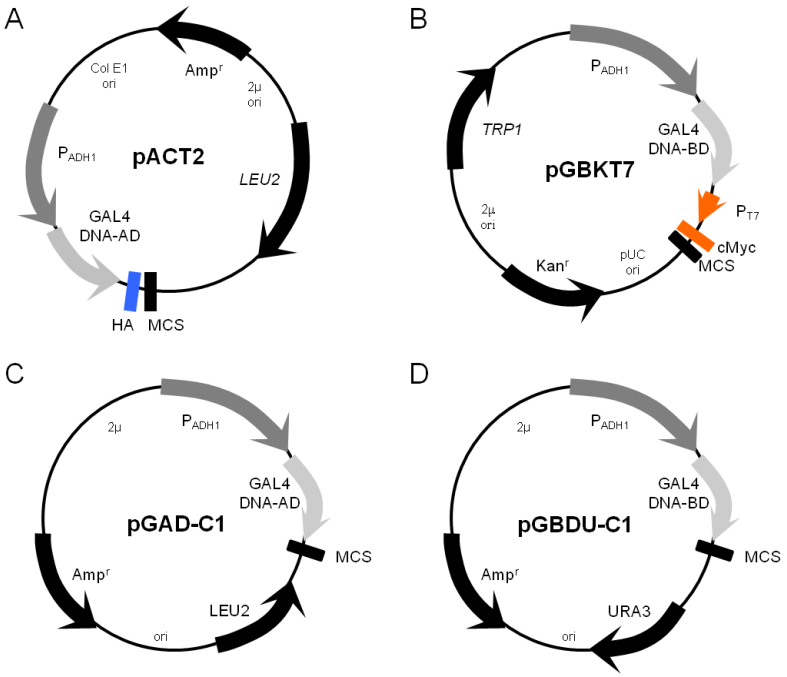

Figure 3-2. Yeast two-hybrid plasmids
Yeast two-hybrid parent vectors used in this study are depicted. Protein coding sequences for Tlg2 were cloned into the multiple cloning sites (MCS) of the Matchmaker pACT2 DNA AD (A) and pGBKT7 DNA BD (B) vectors. Full length Cog1 to Cog4 protein coding sequences were cloned into the MCS of the pGAD-C1 DNA AD (C) and pGBDU-C1 BD (D) vectors.

All yeast two-hybrid assays were performed with the appropriate positive and negative interaction controls. The p53 protein, an important regulator of cell proliferation, was originally identified as an interacting partner of the Large T antigen in SV40-transformed cells (Lane & Crawford, 1979). For this study, the interaction between the Gal4 BD p53 (encoded by plasmid pGBKT7-53 or pGBDU-53) and Gal4 AD SV40 Large T antigen (encoded by plasmid pTD1-1)

fusion proteins was routinely used as a positive interaction control. Plasmids pGBKT7-53 and pTD1-1 are derived from parent vectors pACT2 and pGBKT7, respectively (Figure 3-2, A and B, respectively). pGBDU-53 was generated by subcloning p53 from plasmid pGBKT7-53 into pGBDU-C1. Negative interaction controls were included by co-transforming plasmids encoding Gal4 AD and BD test fusion proteins (i.e. $Tlg2_{cyto}$, $Tlg2_{cyto}\Delta N36$, $Tlg2_{cyto}\Delta Habc$ and Cog1 to Cog4 Gal4 AD and BD fusion proteins) with either pGBKT7-53 or pGBDU-53 and pTD1-1, respectively.

Yeast two-hybrid assays were initially performed using Gal4 AD $Tlg2_{cyto}$, $Tlg2_{cyto}\Delta N36$ and $Tlg2_{cyto}\Delta Habc$ in combination with Gal4 BD Cog1 to Cog4 fusion proteins. These interactions were then repeated using Gal4 BD $Tlg2_{cyto}$, $Tlg2_{cyto}\Delta N36$ and $Tlg2_{cyto}\Delta Habc$ in combination with Gal4 AD Cog1 to Cog4 fusion proteins. Cog1 to Cog4 are collectively referred to as the lobe A subunits of the COG complex (Ungar *et al.*, 2005). These four COG complex subunits are essential for autophagy (Yen *et al.*, 2010) and it is based on this that I included these subunits in my study.

To determine if the Cog1 to Cog4 subunits physically interact with Tlg2, $Tlg2_{cyto}$ was co-expressed with Cog1 to Cog4. The Gal4 AD and BD plasmids encoding $Tlg2_{cyto}$ and Cog1 to Cog4, respectively, encode the nutritional genes *LEU2* and *URA3*. Thus, when co-transformed and expressed, AH109 host cells, which are auxotrophic for leucine and uracil, confer the ability to grow on solid SD media deficient in leucine and uracil (Figure 3-3, control panel). Yeast transformants that confer the ability to grow on leucine, uracil and histidine deficient selective agar (SD-leu,-ura-his, denoted as –his in Figure 3-3) indicate reconstitution of the Gal4 transcriptional factor and therefore a positive interaction between the transformed AD and BD fusion proteins. For all subsequent yeast two-hybrid figures lanes 1 to 4 indicate serial dilution of 1, 0.1, 0.001 and 0.0001, respectively. Co-transformed AD-$Tlg2_{cyto}$ and BD-Cog2 resulted in successful growth at a dilution factor of up to 0.1 (Figure 3-3, -his panel, lane 2). This is indicative of a positive protein-protein interaction. When AD-$Tlg2_{cyto}$ was co-transformed with BD-Cog1, BD-Cog3 and BD-Cog4 no growth was observed (Figure 3-3, -his panel) thereby suggesting no, or very weak, protein-protein interaction. In order to control for auto- and non-specific activation of the plasmid encoding AD-$Tlg2_{cyto}$ the ability of AD-$Tlg2_{cyto}$ to interact with BD-p53 (encoded by pGBDU-53) was tested. As expected this

combination produced no growth on selective agar deficient in leucine, uracil and histidine (Figure 3-3, -his panel) which suggests that auto-activation and non-specific binding between AD-Tlg2$_{cyto}$ and the other components of the assay are not responsible for activation of the histidine reporter gene. Therefore, any novel interaction observed between AD-Tlg2$_{cyto}$ and a previously unknown binding partner is likely to reflect a true interaction provided that the positive interaction control for BD-p53 and positive and negative interaction controls for BD-Cog1 to BD-Cog4 was also successful in the same set. The AD-Large T antigen and BD-p53 positive interaction control produced no growth on selective agar deficient in leucine, uracil and histidine (Figure 3-3, -his panel). This result suggests that the yeast two-hybrid assay, which is known to detect the strong interaction between p53 and the SV40 Large T antigen (Iwabuchi *et al.*, 1993), was unable detect this interaction on this occasion. This could be due to a number of factors. For example, differences in the level of transcriptional activation between the different plasmids encoding Gal4 DNA AD and BD fusion proteins may give rise to the observed variability between interactions (Durfee *et al.*, 1993). Failure of any growth produced by the p53 and SV40 Large T antigen positive interaction control renders all of the above interactions inconclusive. Yeast two-hybrid interactions for AD-Tlg2$_{cyto}\Delta$N36 (Figure 3-4) and AD-Tlg2$_{cyto}\Delta$Habc (Figure 3-5) were performed in parallel with the above. Positive interaction controls for BD-Cog1 to BD-Cog4 for the series of AD-Tlg2$_{cyto}$, AD-Tlg2$_{cyto}\Delta$N36 and AD-Tlg2$_{cyto}\Delta$Habc interactions with BD-Cog1 to BD-Cog4 are presented in Figure 3-6 and will be discussed at the end of this series of experiments. The interactions presented in Figure 3-3 were repeated on at least three separate occasions with each producing different results. This variability highlights the importance of including the appropriate positive and negative interaction controls. Successful expression of all of the above fusion protein constructs were assessed in parallel with the yeast two-hybrid experiments (refer to Figure 3-7) and were prepared as outlined under section 2.12.2 (summarised in Figure 2-5).

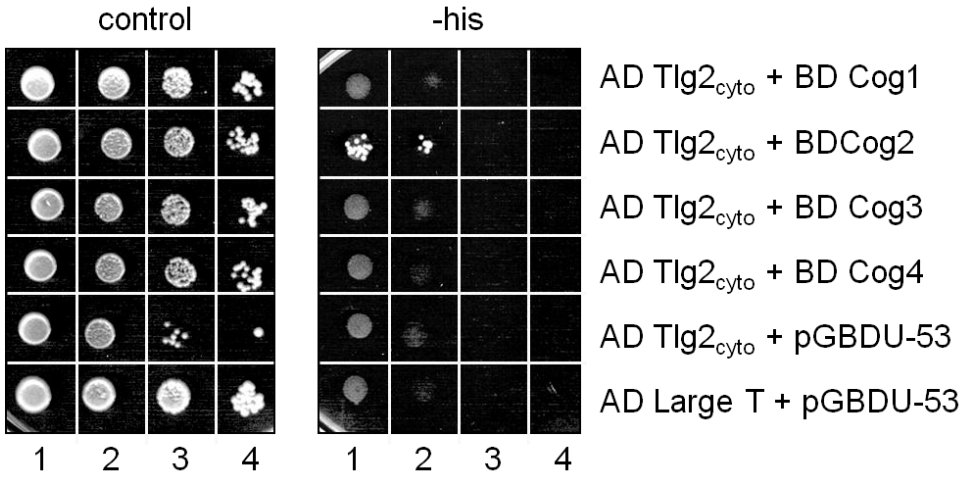

Figure 3-3. Yeast two-hybrid interactions between AD-Tlg2$_{cyto}$ and BD Cog constructs
A single colony of each double transformant was inoculated into 10 ml SD minimal media deficient in the amino acids leucine and uracil (SD-leu-ura) and incubated overnight at 30°C. Cells were diluted to an OD_{600} of 0.2 in fresh SD-leu-ura media the following day and further incubated at 30°C until an OD_{600} of 1.0. Cells were harvested and resuspended at an OD_{600} of 1.0 in sterile dH_2O. Ten-fold serial dilutions were prepared for each culture to generate samples with an OD_{600} of 1.0, 0.1, 0.01 and 0.001. 5 µl of each dilution was spotted out in triplicate onto solid SD-leu-ura (control panel) and SD-leu-ura-his (-his panel). All plates were then incubated upside-down at 30°C. Yeast growth was recorded after 3 to 5 days.

To further investigate if Tlg2 and Cog1 to Cog4 interact, two additional truncated versions of Tlg2 was employed in order to map the specific domains of Tlg2 responsible for mediating any observed associations with the COG subunits. The first 36 N-terminal residues of Tlg2 mediates binding to its SM protein Vps45 via a so-called mode 2 interaction (Dulubova *et al.*, 2002; Carpp *et al.*, 2006). To investigate if the N-terminal peptide of Tlg2 also mediates association with COG subunits, AD-Tlg2$_{cyto}$ΔN36 was co-transformed with BD-Cog1 to BD-Cog4 into *S.cerevisiae* strain AH109 (section 2.5.3) and subsequently assessed for growth on the appropriate solid SD media. Successful co-transformation was assessed by growth of double transformants on solid SD media deficient in leucine and uracil (Figure 3-4, control panel). All double transformants produced growth thereby indicating successful expression of the fusion proteins encoded by the transformed plasmids. Positive interaction was assessed by growth of double transformants on solid SD media deficient in leucine, uracil and histidine (Figure 3-4, -his panel). No growth was observed for AD-Tlg2$_{cyto}$ΔN36 and BD-Cog1, BD-Cog2 and BD-Cog3 whereas a weak interaction was seen for AD-Tlg2$_{cyto}$ΔN36 and BD-Cog4 (Figure 3-4, -his panel). Both the negative AD-Tlg2$_{cyto}$ΔN36 and BD-p53 and positive AD-Large T antigen and BD-p53 interactions were successful. Based on these results

the interaction between AD-Tlg2$_{cyto}$ΔN36 and BD-Cog4 likely reflects a true interaction.

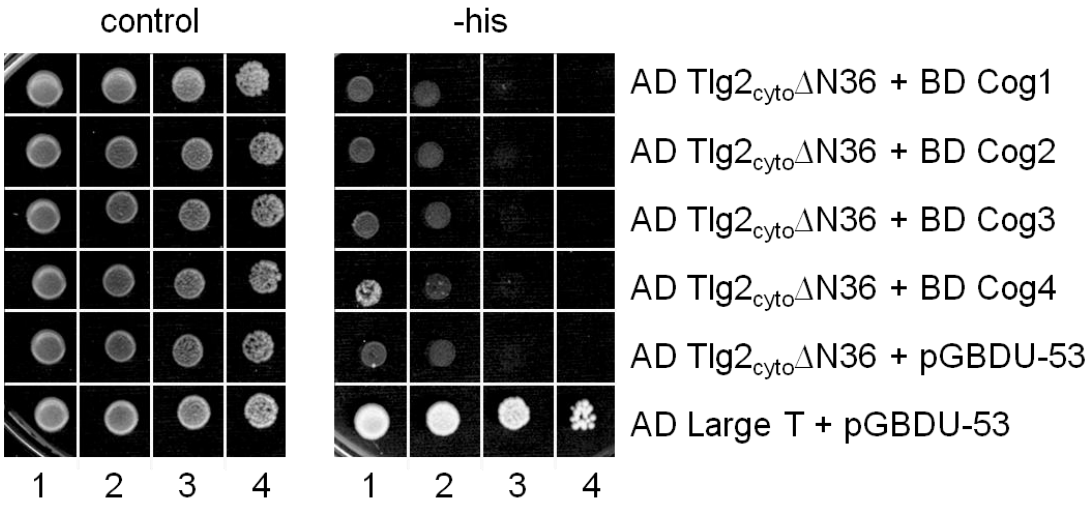

Figure 3-4. Yeast two-hybrid interactions between AD Tlg2$_{cyto}$ΔN36 and BD Cog constructs
A single colony of each double transformant was inoculated into 10 ml SD minimal media deficient in the amino acids leucine and uracil (SD-leu-ura) and incubated overnight at 30°C. Cells were diluted to an OD_{600} of 0.2 in fresh SD-leu-ura media the following day and further incubated at 30°C until growth reached mid-log phase. Cells were harvested and resuspended at an OD_{600} of 1.0 in sterile dH_2O. Serial dilutions were prepared for each culture to generate samples with an OD_{600} of 1.0, 0.1, 0.01 and 0.001. 5 µl of each dilution was spotted out in triplicate onto solid SD-leu-ura (control panel) and SD-leu-ura-his (-his panel). All plates were then incubated upside-down at 30°C and yeast growth was recorded after 3 to 5 days.

The SNARE domain of Tlg2 mediates binding to the corresponding SNARE domains of its interacting partners Tlg1, Vti1 and Snc2 (Abeliovich *et al.*, 1998; Holthuis *et al.*, 1998a) to form a stable SNARE complex (Sutton *et al.*, 1998; Jahn & Scheller, 2006). More recently sequence and structural homology between the MUN domain of Munc13 and subunits of a number of evolutionarily conserved tethering complexes, including Cog4, have been detected (Pei *et al.*, 2009; Li *et al.*, 2011). The significance of this finding lies in the ability of the MUN domain of Munc13 to bind weakly to the SNARE domain of neuronal Syntaxin 1 thereby promoting SNARE complex formation possibly by accelerating the opening of Syntaxin 1(Ma *et al.*, 2011). In order to determine if the SNARE domain of Tlg2 is also important for mediating binding to Cog1 to Cog4, AD-Tlg2$_{cyto}$ΔHabc was assessed for growth on solid SD media deficient in leucine and uracil (Figure 3-5, control panel) or leucine, uracil and histidine (Figure 3-5, -his panel) when co-transformed with BD-Cog1 to BD-Cog4. All double transformants were successful (Figure 3-5, control panel). No growth and therefore no interactions were observed for AD-Tlg2$_{cyto}$ΔHabc and BD-Cog1 to BD-Cog4. As before, both the positive AD-

Tlg2$_{cyto}$ΔHabc and BD-p53 and negative AD-Large T and BD-p53 interaction controls were successful (Figure 3-5). These results suggest that the SNARE domain is not involved in mediating interactions between Cog1 to Cog4 and Tlg2 however further and more powerful methods of investigation will be required to confirm this observation (refer to section 3.2.2).

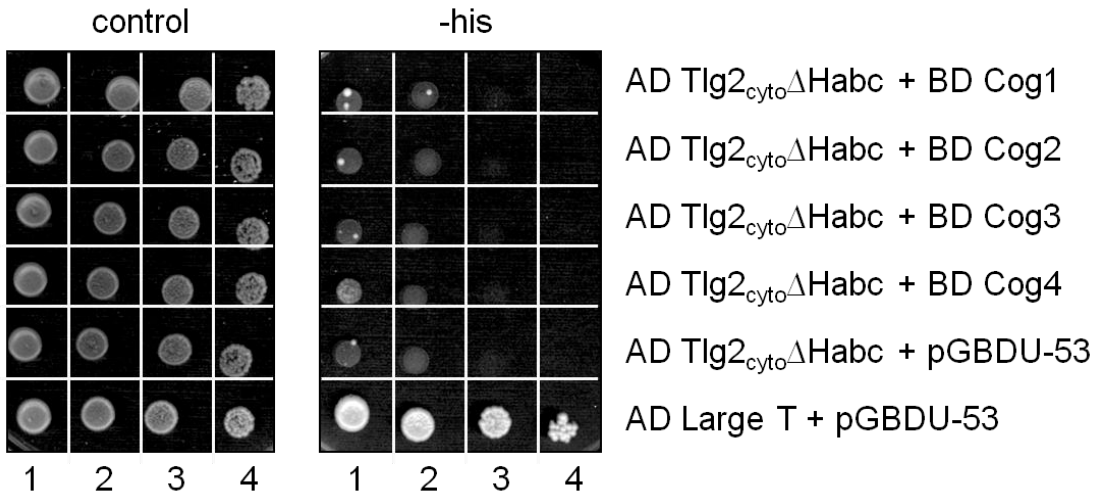

Figure 3-5. Yeast two-hybrid interactions between AD-Tlg2$_{cyto}$ΔHabc and BD Cog constructs
A single colony of each double transformant was inoculated into 10 ml SD minimal media deficient in the amino acids leucine and uracil (SD-leu-ura) and incubated overnight at 30°C. Cells were diluted to an OD_{600} of 0.2 in fresh SD-leu-ura media the following day and further incubated at 30°C until an OD_{600} of 1.0. Cells were harvested and resuspended at an OD_{600} of 1.0 in sterile dH_2O. Ten-fold serial dilutions were prepared for each culture to generate samples with an OD_{600} of 1.0, 0.1, 0.01 and 0.001. 5 µl of each dilution was spotted out in triplicate onto solid SD-leu-ura (control panel) and SD-leu-ura-his (-his panel). All plates were then incubated upside-down at 30°C. Yeast growth was recorded after 3 to 5 days.

Plasmids encoding BD and AD Cog1 to Cog4 do not encode an epitope tag. As an alternative approach to confirm successful protein expression of these constructs, positive interaction controls were included (Figure 3-6, A). These were based on previously reported positive interactions between the respective Cog subunits (Fotso *et al.*, 2005; Ungar *et al.*, 2005). All plasmids encoding AD Cog subunits also encode a *LEU2* selection marker; plasmids encoding BD Cog subunits encode a *URA3* selection marker. Successful co-transformation of the respective Cog positive interaction controls was assessed by growth on solid SD media deficient in leucine and uracil. All Cog positive control double transformants were successful (Figure 3-6, A, control panel). Positive interactions between the appropriate Cog subunits were assessed for growth on solid media deficient in luecine, uracil and histidine (Figure 3-6, A, -his panel). Only the combination between AD-Cog1 and BD-Cog3 produced any growth. Considering that all of the

positive interaction control combinations used in this study have previously been shown to interact we can assume that the yeast two-hybrid assay exhibited low sensitivity for protein-protein interactions on this occasion. Non-specific and/or auto-activation of the histidine reporter gene by BD-Cog1 to BD-Cog4 constructs were excluded for this series of experiments by the inclusion of negative BD-Cog1 to BD-Cog4 and AD-Large T antigen controls (Figure 3-6, B).

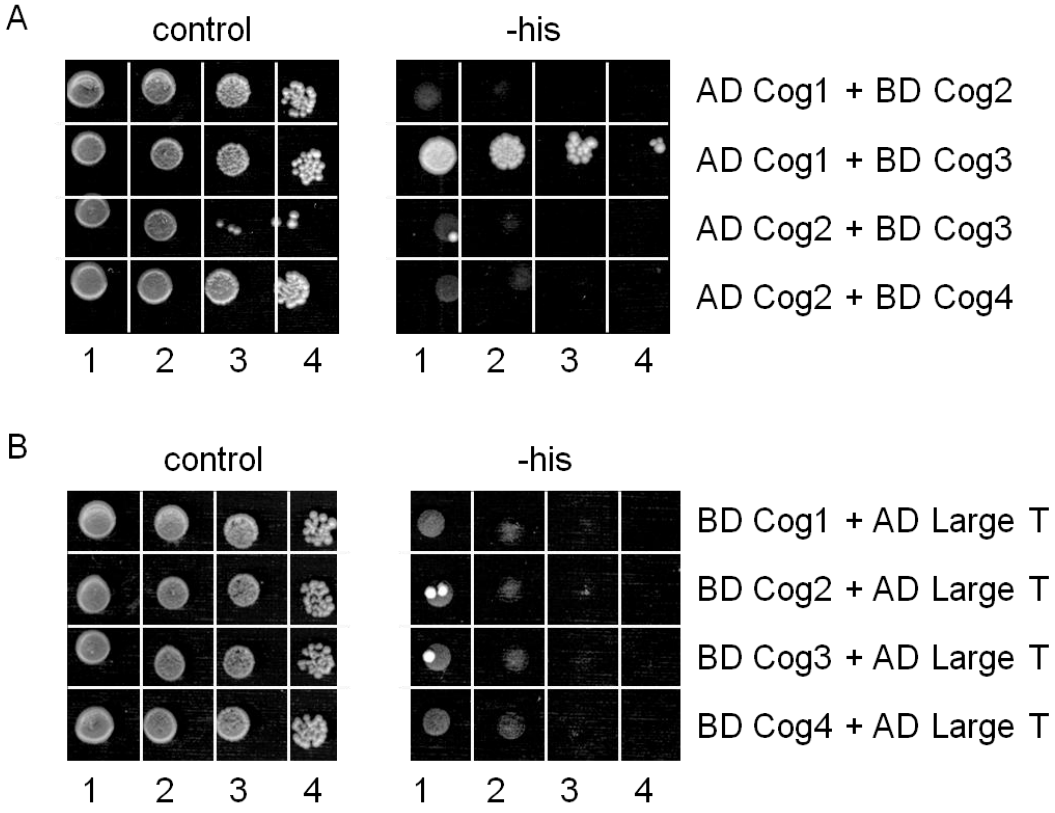

Figure 3-6. Yeast two-hybrid positive and negative interaction controls for BD Cog constructs

A single colony of each double transformant (A and B) was inoculated into 10 ml SD minimal media deficient in the amino acids leucine and uracil (SD-leu-ura) and incubated overnight at 30°C. Cells were diluted to an OD_{600} of 0.2 in fresh SD-leu-ura media the following day and further incubated at 30°C until an OD_{600} of 1.0. Cells were harvested and resuspended at an OD_{600} of 1.0 in sterile dH_2O. Ten-fold serial dilutions were prepared for each culture to generate samples with an OD_{600} of 1.0, 0.1, 0.01 and 0.001. 5 µl of each dilution was spotted out in triplicate onto solid SD-leu-ura (control panel) and SD-leu-ura-his (-his panel). All plates were then incubated upside-down at 30°C. Yeast growth was recorded after 3 to 5 days.

Plasmids encoding AD-$Tlg2_{cyto}$, AD-$Tlg2_{cyto}\Delta N36$ and AD-$Tlg2_{cyto}\Delta Habc$ fusion proteins also encode an HA epitope tag. Expression of AD-$Tlg2_{cyto}$, AD-$Tlg2_{cyto}\Delta N36$ and AD-$Tlg2_{cyto}\Delta Habc$ fusion proteins was confirmed by SDS-PAGE (section 2.3.1) followed by immunoblot analysis (sections 2.3.3 and 2.3.4) of all double transformant whole cell lysates (prepared as described under sections 2.5.4.1 and 2.12.2) using anti-HA antibody (Figure 3-7, A, B and C, respectively).

These lysates were prepared from the same yeast cultures used for the yeast two-hybrid experiments (i.e. they were prepared in parallel).

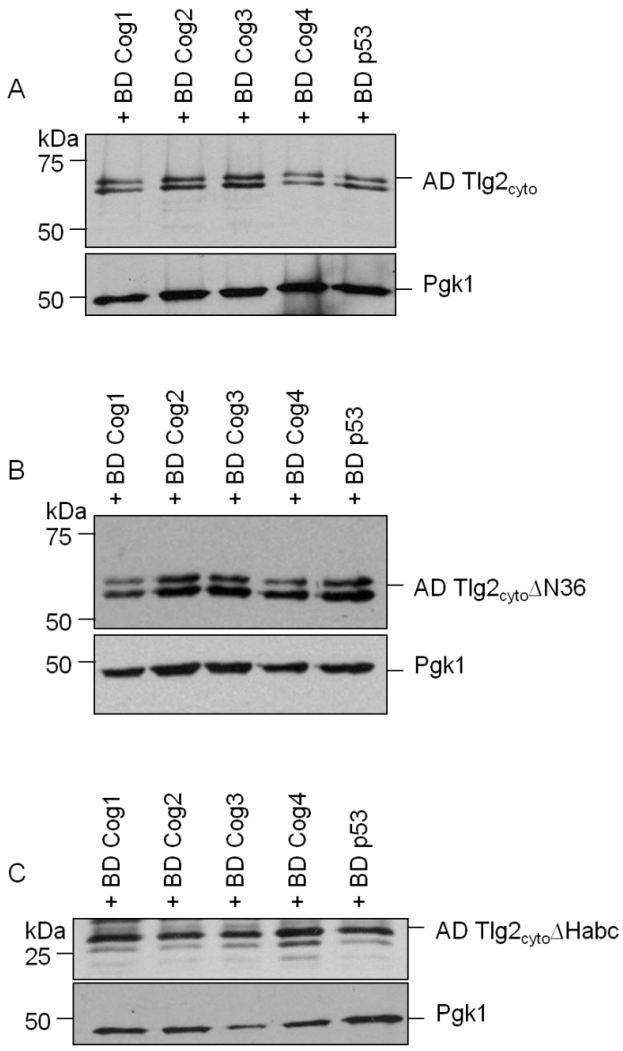

Figure 3-7. Expression of the yeast two-hybrid AD-Tlg2$_{cyto}$, AD-Tlg2$_{cyto}$∆N36 and AD-Tlg2$_{cyto}$∆Habc fusion proteins
Plasmids encoding Gal4 DNA activating domain (AD) Tlg2$_{cyto}$ (A), Tlg2$_{cyto}$∆N36 (B) and Tlg2$_{cyto}$∆Habc (C) fusion proteins, all of which also encode an HA epitope tag, were co-transformed into *S.cerevisiae* strain AH109 with plasmids encoding Gal4 DNA binding domain (BD) Cog1 to Cog4 or BD-p53 (encoded by plasmid pGBDU-p53) fusion proteins. Double transformants were grown to mid-log phase in SD media deficient in leucine and uracil (SD-leu-ura). Whole cell lysates were prepared from equal cell numbers of the double transformants. Equal volumes of proteins contained within the whole cell lysates were resolved by SDS-PAGE followed by immunoblot analysis using anti-HA antibody to detect AD Tlg2$_{cyto}$ (A), Tlg2$_{cyto}$∆N36 (B) and Tlg2$_{cyto}$∆Habc (C). Membranes were subsequently probed for phosphoglycerate kinase 1 (Pgk1; 44.7 kDa) using anti-Pgk1 antibody to control for equal loading across all samples (lower panel, A, B and C). These results are representative of 3 independent experiments (n=3).

All of the above yeast two-hybrid interactions were repeated using BD-Tlg2$_{cyto}$, BD-Tlg2$_{cyto}$∆N36 and BD-Tlg2$_{cyto}$∆Habc in combination with AD-Cog1 to AD-Cog4. The Gal4 DNA BD and AD plasmids encoding Tlg2$_{cyto}$, Tlg2$_{cyto}$∆N36 and

Tlg2$_{cyto}$ΔHabc and Cog1 to Cog4, respectively, encode the nutritional genes *TRP1* and *LEU2*. BD-Tlg2$_{cyto}$ (Figure 3-8), BD-Tlg2$_{cyto}$ΔN36 (Figure 3-9) or BD-Tlg2$_{cyto}$ΔHabc (Figure 3-10) were co-transformed with plasmids encoding AD-Cog1 to AD-Cog4. Positive BD-p53 (encoded by pGBKT7-53) and AD-Large T antigen and negative BD-Tlg2$_{cyto}$, BD-Tlg2$_{cyto}$ΔN36, BD-Tlg2$_{cyto}$ΔHabc and AD-Large T antigen interaction controls were also included. Successful co-transformation and expression of the encoded proteins were assessed by growth on solid SD media deficient in tryptophan and leucine, all of which were positive for growth (Figure 3-8, Figure 3-9, Figure 3-10, control panel). Positive growth was observed for all co-transformations between BD-Tlg2$_{cyto}$ (Figure 3-8) or BD-Tlg2$_{cyto}$ΔN36 (Figure 3-9) and AD-Cog1 to AD-Cog4 when grown on solid SD media deficient in tryptophan, leucine and histidine (-his panel). This is indicative of a positive protein-protein interaction. However, since the negative BD-Tlg2$_{cyto}$ (Figure 3-8, -his panel) or BD-Tlg2$_{cyto}$ΔN36 (Figure 3-9, -his panel) and AD-Large T antigen interaction controls also resulted in growth more stringent selection criteria was employed in order to eliminate any background histidine expression from the *HIS3* reporter gene in the absence of a two-hybrid interaction. This was achieved by the addition of 10 mM of the compound 3-aminotriazole (3AT) to the selective agar deficient in tryptophan, leucine and histidine (denoted –his, +10 mM 3AT). 3AT specifically inhibits the protein product of the *HIS3* gene in a dose-dependent manner thereby minimising the effects of *HIS3* auto-activation (Kishore & Shah, 1988). The low concentration (10 mM) of 3AT relative to that previously used (Reddi & Kumar, 2004) inhibited all previously positive growth produced on solid SD media deficient in tryptophan, leucine and histidine with the exception of the positive BD-p53 and AD-Large T antigen interaction control (Figures 3-8, 3-9 and 3-10). These results either suggest a very weak interaction between the proteins encoded by the BD-Tlg2 and AD-Cog1 to AD-Cog4 constructs, or that these proteins do not interact at all. A complete set of negative AD-Cog1 to AD-Cog4 and BD-p53 controls were included for this series of experiments (Figure 3-11) as a means of excluding auto- or non-specific activation of the *HIS3* reporter gene. Co-transformations and expression of the negative interaction controls were successful, as indicated by positive growth on solid SD media deficient in tryptophan and leucine (Figure 3-11, control panel). As expected, no growth was detected on solid SD-his (Figure 3-11). This indicates that the AD-Cog1 to AD-Cog4 constructs did not result in *HIS3* activation in the absence of a positive protein-protein interaction. A positive AD-Cog2 and BD-Cog1 interaction control

was included for this series of experiments (Figure 3-11). The requirement for a whole series of Cog positive interaction controls only came to my realisation later on during these experiments. I have included the appropriate positive Cog interaction controls for all subsequent yeast-two hybrid assays (refer to Figure 3-6).

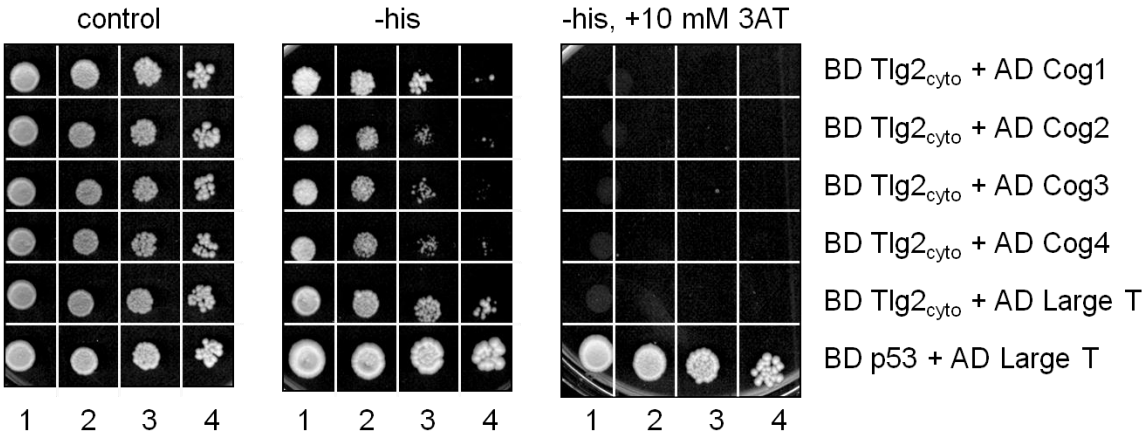

Figure 3-8. Yeast two-hybrid interactions between BD-Tlg2$_{cyto}$ and AD Cog constructs
A single colony of each double transformant was inoculated into 10 ml SD minimal media deficient in the amino acids tryptophan and leucine (SD-trp-leu) and incubated overnight at 30°C. Cells were diluted to an OD_{600} of 0.2 in fresh SD-trp-leu media the following day and further incubated at 30°C until an OD_{600} of 1.0. Cells were harvested and resuspended at an OD_{600} of 1.0 in sterile dH_2O. Ten-fold serial dilutions were prepared for each culture to generate samples with an OD_{600} of 1.0, 0.1, 0.01 and 0.001. 5 µl of each dilution was spotted out in triplicate onto solid SD-trp-leu (control panel), SD-trp-leu-his (-his panel) and SD-trp-leu-his containing 10 mM 3AT (-his, +10 mM 3AT). All plates were then incubated upside-down at 30°C. Yeast growth was recorded after 3 to 5 days.

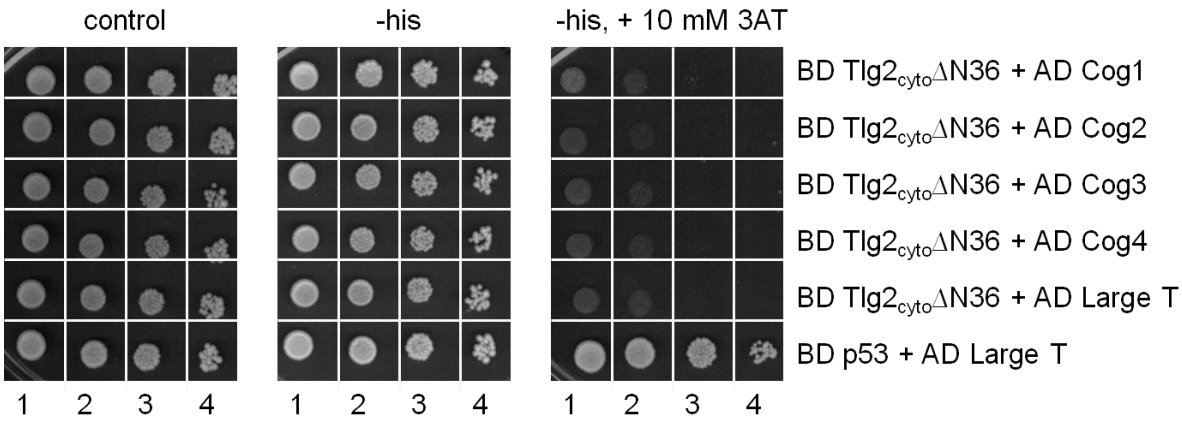

Figure 3-9. Yeast two-hybrid interactions between BD-Tlg2$_{cyto}$ΔN36 and AD Cog constructs
A single colony of each double transformant was inoculated into 10 ml SD minimal media deficient in the amino acids tryptophan and leucine (SD-trp-leu) and incubated overnight at 30°C. Cells were diluted to an OD_{600} of 0.2 in fresh SD-trp-leu media the following day and further incubated at 30°C until an OD_{600} of 1.0. Cells were harvested and resuspended at an OD_{600} of 1.0 in sterile dH_2O. Ten-fold serial dilutions were prepared for each culture to generate samples with an OD_{600} of 1.0, 0.1, 0.01 and 0.001. 5 µl of each dilution was spotted out in triplicate onto solid SD-trp-leu (control panel), SD-trp-leu-his (-his panel) and SD-trp-leu-his containing 10 mM 3AT (-his, +10 mM 3AT). All plates were then incubated upside-down at 30°C. Yeast growth was recorded after 3 to 5 days.

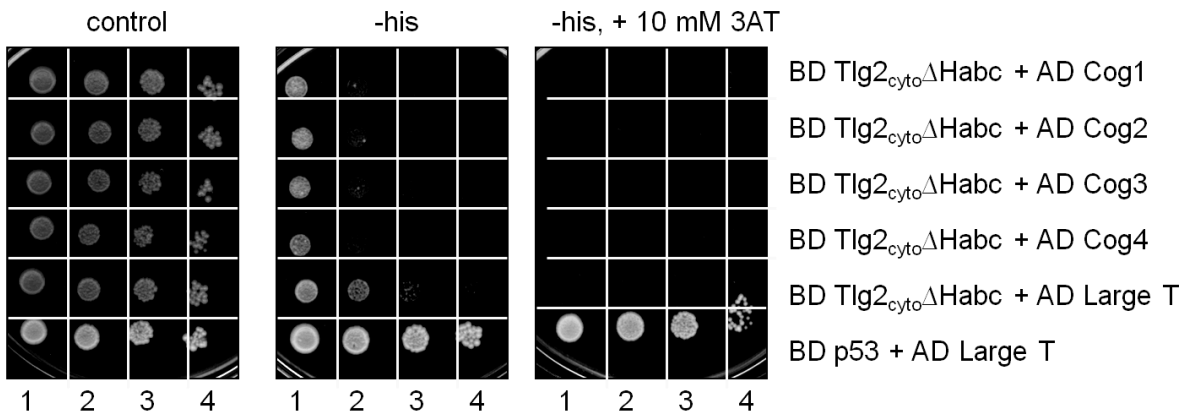

Figure 3-10. Yeast two-hybrid interactions between BD-Tlg2$_{cyto}$ΔHabc and AD Cog constructs

A single colony of each double transformant was inoculated into 10 ml SD minimal media deficient in the amino acids tryptophan and leucine (SD-trp-leu) and incubated overnight at 30°C. Cells were diluted to an OD_{600} of 0.2 in fresh SD-trp-leu media the following day and further incubated at 30°C until an OD_{600} of 1.0. Cells were harvested and resuspended at an OD_{600} of 1.0 in sterile dH_2O. Ten-fold serial dilutions were prepared for each culture to generate samples with an OD_{600} of 1.0, 0.1, 0.01 and 0.001. 5 µl of each dilution was spotted out in triplicate onto solid SD-trp-leu (control panel), SD-trp-leu-his (-his panel) and SD-trp-leu-his containing 10 mM 3AT (-his, +10 mM 3AT). All plates were then incubated upside-down at 30°C. Yeast growth was recorded after 3 to 5 days.

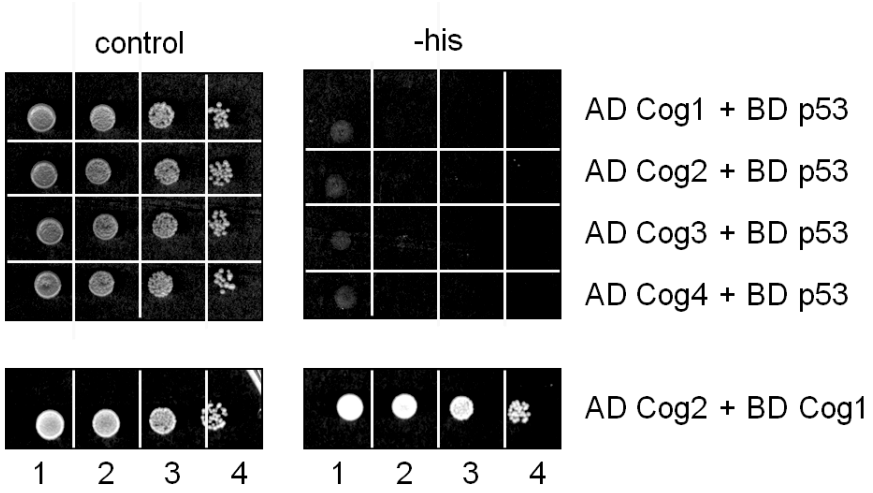

Figure 3-11. Yeast two-hybrid negative and positive interaction controls for AD Cog constructs
A single colony of each double transformant was inoculated into 10 ml SD minimal media deficient in the amino acids tryptophan and leucine (SD-trp-leu) and incubated overnight at 30°C. Cells were diluted to an OD_{600} of 0.2 in fresh SD-trp-leu media the following day and further incubated at 30°C until an OD_{600} of 1.0. Cells were harvested and resuspended at an OD_{600} of 1.0 in sterile dH_2O. Ten-fold serial dilutions were prepared for each culture to generate samples with an OD_{600} of 1.0, 0.1, 0.01 and 0.001. 5 µl of each dilution was spotted out in triplicate onto solid SD-trp-leu (control panel) and SD-trp-leu-his (-his panel). All plates were then incubated upside-down at 30°C. Yeast growth was recorded after 3 to 5 days.

Plasmids encoding BD -Tlg2$_{cyto}$, BD-Tlg2$_{cyto}$ΔN36 and BD-Tlg2$_{cyto}$ΔHabc fusion proteins also encode a cMyc epitope tag. Expression of BD-Tlg2$_{cyto}$, BD-Tlg2$_{cyto}$ΔN36 and BD-Tlg2$_{cyto}$ΔHabc fusion proteins was confirmed by SDS-PAGE (section 2.3.1) followed by immunoblot analysis (sections 2.3.3 and 2.3.4) of all double transformant whole cell lysates (prepared as described under sections 2.5.4.1 and 2.12.2) using anti-cMyc antibody (Figure 3-12).

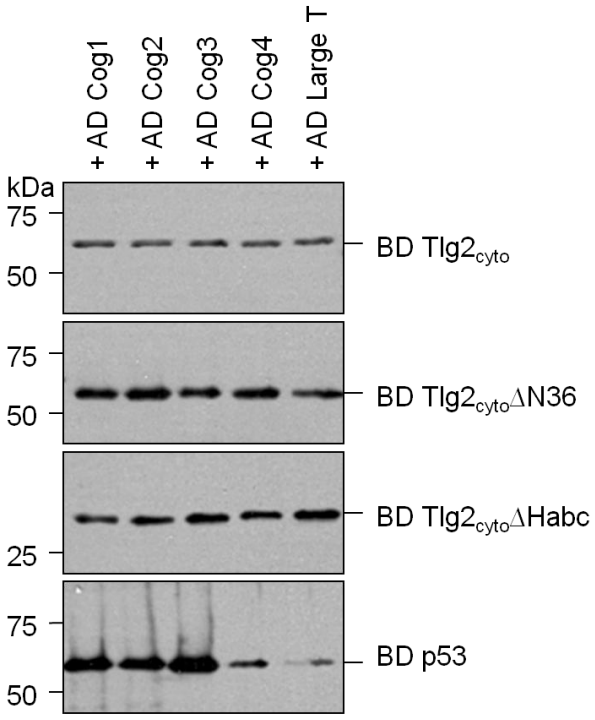

Figure 3-12. Expression of the yeast two-hybrid BD-Tlg2$_{cyto}$, BD-Tlg2$_{cyto}$∆N36, BD-Tlg2$_{cyto}$∆Habc and BD-p53 fusion proteins
Plasmids encoding Gal4 DNA binding domain (BD) Tlg2$_{cyto}$, Tlg2$_{cyto}$∆N36, Tlg2$_{cyto}$∆Habc and p53 (encoded by plasmid pGBKT7-53) fusion proteins, all of which also encode a cMyc epitope tag, were co-transformed into *S.cerevisiae* strain AH109 with plasmids encoding Gal4 DNA activating domain (AD) Cog1 to Cog4 or SV40 large T antigen (encoded by plasmid pTD1-1) fusion proteins. Double transformants were grown to mid-log phase in SD media deficient in leucine and tryptophan (SD-leu-trp). Whole cell lysates were prepared from equal cell numbers of the double transformants. Equal volumes of proteins contained within the whole cell lysates were resolved by SDS-PAGE followed by immunoblot analysis using anti-cMyc antibody to detect BD Tlg2$_{cyto}$, Tlg2$_{cyto}$∆N36, Tlg2$_{cyto}$∆Habc and p53. These results are representative of 3 independent experiments (n=3).

3.2.1.1 Summary of yeast two-hybrid interactions

A summary of the yeast two-hybrid interactions for this study is presented Table 3-1.

Table 3-1 Summary of yeast two-hybrid interactions

	BD-Cog1	BD-Cog2	BD-Cog3	BD-Cog4
AD-Tlg2$_{cyto}$	-	yes	-	-
AD-Tlg2$_{cyto}$∆N36	-	-	-	yes
AD-Tlg2$_{cyto}$∆Habc	-	-	-	-
	AD-Cog1	**AD-Cog2**	**AD-Cog3**	**AD-Cog4**
BD-Tlg2$_{cyto}$	-	-	-	-
BD-Tlg2$_{cyto}$∆N36	-	-	-	-
BD-Tlg2$_{cyto}$∆Habc	-	-	-	-

In addition to differential transcriptional activity it is worth noting that the yeast two-hybrid system is intrinsically prone to producing a large number of false positives possibly due to the leaky *HIS3* reporter gene (Bartel *et al.*, 1993). Moreover, the yeast two-hybrid assay has also been reported to produce false negative in the order of 70-90% (Stellberger *et al.*, 2010). This, together with the previously reported observation that SNARE and Cog proteins weakly associate (Ma *et al.*, 2011) emphasizes the importance of confirming any observed protein-protein associations using alternative and more powerful methods. The inconsistent results obtained for my yeast two-hybrid assays presented here were partially overcome by subsequently repeating all of the yeast two-hybrid interactions using either GST or PrA pull-down assays (performed as described under section 2.12.1). For these series of experiments protein interactions between the different Tlg2 constructs and full-length cytosolic versions of its partner SNARE proteins Tlg1, Vti1 and Snc2, were also assessed.

3.2.2 Pull-down assays

Pull-down assays were employed as a complementary approach to the yeast two-hybrid assay (section 3.2.1) to determine direct physical interaction between members of the yeast endosomal SNARE complex (i.e. Tlg2, Tlg1, Vti1 and Snc2) and subunits of the COG complex. Recombinant fusion protein purification and subsequent pull-down assay results from these experiments are presented below.

3.2.2.1 Expression and purification of recombinant fusion proteins

The well characterised interaction between *S.aureus* PrA and mammalian IgG (Langone, 1982) was employed to purify recombinant PrA-tagged fusion proteins produced in *E.coli* using IgG coated Sepharose beads as described under section 2.11.6. To determine if subunits of the COG complex interact with Tlg2, three different truncated versions of Tlg2 containing C-terminal tagged PrA were produced, as well as PrA by itself, which was included as a negative binding control for all PrA pull-down assays performed. Protein samples were collected at different stages during the purification process for all recombinant fusion proteins. These samples were analysed by SDS-PAGE (section 2.3.1) followed by Coomassie™ blue staining (section 2.3.2) to assess the purity of each of the purified proteins. The first of the Tlg2 constructs contained the entire cytosolic portion of Tlg2 (residues 1-318, denoted $Tlg2_{cyto}$-PrA) (Figure 3-13) and was

expressed from plasmid pCOG025 (Carpp *et al.*, 2006). This construct produced a protein with a molecular weight of 51 kDa. Truncated versions of the cytosolic portion of Tlg2 lacking the first N-terminal 36 amino acids (containing residues 37-309, denoted $Tlg2_{cyto}\Delta$N36-PrA) (Figure 3-13) or the SNARE domain (containing residues 231-309, denoted $Tlg2_{cyto}\Delta$Habc-PrA) (Figure 3-13) was expressed from plasmids pCOG026 (Carpp *et al.*, 2006) and pCOG027. These two constructs produced protein products with molecular weights of 47 kDa and 24 kDa, respectively. Recombinant PrA was expressed from plasmid pCOG022 (Carpp *et al.*, 2006). This plasmid encodes two tandem repeats of PrA thereby producing a protein product with a molecular weight of 15 kDa (Figure 3-13). As mentioned previously, IgG coated Sepharose beads were used to capture and thereby purify all PrA-tagged recombinant fusion proteins. Therefore, the presence of the IgG heavy (50 kDa) and light chains (25 kDa) are visible in the beads before and after samples during the purification process on the Coomassie™ blue stained gels.

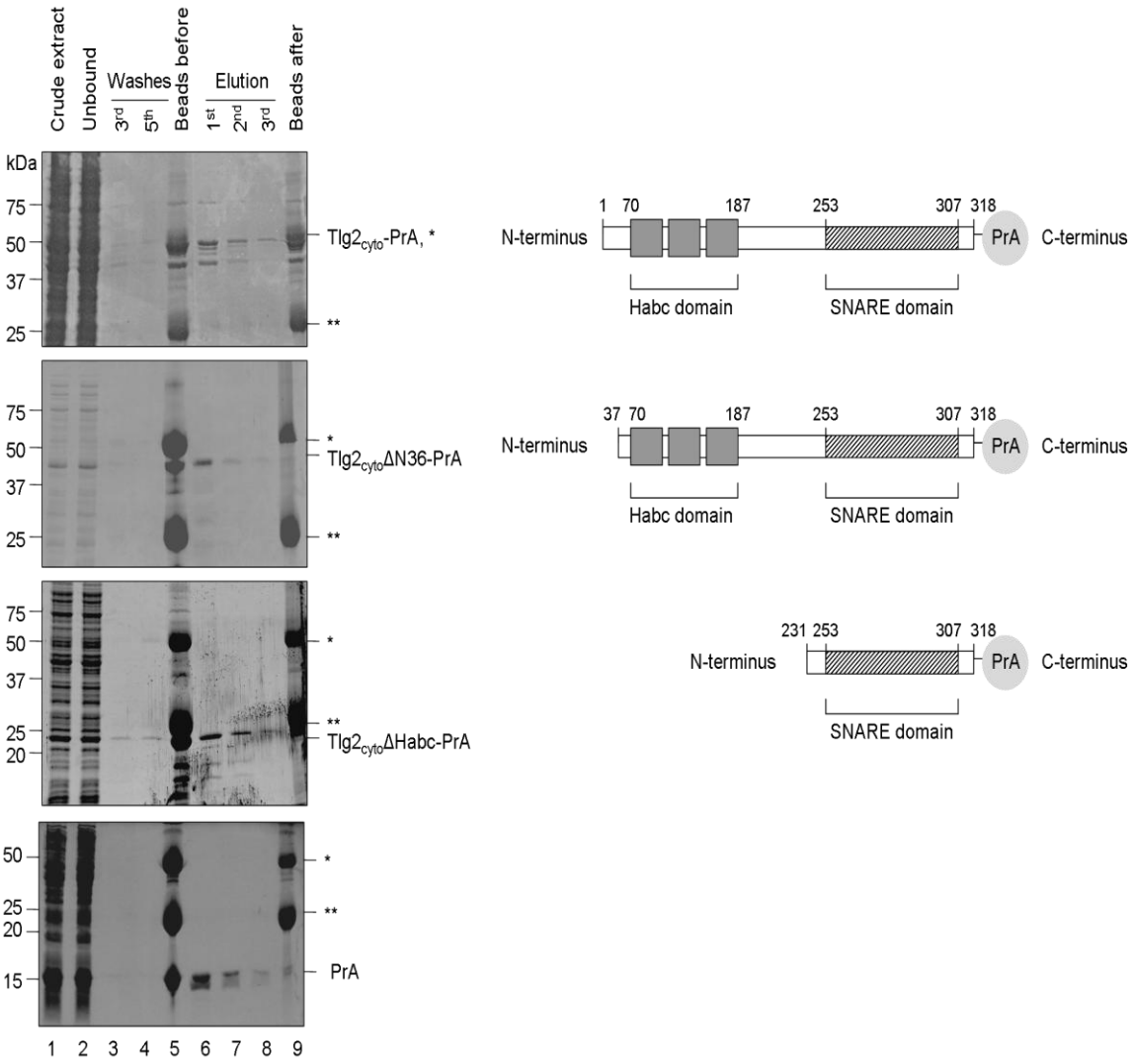

Figure 3-13. Expression and purification of PrA and PrA-tagged Tlg2 constructs
Recombinant PrA-tagged $Tlg2_{cyto}$-PrA, $Tlg2_{cyto}\Delta N36$, $Tlg2_{cyto}\Delta Habc$ and PrA were produced from plasmids pCOG025, pCOG026, pCOG027 and pCOG022. The ORF encoding these proteins were expressed in BL21 StarTM (DE3) bacterial cells and purified from 3, 6, 1 and 6 litres of culture, respectively. SDS-PAGE followed by Coomassie™ blue staining was employed to assess the purity of the protein at different stages during the purification procedure (left hand column). Equal volumes (8 µl) of each sample were analysed. Soluble protein (lane 1) was purified using IgG Sepharose beads. Unbound soluble protein (lane 2) was thoroughly washed from the beads (lanes 3 and 4) and the protein bound to the beads was assessed before (lane 5) and after (lane 9) elution (lanes 6, 7 and 8). IgG heavy (*) and light (**) chains are present at 50 and 25 kDa, respectively (lanes 5 and 9). Positions of molecular weight markers (in kDa) are indicated on the left. Schematic diagrams of the PrA-tagged Tlg2 constructs are presented in the right hand column.

Protein-protein interactions between Tlg2 partner SNARE proteins Snc2, Vti1 and Tlg1 and COG complex subunits were also assessed during this study. The cytosolic portion of Snc2 containing a C-terminal tagged PrA moiety (residues 1-88, denoted $Snc2_{cyto}$-PrA) was recombinantly expressed from plasmid pCOG045 and subsequently purified (Figure 3-14). This construct produced a protein that appears at approximately 30 kDa, which is consistent with previous reports (Carpp *et al.*, 2006). A C-terminally tagged PrA version of the cytosolic portion of Vti1 (residues 1-187, denoted $Vti1_{cyto}$-PrA) was expressed from plasmid pCOG048 (Carpp *et al.*, 2006). As expected, this construct produced a purified protein with a molecular weight of 37 kDa.

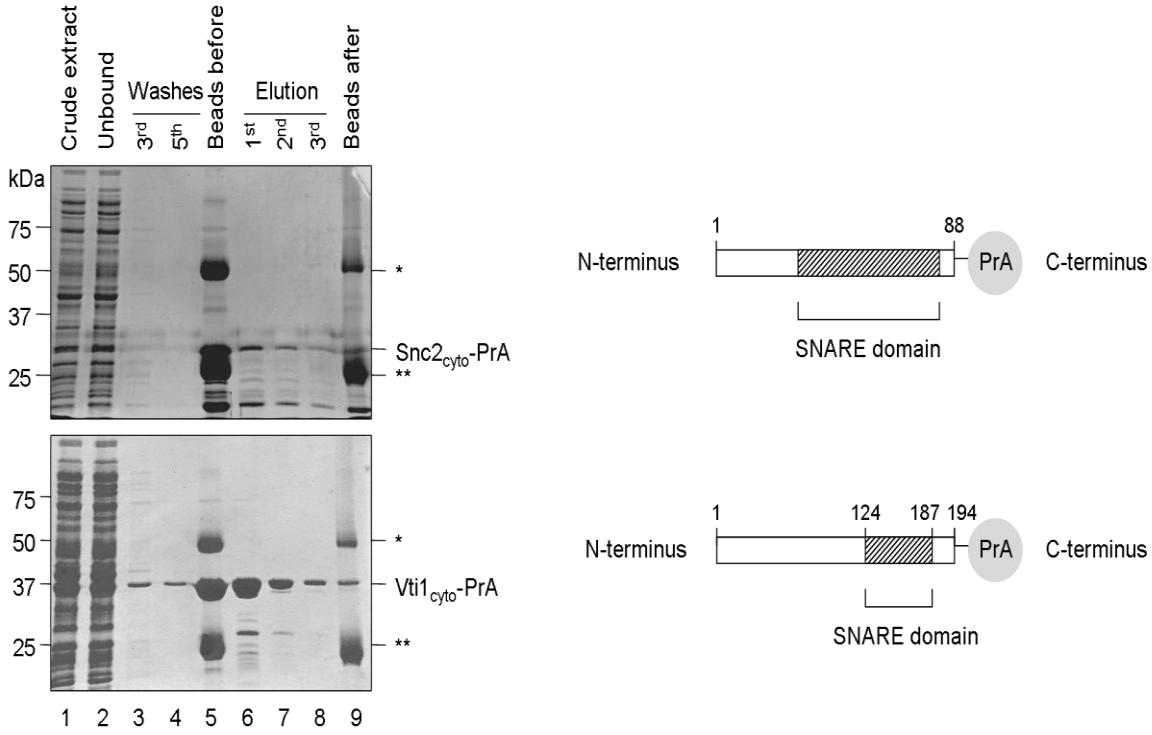

Figure 3-14. Expression and purification of PrA-tagged $Snc2_{cyto}$ and $Vti1_{cyto}$
Plasmids pCOG045 and pCOG048 were used to produce recombinant $Snc2_{cyto}$-PrA and $Vti1_{cyto}$-PrA in BL21 Star™ (DE3) bacterial cells and were purified from 3 litres of culture. The purity of the proteins was assessed at various stages during the purification procedure and was analysed by SDS-PAGE followed by Coomassie™ blue staining (left hand column). Equal volumes (8 µl) of the following samples were analysed: soluble protein before (lane 1) and after (lane 2) affinity purification using IgG Sepharose beads; soluble protein remaining in solution following thorough washing of the bead complex (lanes 3 and 4); the relative amount of protein on the beads before (lane 5) and after (lane 9) elution of the protein from the beads (lanes 6, 7 and 8). IgG heavy (*) and light (**) chains are present at 50 and 25 kDa, respectively (lanes 5 and 9). Positions of molecular weight markers (in kDa) are indicated on the left. Schematic representations of $Snc2_{cyto}$-PrA and $Vti1_{cyto}$-PrA are presented in the right hand column.

The remaining Tlg2 partner SNARE protein Tlg1, together with the Syntaxin 4 and GST negative interaction control proteins were recombinantly produced as GST-tagged fusion proteins. GST binds to glutathione with high affinity (Chasseaud, 1979; Mannervik, 1985) and it is this property that is widely utilised to purify recombinant GST fusion proteins produced in *E.coli* using glutathione coated beads as described under section 2.11.5. For this study, Tlg1 was expressed from plasmid GST-Tlg1 (Coe *et al.*, 1999) which encodes a N-terminal GST-tagged cytosolic version of Tlg1 (residues 1-224, denoted GST-Tlg1$_{cyto}$) (Figure 3-15). A C-terminal GST-tagged version of the cytosolic portion of Syntaxin 4 (residues 1-273, denoted Syntaxin 4$_{cyto}$-GST) was included as a non-functional negative interaction control and was expressed from plasmid pETDuet-Sx4-GST (Figure 3-15) (Aran *et al.*, 2009). GST was expressed from plasmid pETDuet-1-GST (Figure 3-15). Purified GST was used as a negative interaction control for all pull-down assays utilising GST-tagged recombinant fusion proteins.

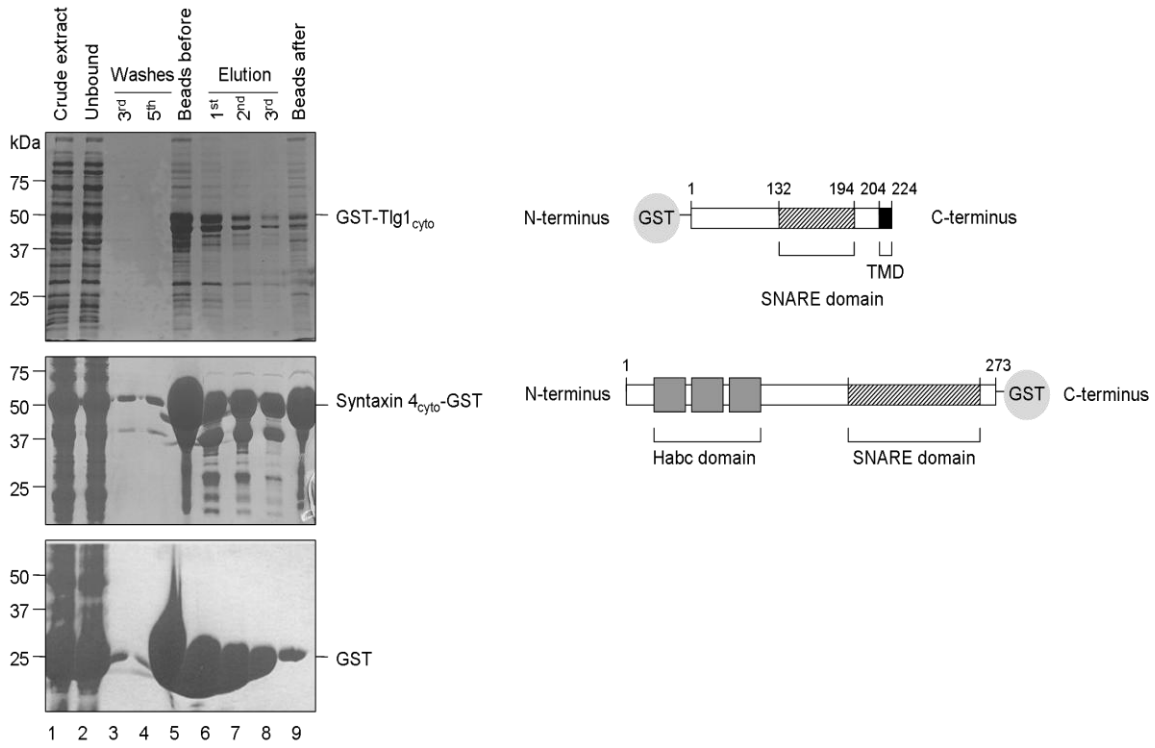

Figure 3-15. Expression and purification of GST-tagged proteins
Plasmids GST-Tlg1, pETDuet-Sx4-GST and pETDuet-1-GST was used to produce recombinant GST-Tlg1$_{cyto}$, Syntaxin 4$_{cyto}$-GST and GST in BL21 Star^{TM} (DE3) bacterial cells and was purified from 3 litres of culture. Protein purity at various stages during the purification procedure was analysed using SDS-PAGE followed by Coomassie™ blue staining (left hand column). Equal volumes (8 µl) of the following samples were analysed: soluble protein present in the cleared whole cell lysate following an overnight induction with 0.5 mM IPTG (lane 1); unbound protein present in the supernatant following a 1 hour incubation with IgG Sepharose beads (lane 2); proteins remaining in solution following washing of the bead complex (lanes 3 and 4); relative amount of protein present on the beads before (lane 5) and after (lane 9) elution from the beads (lanes 6, 7 and 8). Positions of molecular weight markers (in kDa) are indicated on the left. Schematic representations of GST-Tlg1$_{cyto}$, Syntaxin 4$_{cyto}$-GST and GST are indicated in the right hand column.

Eluted recombinant fusion proteins were dialysed against PBS containing 10% (w/v) glycerol prior to snap-freezing and subsequent storage at -80°C. For this study, equal volumes of dialysed GST- or PrA-tagged recombinant fusion protein (sections 2.11.4, 2.11.5 and 2.11.6) were analysed by SDS-PAGE (section 2.3.1) followed by Coomassie™ blue staining (section 2.3.2). Protein concentrations were then normalised for each pull-down assay using the Coomassie™ blue stained gels as a measure of protein concentration. Equal volumes of normalised dialysed recombinant fusion protein was subsequently immobilised to equal volumes of glutathione or IgG coated Sepharose beads (section 2.12.1). This method was employed due to the masking effects caused by the IgG heavy and light chains on some of my PrA-tagged recombinant fusion proteins immobilised to IgG Sepharose coated beads (Figure 3-17). For consistency, I also adopted this method for all my subsequent GST pull-down assays.

Pull-down assays for this study were performed as outlined under section 2.12.1. Briefly, GST- or PrA-tagged recombinant fusion proteins immoblised to glutathione or IgG coated Sepharose beads, respectively, were incubated with yeast cell lysates (prepared as outlined under section 2.5.4.2) containing chromosomally expressed HA-tagged Cog subunits (Table 2-4) (Yen *et al.*, 2010). Following a 2 hour incubation at 4°C, proteins bound to immobilised GST- or PrA-tagged recombinant fusion proteins were captured by centrifugation and subsequent washing of the unbound proteins from the mix. Bound proteins were eluted from the immobilised GST- or PrA-tagged fusion proteins using a reducing buffer followed by heating at 95°C for 5 minutes. Association of HA-tagged Cog subunits to the immobilised recombinant fusion proteins was assessed by SDS-PAGE (section 2.3.1) followed by immunoblot analysis with anti-HA antibody (sections 2.3.3 and 2.3.4).

3.2.2.2 Detection of chromosomally expressed HA-tagged Cog proteins

Yeast cell lysates were prepared from wild type and congenic strains chromosomally expressing HA-tagged Cog1, Cog2, Cog3 and Cog4 to confirm expression of the different Cog constructs (Figure 3-16). HA-specific proteins bands were detected at approximately the correct predicted molecular weight for each of HA-tagged Cog1 to Cog4.

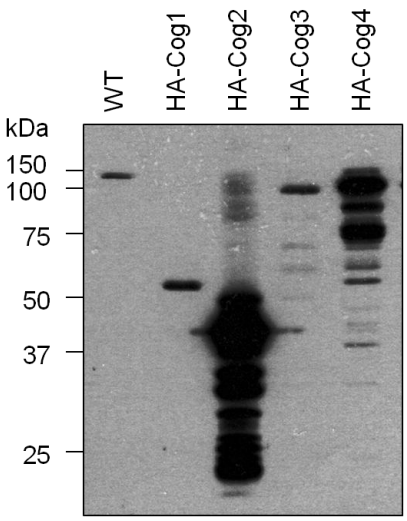

Figure 3-16. Detection of HA-tagged Cog1 to Cog4
Equal volumes of normalised wild type (WT) yeast cell lysate and congenic yeast cell lysate containing chromosomally expressed HA-tagged Cog1, Cog2, Cog3 or Cog4 were analysed by SDS-PAGE (15%) followed by immunoblot analysis using anti-HA antibody. A non-specific HA protein band was seen for the wild type yeast cell lysate just below 150 kDa. Predicted molecular weights for HA-tagged Cog1 to Cog4 were as follows: HA-Cog1, 51 kDa; HA-Cog2, 34 kDa; HA-Cog3, 96 kDa; HA-Cog4, 102 kDa.

3.2.2.3 Tlg2 directly associates with COG complex subunits

$Tlg2_{cyto}$-PrA was pulled down following incubation with yeast cell lysates prepared from wild type (negative control) or congenic strains chromosomally expressing HA-tagged Cog1 to Cog4 (Figure 3-17, top panel, immunoblot analysis; bottom panel, Coomassie™ blue stained gel, lanes 1 to 5) to identify Cog subunits which interact with the cytosolic portion of Tlg2. PrA was separately incubated with lysates prepared from the same yeast strains in order to exclude non-specific binding to the PrA portion of recombinant $Tlg2_{cyto}$-PrA fusion protein (Figure 3-17, top panel, immunoblot analysis; bottom panel, Coomassie™ blue stained gel, lanes 6 to 10). Immunoblot analysis revealed multiple bands for $Tlg2_{cyto}$-PrA that is likely due to IgG cross reactivity with the PrA portion of the recombinant fusion protein (Figure 3-17, top panel, lanes 1 to 5). Binding of HA-tagged Cog2 and Cog4 to $Tlg2_{cyto}$-PrA is also apparent (Figure 3-17, top panel, lanes 3 and 5). The HA-Cog2 specific band partially overlaps with the lower band apparent for $Tlg2_{cyto}$-PrA (Figure 3-17, top panel, lane 3). However, as this protein band appears more intense relative to the lower band seen for $Tlg2_{cyto}$-PrA in WT, HA-Cog1, HA-Cog3 and HA-Cog4, it is reasonable to propose that this is due to binding of some HA-Cog2 to $Tlg2_{cyto}$-PrA. It is evident that some HA-tagged Cog2 and Cog4 bound

non-specifically to PrA (Figure 3-17, top panel, lanes 8 and 10). However, as the protein input for $Tlg2_{cyto}$-PrA appears to be approximately half of the PrA input (Figure 3-17, bottom panel, Coomassie™ blue stained gel) the relative amount of Cog2 and Cog4 bound to PrA compared with $Tlg2_{cyto}$-PrA is much less. Therefore, the $Tlg2_{cyto}$ portion of the $Tlg2_{cyto}$-PrA recombinant fusion protein is responsible for binding a larger proportion of HA-tagged Cog2 and Cog4 compared with PrA by itself. Due to the partial overlap in size between the IgG heavy chain on $Tlg2_{cyto}$-PrA (Figure 3-17, lower pane lanes 1 to 5), I subsequently incorporated my modified protocol of normalising protein concentration prior to immobilising equal volumes of protein to Sepharose beads.

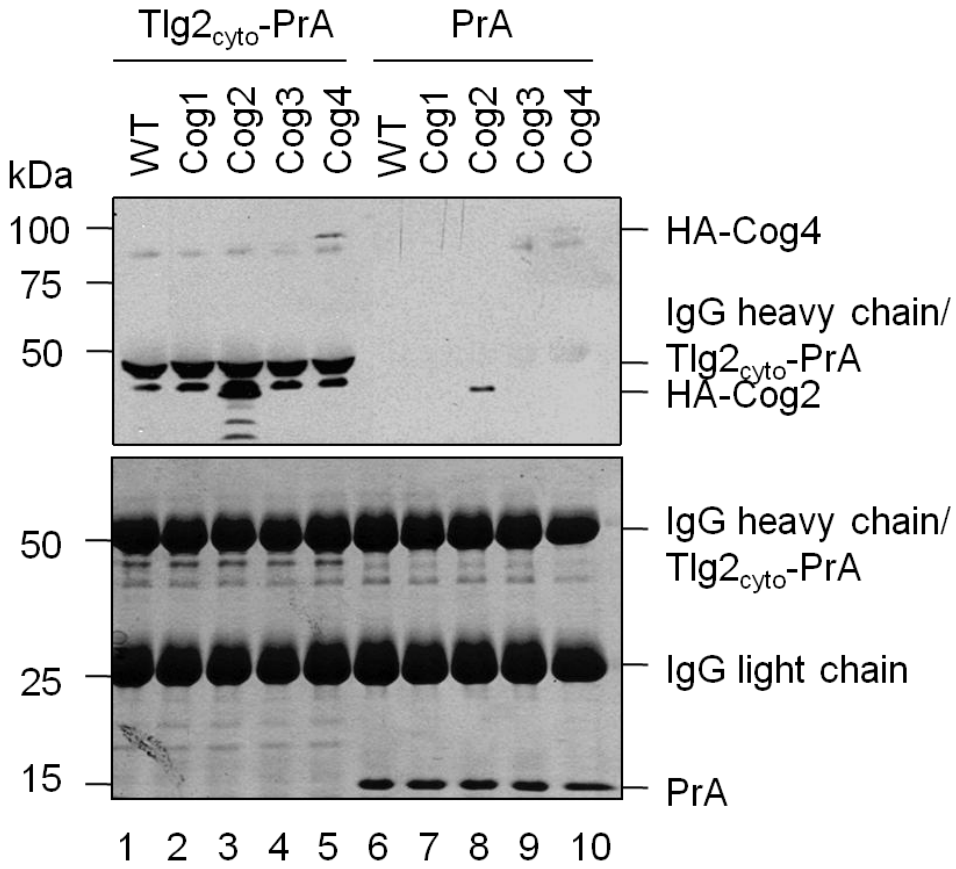

Figure 3-17. $Tlg2_{cyto}$-PrA associates with HA-tagged Cog2 and Cog4
Equal volumes of normalised $Tlg2_{cyto}$-PrA and PrA immobilised to IgG Sepharose beads were incubated with equal volumes of normalised wild type (WT) yeast cell lysate or congenic yeast cell lysate containing chromosomally expressed HA-tagged Cog1 to Cog4 (refer to Table 2-4) as described under section 2.12.1). Sepharose beads and associated proteins were recovered by centrifugation followed by thorough washing of the bead-protein complex. The presence of HA-tagged Cog1 to Cog4 was assessed by SDS-PAGE followed by immunoblot analysis using anti-HA antibody (top panel). Equal $Tlg2_{cyto}$-PrA (51 kDa) and PrA (15 kDa) recombinant fusion protein input was confirmed by SDS-PAGE followed by Coomassie™ blue staining (bottom panel). IgG heavy (50 kDa) (top and bottom panels) and light chains (25 kDa) (bottoms panel) are clearly visible. Associations between HA-tagged Cog2 (~32 kDa) and Cog4 (~100 kDa) were detected (top panel). Input samples amount to 4% of the total protein input. These results are representative of three independent experiments (n=3).

The next step in my investigation was to determine the domains of Tlg2 responsible for mediating binding to Cog2 and Cog4. The SNARE domain of a number of yeast and mammalian SNARE proteins have previously been reported to be involved in binding tethering factors, including subunits of the COG complex (Shestakova *et al.*, 2007; Perez-Victoria & Bonifacino, 2009; Laufman *et al.*, 2011). Similar to the interactions previously established between SM and SNARE proteins (Dulubova *et al.*, 2002; Yamaguchi *et al.*, 2002; Burkhardt *et al.*, 2008), a general and possible conserved mechanism of interaction between tethers and SNAREs may underlie an additional level of specificity and temporal orchestration of membrane fusion events. Recombinant PrA, $Tlg2_{cyto}$-PrA, $Tlg2_{cyto}\Delta$N36-PrA and $Tlg2_{cyto}\Delta$Habc-PrA fusion protein concentrations were normalised prior to immobilising equal volumes of normalised protein to IgG coated sepharose beads (Figure 3-18). This method came with its own challenges as the amount of normalised $Tlg2_{cyto}\Delta$N36-PrA and $Tlg2_{cyto}\Delta$Habc-PrA for this experiment (representative of n=3) was approximately half that of $Tlg2_{cyto}$-PrA and PrA (Figure 3-18) despite multiple efforts to equalise protein concentrations. Non-specific binding of HA-tagged Cog2 to PrA also remained a challenge during the course this study and a number of modifications to my protocol were introduced in an attempt to solve this issue. These included pre-blocking my immobilised proteins with 1% BSA and reducing the binding incubation period from overnight to 2 hours at 4°C. These measures proved variable in their effectiveness. I have therefore used the relative amount of Cog2 bound to my different PrA and PrA-tagged Tlg2 constructs as a measure of a positive protein-protein interaction. Taking all of the above challenges into consideration, Figure 3-19 shows that the SNARE domain of Tlg2 mediates binding to both HA-tagged Cog2 and Cog4. Syntaxin 16, which is the mammalian homolog of yeast Tlg2, has recently been shown to associate with the N-terminal coiled-coil domain of mammalian Cog4 via its SNARE domain (Laufman *et al.*, 2013). The N-terminal coiled-coil domains of the Vps53 and Vps54 subunits of the GARP tethering complex (Perez-Victoria & Bonifacino, 2009), as well as Cog6 (Laufman *et al.*, 2011) and Cog4 (Shestakova *et al.*, 2007), have also been shown to mediate binding to the SNARE domain of their respective syntaxin interacting proteins. Additionally, the N-terminal domains of the GARP and COG complex subunits share some sequence homology with the exocyst complex (Whyte & Munro, 2001) and the Munc13 MUN domain (Pei *et al.*, 2009). The latter has previously been shown to be implicated in SNARE-mediated interactions (Ma *et al.*, 2011). The domains of Cog2 and Cog4 responsible for

mediating interactions with the SNARE domain of Tlg2 remain to be investigated. However, the results presented here support a general mechanism of interaction between syntaxin and tethering proteins.

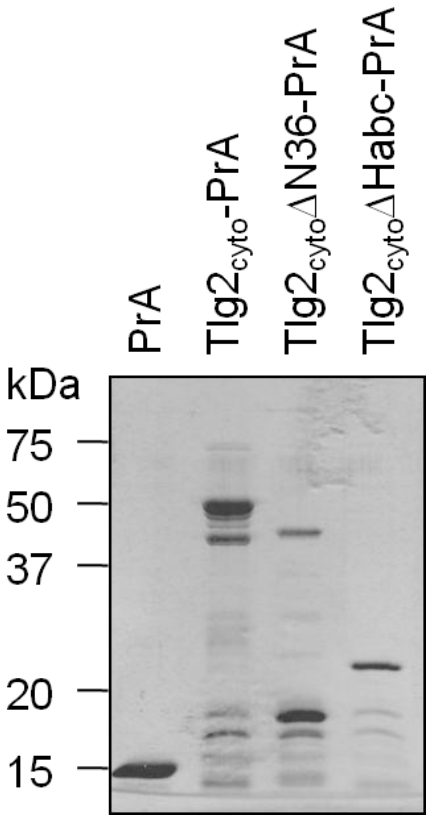

Figure 3-18. Normalised protein concentration for PrA-tagged Tlg2 fusion proteins
Equal volumes of dialysed recombinant PrA, $Tlg2_{cyto}$-PrA, $Tlg2_{cyto}\Delta N36$ and $Tlg2_{cyto}\Delta Habc$ fusion proteins were analysed by SDS-PAGE followed by Coomassie™ blue staining. Equal volumes of proteins normalised for concentration were re-analysed (this image) by SDS-PAGE followed by Coomassie™ blue staining to ensure approximately equal concentrations of protein being immoblised to equal volumes of IgG coated sepharose beads.

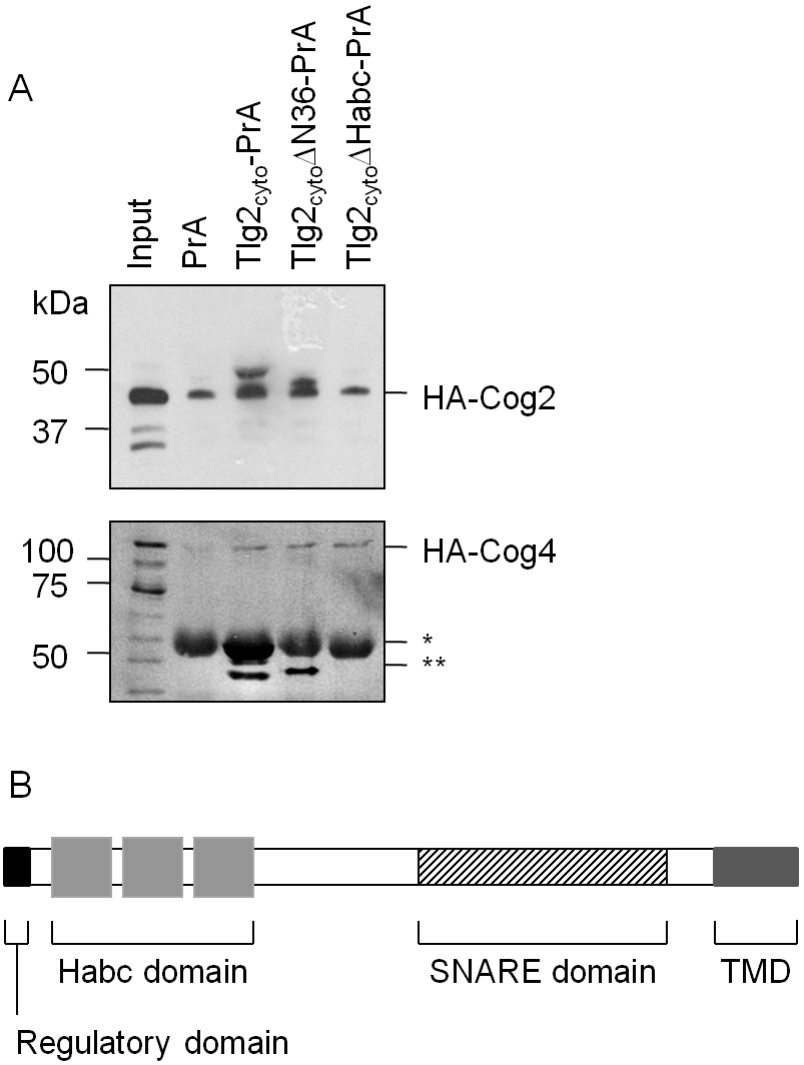

Figure 3-19. The Tlg2 SNARE domain mediates binding to HA-tagged Cog2 and Cog4
A. Equal volumes of normalised recombinant PrA-tagged fusion protein immobilised to IgG coated Sepharose beads was incubated with equal volumes of yeast cell lysates containing chromosomally expressed HA-tagged Cog2 (strain WLY209) or Cog4 (strain WLY208). Bound proteins were eluted from immobilised recombinant fusion proteins. Equal volumes of the eluted protein samples were analysed by SDS-PAGE followed by immunoblot analysis using monoclonal anti-HA antibody. Relative to PrA more HA-tagged Cog2 and Cog4 associates with $Tlg2_{cyto}$-PrA, $Tlg2_{cyto}\Delta$N36-PrA and $Tlg2_{cyto}\Delta$Habc-PrA. This suggests that both Cog2 and Cog4 bind to the SNARE domain of Tlg2. Input samples amount to 4% of the total protein input. *, IgG heavy chain; **, $Tlg2_{cyto}$-PrA and $Tlg2_{cyto}\Delta$N36-PrA specific protein bands. Results are representative of n=3. **B.** Schematic representation of full length Tlg2.

3.2.2.4 Tlg1 directly associates with Cog1

Recombinant PrA, Snc2$_{cyto}$-PrA, Vti1$_{cyto}$-PrA, GST, GST-Tlg1$_{cyto}$ and Syntaxin 4$_{cyto}$-GST fusion protein concentrations were normalised prior to immobilising equal volumes of normalised protein to IgG or glutathione coated Sepharose beads as appropriate (Figure 3-20). Pull-down assays were then performed by incubating equal volumes of immobilised PrA, Snc2$_{cyto}$-PrA, Vti1$_{cyto}$-PrA, GST, GST-Tlg1$_{cyto}$ and Syntaxin 4$_{cyto}$-GST with equal volumes of normalised yeast cell lysates containing chromosomally expressed HA-tagged Cog1. Results from this pull-down assay revealed that Cog1 specifically interacts with the cytosolic portion of Tlg1 as no non-specific binding was detected for GST or the non-functional Syntaxin 4$_{cyto}$-GST control (Figure 3-21, A). No detectable interaction between Cog1 and Snc2$_{ctyo}$-PrA or Vti1$_{cyto}$-PrA was observed (Figure 3-21, B).

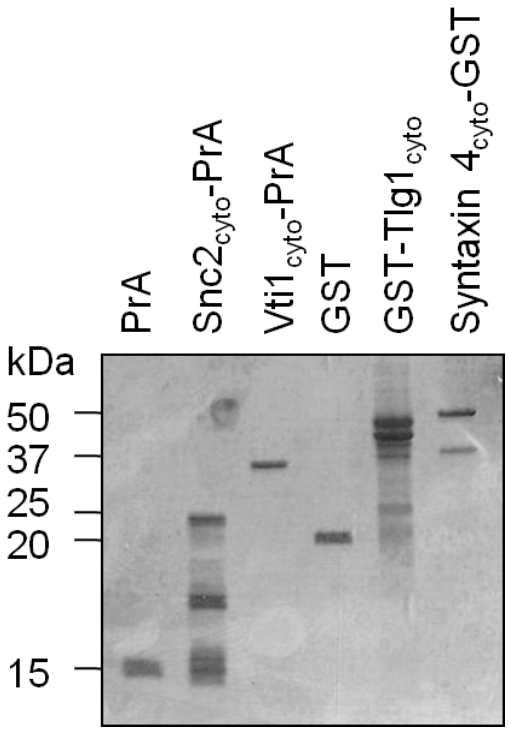

Figure 3-20. Normalised recombinant protein concentration for Tlg2 partner SNARE proteins
Equal volumes of dialysed recombinant PrA, Snc2$_{cyto}$-PrA, Vti1$_{cyto}$-PrA, GST, GST-Tlg1$_{cyto}$ and Syntaxin 4$_{cyto}$-GST fusion proteins were analysed by SDS-PAGE followed by Coomassie™ blue staining. Equal volumes of proteins normalised for concentration were re-analysed (this image) by SDS-PAGE followed by Coomassie™ blue staining to ensure approximately equal concentrations of protein being immoblised to equal volumes of IgG or glutathione coated sepharose beads, as appropriate.

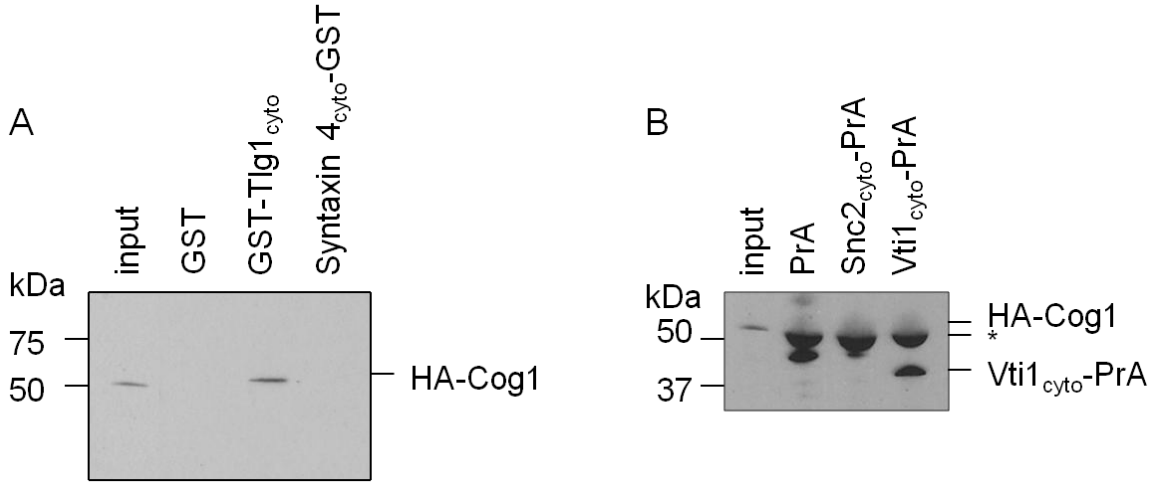

Figure 3-21. HA-Cog1 associates with GST-Tlg1$_{cyto}$
Equal volumes of normalised immobilised GST- or PrA-tagged fusion protein was incubated with equal volumes of normalised yeast cell lysate containing chromosomally expressed HA-tagged Cog1 (strain WLY206). Bound proteins were eluted and equal volumes were subjected to SDS-PAGE followed by immunoblot analysis using monoclonal anti-HA antibody. **A.** HA-tagged Cog1 specifically associates with GST-Tlg1$_{cyto}$. **B.** No detectable associations between HA-Cog1 and Snc2$_{cyto}$-PrA or Vti1$_{cyto}$-PrA were observed. The IgG heavy chain is present at approximately 50 kDa (indicated by *); Vti1$_{cyto}$-PrA is apparent at 37 kDa. Input samples amount to 4% of the total protein input.These results are representative of n=3.

3.2.2.5 Functional significance of the Tlg1 and Cog1 interaction

Previously the Cog6 subunit of the COG complex has been shown to directly interact with the SNARE domain of the mammalian homolog of Tlg1, Syntaxin 6, via its N-terminal coiled-coil domain (Laufman *et al.*, 2011). Subsequent depletion of Cog6 resulted in a marked reduction in the steady-state levels of Syntaxin 6. As a direct result, Syntaxin 6-Syntaxin 16-Vti1-VAMP4 SNARE complex assembly was impaired. In order to investigate the effects of Cog1 depletion on the steady-state levels of Tlg1, yeast whole cell lysates were prepared from wild type (WT) or congenic *cog1* deficient yeast as described under section 2.5.4.1. Equal volumes of normalised yeast cell lysates were subsequently subjected to SDS-PAGE (section 2.3.1) followed by immunoblot analysis (sections 2.3.3 and 2.3.4) with anti-Tlg1, anti-Vti1 and anti-Snc2 as a negative Cog1 interaction controls, and anti-Pgk1 (loading control). Depletion of Cog1 selectively reduced the steady-state levels of its interacting partner Tlg1 (15 ± 1.3%, p=0.042), but not Vti1 or Snc2 (Figure 3-22). This observation supports the idea that the tethering actions provided by COG complex are important in stabilising SNARE protein steady-state levels and/or associations with partner SNARE proteins. Interactions between

COG complex subunits and SNARE proteins are therefore likely to promote subsequent SNARE complex assembly followed by efficient membrane fusion.

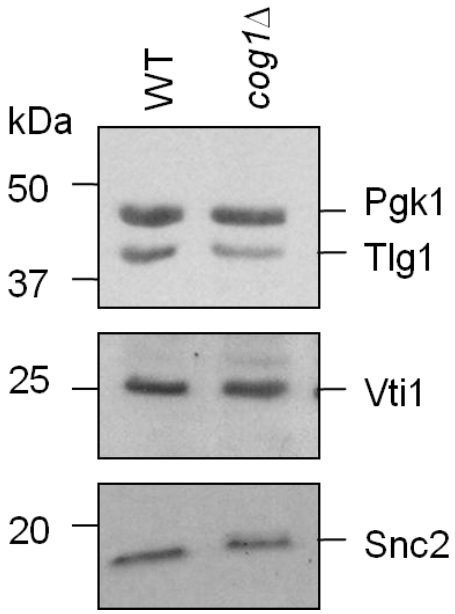

Figure 3-22. Tlg1 whole cell protein levels are selectively reduced in *cog1* deficient yeast
Equal volumes of normalised wild type BY4742 (WT) or congenic *cog1*Δ yeast cell lysate were subjected to SDS-PAGE followed by immunoblot analysis using anti-Tlg1, anti-Vti1 and anti-Snc2 as negative Cog1 interaction controls, and anti-Pgk1 (loading control). Depletion of Cog1 selectively reduced the steady-state levels of Tlg1, but not Vti1 or Snc2. This data is representative of n=3.

3.2.2.6 Tlg1 directly associates with Cog2 and Cog4

Pull-down results for HA-tagged Cog2 and GST-Tlg1$_{cyto}$ revealed that Cog2 selectively associates with the cytosolic portion of Tlg1, but not GST (Figure 3-23, A). Non-specific binding of HA-tagged Cog2 to PrA resulted in inconclusive results for interaction with Snc2$_{cyto}$-PrA and Vti1$_{cyto}$-PrA (Figure 3-23, B).

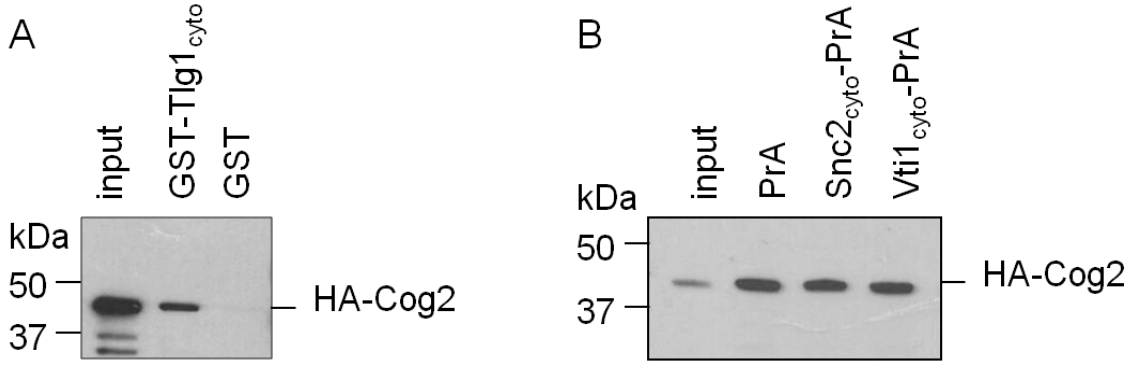

Figure 3-23. HA-Cog2 associates with GST-Tlg1$_{cyto}$
Equal volumes of normalised immobilised GST- or PrA-tagged fusion protein was incubated with equal volumes of normalised yeast cell lysate containing chromosomally expressed HA-tagged Cog2 (strain WLY209). Bound proteins were eluted and equal volumes were subjected to SDS-PAGE followed by immunoblot analysis using monoclonal anti-HA antibody. **A.** HA-tagged Cog2 specifically associates with GST-Tlg1$_{cyto}$. **B.** Non-specific associations between HA-Cog2 and PrA were detected thereby excluding specific Snc2$_{cyto}$-PrA and Vti1$_{cyto}$-PrA interactions. Input samples amount to 4% of the total protein input.These results are representative of n=3.

The Cog3 subunit of the COG complex does not appear to directly associate with GST-Tlg1$_{cyto}$ (Figure 3-24, A), Snc2$_{cyto}$-PrA or Vti1$_{cyto}$-PrA (Figure 3-24, B). Weak but specific interaction between HA-Cog4 and GST-Tlg1$_{cyto}$ was detected (Figure 3-25, A). Cog4 has previously been shown to also interact with the SM protein Vps45 (Laufman *et al.*, 2013), which has a stimulatory effect on SNARE complex assembly (Bryant & James, 2001). Interestingly, addition of Cog4 further enhance Syntaxin 6-Syntaxin 16-Vti1 SNARE complex assembly *in vitro*, as well preventing the formation of non-fusogenic Golgi SNARE complexes (Laufman *et al.*, 2013). Collectively, these results support a role for the COG complex in providing an additional level of specificity for SNARE complex assembly, thereby ensuring fidelity of intracellular transport. Non-specific binding of HA-tagged Cog4 to PrA resulted in inconclusive results for interactions with Snc2$_{cyto}$-PrA and Vti1$_{cyto}$-PrA (Figure 3-25, B). As with the non-specific binding of HA-tagged Cog2 to PrA (Figure 3-23, B), this was a recurring problem despite efforts to reduce non-specific binding.

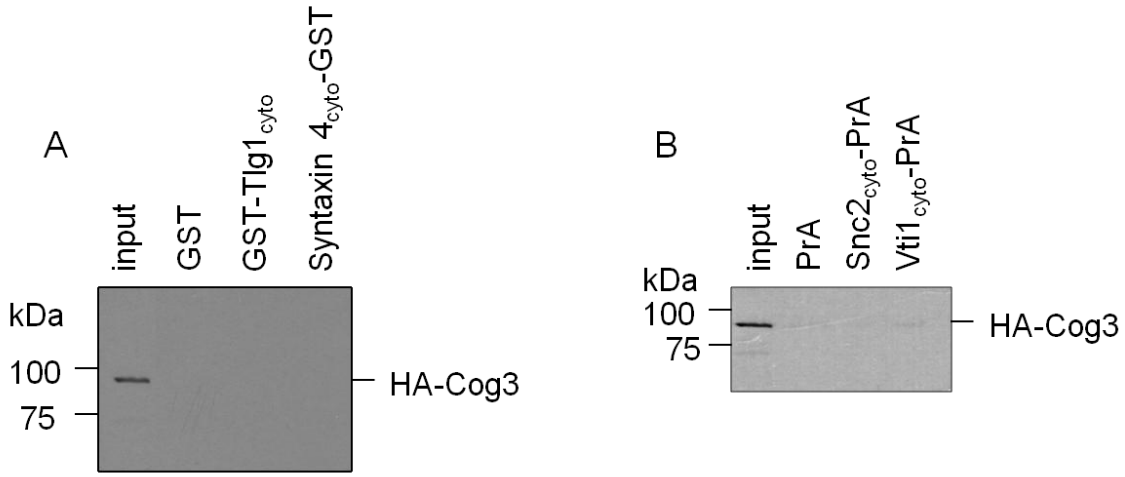

Figure 3-24. HA-Cog3 does not associate with GST-Tlg1$_{cyto}$, Snc2$_{cyto}$-PrA or Vti1$_{cyto}$-PrA
Equal volumes of normalised immobilised GST- or PrA-tagged fusion protein was incubated with equal volumes of normalised yeast cell lysate containing chromosomally expressed HA-tagged Cog3 (strain WLY207). Bound proteins were eluted and equal volumes were subjected to SDS-PAGE followed by immunoblot analysis using monoclonal anti-HA antibody. **A.** No direct interaction between GST-Tlg1$_{cyto}$ and HA-Cog3 was detected. **B.** HA-Cog3 does not appear to associate with Snc2$_{cyto}$-PrA or Vti1$_{cyto}$-PrA. Input samples amount to 4% of the total protein input.These results are representative of n=3.

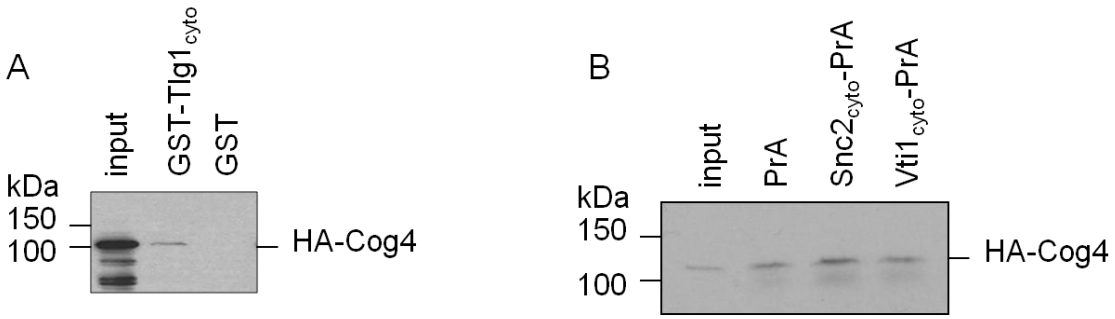

Figure 3-25. HA-Cog4 interacts with GST-Tlg1$_{cyto}$ but not with Snc2$_{cyto}$-PrA or Vti1$_{cyto}$-PrA
Equal volumes of normalised immobilised GST- or PrA-tagged fusion protein was incubated with equal volumes of normalised yeast cell lysate containing chromosomally expressed HA-tagged Cog4 (strain WLY208). Bound proteins were eluted and equal volumes were subjected to SDS-PAGE followed by immunoblot analysis using monoclonal anti-HA antibody. **A.** HA-tagged Cog4 specifically associates with GST-Tlg1$_{cyto}$. **B.** Non-specific associations between HA-Cog4 and PrA were detected. This rendered specific associations between HA-Cog4 and Snc2$_{cyto}$-PrA or Vti1$_{cyto}$-PrA inconclusive. Input samples amount to 4% of the total protein input.These results are representative of n=3.

The observation that Cog4 specifically interacts with the cytosolic portion of Tlg1 (Figure 3-25, A) prompted me to also assess the effects of steady-state Tlg1 levels in Cog4 deficient yeast. Production of a *cog4* deficient yeast strain was first attempted using a one-step gene disruption protocol (section 2.6). This resulted in the absence of geneticin (G418) resistant colonies. I subsequently resorted to obtaining the haploid *cog4* yeast strain by dissecting a diploid strain containing one WT *COG4* allele and another *COG4* allele that was replaced with the geneticin drug resistant gene *kanMX*4 (performed in collaboration with Stephanie Evans, University of Glasgow). Segregation of the haploid strain revealed synthetic lethality of haploid *cog4* which is consistent with previous reports (Kim *et al.*, 2001).

The last in the series of my pull-down experiments investigated interactions between HA-tagged Cog6 and GST-Tlg1$_{cyto}$, Snc2$_{cyto}$-PrA or Vti1$_{cyto}$-PrA. Cog6 has recently been shown to directly interact with the mammalian homolog of Tlg1, Syntaxin 6 (Laufman *et al.*, 2011; Willett *et al.*, 2013). I was therefore curious to investigate if this interaction was conserved in yeast. For completion, I also investigated binding between HA-Cog6 and Snc2$_{cyto}$-PrA or Vti1$_{cyto}$-PrA. Pull-down assay results revealed no detectable interaction between HA-Cog6 and GST-Tlg1$_{cyto}$ (Figure 3-26, A), Snc2$_{cyto}$-PrA or Vti1$_{cyto}$-PrA (Figure 3-26, B). The results presented here do not support conservation in COG-SNARE interactions between mammals and yeast. This may reflect functional redundancy in more complex

biological systems. The non-specific protein band present just below the HA-Cog6 specific protein band was periodically detected in my immunoblot analysis for pull-down assays (Figure 3-26, B). I propose that this band is non-specific as it was also detected in my wild type yeast lysate lacking chromosomally expressed HA-tagged Cog subunits (Figure 3-17, top panel, lane 1).

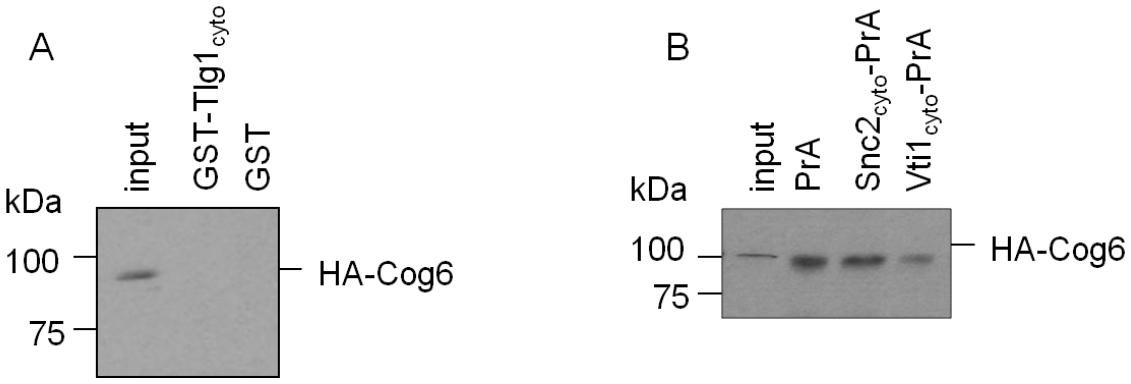

Figure 3-26. HA-Cog6 does not associate with GST-Tlg1$_{cyto}$, Snc2$_{cyto}$-PrA or Vti1$_{cyto}$-PrA
Equal volumes of normalised immobilised GST- or PrA-tagged fusion protein was incubated with equal volumes of normalised yeast cell lysate containing chromosomally expressed HA-tagged Cog6 (strain WLY218). Bound proteins were eluted and equal volumes were subjected to SDS-PAGE followed by immunoblot analysis using monoclonal anti-HA antibody. **A.** No detectable interaction between HA-tagged Cog6 and GST-Tlg1$_{cyto}$ was observed. **B.** Snc2$_{cyto}$-PrA or Vti1$_{cyto}$-PrA does not associate with HA-Cog6. Input samples amount to 4% of the total protein input.These results are representative of n=3.

3.2.2.7 Summary of pull-down interactions

A summary of all the pull-down interaction results obtained are presented in Table 3-2.

Table 3-2 Summary of pull-down interactions

	Cog1	Cog2	Cog3	Cog4	Cog6
Tlg2$_{cyto}$-PrA	-	yes	-	yes	
Tlg2$_{cyto}$ΔN36-PrA	-	yes	-	yes	
Tlg2$_{cyto}$ΔHabc-PrA	-	yes	-	yes	
Vti1$_{cyto}$-PrA	-	-	-	-	-
Snc2$_{cyto}$-PrA	-	-	-	-	-
GST-Tlg1$_{cyto}$	yes	yes	-	yes	-

3.3 Chapter summary

Experiments performed in this chapter provide evidence in support of a direct physical interaction between yeast Tlg2 and the Cog2 and Cog4 subunits of the COG tethering complex (Figure 3-17). The SNARE domain of Tlg2 appears to be important in mediating these associations (Figure 3-19). This observation is consistent with other SNARE-COG associations (Shestakova *et al.*, 2007; Laufman *et al.*, 2011) thereby supporting a possible conserved mechanism of interaction between SNARE proteins and tethering factors. These results will require further confirmation using alternative approaches due to the non-specific binding observed for HA-tagged Cog subunits to PrA. This could include producing recombinant proteins for both the Tlg2 and Cog subunit constructs and allowing interactions between Tlg2 and Cog subunits to occur in an isolated environment that is not influenced by endogenous factors. Specifically, this approach will exclude the possibility of any indirect protein associations that may have occurred using the pull down approach employed during this study. Additionally, affinity purification coupled to mass spectrometry could also be employed to confirm the interaction between Tlg2 and the COG complex subunits.

This chapter also documents associations between Tlg1 and Cog1 (Figure 3-21), Cog2 (Figure 3-23) and Cog4 (Figure 3-25). It remains to be investigated whether the SNARE domain of Tlg1 is also important in mediating these associations. The yeast two-hybrid assays (section 3.2.1) performed in this chapter were inconclusive in determining interactions between the different truncated versions of the cytosolic portion of Tlg2 and full-length Cog1 to Cog4 (section 3.2.1). It is important to note that the plasmids used in this study were derived from a combination of Clontech Matchmaker Gal4 two-hybrid vectors and the pGAD-C1 and pGBDU-C1 vectors previously described (James et al., 1996; Yen et al., 2010). This resulted in incorporating three different nutritional selection markers during these studies, which introduced an element of inconsistency depending on which combination of AD and BD Tlg2 and Cog interactions were assessed. This could potentially be improved in future experiments by subcloning all Cog subunit constructs into Clontech Matchmaker Gal4 two-hybrid vectors. An additional benefit would be the ability to determine successful AD and BD Cog hybrid protein expression by immunoblot analysis using anti-HA and anti-cMyc antibodies (refer to Figure 3-7 and Figure 3-12).

Based on the results obtained in this chapter I propose a model analogous to the Cog4-Sly1-Syntaxin 5 scenario (Laufman *et al.*, 2009; Laufman *et al.*, 2013) whereby Cog4 can simultaneously interact with Vps45 (Laufman *et al.*, 2013) and Tlg2 and subsequently promote SNARE complex assembly through binding of the SM protein Vps45. This model would support the observation that addition of Cog4 to a mammalian *in vitro* system enhances SNARE complex assembly even further compared to just Vps45 by itself (Laufman *et al.*, 2013). Furthermore, the observation that Atg9 is mislocalised in a similar manner in both *tlg2* (Ohashi & Munro, 2010; Nair et al., 2011) and *cog* (Yen *et al.*, 2010) mutant yeast suggests that association between Tlg2 and subunits of the COG complex is required in order to facilitate tethering and subsequent homotypic membrane fusion of Atg9-associated vesicles, which in turn supplies membrane to the autophagosome precursor. The recruitment of the remaining Tlg2 partner SNARE proteins into this system is likely to be mediated by association with distinct Cog subunits (refer to section 3.2.2.4) and/or their partner SNARE proteins. SNARE-Cog interactions are regulated by additional binding partners, including Rab GTPases and SM proteins (Suvorova *et al.*, 2002; Laufman *et al.*, 2013). COG-mediated associations with these accessory proteins may be mediated by Cog subunits which do not interact with SNARE proteins, or alternatively, via distinct domains within Cog subunits that are not involved in SNARE-mediated associations. Collectively, the results presented in this chapter supports the hypothesis that Tlg2 and its partner SNARE proteins is by association with subunits of the COG complex involved in homotypic membrane fusion events regulating autophagosome formation.

Chapter 4 – Regulation of Tlg2 steady-state levels

4.1 Overview and aims

The SM protein Vps45 associates with intracellular membranes predominantly in a Tlg2-dependent manner (Nichols *et al.*, 1998; Bryant & James, 2001). Wild type and *vps45* deficient yeast synthesise Tlg2 to similar levels. However, Tlg2 is subjected to rapid proteasomal degradation in *vps45* deficient yeast, which results in reduced steady-state levels of Tlg2 (Nichols *et al.*, 1998; Bryant & James, 2001). More recently our group has also demonstrated a role for the vacuole in mediating steady-state levels of Tlg2 (Struthers, 2009). This was investigated by comparing steady-state levels of Tlg2 in wild type and congenic yeast lacking active vacuolar proteases [harboring the *pep4-3* mutation, refer to (Woolford *et al.*, 1986)]. The latter contain approximately 2-fold higher steady-state levels of Tlg2, which indicates a role for the vacuole in regulating Tlg2 levels under wild type conditions. Interestingly, Tlg2 steady-state levels are not restored to wild type levels in yeast containing both *vps45*Δ and *pep4-3*Δ mutations (Bryant & James, 2001). Vps45 is required for the efficient delivery of proteins to the proteolytically active endosomal compartment (Piper *et al.*, 1994; Bryant *et al.*, 1998) therefore it was concluded that the proteasome is the principal site of Tlg2 degradation in cells lacking Vps45 (Bryant & James, 2001; Struthers, 2009).

In my previous results chapter I provided evidence in support of a role for Tlg2 in autophagy, which terminates in the vacuole. However, it is not clear whether the vacuolar regulation of Tlg2 in wild type cells occurs via the autophagic pathway.

Ubiquitin is the classic signal for proteasomal-mediated degradation of proteins [reviewed in (Glickman & Ciechanover, 2002)]. Ubiquitin can also signal the entry of proteins, such as Tlg1, into the MVB pathway, which ultimately terminates in the vacuole (Reggiori & Pelham, 2001; Reggiori & Pelham, 2002). It is becoming increasingly evident that autophagy is a more selective process than originally described [reviewed by (Mizushima, 2007)]. The identification of the autophagy receptors p62 and NBR1, which have the ability to simultaneously bind ubiquitin and autophagosome-associated ubiquitin (Ub)-like proteins, provide a means by which protein cargo can be selectively targeted to the vacuole (Pankiv *et al.*, 2007; Kirkin *et al.*, 2009). Previously our lab provided evidence which suggests that Tlg2

is ubiquitinated in both wild type and *vps45*Δ cells (Struthers, 2009). Moreover, preliminary experiments performed by Marion Struthers also demonstrated that Tlg2 is likely to undergo palmitoylation. This reversible post-translational modification may serve to protect Tlg2 from ubiquitin-mediated degradation in a manner analogous to that described for its partner SNARE protein Tlg1 (Valdez-Taubas & Pelham, 2005).

This chapter documents the autophagy-dependent regulation of Tlg2 levels in wild type cells. A role for palmitoylation and the specific palmitoyltransferases involved in the regulation of Tlg2 levels was also investigated

4.2 Results

4.2.1 Vps45 regulates Tlg2 steady-state protein levels

The SM protein Vps45 has a well described role in endosomal trafficking in yeast (Cowles *et al.*, 1994). Vps45 interacts with Tlg2 via two distinct binding modes (Carpp et al., 2006; Ferguson et al., 2009; Bryant et al., 2001). The Vps45-Tlg2 interaction is important for promoting SNARE complex assembly and stabilising Tlg2 steady-state levels (Nichols *et al.*, 1998; Bryant & James, 2001). The effect of Vps45 depletion on Tlg2 steady-state levels was confirmed in this study. It is evident from Figure 4-1 that Tlg2 levels are reduced to near undetectable levels in cells lacking Vps45 (*vps45*Δ).

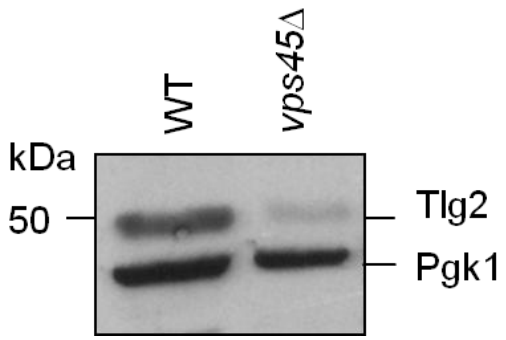

Figure 4-1. Vps45 deficient cells exhibit reduced cellular levels of Tlg2
Immunoblot analysis was employed to assess the steady-state levels of endogenous Tlg2 in wild type yeast cells (BY4742) compared with the congenic Vps45 deficient strain (*vps45*Δ). Equal volumes of cell lysates that were normalised for cell count were subjected to SDS-PAGE followed by immunoblot analysis using antisera against Tlg2. The same membrane was subsequently probed with anti-Pgk1 as a loading control.

4.2.2 Tlg2 steady-state protein levels are regulated by the vacuole

Reduction of Tlg2 cellular levels in Vps45 deficient cells is mediated by rapid proteasomal degradation (Bryant and James, 2001). Our group has also demonstrated a role for the vacuole in regulating Tlg2 protein levels under wild type conditions (Struthers, 2009). This observation is consistent across different strain backgrounds: wild types RPY10 and SEY6210 and their corresponding congenic *pep4-3* mutant strains, SF838-9D and RMY8, respectively (Figure 4-2). Marion Struthers estimated the relative increase in Tlg2 steady-state levels in *pep4-3* versus wild type strains to be approximately 2-fold (Struthers, 2009). For this study, I calculated a 1.2- to 1.4-fold increase in the levels of Tlg2 in *pep4-3* cells when compared with wild type cells (Figure 4-2, B). Levels of Pgk1 were used as a loading control in all cases. This discrepancy is likely due to the dynamic nature of this process and/or the densitometry methods employed to determine the levels of Tlg2 steady-state levels.

A

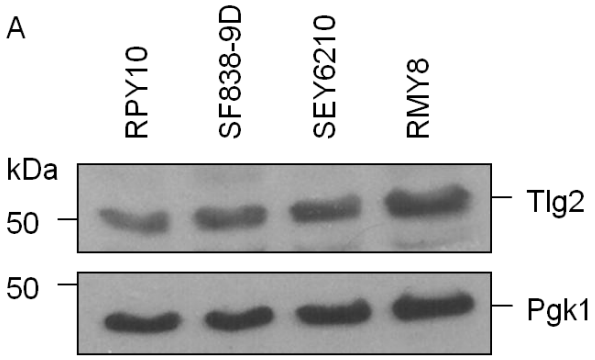

B

pep4-3/PEP4	Relative levels of Tlg2
SF838-9D/RPY10	1.4 ± 0.10 (p=0.02)
RMY8/SEY6210	1.2 ± 0.19 (p=0.350)

Figure 4-2. Endogenous levels of Tlg2 is elevated in cells deficient in vacuolar activity
A. Immunoblot analysis was employed to assess the steady-state levels of endogenous Tlg2 in wild type yeast cells (RPY10 and SEY6210) compared with their congenic *pep4-3* (vacuolar protease) deficient strains (SF838-9D and RMY8, respectively). Equal volumes of cell lysates that were normalised for cell count were subjected to immunoblot analysis using antisera against Tlg2 followed by probing the same membrane with anti-Pgk1 as a loading control. **B.** Densitometry was subsequently performed with the use of the ImageJ 1.46r gel analysis tool (National Health Institute). Protein levels of Tlg2 contained within *pep4-3* and congenic wild type strains were normalised to Pgk1 levels. The relative amount of Tlg2 present was calculated (*pep4-3*/PEP4). Standard deviations of the mean relative values and p-values are indicated (n=3).

Inactivation of vacuolar proteases by the *pep4-3* mutation in a Vps45 deficient background does not restore Tlg2 steady-state levels to that seen in the congenic wild type strain (Bryant and James, 2001). As before, this observation is reproducible (Figure 4-3) and consistent with previous reports suggesting that Vps45 is required for the entry of proteins, including Tlg2, into the proteolytically active endosomal system (Bryant et al., 1998; Piper et al., 1994).

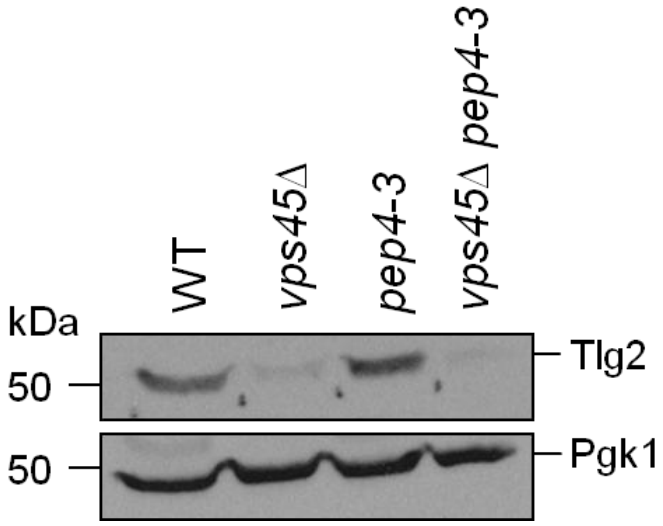

Figure 4-3. Regulation of Tlg2 steady-state levels by the vacuole is dependent on Vps45
Tlg2 steady-state levels were compared in wild type RPY10 (WT) and the following congenic yeast strains: lacking Vps45 (*vps45*Δ), containing inactive vacuolar proteases (*pep4-3*) or lacking both Vps45 and active vacuolar proteases (*vps45*Δ *pep4-3*). Proteins contained within whole cell lysates (normalised for cell number) were subjected to SDS-PAGE followed by immunoblot analysis using anti-Tlg2 and anti-Pgk1, as a loading control.

4.2.3 Tlg2 is regulated in an autophagy-dependent manner

Evidence of a role for Tlg2 in autophagy has previously been provided (section 1.1.4 and 1.2.3). We have demonstrated that Tlg2 levels are regulated by vacuolar proteases under wild type conditions however it remains to be investigated whether this regulation is through the autophagic pathway. The autophagic adaptors, p62 and NBR1, are both continuously and selectively degraded by autophagy (Bjorkoy *et al.*, 2005; Pankiv *et al.*, 2007; Kirkin *et al.*, 2009). More recently Atg1, a protein implicated during the early stages of autophagosome formation, was also shown to be degraded by the vacuole via autophagy (Nakatogawa *et al.*, 2012). Given Tlg2's role in autophagy, it is attractive to hypothesise that Tlg2 is also a substrate for autophagy. I set out to test this hypothesis and investigate whether autophagy plays a role in the regulation of

Tlg2 levels. I achieved this by generating autophagy deficient yeast strains (*cog1*Δ and *atg1*Δ) and used immunoblot analysis to assess the steady-state levels of Tlg2 in these compared to wild type cells.

Autophagy can be selectively disrupted by *atg1*Δ and *cog1*Δ mutations. More specifically, depletion of Atg1 and Cog1 result in incomplete autophagosome formation and thereby disruption of autophagy (Matsuura *et al.*, 1997; Kamada *et al.*, 2000; Kabeya *et al.*, 2005; Yen *et al.*, 2010). For this study, I produced both *atg1*Δ and *cog1*Δ cells in the RPY10 background by homologous recombination as described under section 2.6 (Longtine *et al.*, 1998). Kanamycin resistant (KanR) gene disruption cassettes containing 5' and 3' flanking regions homologous to the target gene's ORF (either C*OG1* or *ATG1*) were generated by PCR (section 2.2.4) using the appropriate primer pairs (listed in Table 2-7) and plasmid pYORC-YC018C (Seron *et al.*, 1998) as a DNA template (refer to Table 2-6 for plasmid details). The expected size for both *COG1* KanR and *ATG1* KanR was 1.5 kb. PCR products were analysed by agarose gel electrophoresis (section 2.2.2) and DNA products of the correct expected size were generated (Figure 4-4).

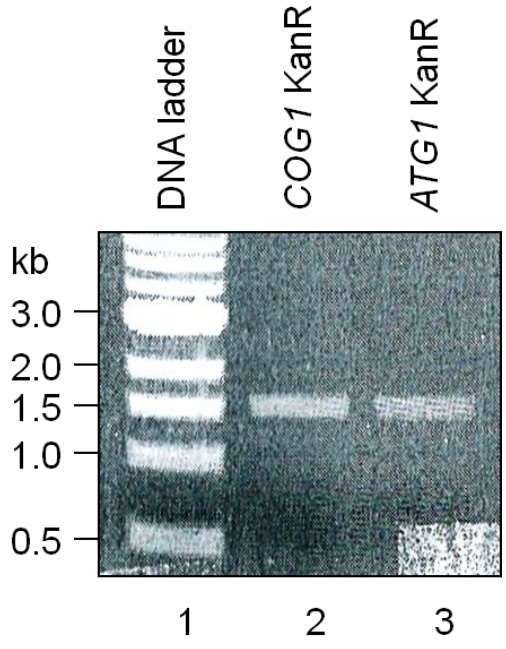

Figure 4-4. *COG1* and *ATG1* KanR modules produced by PCR
PCR was employed to generate linear KanR modules flanked by homologous regions to the *COG1* (lane 2) and *ATG1* (lane 3) specific gene sequences using forward primer *COG1* KAN5' or *ATG1* KAN5' and reverse primer *COG1* KAN3' or *ATG1* KAN3 (refer to Table 2-7), respectively, and plasmid pYORC–YC018C (Table 2-6) as a template. The expected size for both the *COG1* (lane 2) and *ATG1* (lane 3) KanR modules was 1.5 kb. A DNA ladder is included (lane 1) and the corresponding values (in kilobase pairs, kb) are indicated on the left.

The *ATG1* KanR and *COG1* KanR gene disruption cassettes (Figure 4-4) were transformed into wild type RPY10 cells as described under section 2.5.3. Integration of the selectable KanR marker into the correct ORF was identified by whole cell PCR analysis (section 2.2.4) using either *ATG1*- or *COG1*- specific primer pairs (listed in Table 2-7). Figure 4-5 shows that the selectable *COG1* KanR marker successfully integrated into the *COG1* locus of one of the candidate *cog1*Δ cells screened. This is indicated by a PCR product equivalent in size to the *COG1* KanR product of 1.5 kb. Wild type *COG1* (amplified from RPY10 genomic DNA, prepared as outlined under section 2.5.5) and the *COG1* KanR gene disruption cassette were included in the analysis as a means of comparison. This confirmed successful generation of yeast strain YMC001 (RPY10 *cog1*Δ::*KAN*) (Table 2-4).

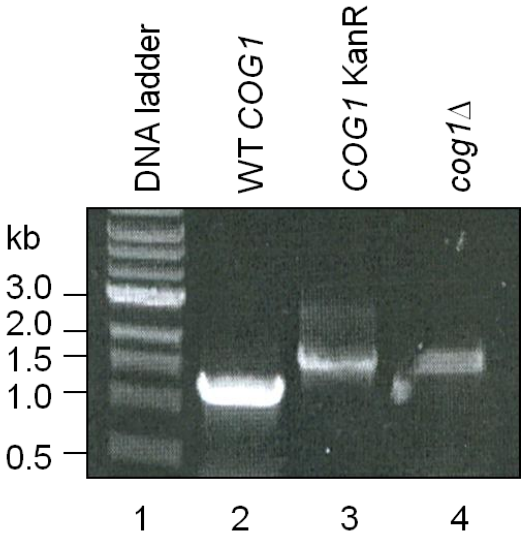

Figure 4-5. Integration of the *COG1* KanR module into the *COG1* locus
Linear *COG1* KanR modules produced by PCR were transformed into wild type RPY10 yeast cells. Whole-cell PCR analysis was perfomed on candidate colonies using the *COG1*-specific primer pairs *COG1* 5' and *COG1* 3' (refer to Table 2-7) to determine successful integration of the linear Cog1 KanR module into the correct locus by homologous recombination. The wild type (WT) *COG1* DNA fragment is 1.25 kb in length (lane2) and the *COG1* KanR module 1.5 kb (lane 3). The candidate colony screened by PCR analysis using the above mentioned primer pairs produced a 1.5 kb DNA fragment (lane 4). This corresponds to the size of the *COG1* KanR module thereby confirming successful intergration of the module into the correct locus and thereby the production of yeast strain YMC001 (RPY10 *cog1*Δ::*KAN*; Table 2-4). A DNA ladder is included (lane 1) and the corresponding values (in kb) are indicated on the left.

Integration of the *ATG1* KanR marker into the *ATG1* locus was confirmed by whole cell PCR analysis (section 2.2.4) of candidate *atg1*∆ cells (Figure 4-6, A). Wild type *ATG1* (amplified from RPY10 genomic DNA, prepared as outlined under section 2.5.5) and the *ATG1* KanR gene disruption cassette was included in the analysis for comparison. The presence of a non-specific DNA band at just under 1.0 kb in the candidate *atg1*∆ PCR product lane (Figure 4-6, A; lane 4) prompted me to perform a controlled PCR in order to test the specificity of my *ATG1* 5' and *ATG1* 3' primer pairs in amplifying the *ATG1* KanR module present in the *ATG1* locus of candidate *atg1*∆ cells. The *ATG1* 5' and *ATG1* 3' primers were unable to independently amplify a DNA product in the presence of whole cell DNA template (Figure 4-6, B; lanes 3 and 4). In the absence of DNA template, the *ATG1* 5' and *ATG1* 3' primer pair was unable to produce a product (Figure 4-6, B; lane 6). Only when added together in a PCR in the presence of a DNA template was a DNA product of 1.0 and 1.5 kb produced (Figure 4-6, B; lane 5). This suggests that the *ATG1* 5' and *ATG1* 3' primer pair was specifically targeted to the *ATG1* locus and that the DNA fragment present at 1.5 kb is indeed the *ATG1* KanR module. This confirmed successful integration of the *ATG1* KanR module into the *ATG1* locus and thereby the generation of yeast strain YMC002 (RPY10 *atg1*∆::*KAN*) (Table 2-4).

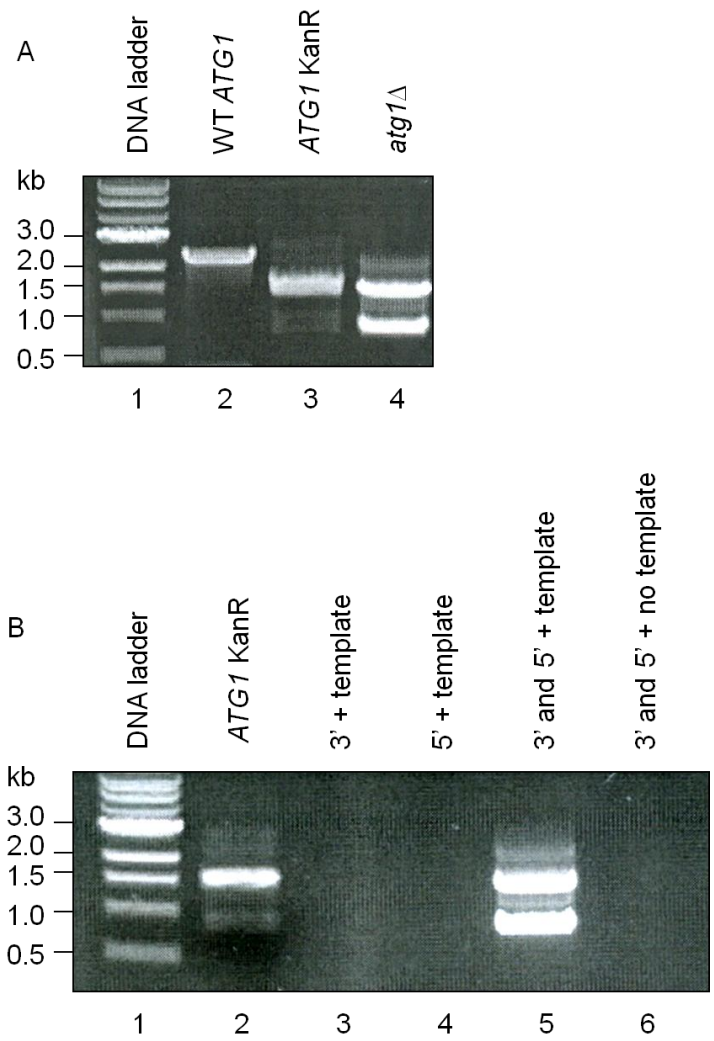

Figure 4-6. Integration of the *ATG1* KanR module into the *ATG1* locus
(A) Linear *ATG1* KanR modules generated by PCR were transformed into wild type RPY10 yeast cells. Whole-cell PCR analysis was performed on two candidate colonies (lanes 4 and 5) using the *ATG1*-specific primer pairs *ATG1* 5' and *ATG1* 3' to determine if the *ATG1* KanR module integrated successfully into the *ATG1* locus. The wild type (WT) *ATG1* DNA fragment is 2.7 kb in length and the *ATG1* KanR module 1.5 kb. The two candidate colonies that were screened produced two identical DNA fragments each that were 1.5 and just under 1.0 kb in length. The 1.5 kb fragment corresponds to the size of the *ATG1* KanR module however the presence of the smaller fragment was further investigated. (B) The specificity of the primer pairs used was further investigated. PCR samples were set up to contain the 3' primer (lane 3), the 5' primer (lane 4) or the 3' and 5' primers together (lane 5) with the template to be screened, or the 3' and 5' primer together in the absence of template DNA (lane 6). The *ATG1* KanR module was included as a control (lane 2). The reaction mix that contained both the 3' and 5' primers together with the template (lane 5) was the only sample to produce a positive result therefore it can be concluded that the primers were specifically targeted to the *ATG1* locus and that the DNA fragment present at 1.5 kb is indeed the *ATG1* KanR module. It can thus be confirmed with confidence that the *ATG1* KanR module successfully integrated into the correct locus and thereby the production of YMC002 (RPY10 *atg1*Δ::*KAN*). A DNA ladder is included (A and B, lane 1) and the corresponding values (in kb) are indicated on the left of each of A and B.

Following construction of the *atg1*Δ and *cog1*Δ RPY10 strains, I went on to investigate the steady-state levels of Tlg2 in wild type compared with autophagy deficient cells. In addition to the RPY10 background strains, I also included wild type, *vps45*Δ, *atg1*Δ and *cog1*Δ BY4742 cells (Table 2-4) in order to exclude strain specific effects. Whole cell lysates were prepared using the rapid Twirl buffer lysis protocol (section 2.5.4.1). Equal volumes of normalised whole cell lysate for wild type, *vps45*Δ (control), *atg1*Δ and *cog1*Δ RPY10 and BY4742 cells were resolved by SDS-PAGE (section 2.3.1) followed by immunoblot analysis (sections 2.3.3 and 2.3.4) with anti-Tlg2 and as a loading control, anti-Pgk1 (Figure 4-7). Tlg2 steady-steady levels undergo an approximate 2-fold increase in Atg1deficient cells in both the RPY10 (Figure 4-7, A; 1.8 ± 0.93, p=0.458) and BY4742 (Figure 4-7, B; 2.0 ± 0.59, p=0.132) background when compared with their congenic wild type strains. Similarly, Tlg2 steady-state levels increased by approximately 1.5 to 2-fold in Cog1 deficient cells (Figure 4-7, A; 1.56 ± 0.25, p=0.258; Figure 4-7, B; 2.2 ± 0.1, p=0.158). As was expected and previously reported (Nichols *et al.*, 1998; Bryant & James, 2001), Tlg2 steady-state levels were near undetectable in Vps45 deficient cells (Figure 4-7, A; 0.34 ± 0.42, p=0.315; Figure 4-7 B; 0.35 ± 0.09, p=0.186). These results suggest that the portion of Tlg2 degraded by the vacuole under wild type conditions is, at least in part, via an autophagy-dependent mechanism.

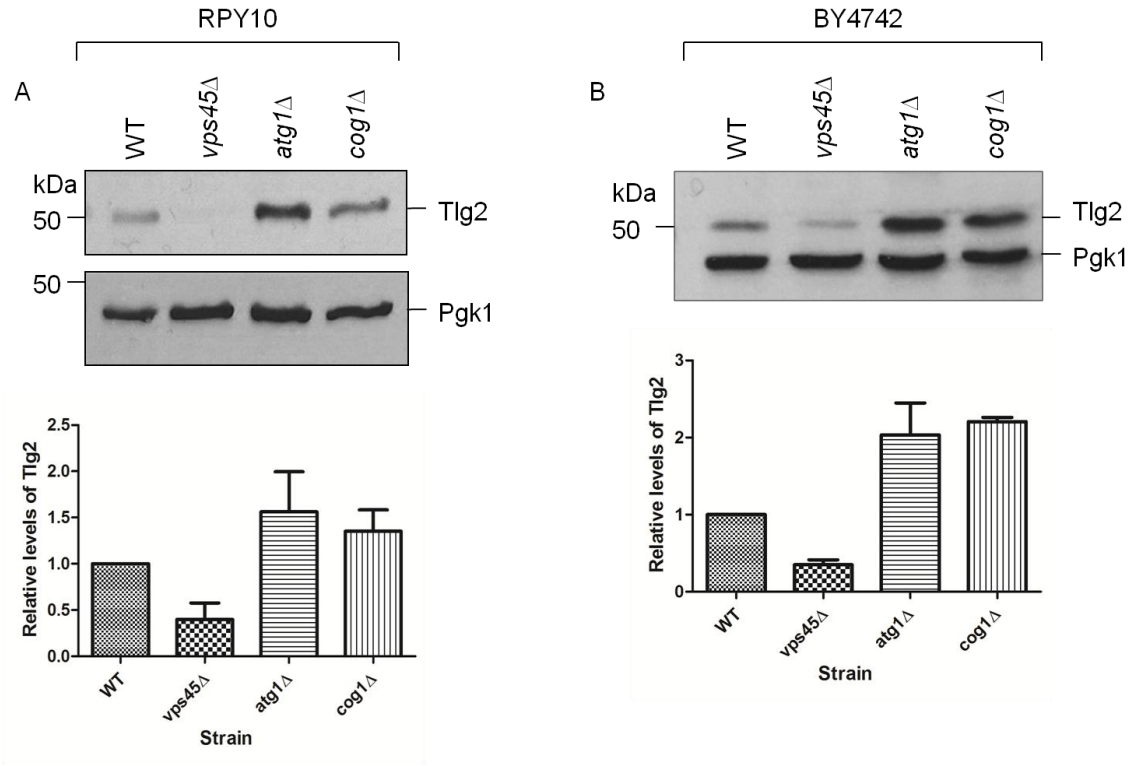

Figure 4-7. Tlg2 steady-state levels are increased in autophagy deficient cells
Immunoblot analysis was employed to assess the steady-state levels of endogenous Tlg2 in wild type RPY10 (**A**) and BY4742 (**B**) cells compared with their corresponding congenic Vps45 (*vps45*Δ) and autophagy deficient strains (*atg1*Δ and *cog1*Δ). Equal volumes of cell lysates that were normalised for cell count were subjected to SDS-PAGE followed by immunoblot analysis using antisera against Tlg2. The same membranes were subsequently probed with anti-Pgk1 as a loading control. Densitometry was performed with the use of the ImageJ 1.46r gel analysis tool (National Health Institute). Tlg2 protein levels were normalised to Pgk1. Levels of Tlg2 contained within Vps45 and autophagy deficient cells were compared with their corresponding congenic wild type strain. This is presented as a bar graph underneath each corresponding immunoblot. These results are representative of three independent experiments (n=3).

I also set out to produce *atg1*Δ and *cog1*Δ mutant cells in a Vps45 deficient background to determine if Vps45 is required for the autophagy-dependent regulation of Tlg2 cellular levels. I initially tried to produce these double mutants in the RPY10 background. However, the two-step gene replacement protocol employed (Sherman, 1997) was unsuccessful. I subsequently mated the BY4742 *vps45*Δ strain with congenic *atg1*Δ or *cog1*Δ strains of opposite mating types (MATa or MATα) followed by sporulation and tetrad dissection (performed in collaboration with Stephanie Evans, University of Glasgow). It was evident following tetrad dissection analysis that the BY4742 *vps45*Δ *cog1*Δ strain was synthetically lethal. The resulting tetratype contained four different genotypes: two parental, and two recombinant types. Synthetic lethality was recognised by the absence of growth of the two recombinant-type ascospores, which was the result

of a single cross-over event between two loci. The two parental-type ascospores produced growth. Thus, half of all the tetrad dissections were lethal. It is worth mentioning here that both *COG1* and *VPS45* reside on chromosome VII. Synthetic lethality, which was a direct result of successful homologous recombination, indicated that *COG1* and *VPS45* are not genetically linked despite being present on the same chromosome. I then focussed my attention on producing BY4742 *vps45*Δ *atg1*Δ in the same manner. Tetrad dissection analysis revealed a non-Mendelian spore arrangement in which a greater proportion were non-recombinant-type ascospores. This is indicative of gene linkage, which is consistent with both *VPS45* and *ATG1* being present on chromosome VII.

4.2.4 A role for palmitoylation in the regulation of Tlg2

Protein palmitoylation (section 1.2.5.1) is a reversible post-translation modification involving the addition of a palmitate molecule to a cysteine residue via a thioester bond [reviewed in (Salaun *et al.*, 2010)]. This reaction is mediated by substrate specific palmitoyltransferases (Roth et al., 2002; Lobo et al., 2002). A wide variety of different proteins have been found to undergo palmitoylation, including SNARE proteins (He et al., 2009) and this modification has been shown to play a role in regulating protein function (Veit *et al.*, 1996), localisation (He et al., 2009) and stability (Couve et al., 1995).

The Tlg2 partner SNARE proteins, Tlg1 and Snc2, are both subject to palmitoylation (Couve *et al.*, 1995; Valdez-Taubas & Pelham, 2005). More specifically, the palmitoyltransferase Swf1 was identified as the enzyme responsible for modifying cysteine residues near or within the transmembrane domains of both Tlg1 and Snc2. Palmitoyltransferases all share a conserved Asp-His-His-Cys (DHHC) motif and are collectively referred to as the DHHC protein family. There are at least seven members belonging to this group of proteins in yeast (Linder & Deschenes, 2004) and it has been suggested that palmitoyltransferase substrates share common features. For example, Swf1 appears to preferentially bind substrates containing cysteine residues adjacent to or within transmembrane domains (Roth *et al.*, 2006). Tlg2 conforms to this latter group with two potential sites of palmitoylation already identified (Valdez-Taubas & Pelham, 2005). However, it remains to be determined whether Tlg2 is also subject

to palmitoylation. Thus, I set out to determine if Tlg2 is palmitoylated in wild type and Swf1 deficient cells.

It has been observed that unpalmitoylated proteins that normally undergo palmitoylation are less stable than their modified counterparts (Couve *et al.*, 1995; Valdez-Taubas & Pelham, 2005). Hydroxylamine selectively cleaves thioester-linked palmitates from proteins (Chamberlain & Burgoyne, 1998). These two observations were used in combination as an initial approach to determine if Tlg2 is palmitoylated. The protocol employed during this study (refer to section 2.8.1) has previously been described (Valdez-Taubas & Pelham, 2005). Yeast lysates containing equal quantities of protein extract (estimated as outlined under section 2.9) were prepared from wild type or *swf1*Δ cells transformed with pNB701 (empty vector) or pMAZ006 (encoding HA-Tlg2) (Table 2-6). Yeast lysates were treated with either 1M hydroxylamine pH 7.5 or 1M Tris-HCl pH 7.5, as a control. 20 µl of each sample was subjected to SDS-PAGE (section 2.3.1) followed by immunoblot analysis (sections 2.3.3 and 2.3.4) with anti-HA and anti-Pgk1. It is evident that wild type yeast lysates treated with hydroxylamine contained reduced levels of HA-Tlg2 (76 ± 13%) compared with lysates treated with the control compound Tris-HCl (Figure 4-8, A, lanes 3 and 4, respectively; B). In contrast, hydroxylamine and Tris-HCl treated *swf1*Δ yeast lysates contained comparable levels of HA-Tlg2 (Figure 4-8, A, lanes 7 and 8, respectively). The absence of HA-Tlg2 reactive bands in the wild type (Figure 4-8, A, lanes 1 and 2) and *swf1*Δ empty vector controls (Figure 4-8, A, lanes 5 and 6) confirmed specificity of the anti-HA antibody to HA-Tlg2. The reduction observed in Tlg2 levels following hydroxylamine treatment of wild type cell lysates indicate that Tlg2 may be subject to palmitoylation and that Swf1 may function in this process.

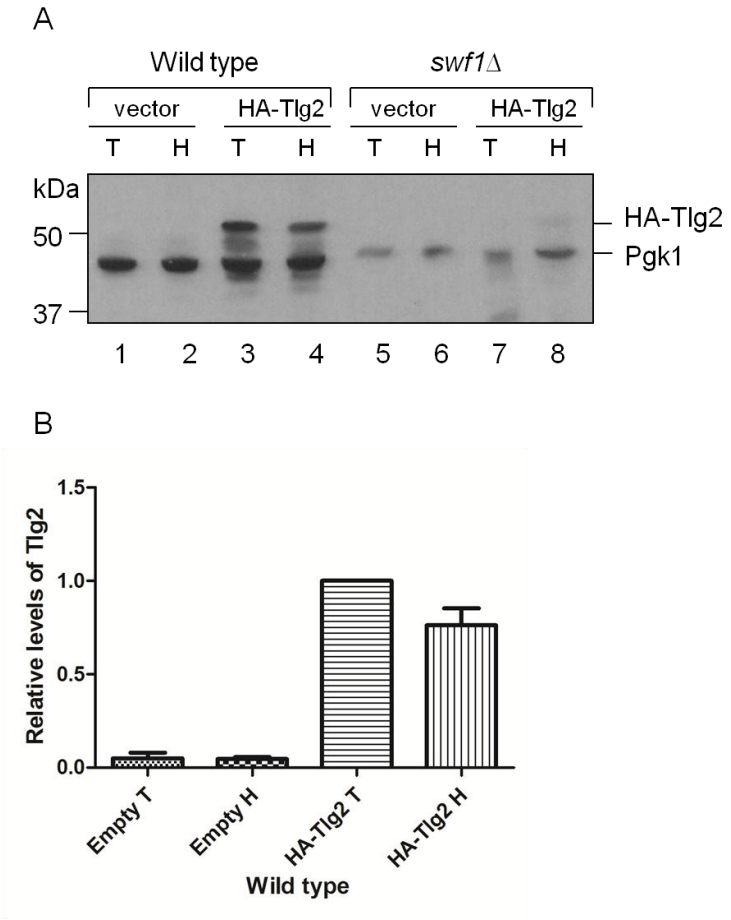

Figure 4-8. Cellular levels of HA-Tlg2 are reduced following treatment with hydroxylamine in wild type cells
A. Yeast lysates containing equal quantities of protein extract were prepared from wild type BY4742 or congenic *swf1*Δ cells transformed with pNB701 (empty vector) or pMAZ006 (encoding HA-Tlg2). 50 µg of protein extract in no more than 50 µl was treated with 1M hydroxylamine (H) or as a control, 1M Tris-HCl (T). Proteins were precipitated and resuspended in 100 µl of 1X LSB prior being heated at 65°C for 15 minutes. 20 µl of each sample was subjected to SDS-PAGE followed by immunoblot analysis with anti-HA and anti-Pgk1 as a loading control. **B.** Densitometry was performed using the ImageJ 1.46r gel analysis tool (NHI). HA-Tlg2 protein levels were normalised to Pgk1. HA-Tlg2 protein levels contained within wild type cells treated with Tris or hydroxylamine and harboring an empty plasmid or a plasmid encoding HA-Tlg2 were assessed and are expressed as a fraction of the HA-Tlg2 Tris treated protein levels.

I went on to investigate the steady-state levels of endogenous Tlg2 in wild type and *swf1*Δ cells, both of which contain active vacuolar proteases. I predicted, based on previous reports for Tlg1 and Snc2 (Valdez-Taubas & Pelham, 2005), that Swf1-dependent palmitoylation of Tlg2 would result in reduced steady-state levels of endogenous Tlg2 in *swf1*Δ compared with wild type cells. It is evident from Figure 4-9 that Swf1 deficient cells exhibit reduced levels of endogenous Tlg2 (49 ± 24%, p=0.034) and Tlg1 (45 ± 23%, p=0.209) compared with wild type cells. This provides further evidence to support a role for Swf1 in mediating palmitoylation of Tlg2 which in turn regulates steady-state levels of the protein

perhaps by protecting it from ubiquitination and subsequent degradation in a manner analogous to that described for Tlg1 (Valdez-Taubas & Pelham, 2005). The degradation observed for Tlg2 in Figure 4-9 can occur via either the proteasome or vacuole under these conditions. The vacuolar contribution to this effect can be further investigated in future experiments by introducing *pep4-3* mutant into the wild type and *swf1*Δ genetic backgrounds.

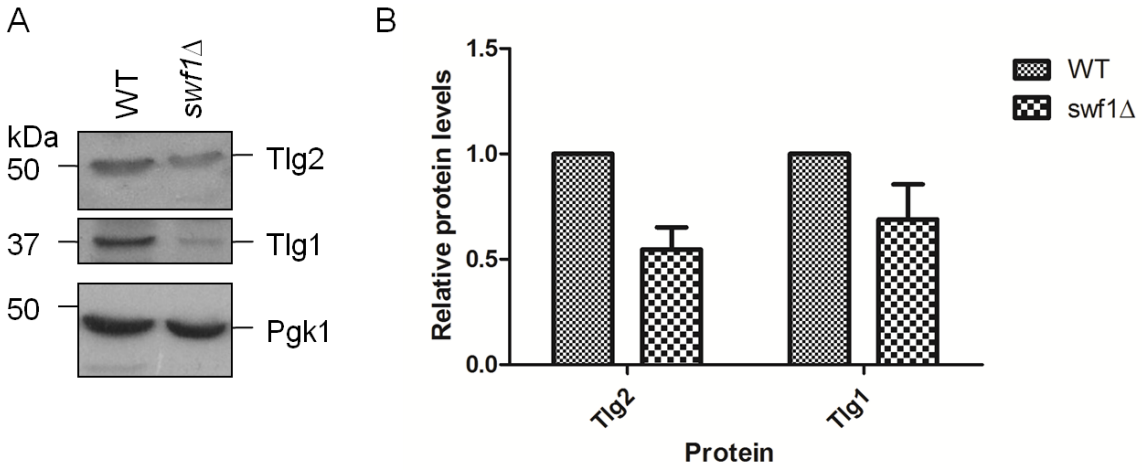

Figure 4-9. Endogenous levels of Tlg2 and Tlg1 are reduced in Swf1 deficient cells
A. Equal volumes of normalised wild type BY4742 (WT) or congenic *swf1*Δ yeast cell lysate were subjected to SDS-PAGE followed by immunoblot analysis using anti-Tlg2, anti-Tlg1 (positive control for Swf1-dependent palmitoylated protein) and anti-Pgk1 (loading control). Depletion of Swf1 reduced the steady-state levels of both Tlg2 and Tlg1. **B.** Densitometry analysis was performed using the ImageJ1.46r gel analysis tool (NHI). Tlg2 and Tlg1 protein levels were normalised to Pgk1 and compared to their respective wild type levels. These results are representative of n=3.

To further investigate palmitoylation of Tlg2, I performed resin-assisted capture of Tlg2 from wild type and *swf1*Δ cells. The acyl-RAC method (described in section 2.8.2) allows rapid identification of novel S-acylated protein species via resin-assisted capture (Forrester *et al.*, 2011). Briefly, yeast lysates prepared from wild type and Swf1 deficient cells were treated with the compound methyl methanethiosulfonate (MMTS) for 3 hours at 40°C to block unmodified cysteine residues. Proteins were precipitated, resuspended and subsequently incubated with thiopropyl Sepharose® beads in 0.5 M hydroxylamine or 0.5 M Tris-HCl as a control. Approximately 20 µl of the resuspended precipitated protein (400 µl) was saved as the total input. The protein-bead slurry samples were incubated overnight at room temperature and subsequently separated from the unbound proteins by centrifugation. The unbound fraction was transferred into a fresh

eppendorf tube and prepared for analysis as outlined in section 2.8.2 The thiopropyl Sepharose® bead-protein complex was thoroughly washed prior to eluting bound proteins from the beads by the addition of 4X LSB containing DTT. 15 µl of each sample was subjected to SDS-PAGE (section 2.3.1) followed by immunoblot analysis (sections 2.3.3 and 2.3.4) with anti-Tlg2 and anti-Pgk1 as a loading control. A schematic summary of the acyl-RAC protocol employed during this study is depicted in Figure 4-10.

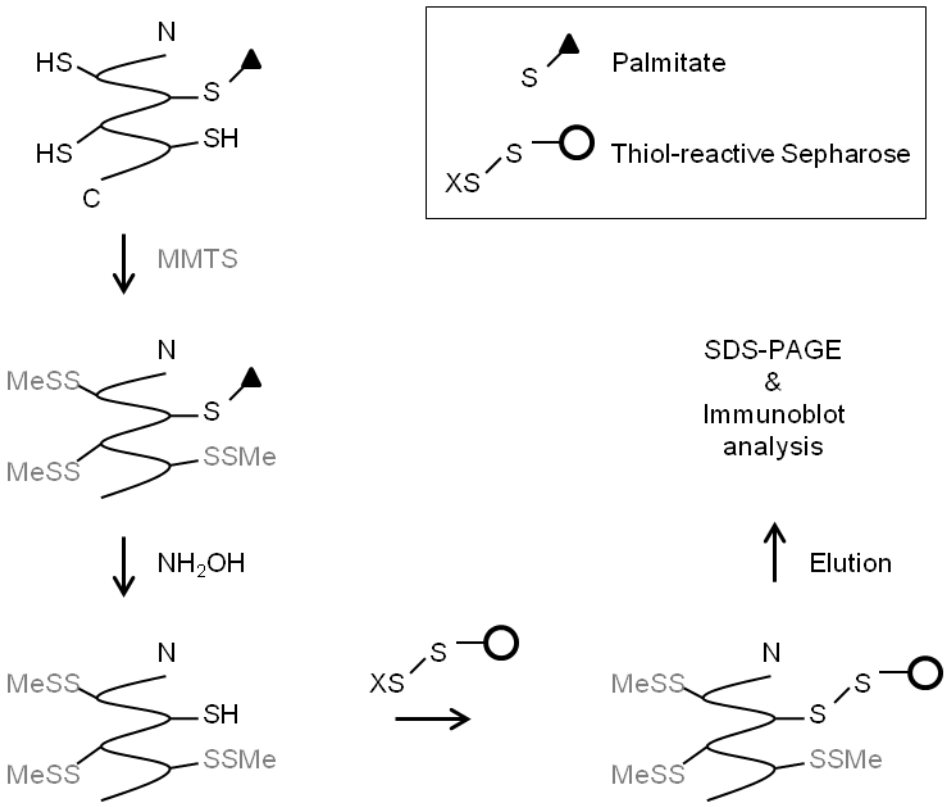

Figure 4-10. Schematic overview of resin-assisted capture of S-acylated proteins
Free cysteine residues present in proteins contained within yeast cell lysates were blocked with methyl methanethiosulfonate (MMTS).Thioester linked palmitate molecules were subsequently cleaved by the addition of neutral hydroxylamine (NH_2OH), or as a control Tris-HCl, in order to expose previously palmitoylated cysteine residues. The newly liberated thiols were captured with thiopropyl Sepharose® beads. The unbound proteins were transferred into a clean tube and the remaining bead-protein complex was thoroughly washed prior to eluting bound proteins from the beads using DTT. 15 µl of each sample was analysed by SDS-PAGE followed by immunoblot analysis using anti-Tlg2 and anti-Pgk1 as a loading control. Figure adapted from (Forrester *et al.*, 2011).

Analysis of wild type yeast lysates treated with hydroxylamine produced a Tlg2 specific protein band in the bound protein fraction (Figure 4-11, A). This band is absent in the Tris-HCl treated bound fraction, demonstrating that Tlg2 was recovered in a hydroxylamine-dependent manner. It is evident that, compared with

the unbound hydroxylamine treated fraction, only a small proportion of Tlg2 bound to the thiopropyl Sepharose® beads. This is likely to reflect a dynamic or transient process, i.e. at any point in time only a small percentage of Tlg2 present in the cell is palmitoylated. The absence of a Tlg2 specific band in the hydroxylamine treated bound fraction in *swf1*Δ cells (Figure 4-11, B) provides evidence that Tlg2 is palmitoylated in a Swf1-dependent manner. I attempted to include Snc2 and Tlg1 in my analysis as internal positive controls for palmitoylation however the respective antisera were consistently unable to detect endogenous levels of Snc2 and Tlg1 during the course of this work.

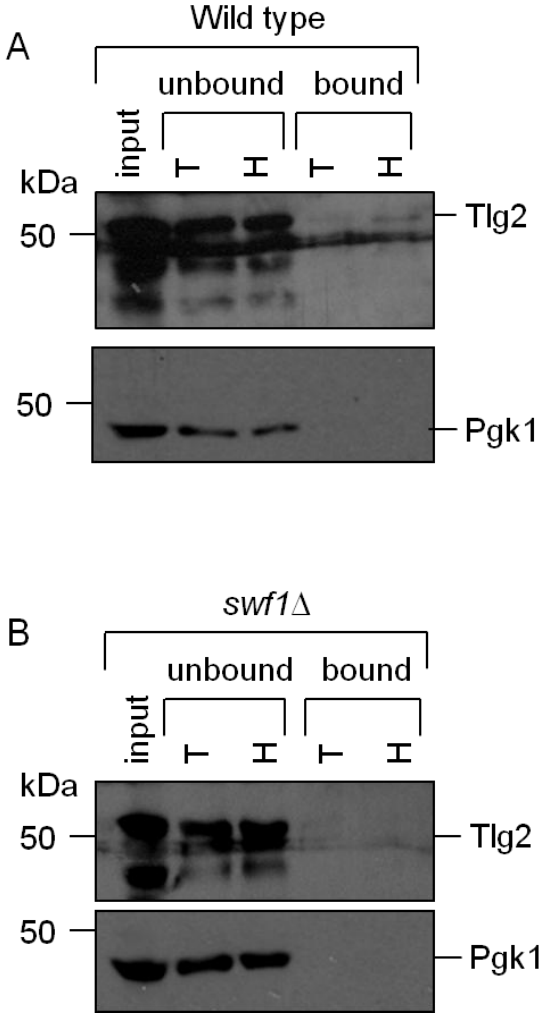

Figure 4-11. Endogenous Tlg2 is palmitoylated in wild type but not Swf1 deficient cells
Free cysteine residues present in proteins contained within wild type (**A**) and *swf1*Δ (**B**) yeast lysates were blocked with MMTS. Thioester linked palmitate moieties were subsequently cleaved by the addition of neutral hydroxylamine, or as control, Tris-HCl. Previously palmitoylated cysteine residues were now exposed in the hydroxylamine treated samples but not in the Tris-HCl treated samples. The addition of thiopropyl Sepharose® beads to the mix allowed for the capture of palmitoylated proteins now containing free cysteine residues. Unbound proteins were separated from the bead-protein complex by centrifugation. The bead-protein complex was thoroughly washed prior to eluting bound proteins from the beads. Samples were analysed by SDS-PAGE followed by immunoblot detection of Tlg2 and Pgk1 as a loading control.

Protein palmitoylation has been implicated in a range of functions including regulation of membrane interactions, intracellular sorting and protein stability (Veit *et al.*, 1996; Vogel & Roche, 1999; Valdez-Taubas & Pelham, 2005). It is unique in the sense that it is the only dynamic type of fatty acylation, thus palmitoylation may serve as a potential activation or signalling modification (Drisdel *et al.*, 2006). In order to determine if palmitoylation of Tlg2 plays a role in protecting Tlg2 from autophagy-mediated degradation, or alternatively, signal Tlg2 to the vacuole by autophagy, I performed resin-assisted capture of Tlg2 in wild type and *atg1*Δ cells as described for Figure 4-11. I predicted that the level of palmitoylated Tlg2 in *atg1*Δ cells would remain similar to that observed for wild type cells if palmitoylation served to protect Tlg2 from being degraded. On the contrary, disruption of autophagy would result in an increase of palmitoylated Tlg2 if palmitoylation served to signal Tlg2 to the vacuole in an autophagy-dependent manner.

Visual analysis indicated that the relative amount of Tlg2 recovered in the hydroxylamine treated bound fraction in wild type (WT) (Figure 4-12, A) and *atg1*Δ cells (Figure 4-12, B) are comparable. This portion reflects palmitoylated Tlg2. Densitometry analysis revealed that the percentage of Tlg2 present in the hydroxylamine bound fraction relative to the hydroxylamine unbound fraction was 18.2 ± 0.3% and 13.9 ± 3.2% in WT and *atg1*Δ cells, respectively (n=3). These data supports a role for palmitoylation in protecting Tlg2 from degradation possibly in a manner analogous to that previously described for Tlg1(Valdez-Taubas & Pelham, 2005). Lack of Tlg1 palmitoylation by Swf1 leads to Tul1-mediated ubiquitination of this protein. This signals the entry of Tlg1 into the MVB pathway and ultimate degradation by the vacuole (Reggiori & Pelham, 2001; Reggiori & Pelham, 2002).

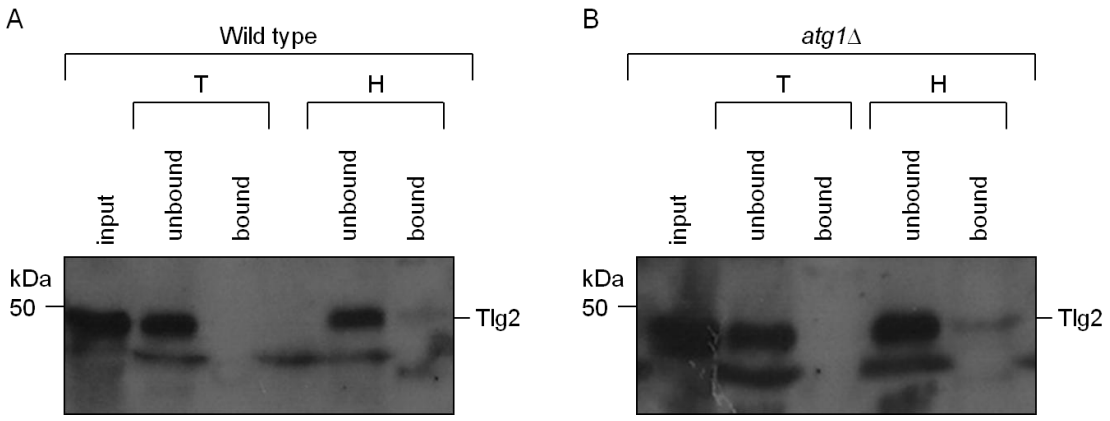

Figure 4-12. Levels of Tlg2 palmitoylation is comparable in wild type and *atg1*Δ cells
Wild type (WT) and *atg1*Δ extracts were treated with MMTS to block unmodified cysteine residues. Thioester linked palmitate molecules were subsequently cleaved by the addition of neutral hydroxylamine, or as a control, Tris-HCl. Palmitoylated proteins containing newly exposed cysteine residues were recovered by the addition of thiopropyl Sepharose® beads. Unbound proteins were separated from the bead-protein complex by centrifugation and bound proteins were eluted. Samples were analysed by SDS-PAGE followed immunoblot detection of Tlg2.

4.3 Chapter summary

This chapter documents a series of functional studies investigating the regulation of Tlg2 steady-state levels. I presented data to demonstrate that Tlg2 is regulated, at least in part, by the vacuole in wild type but not in Vps45 deficient cells (Figure 4-2 and Figure 4-3) and that autophagy plays a role in regulating Tlg2 levels under these conditions (Figure 4-7). Additionally, I demonstrated that Tlg2 undergoes Swf1-dependent palmitoylation (Figure 4-8, Figure 4-9 and Figure 4-11) and provide evidence to suggest that this reversible post-translational modification may serve to protect Tlg2 from being selectively degraded (Figure 4-12).

It is interesting to note that the steady-levels of Tlg2 were consistently higher in *atg1*Δ compared with *cog1*Δ cells, both of which disrupt autophagy (Figure 4-7). Subunits of the COG complex have previously been shown to directly associate with Atg proteins (Yen *et al.*, 2010). It is likely that Atg1 or its associated proteins are required for the efficient recruitment of Cog1 to the pre-autophagosomal structure (PAS). The kinase activity of Atg1 is regulated by autophosphorylation of residues present in its kinase domain. Mutation of the threonine 226 and serine 230 residues to alanine (T226A and S230A, respectively) result in loss of Atg1 kinase activity (Kijanska *et al.*, 2010). Phosphorylation of these residues is required to stabilise the structural conformation of the activation segments

(contained within the kinase domain), which in turn is suitable for substrate binding, catalytic activity and thereby autophagy induction (Goldberg *et al.*, 1996; Johnson *et al.*, 1996; Kijanska *et al.*, 2010). Thus, in the absence of Atg1, Cog1 would not be recruited to the site of autophagy initiation. Moreover, in the absence of Cog1, alternative proteins might functionally complement Cog1, whereas in the case of Atg1, this complementation may be less efficient. The remaining lobe A COG subunits have previously been shown to associate with Atg9, Atg12 and Atg17, all of which forms part of the core complex operating during the initial stages of autophagy induction (section 1.1.4) (Yen *et al.*, 2010). In the absence of Cog1, the Cog2, Cog3 and Cog4 subunits may mediate recruitment of the COG complex to the site of autophagy induction.

To further investigate the effects of palmitoylation of Tlg2, I would suggest future experiments whereby candidate cysteine residues that could serve as palmitoylation sites of Tlg2 be mutated. It would be interesting to investigate the steady-state levels and cellular distribution of Tlg2 under these conditions. Furthermore, palmitoyltransferases have previously been reported to have overlapping substrate specificities (Roth *et al.*, 2006). Therefore, performing acyl-RAC of Tlg2 in null mutants of the remaining six palmitoyltransferase proteins already identified in *S.cerevisiae* may provide further insight into the specificity of Swf1-mediated palmitoylation of Tlg2.

Collectively, the results presented in this chapter provide evidence in support of a role for autophagy and Swf1-dependent palmitoylation in the regulation of Tlg2 steady-state levels.

Chapter 5 – The T238N mutation in yeast Vps45

5.1 Overview and aims

Severe congenital neutropenia comprises a group of genetic disorders that is characterised by an increased susceptibility of neutrophil granulocytes and their precursors to undergo apoptosis (Klein, 2009). Neutrophil disorders are premalignant in nature and confer a predisposition to severe infections. Mutations in at least five different genes have been associated with this condition with the majority inherited in an autosomal dominant pattern (Dale *et al.*, 2000; Hernandez *et al.*, 2003; Person *et al.*, 2003). Less frequently, this condition is inherited in an autosomal recessive manner (Boztug *et al.*, 2009). Interestingly, a number of these congenital neutropenia associated genes encode endosomal-lysosomal related proteins (Nagle *et al.*, 1996; Dell'Angelica *et al.*, 1999). Two independent groups have recently associated homozygous Thr224Asn and Glu238Lys mutations of human *VPS45* with a rare form of congenital neutropenia (Stepensky *et al.*, 2013; Vilboux *et al.*, 2013). Vps45 regulates traffic through the endosomal system by regulating SNARE complex formation (Bryant & James, 2001). Vps45 deficient yeast cells display multiple phenotypes including reduced levels of its cognate syntaxin Tlg2 (Nichols *et al.*, 1998; Bryant & James, 2001).

The work presented in this chapter was a collaborative contribution to the data published in (Stepensky *et al.*, 2013). This chapter documents my introduction of Thr238Asn (T238N), which is analogous to Thr224Asn in the human protein, into yeast Vps45. Phenotypic and functional analysis of the yeast T238N Vps45 mutation was subsequently performed to investigate the effect of the patients' mutation on Vps45 function.

5.2 Results

5.2.1 Generation of the Vps45 T238N mutation in yeast

The introduction of the T238N Vps45 mutation in yeast was performed by site-directed mutagenesis (SDM) using a PCR-based approach. High copy (HC) (pCOG070) or low copy (LC) (pNB706) yeast expression plasmids (listed in Table 2-6) encoding a C-terminally HA-tagged version of wild type Vps45 was used as a template to produce a single codon change (ACA to AAT at codon position 238) in *VPS45* to create yeast expression plasmids pMC007 and pMC004, respectively, encoding HA-tagged Vps45T238N (listed in Table 2-6). The *VPS45* T238N For and *VPS45* T238N Rev primers (listed in Table 2-7) were employed for this purpose. Negative reaction controls were included using only *VPS45* T238N For primer in combination with the appropriate DNA template (either pCOG070 of pNB706). An aliquot of the products from these reactions was analysed by agarose gel electrophoresis (Figure 5-1) to check for presence of a higher proportion of DNA in the positive reactions (containing both forward and reverse primers in combination with HC or LC plasmid DNA template) (Figure 5-1, lanes 2 and 4, respectively) compared with their corresponding negative reaction controls (Figure 5-1, lanes 3 and 5).

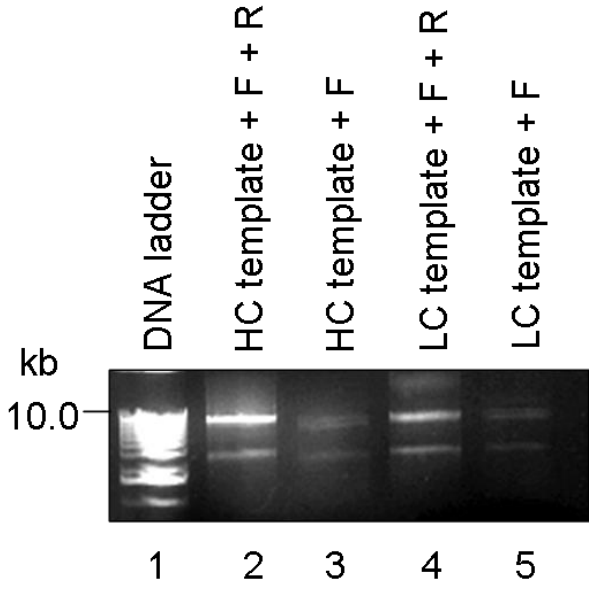

Figure 5-1. Products of site-directed mutagenesis for the production of yeast Vps45 T238N
Site-directed mutagenesis was performed on template double-stranded plasmid DNA using a PCR-based approach. The desired mismatched bases were incorporated into the centre of the primer pairs, which were complimentary to each other. Negative controls for each of the high copy (HC) or low copy (LC) plasmid DNA was included by omitting the reverse primer in each reaction. Following the reaction, equal volumes of product was analysed by agarose gel electrophoresis.

The remaining products were treated with the restriction endonuclease *DpnI* to selectively digest methylated template DNA (section 2.2.5). *DpnI*-resistant molecules were recovered by transforming *E.coli* to antibiotic resistance as outlined under section 2.11.2. Plasmid DNA was isolated from antibiotic resistant colonies and processed for DNA sequencing to confirm successful SDM. The *VPS45*T238N DNA sequences obtained following DNA sequence analysis were aligned with wild type *VPS45* DNA sequence (NCBI accession number NM_001180960) using Vector NTI® Software (Invitrogen Ltd.). A partial DNA sequence alignment for pMC007 (HC plasmid encoding HA-tagged Vps45T238N) with wild type *VPS45* is shown in Figure 5-2. This confirmed successful SDM of the 238th codon (nucleotide 714) from threonine (Thr) to asparagine (Asn) (ACA to AAT). The DNA sequence alignment results for pMC004 (LC plasmid encoding HA-tagged Vps45T238N) with wild type V*PS45* also revealed successful SDM (alignment not shown).

```
T238N        AGA-TGGCT-AAGAAGTTTCCTATGAGATTGGTAAAAACGAAAGAACttttttttGATTTT  69
             ||| ||||| ||||||||||||||||||||||||||||||||||||||||||||||||||||
WT VPS45     AGATTGGCTAAAGAAGTTTCCTATGAGATTGGTAAAAACGAAAGAACTTTTTTTGATTTT  654

T238N        CCTGTGATGGATTCGACACCTGTGTTACTAATTTTAGATCGTAATACTGATCCTATAAAT  129
             ||||||||||||||||||||||||||||||||||||||||||||||||||||||||||||
WT VPS45     CCTGTGATGGATTCGACACCTGTGTTACTAATTTTAGATCGTAATACTGATCCTATAACA  714

T238N        CCTTTACTTCAACCTTGGACCTACCAATCAATGATCAATGAGTATATAGGCATTAAGCGG  189
             ||||||||||||||||||||||||||||||||||||||||||||||||||||||||||||
WT VPS45     CCTTTACTTCAACCTTGGACCTACCAATCAATGATCAATGAGTATATAGGCATTAAGCGG  774

T238N        AATATAGTTGATTTATCGAAAGTGCCTAGAATTGATAAAGACCTGGAGAAGGTCACCTTA  249
             ||||||||||||||||||||||||||||||||||||||||||||||||||||||||||||
WT VPS45     AATATAGTTGATTTATCGAAAGTGCCTAGAATTGATAAAGACCTGGAGAAGGTCACCTTA  834
```

Figure 5-2. Partial DNA sequence alignment for pMC007 and yeast wild type *VPS45*
DNA sequence analysis results for the newly generated high copy (HC) yeast expression plasmid pMC007 (encoding HA-tagged Vps45T238N) were aligned with the wild type *VPS45* DNA sequence using Vector NTI® to confirm successful site-directed mutagenesis (SDM) at the 238th codon from ACA (encoding threonine, Thr) to AAT (encoding asparagines, Asp) (highlighted in grey).

5.2.2 The yeast Vps45 T238N position localises to domain 3a

Mutations in domain 3a of the SM family of proteins (section 1.3.1) have previously been shown to be defective in SNARE complex assembly and/or assembled SNARE complex binding (Boyd *et al.*, 2008; Hashizume *et al.*, 2009). I performed a multiple sequence alignment with yeast Vps33, yeast Vps45 and human Vps45 in order to determine if the yeast Vps45 T238N and the analogous human mutation, Vps45 T224N, localises to domain 3a (Figure 5-3). The crystal structure and domain regions for the SM protein Vps33 have recently been reported (Baker *et al.*, 2013). Sequence alignment analysis revealed that both the yeast and human mutation localise to a region within the domain 3a sequence. Steric hindrance induced by the yeast T238N and human T224N mutations may likely affect binding to their respective cognate syntaxin proteins, Tlg2 and Syntaxin 16. Functional analysis was employed to further investigate the effects of the yeast Vps45 T238N mutation (sections 5.2.3, 5.2.4 and 5.2.5).

```
Vps33       TNSIITNV--------VSIGNLSKRCSHLLKKRIDEH-QTENDLFIKGTLYGERTNCGLE
yVps45      TNSLVSVLLSLKIKPDIRYEGASKICERLAKEVSYEIGKNERTFF-------DFPVMDST
hVps45      TQGLTALLLSLKKCPMIRYQLSSEAAKRLAECVKQVI-TKEYELF-------EFRRTEVP
            *:.: : :        :     *: ..:* :        .*  :*       :

Vps33       MDLIILERNTDPITPLLTQLTYAGILDDLYEFNSG---------IKIKEKDMNFNYKEDK
yVps45      PVLLILDRNTDPITPLLQPWTYQSMINEYIGIKRNIVDLSKVPRIDKDLEKVTLSSKQDA
hVps45      PLLLILDRCDDAITPLLNQWTYQAMVHELLGINNNRIDLSRVPGISKDLREVVLSAENDE
              *:**:*  * *****   ** .::.:   ::          *. . ..: :. ::*

Vps33       IWNDLKFLNFGSIGPQLNKLAKELQTQY-DTRHKAESVHEIKEFVDSLGSLQQRQAFLKN
yVps45      FFRDTMYLNFGELGDKVKQYVTTYKDKT-QTNSQINSIEDIKNFIEKYPEFRKLSGNVAK
hVps45      FYANNMYLNFAEIGSNIKNLMEDFQKKKPKEQQKLESIADMKAFVENYPQFKKMSGTVSK
            :: :  :***..:* ::::     : :  . . : :*: ::* *::.  .::: .. : :
```

Figure 5-3. Sequence alignment of yeast Vps33 domain 3a with yeast and human Vps45
A multiple amino acid sequence alignment was performed for yeast Vps33 (yVps33) (NCBI accession number NP_013500), Vps45 (yVps45) (NCBI accession number NP_011420) and human Vps45 (hVps45) (NCBI accession number AAF86643) using the European Bioinformatics Institute multiple sequence alignment tool (available at http://www.ebi.ac.uk). The SM protein domain 3a structural region is indicated in light grey and was taken from (Baker *et al.*, 2013). The conserved threonine (T) residue at position 238 and 224 in yeast and human Vps45, respectively, is indicated in dark grey. * indicates regions that are 100% conserved.

5.2.3 Tlg2 is destabilised by the Vps45 T238N mutation in yeast

In order to investigate the effect of the patients' mutation on Vps45 function, I introduced the analogous mutation, Vps45T238N, or the wild type Vps45 protein into SEY6210 and RPY10 yeast cells lacking endogenous Vps45. Cells lacking endogenous Vps45 but harboring pMC007 (encoding Vps45T238N) have reduced levels of HA-tagged Vps45 by 44.4 ± 7.3% (p=0.049, n=3) compared with cells expressing wild type Vps45 from pCOG070. Tlg2 cellular were similarly reduced by 44.5 ± 9.4% (p=0.024, n=3) compared with cells expressing wild type Vps45 under the same conditions (Figure 5-4). This investigation was repeated in SEY6210 and RPY10 and their corresponding *vps45*Δ cells harboring the LC yeast expression plasmids pNB706 (encoding wild type Vps45) or pMC004 (encoding Vps45T238N) (Figure 5-5). The observations made for this series of experiments was identical to that reported for Figure 5-4. The plasmids encoding wild type Vps45 and Vps45 T238N are identical in all respects apart from the mutation of codon 238 (ACA to AAT). These results indicate that the T238N mutation in yeast Vps45 destabilises the protein.

The analogous mutation in human Vps45 (T224N) resulted in a similar effect on Vps45 expression in lymphoblastic cell lines derived from affected patients (Stepensky *et al.*, 2013). Vilboux and colleagues reported a similar effect on Vps45 expression in fibroblast cells derived from affected patients (Vilboux *et al.*, 2013). Additionally, the cellular level of the Vps45 binding partner Syntaxin 16, which is the ortholog of yeast Tlg2, was also reduced. Consistent with a role for the Vps45 domain 3a being crucial in its ability to promote SNARE complex assembly and/or binding to assembled SNARE complexes (section 5.2.2), human *VPS45* bearing the T224N mutation was diffusely localised throughout the cytoplasm of affected patients' neutrophils and fibroblasts. This reflects a likely obstruction in the ability of Vps45 to bind its cognate syntaxin, which provides the principal binding site for Vps45 on intracellular membranes (Nichols *et al.*, 1998). This effect may be secondary to a misfolding error caused by the single amino acid change in Vps45 T224N and similarly, in yeast Vps45 T238N. This may render Vps45 T224N unable to associate with membranes which may lead to it being rapidly degraded as a consequence. Vps45 has previously been shown to regulate Tlg2 steady-state levels (Nichols *et al.*, 1998; Bryant & James, 2001). Thus, the reduction observed in Tlg2 and Syntaxin 16 steady-levels in cells

harboring the *VPS45* T238N and T224N mutations, respectively, may be secondary to Vps45 being unstable under these conditions.

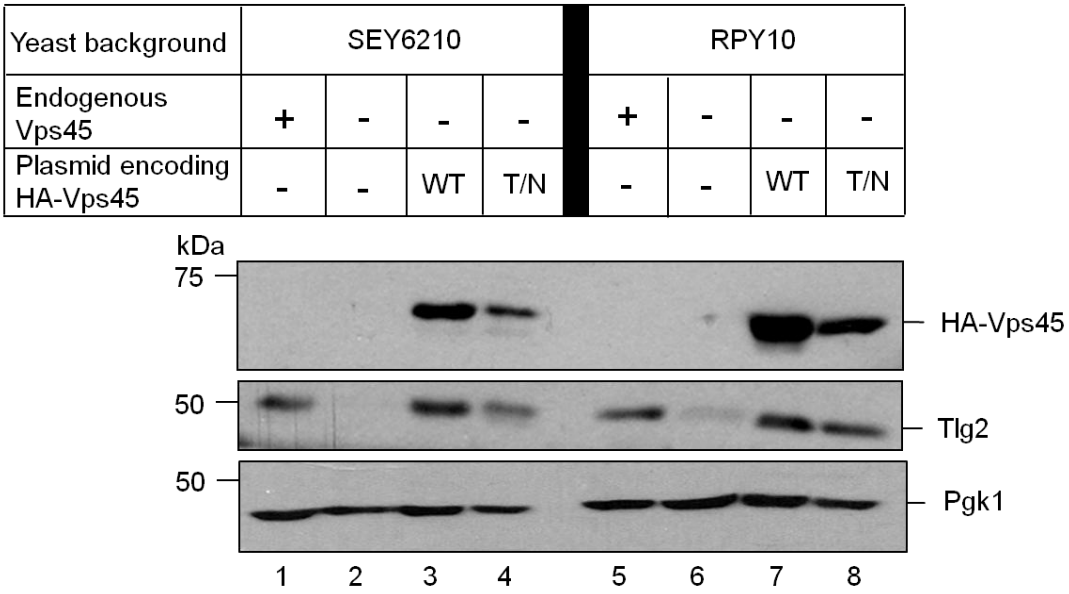

Figure 5-4. Yeast cells harboring the Vps45T238N mutation exhibit reduced cellular levels of Vps45 and Tlg2
Steady-state protein levels of Tlg2 was detected by immunoblot analysis in SEY6210 (lanes 1 to 4) or RPY10 cells (lanes 5 to 8) containing (+) or lacking (-) endogenous Vps45. In addition, HA-tagged versions of either wild type (WT) Vps45 or Vps45T238N (T/N) and endogenous Tlg2 were assessed in cells lacking endogenous Vps45 but harboring plasmids pCOG070 (encoding HA-tagged wild type Vps45) or pMC007 (encoding HA-tagged Vps45T238N). Levels of Pgk1 were assessed as a loading control in all cases. These results are representative of three independent experiments (n=3).

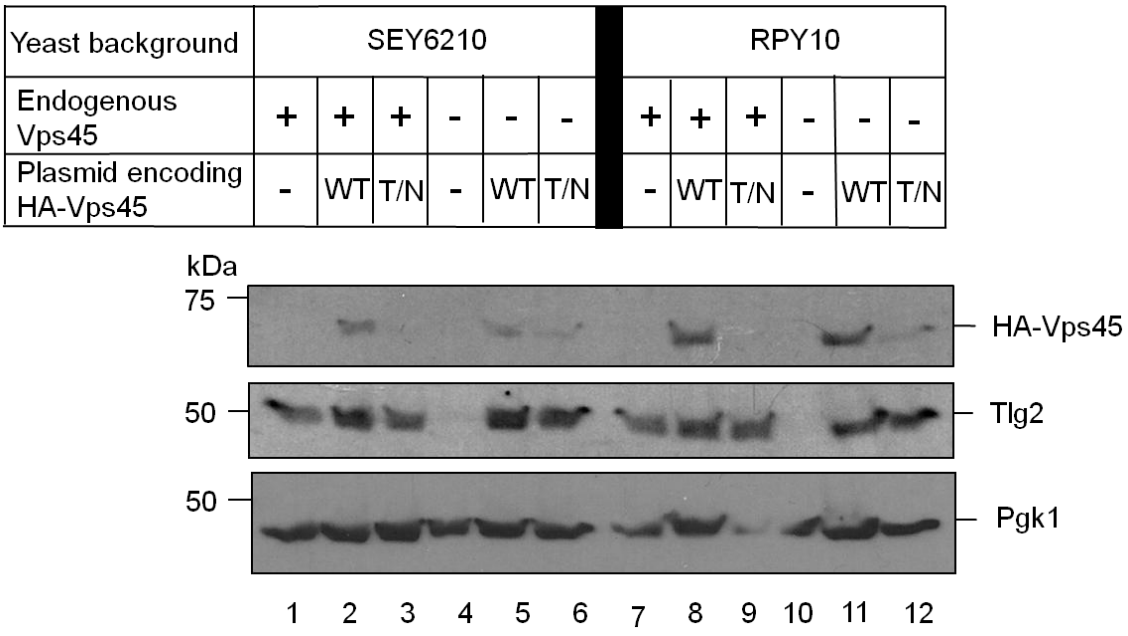

Figure 5-5. Cellular levels of Vps45 and Tlg2 are reduced in cells harboring low copy yeast expression plasmids encoding Vps45T238N
Steady-state protein levels of Tlg2 was detected by immunoblot analysis in SEY6210 (lanes 1 to 6) or RPY10 cells (lanes 7 to 12) containing (+) or lacking (-) endogenous Vps45 but harboring pNB706 (encoding HA-tagged wild type Vps45, WT) or pMC004 (encoding HA-tagged Vps45T238N, T/N). In addition, HA-tagged versions of either wild type Vps45 (WT) or Vps45T238N (T/N) were also assessed in cells containing (+) or lacking (-) endogenous Vps45. Levels of Pgk1 were assessed as a loading control in all cases. These results are representative of three independent experiments (n=3).

5.2.4 CPY is correctly sorted in yeast harboring the Vps45T238N mutation

Newly synthesised vacuolar proteins are transported to the vacuole by two distinct routes known as the carboxypeptidase Y (CPY) and alkaline phosphatase pathways (Conibear & Stevens, 1998). The former constitutes the principal pathway for the delivery of newly synthesised proteins, including CPY, to the vacuole. CPY is a soluble vacuolar hydrolase that normally resides within the vacuole. Vps45 was originally identified in yeast through isolation of mutants defective in the delivery and processing of multiple vacuolar hydrolases, including CPY (section 1.3.4) (Robinson *et al.*, 1988). Vacuolar protease sorting (*vps)* mutants have subsequently been classified into six distinct groups (A-F) based on vacuolar morphology (Raymond *et al.*, 1992). Vps45 belongs to the class D *vps* mutants and is required for traffic between the TGN and endosomes (Cowles *et al.*, 1994; Piper *et al.*, 1994). In order to investigate if the Vps45T238N mutation results in a vacuolar protein sorting phenotype in yeast, I set out to perform a CPY overlay assay as described under section 2.7. SEY6210 and RPY10 and their

congenic *vps45*Δ strains were transformed with YEp352 (empty vector), pCOG070 (encoding wild-type Vps45, WT) or pMC007 (encoding Vps45T238N, T/N). Analysis revealed that CPY was only secreted in *vps45*Δ cells harboring the empty vector (Figure 5-6). This indicates that Vps45T238N was able to complement the CPY sorting defect of *vps45*Δ mutant cells despite being present at reduced cellular levels compared to those found in wild type cells (Figure 5-4 and Figure 5-5).

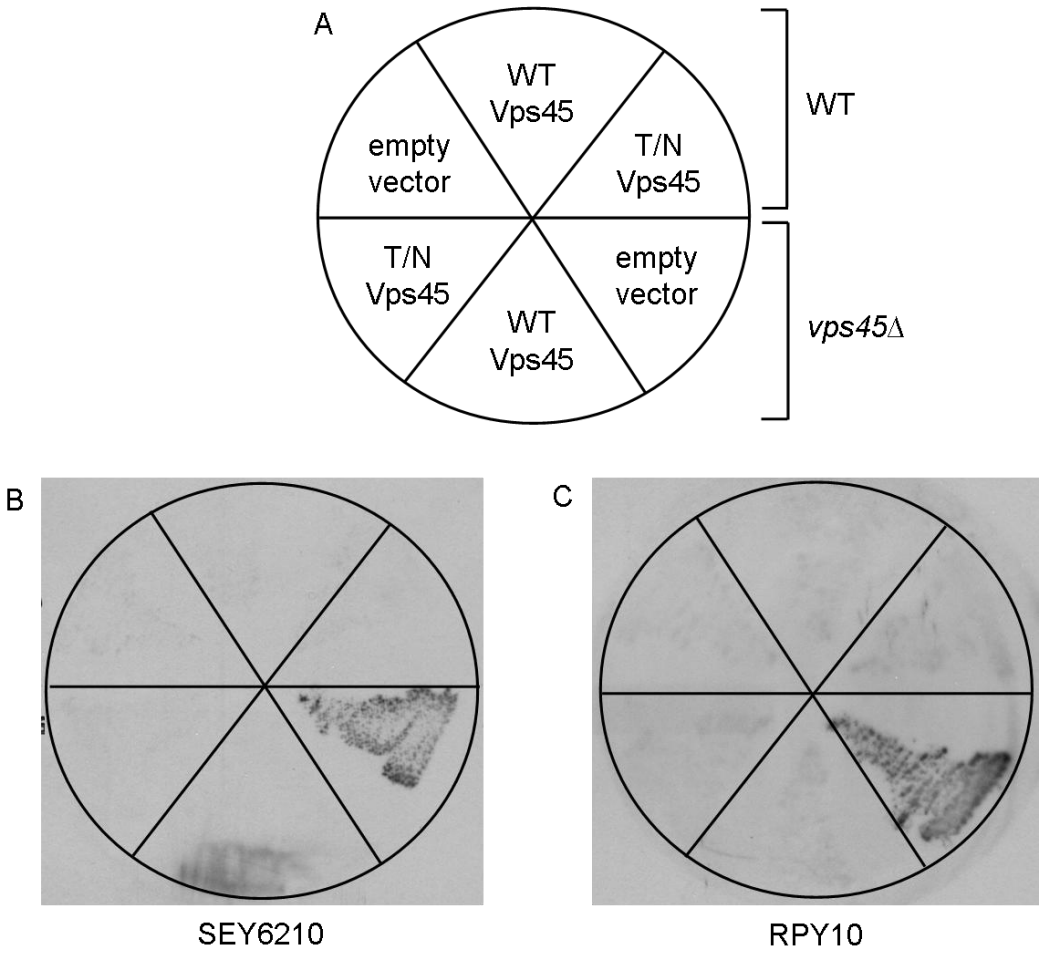

Figure 5-6. CPY is correctly sorted in yeast harboring the Vps45T238N mutation
A. Assay template. **B and C.** Secretion of caboxypeptidase Y (CPY) was assessed in SEY6210 and RPY10 yeast cells containing wild type (WT) Vps45 or lacking Vps45 (*vps45*Δ). In addition, secretion of CPY was assessed in WT and *vps45*Δ SEY6210 and RPY10 harboring plasmids Yep352 (empty vector), pCOG070 (encoding wild type Vps45; WT Vps45) or pMC007 (encoding Vps45T238N; T/N Vps45).

5.2.5 The T238N mutation in yeast *VPS45* leads to increased apoptosis

Fibroblasts, bone marrow and neutrophils from patients carrying the homozygous T224N mutation in human *VPS45* exhibit accelerated rates of apoptosis (Stepensky *et al.*, 2013; Vilboux *et al.*, 2013). The abnormal diffuse cytoplasmic cellular distribution of human Vps45 bearing the T224N mutation (Vilboux *et al.*, 2013) may directly result in perturbed delivery of protein cargo from the TGN to the endosomal pathway. Stepensky and colleagues (Stepensky *et al.*, 2013) speculated that, similar to the *ELANE* and *G6PC3* variants of congenital neutropenia (Grenda *et al.*, 2007; Boztug *et al.*, 2009), Vps45T224N may induce a block in the earlier secretory pathway, which in turn may lead to overwhelming endoplasmic reticulum (ER) stress and subsequent apoptosis.

Hydrogen peroxide (H_2O_2) has previously been shown to induce ER stress and subsequent apoptosis in *S.cerevisiae* as a direct result of reactive oxygen species (ROS) accumulation (Madeo *et al.*, 1999). This has validated yeast as a model system in which to study programmed cell death in higher eukaryotes (Frohlich & Madeo, 2001). In order to investigate if yeast cells harboring the analogous mutation in Vps45 (Vps45T238N) also exhibit increased apoptosis, I set out to perform H_2O_2 halo assays as outlined under section 2.10 (Gourlay & Ayscough, 2005). Briefly, yeast cells were grown overnight in YPD or selective media and diluted to an OD_{600} of 0.1 the following day. 1 ml of cells at an OD_{600} = 0.1 was evenly spread onto YPD or selective agar. Excess culture was removed and the agar was allowed to dry. Each strain was prepared in triplicate. Sterile filter discs saturated with 10 µl of solvent blank (sterile dH_2O), 0.3 mM, 0.6 mM or 1.5 mM H_2O_2 was carefully positioned onto each lawn of cells as depicted in Figure 5-7. The agar plates, which were prepared in triplicate and each containing four discs of solvent blank or H_2O_2, were incubated for 3 to 5 days at 30°C. The area of the halo, which was defined as the area where no cell growth has occurred, was measured in arbitrary units using the ImageJ 1.46r analysis tool (National Health Institute). The relative apparent sensitivity of each strain to H_2O_2 was calculated as described previously (Gourlay & Ayscough, 2005).

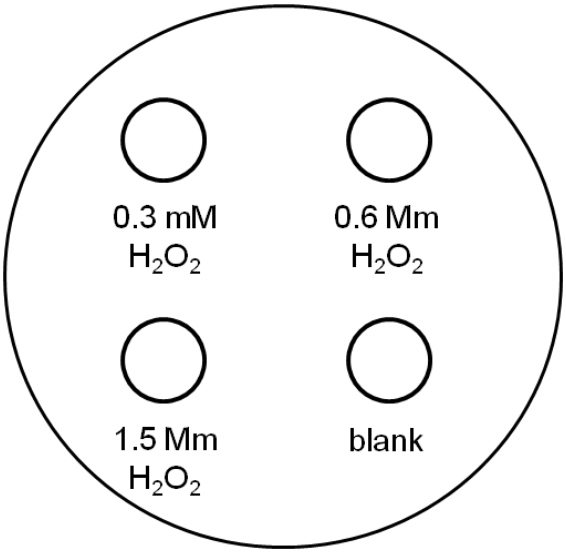

Figure 5-7. H_2O_2 halo assay template
YPD or selective agar was evenly covered with the desired yeast culture (OD_{600}=0.1). Agar plates were allowed to dry prior to carefully placing sterile filter discs saturated with 10 µl of solvent blank (dH_2O), 0.3 mM, 0.6 mM or 1.5 mM H_2O_2 onto the dried lawn of cells. Plates were incubated for 3 to 5 days at 30°C and halo areas were measured as previously described (Gourlay & Ayscough, 2005).

My initial H_2O_2 halo assay investigated the relative H_2O_2 sensitivity of SEY6210 (Figure 5-8, A) and RPY10 cells (Figure 5-8, B) containing or lacking endogenous Vps45 but harboring YEp352 (empty vector) with *vps45*Δ cells harboring pCOG070 (encoding wild type Vps45) or pMC007 (encoding Vps45T238N). Analysis of the halo areas revealed that SEY6210 and RPY10 *vps45*Δ cells harboring YEp352 was approximately 1.7 ± 0.1 (p=0.006) and 3.8 ± 1.1 (p=0.047) times more sensitive to H_2O_2-induced ER stress compared with their corresponding wild type cells. Vps45 deficient SEY6210 and RPY10 cells harboring pCOG070 (encoding wild type Vps45) was able to restore H_2O_2 sensitivity to that observed for their corresponding wild type cells (0.9 ± 0.1, p=0.214 and 0.8 ± 0.2, p=0.212). Vps45T238N was only able to partially restore the apoptotic phenotype observed for Vps45 deficient cells and remained approximately 1.2 ± 0.5 (p=0.472) and 2.9 ± 1.6 (p=0.176) times more sensitive to H_2O_2, respectively.

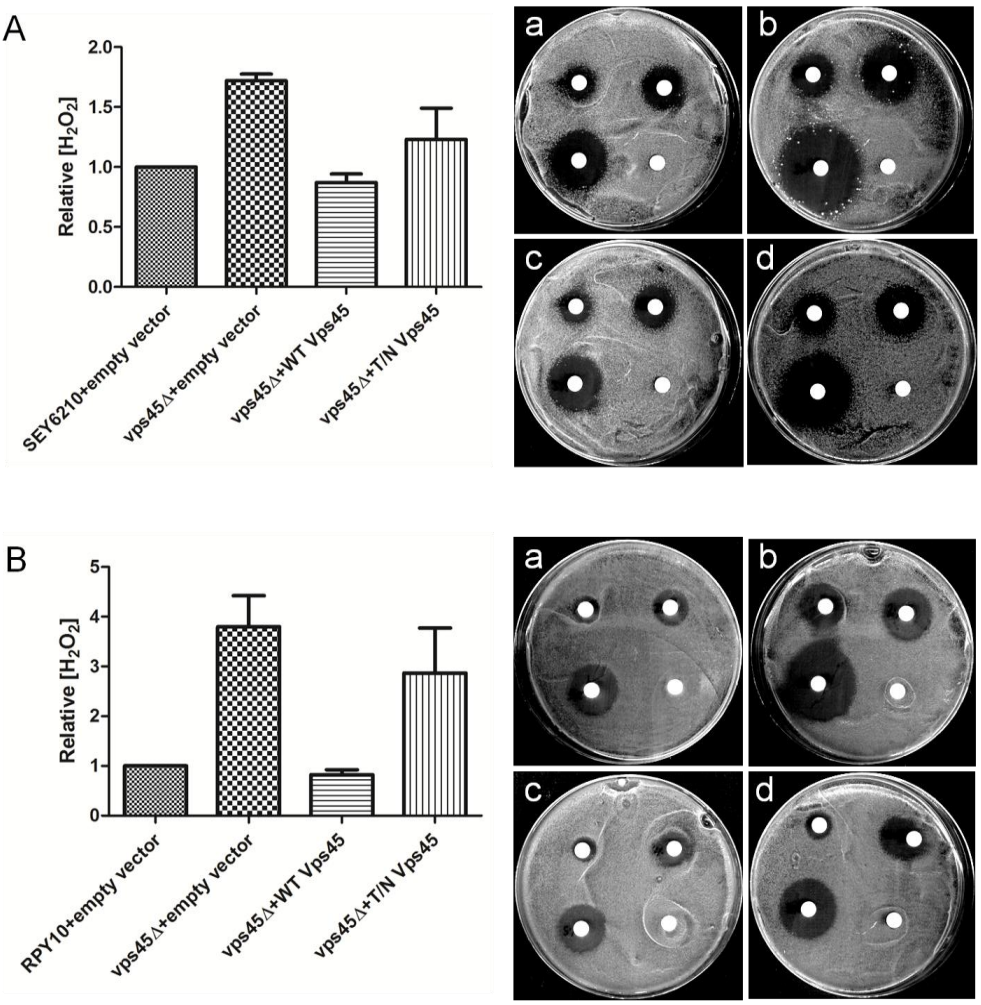

Figure 5-8. *vps45*Δ and Vps45T238N lead to increased apoptosis
The relative hydrogen peroxide (H_2O_2) sensitivity was calculated in SEY6210 (**A**) and RPY10 (**B**) cells containing (**a**) or lacking Vps45 (*vps45*Δ) (**b**) but harboring YEp352 (empty vector) and congenic *vps45*Δ cells harboring pCOG070 (encoding wild type Vps45, WT Vps45) (**c**) or pMC007 (encoding Vps45T238N, T/N Vps45) (**d**) as previously described (Gourlay & Ayscough, 2005).

The next step in my investigation was to determine if the increased sensitivity to H_2O_2 was specific to the class D *vps* mutants. For this assay I included RPY10 cells (all listed in Table 2-4) deficient in Vps45 (class D), Vps21 (class D) and Vps27 (class E) (Raymond *et al.*, 1992; Piper *et al.*, 1995). Additionally, I included RPY10 cells harboring the *pep4-3* mutation (lacking active vacuolar proteases) in a wild type and Vps45 deficient background. As an internal control for cells known to be sensitive to oxidative stress I included RPY10 *end3*Δ (Gourlay & Ayscough, 2005) cells in a *pep4-3* background. Lastly, to exclude the effect of reduced cellular levels of Tlg2 on the apoptotic phenotype observed in Vps45 deficient cells I also included RPY10 *tlg2*Δ cells in my assay. Halo assay analysis (Figure 5-9) revealed that cells deficient in Vps45 either by itself or in combination with *pep4-3*

exhibited the most severe apoptotic phenotype. Vps45 deficient and *vps45*Δ *pep4-3* cells were 2.4 ± 0.03 and 2.9 ± 0.3 times more sensitive to H_2O_2 when compared with wild type cells, respectively. Cells harboring the *pep4-3* and *pep4-3 end3*Δ mutations were 1.4 ± 0.2 and 1.7 ± 0.1 times more sensitive to H_2O_2 compared with wild type cells. Vps21 (class D *vps* mutant) and Vps27 (class E *vps* mutant) deficient cells only exhibited a slight increase of 1.2 ± 0.07 and 1.0 ± 0.03, respectively, in their relative H_2O_2 sensitivities when compared with wild type cells. The H_2O_2 sensitivity of Tlg2 deficient cells was comparable to that observed for wild type cells (1.1 ± 0.2). Collectively these results imply that the observed increased sensitivity of Vps45 deficient cells to H_2O_2 is specific to Vps45, and not to the *vps* class D mutants as a whole. This potentially identifies a previously uncharacterised phenotype of Vps45, which is consistent with the apoptotic phenotype observed in neutrophil and fibroblast cells of patients' affected by the Vps45 T224N variant of congenital neutropenia (Stepensky *et al.*, 2013; Vilboux *et al.*, 2013). This apoptotic phenotype is unrelated to the vacuolar protein sorting phenotype previously described for *vps* mutants (Cowles *et al.*, 1994; Piper *et al.*, 1994). The mechanism by which Vps45 deficient cells and yeast expressing Vps45T238N give rise to increased H_2O_2 sensitivity remains unclear and will require further investigation.

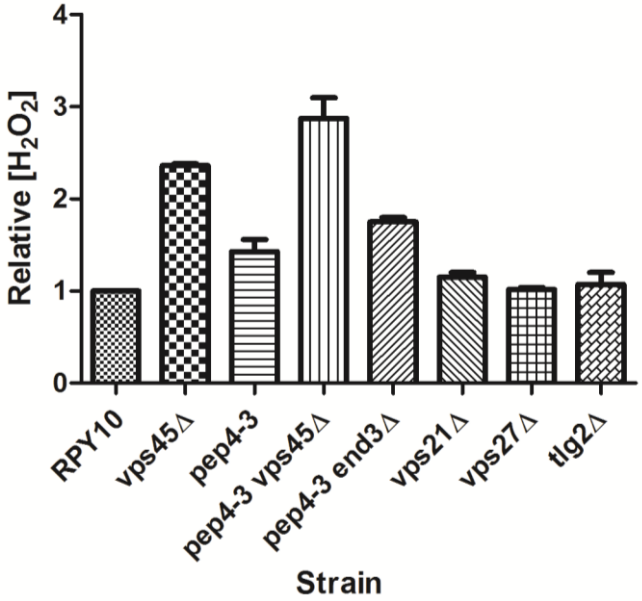

Figure 5-9. Vps45, but not Vps21 or Vps27 deficient cells, lead to increased H_2O_2-induced apoptosis
The relative hydrogen peroxide (H_2O_2) sensitivity was calculated in RPY10 wild type and congenic *vps45*Δ, *pep4-3*, *vps45*Δ *pep4-3*, *pep4-3 end3*Δ, *vps21*Δ (class D *vps* mutant), *vps27*Δ (class E *vps* mutant) and *tlg2*Δ cells as previously described (Gourlay & Ayscough, 2005).

5.2.6 Chapter summary

Homozygous Thr224Asn mutations in human *VPS45* have recently been associated with a rare form of congenital neutropenia (Stepensky *et al.*, 2013; Vilboux *et al.*, 2013). This chapter documents analysis of the analogous mutation, Thr238Asn, in yeast Vps45.

This chapter describes the generation and confirmation of low copy (pMC004) and high copy (pMC007) yeast expression plasmids encoding Vps45T238N (Figure 5-1 and Figure 5-2). This was performed by SDM using the corresponding plasmids encoding wild type Vps45 (pNB706 and pCOG070, respectively) as a template followed by subsequent DNA sequence analysis. Yeast cells containing or lacking endogenous Vps45 and expressing Vps45T238N from a plasmid (either pMC004 or pMC007) have reduced cellular levels of Vps45 and its cognate SNARE Tlg2 compared with cells expressing wild type Vps45 (from pNB706 or pCOG070, respectively) under the same conditions (Figure 5-4 and Figure 5-5). Tlg2 has a half life of >2 hours in wild type cells. However, in *vps45*Δ cells this is reduced to approximately 20 minutes despite being synthesised to levels comparable with wild type cells (Bryant & James, 2001). Based on this observation, my results are likely to indicate that the T238N mutation destabilises yeast Vps45. This may perturb efficient cargo delivery from the TGN to the endosomal pathway and in effect may partially block the earlier secretory pathway. This in turn may lead to increased ER stress and subsequent apoptosis as seen in patients with the *ELA2* variant of congenital neutropenia (Grenda *et al.*, 2007). Furthermore, I have demonstrated that T238N mutation in yeast Vps45 does not result in a vacuolar protein sorting defect but instead is able to complement wild type Vps45 in its ability to restore CPY trafficking despite being present at much reduced cellular levels (Figure 5-6).

Congenital neutropenia is characterised by a low absolute neutrophil count which predisposes affected individuals to severe infections (Klein, 2009). I have provided evidence that yeast cells harboring Vps45T238N exhibit an increased sensitivity to H_2O_2-induced ER stress, which leads to accelerated apoptosis (Figure 5-8). This is in agreement with observations made on neutrophil and fibroblast cells isolated from patients affected with the analogous mutation, Vps45T224N (Stepensky *et al.*, 2013; Vilboux *et al.*, 2013). I have provided evidence to show that this effect

appears to be specific to Vps45, and not class D *vps* mutants as a whole (Figure 5-9). Therefore, this work has identified a novel phenotype of *vps45* mutant cells. However, the mechanism by which this apoptotic phenotype is induced remains to be investigated. This may provide us with new insight into the molecular functions of Vps45.

Chapter 6 – Autophagy and endosomal trafficking in *C.elegans* development

6.1 Overview and aims

C.elegans post-embryonic development proceeds through four larval stages, referred to as L1 to L4, prior to reaching adulthood (section 1.5.1) (Singh & Sulston, 1978). The end of each of the four larval stages is defined by moulting of the cuticle which is synthesised five times during development: once in the embryo and subsequently at the end of each of the four larval stages prior to moulting [reviewed in (Page & Johnstone, 2007)]. The cuticle is synthesised by an underlying hypodermal cell layer that surrounds the body of the animal (section 1.5.2). Newly synthesised cuticular components are secreted via the apical membrane of the hypodermal cells. Each moult is preceded by a large increase in abundance of intracellular membranes and vesicles, as observed by transmission electron microscopy, within the hypodermal cells which reflects increased synthetic activity of cuticular components that is predominantly composed of soluble collagen proteins (Singh & Sulston, 1978; Page & Johnstone, 2007). This increased abundance in intracellular membranes and vesicles associated with cuticle synthesis is rapidly cleared following each moult. However, the molecular mechanisms involved in this clearance remain to be investigated.

Lysosomal degradative pathways, including the endocytic and autophagy pathways, are implicated in cellular remodelling during *C.elegans* development (Gengyo-Ando *et al.*, 2007; Kovacs & Zhang, 2010; Sato & Sato, 2013). *C.elegans* VPS-45 has previously been shown to be implicated in nematode viability, development and the endocytic pathway (Gengyo-Ando *et al.*, 2007). Additionally, the quantity of autophagic vacuoles in hypodermal cells is significantly elevated at the end of each of the four larval stages (Kov *et al.*, 2000) which coincides with the clearance of the pre-moult increase in intracellular components.This chapter documents the role of autophagy and endosomal trafficking and associated proteins, including VPS-45, in mediating the clearance of the pre-moult increase in intracellular membranes and vesicle.

6.2 Results

C.elegans cuticle components, including collagen proteins, exhibit a unique temporal pattern of expression (Cox *et al.*, 1981a; Johnstone & Barry, 1996; Johnstone, 2000). Synthesis of cuticle components peak during the moulting periods and is much reduced during the inter-moult periods. Monomeric cuticle collagens are synthesised as pro-collagens and configure into trimeric structures within the ER. Cuticle collagens polymerise upon secretion from the hypodermal cells and remain intact as the mature cuticle. The *C.elegans* cuticle is highly resistant to solubilisation (Cox *et al.*, 1981b). Thus, the soluble DPY-7 and DPY-10 protein that can be detected using standard immunoblot analysis of solubilised *C.elegans* whole animal extracts reflects the intracellular portion of these proteins within the secretory system. The cuticle collagen proteins DPY-7 and DPY-10 have been shown to be obligate partners and co-localise within the cuticle (McMahon 2003). Glycine substitution mutations in either *dpy-7* or *dpy-10* accumulate not only more soluble protein than their respective wild type counterparts, but also accumulate more of their obligate DPY-10 or DPY-7 wild type partner protein, respectively. This reflects accumulation within the secretory system of the mutant glycine substitution monomers and their respective wild type obligate partners, presumably as they are recognised as being misfolded within the ER. In addition to collagen glycine substitution mutations, whereby the resultant protein's function is compromised, loss-of-function mutations have also been described previously (McMahon *et al.*, 2003). The *dpy-7(qm63)* mutation is a complete deletion of the *dpy-7* gene. The phenotype exhibited by *dpy-7(qm63)* mutant nematodes is identical to that described for the splice site mutant of *dpy-10(e128)*, which results in a premature stop codon and thereby transcription of a very short peptide. Thus, both *dpy-7(qm63)* and *dpy-10(e128)* are considered to be null mutants. In contrast to the glycine substitution mutants, *dpy-7* and *dpy-10* null mutants result in the absence of any detectable soluble DPY-7 and DPY-10, respectively, as well as their corresponding wild type or glycine substitution obligate DPY-10 or DPY-7 partners.

Furthermore, *dpy-7* and *dpy-10* null mutant nematodes exhibit identical phenotypes: they are shorter and fatter than their wild type N2 counterparts, a phenotype that is classified as dumpy (Dpy). Glycine substitution mutant alleles in *dpy-7* and *dpy-10* induce a phenotype that is identical to that described for the null

mutants when cultured at 25°C. However, this Dpy phenotype is less exaggerated at 20°C. This indicates some residual function in the mutant protein at lower temperatures. Therefore, glycine substitution mutant alleles in *dpy-7* and *dpy-10* behave as partial loss-of-function at 20°C. The Dpy phenotype was utilised in this study to identify *C.elegans* harboring homozygous *dpy-10(sc48)* glycine substitution or *dpy-10(e128)* null mutations at 20°C (section 6.2.1 and 6.2.2).

The temporal behaviour of the DPY-10 protein in wild type, *dpy-10(sc48)* glycine substitution and *dpy-10(e128)* null mutants is known. Both DPY-7 and DPY-10 protein accumulate intracellularly in the *dpy-10(sc48)* glycine substitution mutants and are retained within the secretory membrane organelles, most likely within the ER where collagen trimerisation occurs. The observable accumulation in glycine substitution collagen proteins disappear at a time during the moulting cycle that coincides with the disappearance of the increased abundance of intracellular membranes and vesicles. Thus, it can be assumed that the process responsible for the clearance of the increased intracellular content after each moult is also involved in removing the secretory membranes and mutant collagens retained within. Studying the temporal and spatial behaviour of DPY-7, an obligate partner of DPY-10, at the protein level in wild type and glycine substitution mutant backgrounds therefore provides us with a molecular tool to indirectly investigate the mechanism(s) that regulate the appearance and disappearance of the intracellular increase in membranes and vesicles preceding each moult.

The temporal behaviour of DPY-7, the obligate partner of DPY-10, is known in wild type, *dpy-10(sc48)* and *dpy-10(e128)* mutant backgrounds (McMahon *et al.*, 2003). Thus, to assess a role for autophagy and endosomal trafficking in regulating the cyclical appearance and disappearance of the intracellular increase in membranes and vesicle preceding each moult, I initially set out to generate double mutants between the *dpy-10(sc48)* glycine substitution and *dpy-10(e128)* null mutant and either endosomal trafficking [*vps-45(tm246)*] or autophagy [*unc-51(e369)*] deficient strains (sections 6.2.1 and 6.2.2). In particular, I was interested in studying the temporal behaviour and cuticular localisation of the DPY-10 obligate partner, DPY-7, in these newly generated strains (sections 6.2.4.2, 6.2.5.1, 6.2.5.1and 6.2.5.2). Additionally, I also characterised the phenotypes of these mutant *C.elegans* in order to gain a better understanding of the role of

autophagy and endosomal trafficking under these conditions (sections 6.2.3 and 6.2.4).

6.2.1 Disruption of autophagy in *dpy-10* mutant backgrounds

The molecular understanding of autophagy has almost exclusively originated from genetic screens performed in the yeast *S.cerevisiae* (Xie & Klionsky, 2007; Nakatogawa *et al.*, 2009). Many of the autophagy related genes, or *ATG* genes, have orthologs in higher eukaryotes, including *C.elegans*. *unc-51* (uncoordinated gene 51) is the *C.elegans* ortholog of *atg1 (*Matsuura et al., 1997). Similar to yeast *atg1*∆, *C.elegans unc-51* mutants are viable but result in mislocalization of the autophagy marker GFP-LGG-1, the worm homolog of yeast Atg8 and mammalian LC3 (Melendez *et al.*, 2003). *C.elegans unc-51* mutants are mostly paralyzed, egg-laying defective and dumpy (Brenner, 1974; Ogura *et al.*, 1994; Aladzsity *et al.*, 2007). Research has mainly focused on the neuronal aspects of this phenotype. However, the Dpy phenotype is consistent with a role for UNC-51 in cuticle formation. These behavioural and phenotypic characteristics allow for the visual identification of *unc-51* mutant *C.elegans* strains.

C.elegans genetic crosses were performed as outlined under section 2.13.6. Briefly, male N2 *C.elegans* were mated with IA337 [*dpy-10(sc48)*] or CB128 [*dpy-10(e128)*] hermaphrodites at 20°C and resulting heterozygous *dpy-10(sc48)* or *dpy-10(e128)* male offspring were subsequently mated at 20°C with CB369 [*unc-51(e369)*] hermaphrodites (Figure 6-1). Hermaphrodite offspring from the latter two crosses were cloned out onto separate plates and were visually monitored for segregating homozygous *dpy-10(sc48); unc-51(e369)* or *dpy-10(e128); unc-51(e369)* progeny. Candidate homozygous *dpy-10(sc48); unc-51(e369)* or *dpy-10(e128); unc-51(e369)* progeny were further selected and visually monitored at 20°C for segregating identical offspring based on phenotype (mostly paralyzed and dumpy). The newly generated IA835 [*dpy-10(sc48); unc-51(e369)*] (Figure 6-2) and IA836 [*dpy-10(e128); unc-51(e369)*] (Figure 6-3) strains were routinely cultured at 20°C and were used for further investigations as outlined under sections 6.2.3 and 6.2.4.

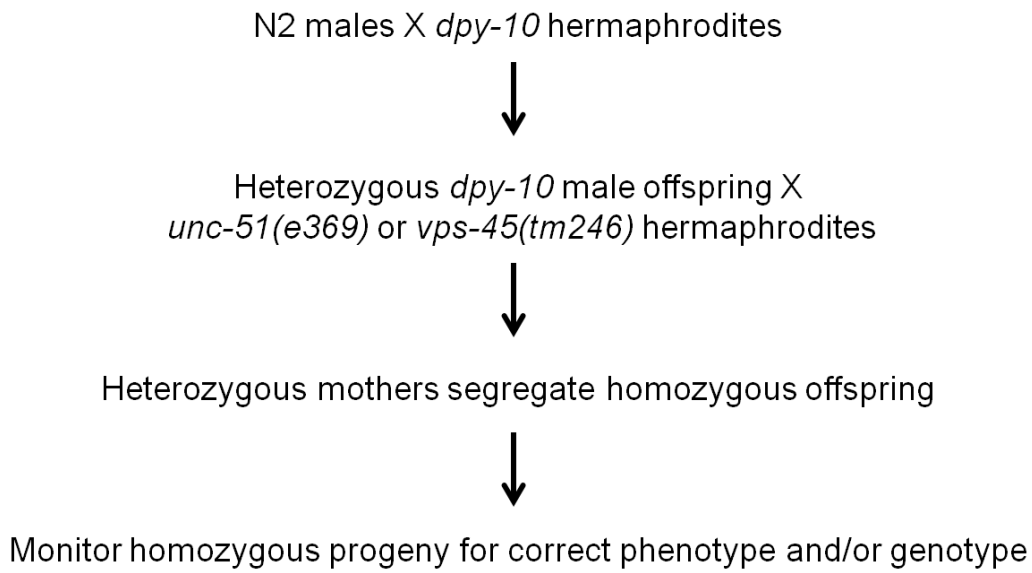

Figure 6-1. Summary of *C.elegans* genetic crosses
Wild type (N2) males were mated with *dpy-10(sc48)* (strain I337) or *dpy-10(e128)* (strain CB128) hermaphrodites. Resulting heterozygous *dpy-10(sc48)* or *dpy-10(e128)* male offspring were subsequently mated with *unc-51(e369)* (strain CB369) or *vps-45(tm246)* (strain IA757) hermaphrodites to produce strains IA835 [*dpy-10(sc48); unc-51(e369)*] and IA836 [*dpy-10(e128); unc-51(e369)*] or IA779 [*dpy-10(sc48);vps-45(tm246)*] and IA823 [*dpy-10(e128); vps-45(tm246)*], respectively. Heterozygous mothers from the latter cross segregated homozygous double mutant offspring whose progeny were subsequently monitored for the correct phenotype and/or genotype.

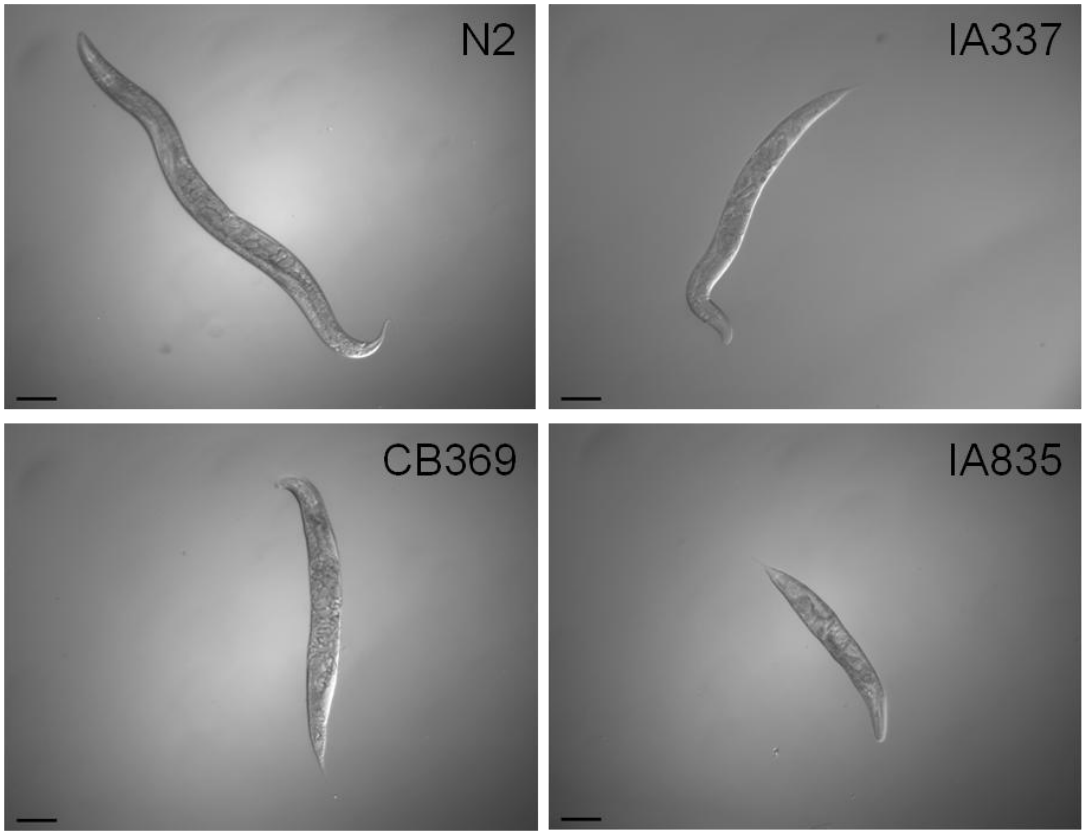

Figure 6-2. Phenotypic identification of *C.elegans* strain IA835
Variation in the severity of the dumpy phenotype at 20°C is evident between different adult *C.elegans* strains shown at the same magnification (scale bar represents 100 µm). Wild type strain (N2), *dpy-10(sc48)* mutant (IA337), *unc-51(e369)* mutant (CB369), *dpy-10(sc48); unc-51(e369)* double mutant (IA835).

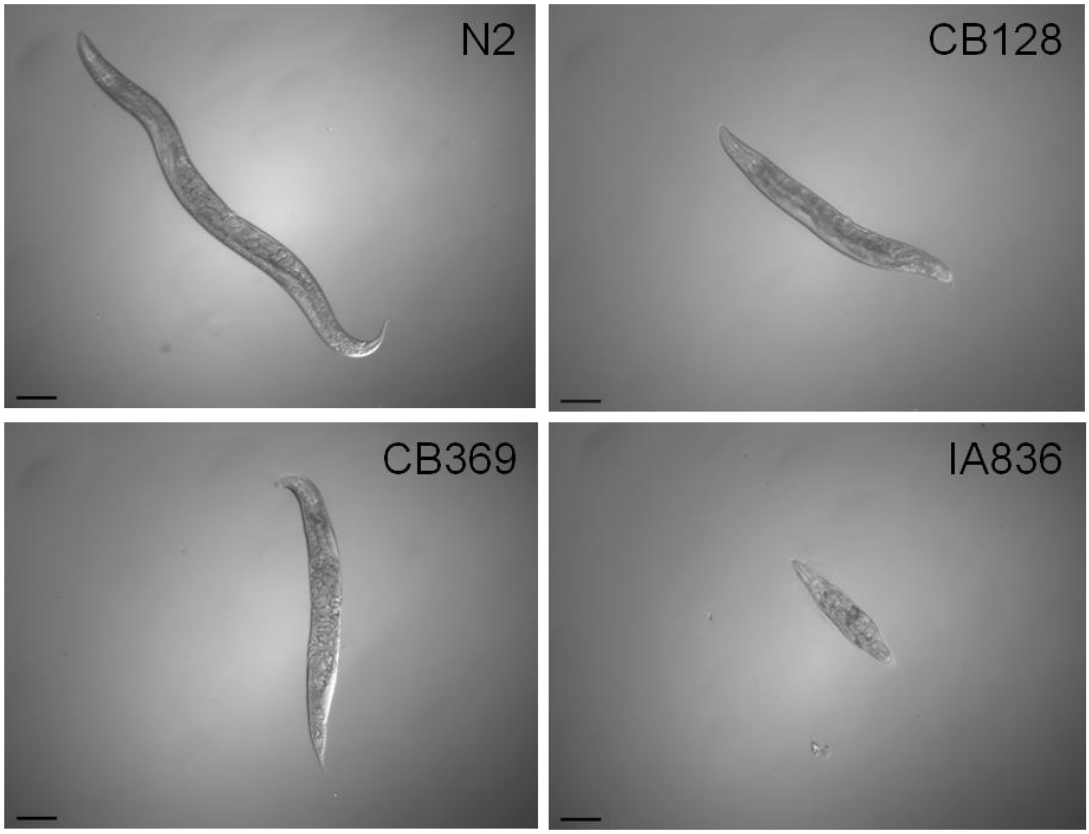

Figure 6-3. Phenotypic identification of *C.elegans* strain IA836
Variation in the severity of the dumpy phenotype at 20°C is evident between different adult *C.elegans* strains shown at the same magnification (scale bar represents 100 µm). Wild type strain (N2), *dpy-10(e128)* mutant (CB128), *unc-51(e369)* mutant (CB369), *dpy-10(e128); unc-51(e369)* double mutant (IA836).

6.2.2 Disruption of endosomal trafficking in *dpy-10* mutant backgrounds

C.elegans VPS-45 is ubiquitously expressed during nematode development and shares high sequence homology with yeast Vps45 and mVps45 (Bock *et al.*, 2001). *C.elegans* harboring homozygous *vps-45(tm246)* deletion alleles (strain IA757; refer to Table 2-5) are temperature sensitive and exhibit endocytosis and moulting defects (Gengyo-Ando *et al.*, 2007). The *tm246* mutation contains a deletion extending from the promoter to the fourth exon (depicted in Figure 6-4) and is likely to be a null allele. Identifying this mutant allele based on phenotype is difficult as it does not exhibit an obvious phenotypic defect. Thus, the *tm246* deletion allele was detected by single worm PCR which easily permits genotyping.

The *vps-45(tm246)* homozygous mutant alleles were introduced into the *dpy-10(sc48)* and *dpy-10(e128)* mutant backgrounds to investigate a role for

endosomal trafficking in the clearance of excess intracellular membranes and vesicles following each moult. Male N2 *C.elegans* were mated with IA337 [*dpy-10(sc48)*] or CB128 [*dpy-10(e128)*] hermaphrodites at 20°C and resulting heterozygous *dpy-10(sc48)* or *dpy-10(e128)* male offspring were subsequently mated at 15°C with IA757 [*vps-45(tm246)*] hermaphrodites (Figure 6-1). Homozygous *vps-45(tm246)* animals segregating from heterozygous mothers were identified by PCR amplification using single worm genomic DNA as a template (section 2.13.4) and primers spanning the *vps-45(tm246)* deletion region. More specifically, PCR amplification (prepared as outlined in Table 2-8) contained three primers: two forward primers and one reverse primer (Figure 6-4). The two forward primers (*vps-45* WT sense and vps-*45 tm246* sense2, Table 2-7) were either specific to amplifying the wild type *vps-45* or *vps-45(tm246)* allele and produced DNA products that were 629 and 490 bp, respectively. The reverse primer (*vps-45 tm246* anti2, Table 2-7) was common to both the wild type vps-*45* and mutant *vps-45(tm246)* alleles. This allowed for the identification of heterozygous or homozygous *vps-45(tm246)* mutant *C.elegans*. Figure 6-5 show PCR confirmation of homozygosity of the *vps-45(tm246)* alleles in the newly generated IA779 [*dpy-10(sc48); vps-45(tm246)*] and IA823 [*dpy-10(e128); vps-45(tm246)*] double mutant strains. The presence of homozygous *dpy-10(sc48)* or *dpy-10(e128)* alleles in the IA779 and IA823 double mutant strains were identified based on the Dpy phenotype they exhibit (Figure 6-6and Figure 6-7, respectively). These are true-breeding strains thus all subsequent progeny are homozygous for the mutant alleles identified.

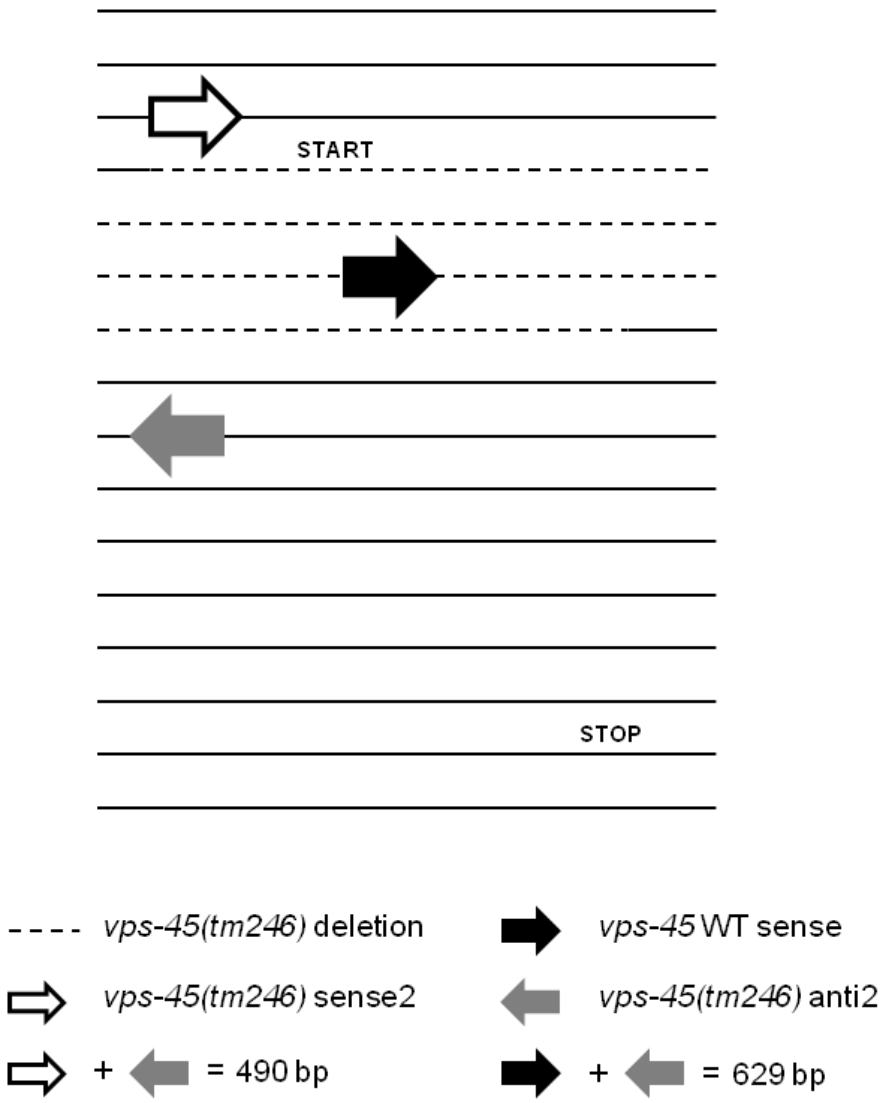

Figure 6-4. Schematic diagram of *vps-45* and *vps-45(tm246)* PCR analysis
Single worm PCR amplification was employed to confirm homozygosity of the *vps-45(tm246)* allele in the newly generated IA779 [*dpy-10(sc48); vps-45(tm2346)*] and IA823 [*dpy-10(e128); vps-45(tm246)*] strains. Each PCR contained three primers in order to detect homozygous or heterozygous vps-*45* or *vps-45(tm246)* alleles. The *vps-45* WT sense and *vps-45(tm246)* sense2 forward primers were designed to amplify the wild type *vps-45* or *vps-45(tm246)* alleles, respectively. The reverse primer [*vps-45(tm246)* anti2] was common to both the wild type and mutant alleles. Wild type VPS-45 and vps-45(tm246) DNA products were 629 and 490 bp, respectively.

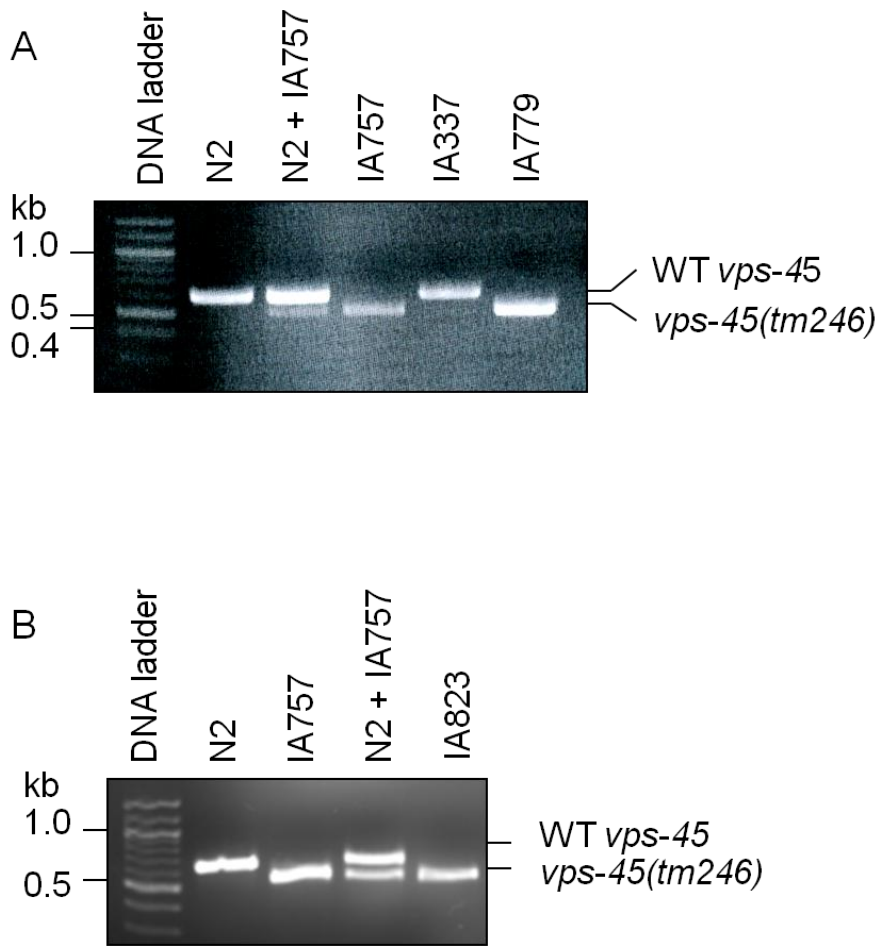

Figure 6-5. PCR analysis confirming homozygosity of *vps-45(tm246)* in strains IA779 and IA823

vps-45 specific primers *vps-45* WT sense, *vps-45 tm246* sense2 and *vps-45 tm246* anti2 (refer to Table 2-7) were used in combination with single worm genomic DNA as a template for PCR (as depicted in Figure 6-4) to confirm homozygosity of the *vps-45(tm246)* alleles in strains IA779 [*vps-45(tm246)*;*dpy-10(sc48)*] (A) and IA823 [*vps-45(tm246)*;*dpy-10(e128)*] (B). **A.** Control PCR reactions were included for the wild type (N2), N2 + *vps-45(tm246)* (IA757) [mock *vps-45(tm246)* heterozygous sample], IA757 and *dpy-10(sc48)* (IA337) strains. **B.** Control PCR reactions were included for the N2, IA757 and N2 + IA757 [mock *vps-45(tm246)* heterozygous sample] strains. PCR products were analysed by agarose gel electrophoresis (2%). The PCR products for the wild type *vps-45* and *vps-45(tm246)* alleles are 629 and 480 base pairs (bp), respectively.

Figure 6-6. Phenotypic identification of *C.elegans* strain IA779
Variation in the severity of the dumpy phenotype at 20°C is evident between different adult *C.elegans* strains shown at the same magnification (scale bar represents 100 µm). Wild type strain (N2), *dpy-10(sc48)* mutant (IA337), *vps-45(tm246)* mutant (IA757), *dpy-10(sc48); vps-45(tm246)* double mutant (IA779).

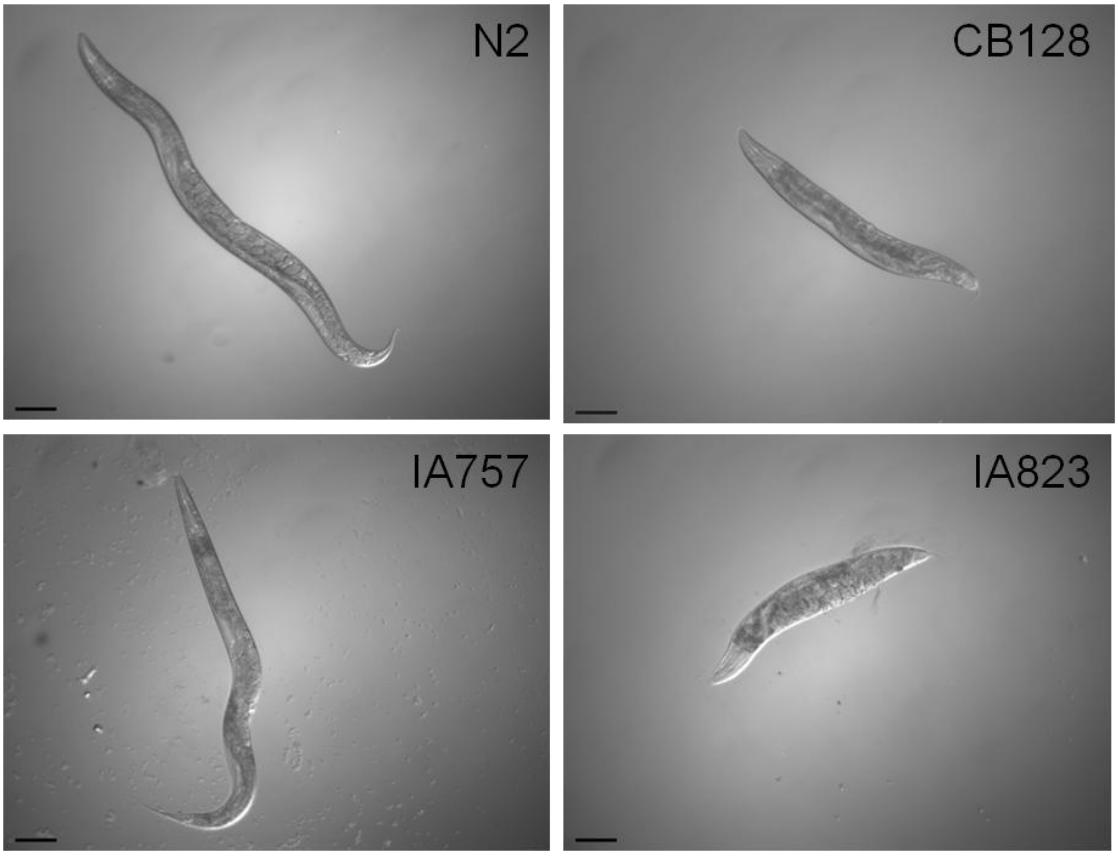

Figure 6-7. Phenotypic identification of *C.elegans* strain IA823
Variation in the severity of the dumpy phenotype at 20°C is evident between different adult *C.elegans* strains shown at the same magnification (scale bar represents 100 µm). Wild type strain (N2), *dpy-10(e128)* mutant (CB128), *vps-45(tm246)* mutant (IA757), *dpy-10(e128); vps-45(tm246)* double mutant (IA823).

6.2.3 Characterisation of *C.elegans* strains

The phenotypic characteristics of the *C.elegans* strains used during this study is summarised in Table 2-5. Adult body lengths of the newly generated autophagy deficient IA835 and IA836 and endosomal trafficking deficient IA779 and IA823 double mutant strains were compared with wild type and their respective single mutant strains at 15°C. The data presented in Figure 6-8 were obtained by measuring 10 adult nematodes from each individual strain and determining the mean body length. Adult N2, IA337 and CB128 nematodes continuously cultured at 15°C measured 1201 ± 65 µm, 861 ± 18 µm and 741 ± 66 µm, respectively (Figure 6-8). These results are consistent with a Dpy phenotype exhibited by the IA337 (p=0.001) and CB128 (p=0.001) strains when compared with wild type *C.elegans*. Adult nematodes from the newly generated autophagy deficient IA835 (819 ± 93 µm, p=0.005) and IA836 (736 ± 46 µm, p=0.01) double mutant strains

consistently measured shorter than the CB369 autophagy deficient single mutant strain (991 ± 49 µm) (Figure 6-8, A). Similarly, endosomal trafficking deficient IA779 (992 ± 55 µm, p=0.201) and IA823 (718 ± 81 µm, p=0.014) double mutant strains also measured shorter than the endosomal trafficking deficient single mutant strain IA757 (1066 ± 55 µm) (Figure 6-8, B). CB369 (Aladzsity *et al.*, 2007) and IA757 adult nematodes measure shorter than wild type N2 nematodes (Brenner, 1974) grown under the same conditions (p=0.019 and p=0.041, respectively). Consistent with previous reports, this observation indicates a role for both autophagy and endosomal trafficking in normal *C.elegans* growth (Aladzsity *et al.*, 2007).

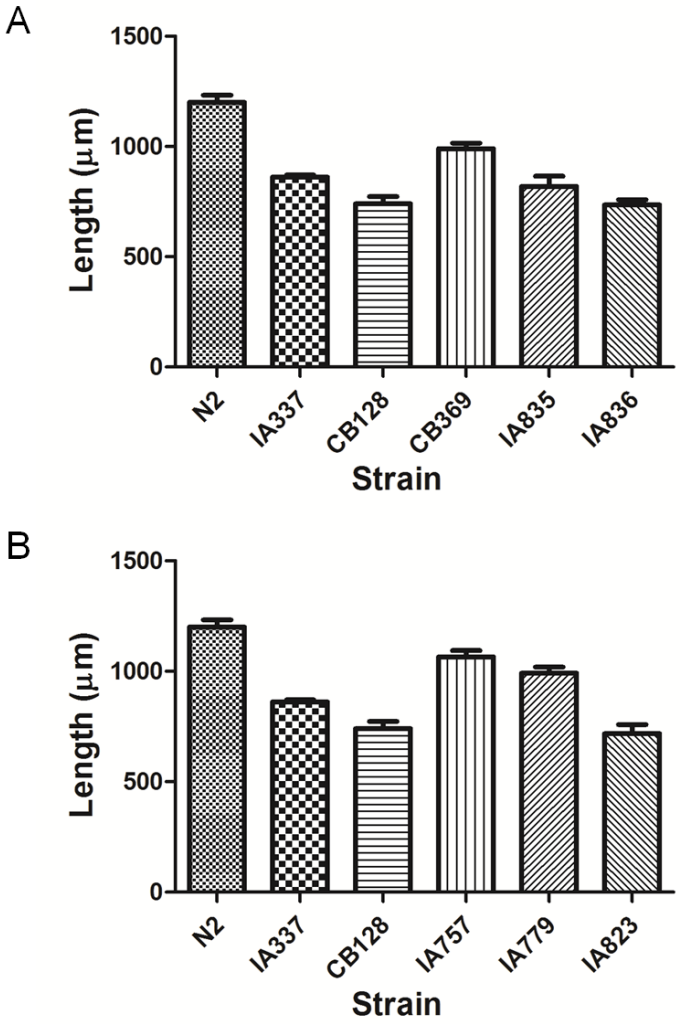

Figure 6-8. Mutant *C.elegans* body size
Adult nematode body lengths were measured for autophagy (CB369) and endosomal trafficking deficient (IA757) strains (**A** and **B**, respectively) in the wild type (N2), *dpy-10(sc48)* glycine substitution (IA337) *and dpy-10(e128)* null mutant (CB128) backgrounds. Measurements were obtained from 10 adult nematodes for each individual strain continuously cultured at 15°C. Error bars represent the standard deviation of the measurements.

C.elegans larval development at 15°C was measured for endosomal trafficking deficient single and double mutant strains (Figure 6-9). This analysis was not performed for the autophagy deficient strains due to severe egg-laying deficiencies (refer to section 6.2.4). The N2 larval development duration recorded during this study was 93.5 ± 13.4 hours (3.9 days) compared with 114 ± 25.5 hours (4.8 days) for endosomal trafficking deficient nematodes (strain IA757). Larval development for the *dpy-10(sc48)* and *dpy-10(e128)* single mutant strains was 93.5 ± 13.4 (3.9 days) and 113.5 ± 19.1 hours (4.7 days). This compared with 112 ± 14.1 (4.7 days) and 120 ± 17.7 hours (5 days) for strains IA779 and IA823, respectively.

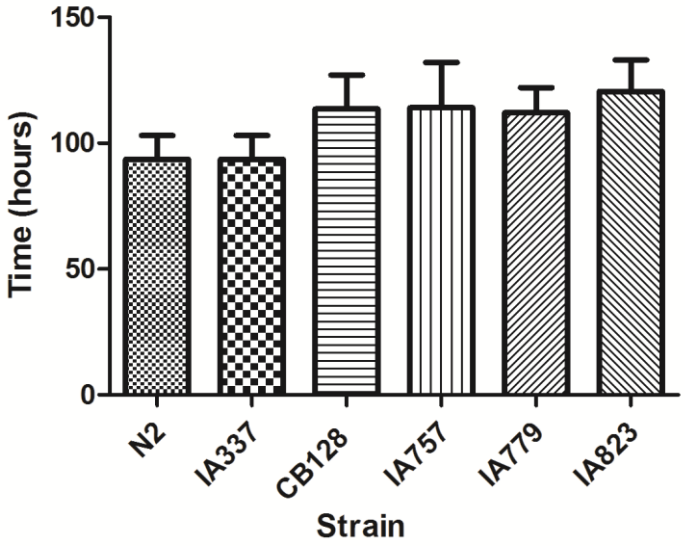

Figure 6-9. Larval development for endosomal trafficking deficient *C.elegans*
Larval development for N2 (wild type), IA337 [*dpy-10(sc48)*], CB128 [*dpy-10(e128)*], IA757 [vps-*45(tm246)*], IA779 [*dpy-10(sc48); vps-45(tm46)*] and IA823 [*dpy-10(e128); vps-45(tm246)*] was monitored. The duration is expressed in hours. This data was collected from 70 nematodes from each individual strain continuously cultured at 15 °C. Error bars represent the standard deviation of the measurements.

Embryonic lethality for N2, IA337, CB128, IA757, IA779 and IA823 continuously cultured at 15°C was 26%, 10%, 9%, 9%, 6% and 63% respectively (Figure 6-10). Collectively these results indicate that the *vps-45(tm246)* and *dpy-10(e128)* mutant alleles produced the biggest impact on post-embryonic development. In particular, embryonic viability was greatly reduced in the *vps-45(tm246); dpy-10(e128)* double mutant strain (IA823). Loss of both VPS-45 and DPY-10 protein function produced a compounding effect as regards to embryonic lethality therefore VPS-45 function is required for normal embryonic development in the *dpy-10(e128)*

mutant strain, and vice versa. This compounding effect on embryonic lethality was not observed for the *dpy-10(sc48)* mutant strain. At 15°C, the *dpy-10(sc48)* allele exhibits a considerable amount of function in the *vps-45(tm246)* mutant background and is successfully secreted and present within the cuticle. This suggests that the biological impact produced by the *vps-45(tm246)* mutant allele in the *dpy-10(e128)* null and *dpy-10(sc48)* glycine substitution mutant backgrounds are mechanistically different.

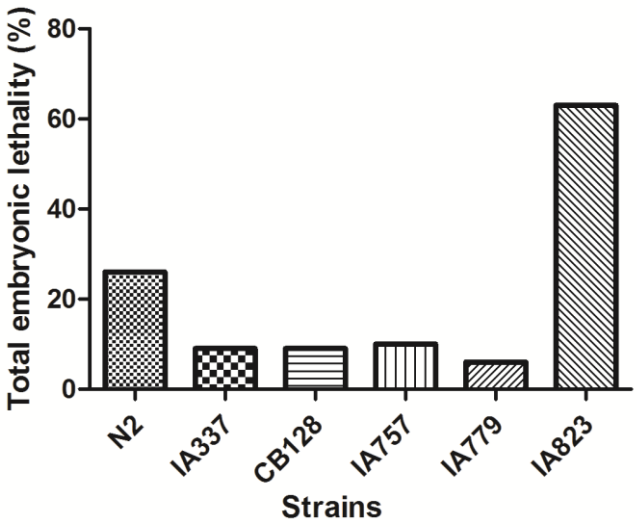

Figure 6-10. *C.elegans* embryonic viability measured at 15°C
C.elegans larval development was measured for strains N2 (wild type), IA337 [*dpy-10(sc48)*], CB128 [*dpy-10(e128)*], IA757 [vps-*45(tm246)*], IA779 [*dpy-10(sc48); vps-45(tm46)*] and IA823 [*dpy-10(e128); vps-45(tm246)*] continuously cultured at 15°C. Seventy eggs for each strain were picked and the duration to adulthood was monitored. The number of eggs that remained uhatched was quantified as a percentage of the total eggs picked.

6.2.4 *C.elegans* development and a role for autophagy

The newly generated IA835 and IA836 autophagy deficient strains (Table 2-5) were further investigated to determine the role of autophagy in the clearance of the surge in intracellular membrane preceding each moult.

I initially set out to investigate if the IA835 double mutant strain accumulates more DPY-7 compared with its respective single mutant strains, IA337 and CB369. The IA337 strain accumulates more DPY-7 than the wild type N2 strain. However, the overall levels of DPY-7 in the autophagy deficient mutant CB369 strain have not been investigated previously. I hypothesised that if autophagy played a role in the

clearance of the surge in intracellular membrane following each moult, the autophagy deficient CB369 strain would accumulate more DPY-7 when compared with the N2 strain. Furthermore, the IA835 double mutant strain would accumulate more DPY-7 than both the IA337 and CB369 strains if autophagy was involved in this clearance process. I relied on obtaining mixed staged *C.elegans* cultures due to the difficulties predicted in synchronising the different mutant strains employed for this investigation. In particular, the IA835 strain was difficult to maintain due to their unusually slow development and severe phenotypes, even at 15°C. These challenges also prevented me from preparing frozen stocks of this strain as I was never able to get enough animals cultured for this purpose. The same difficulties were encountered for the IA836 strain which exhibited an even more severe phenotype (section 6.2.4.1)

6.2.4.1 Morphological characterisation of autophagy deficient *C.elegans*

This investigation subsequently progressed into an observational study. I further characterised the phenotypes of IA835 and IA836 at 15°C, 20°C and 25°C using light microscopy (2.13.7). Homozygous *unc-51(e369)* nematodes are egg-laying deficient and dumpy (refer to Table 2-5) however temperature sensitivities have not been reported for these behavioural and phenotypic defects (Brenner, 1974). The dumpy phenotype of the *dpy-10(sc48)* glycine substitution mutant is more pronounced but not lethal at the non-permissive temperatures of 20°C and 25°C (personal communication with Dr Iain Johnstone). The dumpy phenotype of the *dpy-10(e128)* null mutant is not temperature sensitive and appears similar at 15°C, 20°C and 25°C. It was evident at low magnification that the gross morphology and dumpy phenotype of the IA835 (Figure 6-11, A) and IA836 (Figure 6-11, B) nematodes gradually worsened with increasing temperatures of 20°C and 25°C. This change in morphology and dumpy phenotype was more severe than their respective single mutants which are indicative of a compounding effect caused by the double *dpy-10(sc48);unc-51(e369)* and *dpy-10(e128); unc-51(e369)* mutant alleles, respectively. The more pronounced dumpy phenotype in the IA836 double mutant strain at 20°C and 25°C was unexpected as the dumpy phenotype in the respective single CB128 or CB369 mutant strains do not exhibit temperature sensitivities. IA836 nematodes cultured at 25°C typically displayed a burst phenotype which suggests a weak cuticle (Figure 6-11, B). This phenotype is not observed for the CB128 and CB369 single mutant strains. As before, this implies a

compounding effect caused by the *dpy-10(e128)* and *unc-51(e369)* alleles and a possible and previously uncharacterised role for *unc-51* in cuticle formation.

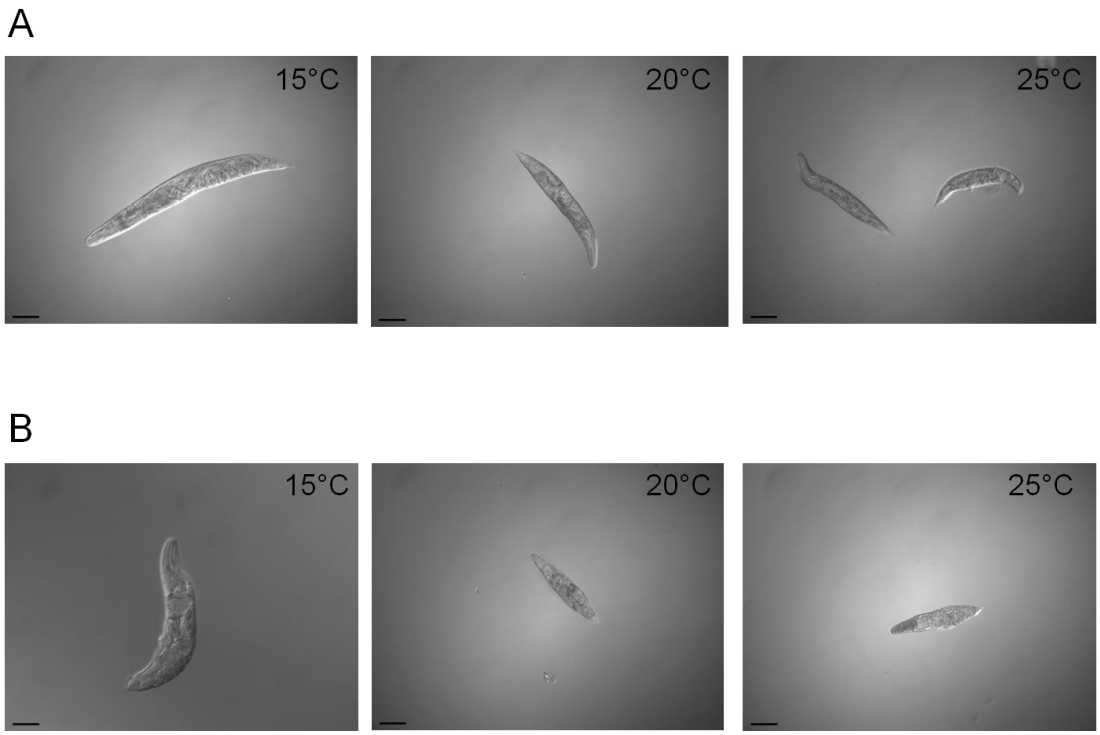

Figure 6-11. The IA835 and I836 dumpy phenotypes at 15°C, 20°C and 25°C
A and **B.** The morphological appearance and dumpy phenotype of IA835 (A) and IA836 (B) adult nematodes is more pronounced at 20°C and 25°C. Scale bars represent 100 µm.

Upon closer inspection, it became evident that the IA835 strain exhibited severe moulting (Figure 6-12, A) and egg-laying deficiencies (Figure 6-12, B) at 20°C. The gross cellular structures occasionally became distorted, possibly due to swelling of the intestines, and optically dense with no embryos visible intracellularly (Figure 6-12, C). Shed cuticles appeared to contain a large amount of extracellular content, particularly at 25°C (Figure 6-12, D).

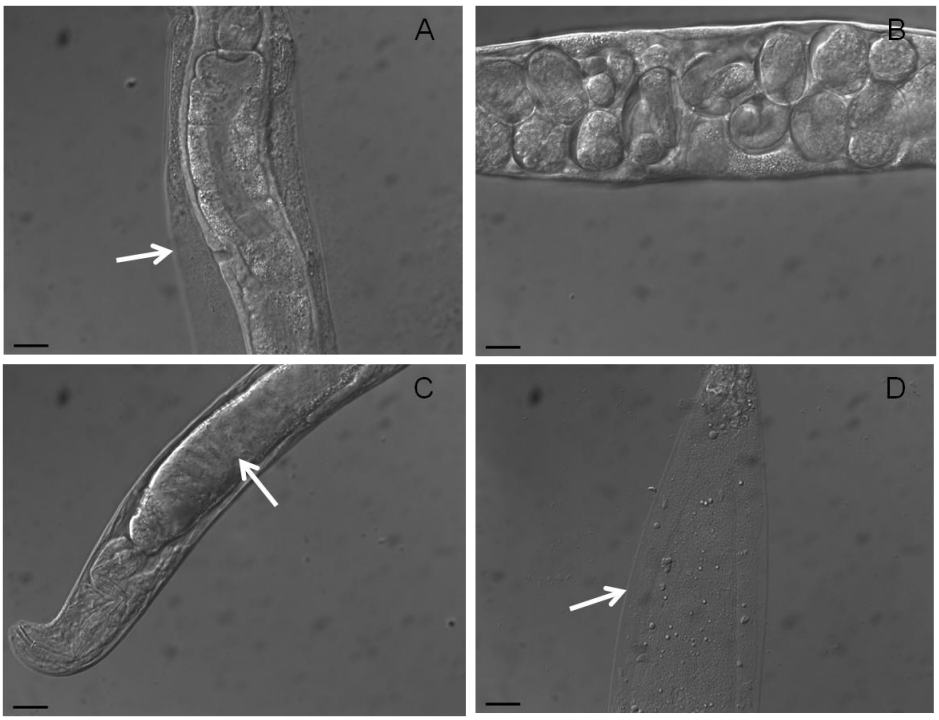

Figure 6-12. IA835 phenotypic characteristics
Light microscopy images showing strain IA835 [*dpy-10(sc48); unc-51(e369)*] adult nematodes. **A.** IA835 nematodes exhibit severe moulting defects at 20°C. The white arrow indicates the old cuticle containing extracellular content (dense granular-like structures within the shed cuticle). **B.** IA835 adult nematode displaying an egg-laying deficiency at 20°C. **C.** Dense cellular structure at 20°C, possibly caused by swelling of the intestines (indicated by white arrow). **D.** Aberrant shed cuticle (indicated by white arrow) from nematode cultured at 25°C. Scale bar represents 10 µm.

Similarly, the IA836 strain exhibited severe moulting and egg-laying deficiencies (Figure 6-13, A) at 20°C. The pharynx of the IA836 nematodes was often noted to be twisted (Figure 6-13, B). This was possibly secondary due to the severe dumpy phenotype. As for the IA835 strain, ghost cuticles of the IA836 strain also appeared to contain a large amount of extracellular content (Figure 6-13, C). This phenotype is not observed in the IA337, CB128 or CB369 single mutant strains. However, due to the apparent compounding effects caused by the double mutant alleles in IA835 and IA836 strains, the extracellular content present in the shed cuticles are likely due to a lysosomal trafficking defect induced by the *unc-51(e369)* mutation. IA836 nematodes cultured at 25°C typically exhibited a burst phenotype with very few embryos present (Figure 6-13, D). Overall the phenotypes and behavioural characteristics observed in the IA835 and IA836 double mutant strains are much more severe than their respective single mutant strains. This suggests that the mutant alleles, and thereby autophagy, contribute function to *C.elegans* development and cuticle synthesis.

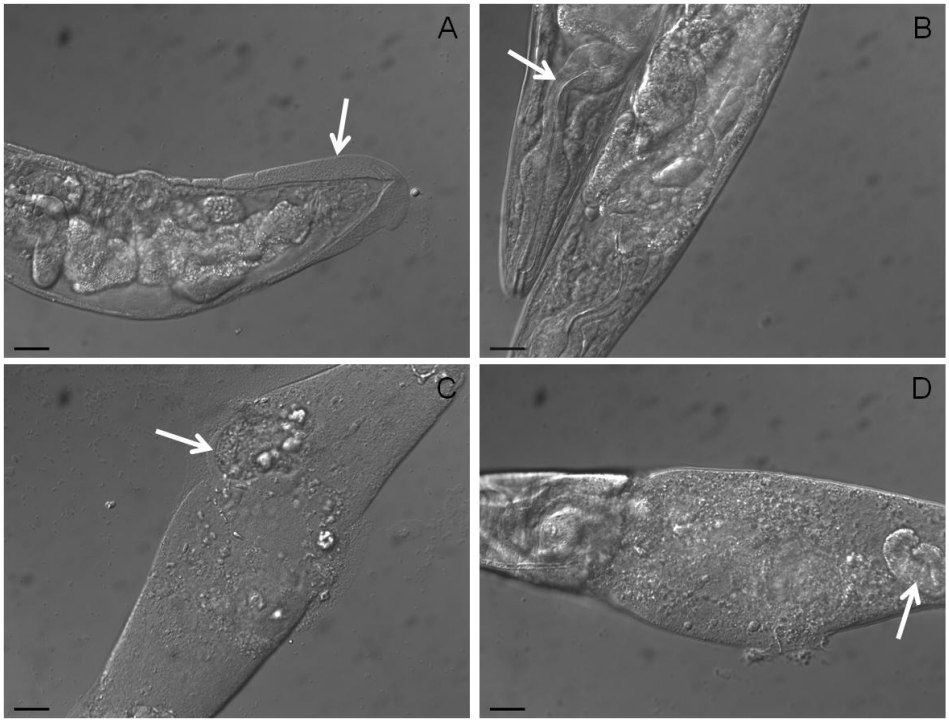

Figure 6-13. IA836 phenotypic characteristics
Light microscopy images showing strain IA836 [*dpy-10(e128); unc-51(e369)*] adult nematodes. **A.** IA836 nematodes exhibit severe moulting (indicated by white arrow) and egg-laying defects at 20°C. **B.** Twisted pharynx observed in IA835 nematodes at 20°C. **C.** Aberrant shed cuticle (indicated by white arrow) containing extracellular content at 20°C. **D.** Burst IA836 adult nematode containing a single dead embryo at 25°C. Scale bar = 10 µm.

6.2.4.2 Cuticular localisation of DPY-7 in autophagy deficient *C.elegans*

Immunofluorescence microscopy was employed to investigate the localisation of DPY-7 in the IA835 and IA836 double mutant strains compared with their respective single mutant strains. I was particularly interested in the pattern of DPY-7 localisation in the cuticles of the IA835 and IA836 double mutant strains. These observations would provide insight into the role of autophagy in the clearance and recycling of DPY-7 and its obligate partner DPY-10.

Immunofluorescent staining for this study was performed as outlined under section 2.13.8. DPY-7 localises to the cuticular annular furrows in a regular and uninterrupted manner in adult N2 nematodes (Figure 6-14, A) (McMahon *et al.*, 2003). This pattern becomes fragmented in the *dpy-10(sc48)* glycine substitution mutant background (Figure 6-14, B) (McMahon *et al.*, 2003). In contrast, DPY-7 staining is completely absent in the *dpy-10(e128)* null mutant background (Figure 6-14, C) (McMahon *et al.*, 2003). The cuticular localisation for DPY-7 in CB369 nematodes has not been reported previously. Immunofluorescence staining

revealed that the cuticular localisation for DPY-7 in CB369 appear similar to that described for the N2 strain: regular and uninterrupted within the cuticular furrows (Figure 6-14, D). Localisation of DPY-7 in the IA835 double mutant strain appeared even more fragmented than observed for the IA337 strain (Figure 6-14, E). This suggests, as previously discussed for the light microscopy analysis (section 6.2.4.1), that the DPY-7 glycine substitution mutant collagen is effectively less functional at 20°C in the autophagy defective background. In contrast, disruption of autophagy was unable to recover the presence of cuticular DPY-7 in the *dpy-10(e128)* background (strain IA836) (Figure 6-14, F).

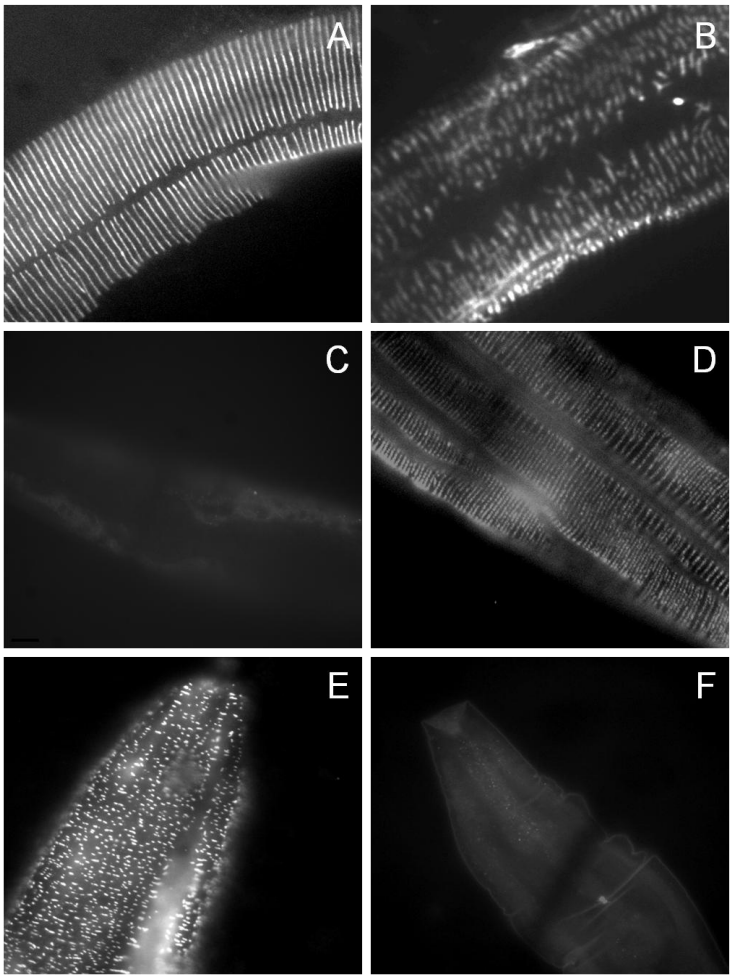

Figure 6-14. DPY-7 cuticular localisation in the IA835 and IA836 double mutant strains
Autophagy deficient adult nematodes continuously cultured at 20°C were assessed for DPY-7 localisation using immunofluorescence microscopy as outlined under section 2.13.8. All images were taken at the same magnification. **A.** N2 **B.** IA337 [*dpy-10(sc48)*] **C.** CB128 [*dpy-10(e128)*] **D.** CB369 [*unc-51(e369)*] **E.** IA835 [*dpy-10(sc48); unc-51(e369)*] **F.** IA836 [*dpy-10(e128); unc-51(e369)*].

6.2.5 *C.elegans* development and a role for endosomal trafficking

6.2.5.1 Cuticular localisation of DPY-7 in endosomal trafficking deficient *C.elegans*

The role for endosomal trafficking, and in particular *VPS-45*, was investigated in the clearance of the intracellular surge in membranes and vesicles following each moult. Firstly, I investigated DPY-7 cuticular staining patterns for IA337, CB128, IA757, IA779 and IA823 at 15°C (Figure 6-15). Consistent with previous reports, the cuticular localisation for DPY-7 in N2 appeared regular and uninterrupted within the cuticular furrows (Figure 6-15, A) (McMahon *et al.*, 2003). DPY-7 appeared fragmented and localised to the cuticular furrows in strain IA337 (Figure 6-15, B). DPY-7 cuticular staining was absent in CB128 (Figure 6-15, C). Cuticular DPY-7 in IA757 (Figure 6-15, D) exhibit a similar pattern of localisation when compared with N2 nematodes (Figure 6-15, A): regular and uninterrupted within the cuticular furrows. Cuticular DPY-7 localisation in the IA779 strain still localised within the cuticular furrows (Figure 6-15, E). Although DPY-7 remained to be fragmented, it was also noted to be more abundant than that observed for IA337. This suggests that loss of VPS-45 function augments DPY-7 function in the *dpy-10(sc48)* mutant background. Disruption of VPS-45 function may impair the clearance of the glycine substitution DPY-7 mutant collagen from the ER under these conditions and thus allow for more partially functional DPY-7 to be secreted. In contrast, disruption of endosomal trafficking in the *dpy-10(e128)* background did not recover the presence of DPY-7 within the cuticle (Figure 6-15, F).

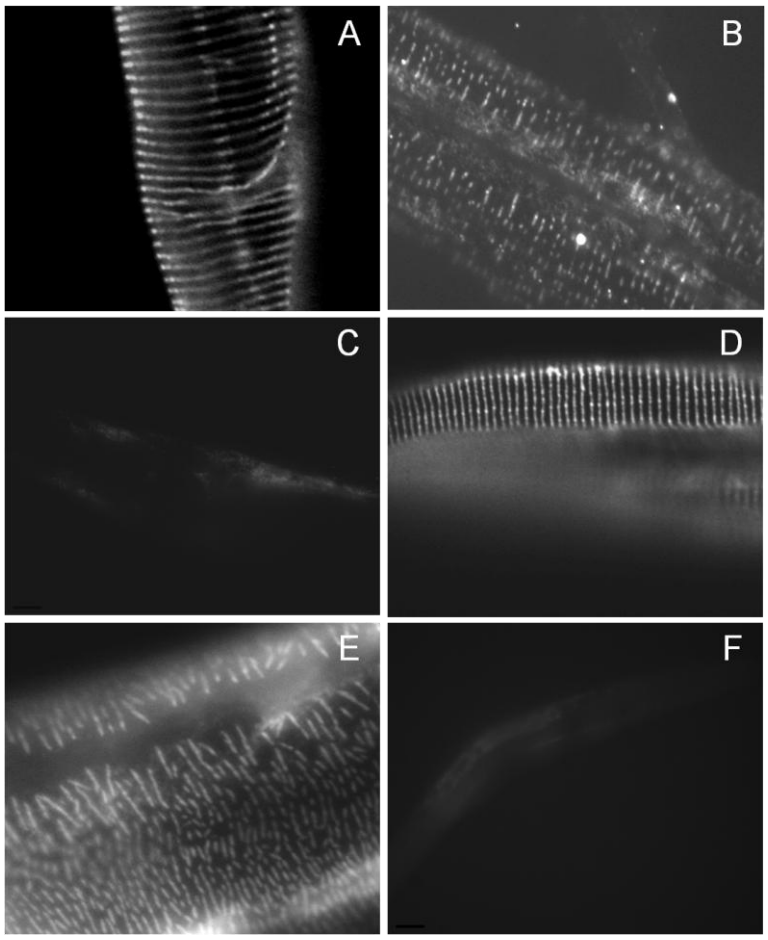

Figure 6-15. DPY-7 cuticular localisation in the IA779 and IA823 double mutant strains
Endosomal trafficking deficient adult nematodes continuously cultured at 15°C were assessed for DPY-7 localisation using immunofluorescence microscopy as outlined under section 2.13.8. All images were taken at the same magnification. **A.** N2 **B.** IA337 [*dpy-10(sc48)*] **C.** CB128 [*dpy-10(e128)*] **D.** IA757 [vps-45*(tm246)*] **E.** IA779 [*dpy-10(sc48); vps-45(tm246)*] **F.** IA823 [*dpy-10(e128); vps-45(tm246)*].

6.2.5.2 Monitoring soluble DPY-7 in endosomal trafficking deficient *C.elegans*

The role for endosomal trafficking in the clearance of the pre-moult surge in intracellular content was further investigated in the *dpy-10(sc48)* and *dpy-10(e128)* mutant backgrounds. In order to determine if endosomal trafficking is involved in the clearance of the pre-moult surge in intracellular membranes and vesicles I set out to investigate if more DPY-7 accumulates in the *dpy-10(sc48)* and *dpy-10(e128)* mutant backgrounds when endosomal trafficking is disrupted.

C.elegans whole animal lysates were prepared from mixed stage cultures continuously cultured at 15°C as described under section 2.13.5. Equal amounts of whole cell lysate (normalised against actin) was subjected to SDS-PAGE

(section 2.3.1) followed by immunoblot analysis (sections 2.3.3 and 2.3.4) with anti-DPY-7 and as a loading control, anti-actin (Table 2-2). Figure 6-16 shows the extent of DPY-7 accumulation in endosomal trafficking deficient strains in wild type and *dpy-10(sc48)* glycine substitution mutant backgrounds. More DPY-7 accumulated intracellularly in IA337 when compared with the N2 strain (4.3 ± 1.6, p=0.205). This increased abundance of DPY-7 is not reflected in the secreted DPY-7 portion when compared with N2 nematodes (Figure 6-15). Similarly, disruption of endosomal trafficking resulted in more DPY-7 accumulation when compared with the N2 strain (1.7 ± 2.1, p=0.915) however the extent of DPY-7 accumulation was less than that observed for IA337. This observation suggests that more soluble DPY-7 remains following each moult thereby supporting a role for endosomal trafficking in the clearance of the pre-moult surge in intracellular components. Interestingly, *dpy-10(sc48); vps-45(tm246)* nematodes (strain IA779) accumulated even more DPY-7 when compared with N2 (5.1 ± 4.2, p=0.402) and its respective single mutant strains, IA337 and IA757. Given that more cuticular DPY-7 is also seen in the IA779 strain compared with N2 nematodes (Figure 6-15), the extent at which mutant DPY-7 accumulates intracellularly in the IA779 strain may be underestimated in Figure 6-16.

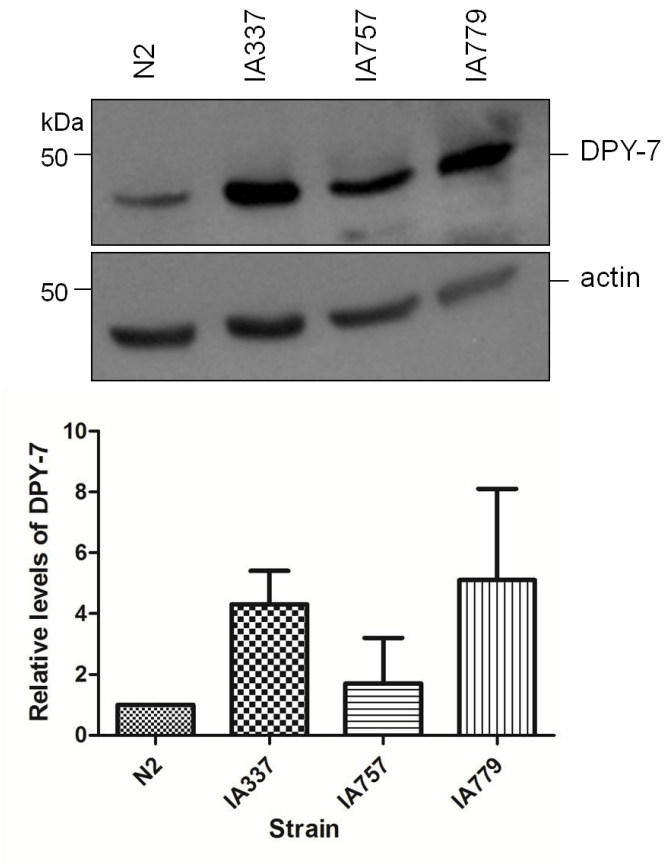

Figure 6-16. Soluble DPY-7 accumulates in strain IA779
Mixed stage cultures of *C.elegans* strains N2 (wild type), IA337 [*dpy-10(sc48)*], IA757 [*vps-45(tm246)*] and IA779 [*dpy-10(sc48); vps-45(tm246)*] continuously grown at 15°C was assessed for DPY-7 accumulation by SDS-PAGE followed by immunoblot analysis with anti-DPY-7 and as a loading control, anti-actin. Densitometry analysis was performed with the use of ImageJ 1.46r Gel Analysis tool (National Health Institute). DPY-7 levels for IA337, IA757 and IA779 were normalised against actin and are expressed relative to wild type DPY-7 levels. Error bars represent the standard deviation of the mean relative levels of DPY-7 (n=2).

Figure 6-17 shows the extent of DPY-7 accumulation in endosomal trafficking deficient strains in wild type and *dpy-10(e128)* null mutant backgrounds. Soluble DPY-7 was detected in N2 and the endosomal trafficking deficient single mutant strain IA757. The latter accumulated more DPY-7 compared with N2 nematodes. DPY-7 was undetectable in both CB128 and IA823 nematodes. These results suggest that strain IA823 does not accumulate soluble DPY-7 and that disruption of autophagy in the *dpy-10(e128)* null mutant background is unable to recover DPY-7 levels. This observation is consistent with the absence of cuticular DPY-7 in strain IA823 (section 6.2.5.1; Figure 6-15).

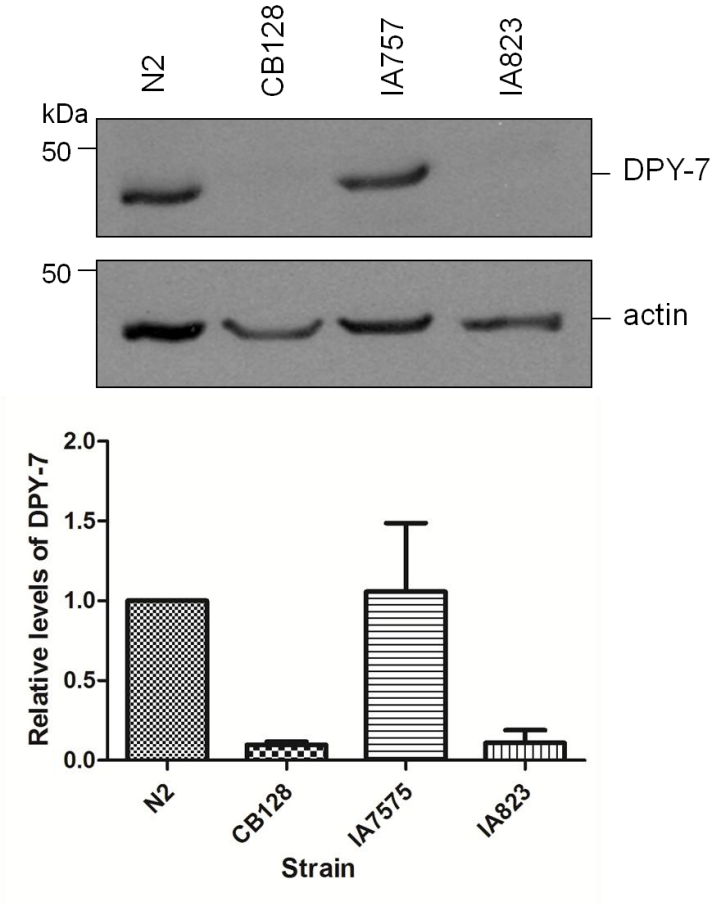

Figure 6-17. Soluble DPY-7 is undetectable in strain IA823
Mixed stage cultures of *C.elegans* strains N2 (wild type), CB128 [*dpy-10(e128)*], IA757 [*vps-45(tm246)*] and IA823 [*dpy-10(e128); vps-45(tm246)*] continuously grown at 15°C was assessed for DPY-7 accumulation by SDS-PAGE followed by immunoblot analysis with anti-DPY-7 and as a loading control, anti-actin. Densitometry analysis was performed with the use of ImageJ 1.46r Gel Analysis tool (National Health Institute). DPY-7 levels for CB128, IA757 and IA823 were normalised against actin and are expressed relative to wild type DPY-7 levels. Error bars represent the standard deviation of the mean relative levels of DPY-7 (n=2).

6.3 Chapter summary

This chapter documents investigations into the role of autophagy and endosomal trafficking in the clearance of the pre-moult increase in abundance of intracellular membranes and vesicles. I have demonstrated for the first time that the introduction of homozygous *unc-51(e369)* and *vps-45(tm246)* mutant alleles in the *dpy-10(sc48)* glycine substitution and *dpy-10(e128)* null mutant backgrounds produce compounding phenotypic, morphological and behavioural effects (sections 6.2.3). Consistent with previous reports, these results implicate a role for autophagy and endosomal trafficking in *C.elegans* development and in particular cuticle formation (Kov *et al.*, 2000; Gengyo-Ando *et al.*, 2007; Kovacs & Zhang, 2010; Sato & Sato, 2013). I have provided evidence in support of a role for autophagy in membrane turnover during *C.elegans* development (section 6.2.4). I have also provided quantitative evidence in support of a role for endosomal trafficking in the clearance of the pre-moult increase in intracellular content (section 6.2.5).

Further work will be required to elucidate the mechanisms involved in the autophagy and endosomal trafficking-dependent regulation of intracellular membrane and vesicle turnover during *C.elegans* development and their respective roles in cuticle formation. Investigations using more powerful techniques, including electron microscopy, may provide more insight into the pathologies induced under these mutant conditions. For example, investigating the structural differences in the cuticles of wild type and autophagy deficient *C.elegans* strains may provide more insight into the burst phenotypes observed under autophagy deficient conditions.

Chapter 7 – Discussion

Autophagy is a well-studied ubiquitous degradative process that operates to assist in the maintenance of cellular health, particularly under stress conditions (Choi *et al.*, 2013). Regulation of this process is crucial and mutations in genes operating in this pathway have demonstrated its significance in a number of physiological processes and pathologies (Yue *et al.*, 2003; Mizushima & Levine, 2010). The primary focus of the work presented in this thesis was aimed at gaining a better understanding of the molecular fusion machinery involved in autophagy by using the yeast model system *S.cerevisiae*. Specifically, I investigated a role for autophagy in regulation of the endosomal SNARE protein Tlg2, which has previously been shown to regulate autophagy in yeast (Abeliovich *et al.*, 1999; Ohashi & Munro, 2010; Nair *et al.*, 2011). The SM protein Vps45 associates with membranes predominantly via interaction with Tlg2 and is also required for stable expression of Tlg2 (Nichols *et al.*, 1998; Bryant & James, 2001). I investigated the functional effects of the Vps45 T238N mutation in yeast (Stepensky *et al.*, 2013). I concluded my work by investigating a role for autophagy and endosomal trafficking in the post-embryonic development of the nematode *C.elegans*.

7.1 Endosomal SNAREs and autophagy

The endosomal syntaxin Tlg2 has previously been shown to regulate autophagy in yeast (Abeliovich *et al.*, 1999; Ohashi & Munro, 2010; Nair *et al.*, 2011). In particular, deletion of *tlg2* inhibits the accumulation of Atg9, which is a membrane constituent of lipid bilayers supplying the growing isolation membrane, at the site of autophagy initiation (i.e. the PAS) (Noda *et al.*, 2000; Ohashi & Munro, 2010; Nair *et al.*, 2011). There is increasing evidence to support a role for the endosomal and Golgi systems in providing this membrane source and substantial co-localisation for Atg9-GFP and endocytic compartments has been observed (Ohashi & Munro, 2010; Longatti & Tooze, 2012). Consistent with this, the COG complex, which functions in Golgi transport (section 1.4.1) has also been shown to regulate autophagy in yeast and similar to *tlg2*, *cog* mutants also result in the dispersed localisation of Atg9 (Yen *et al.*, 2010). These observations implicate a role for Tlg2 and the COG complex in the efficient anterograde delivery of Atg9 to the forming autophagosomes and/or expansion of the isolation membrane at the PAS. The results presented in chapter 3 supports my hypothesis that Tlg2 and its

partner SNARE proteins regulate autophagy by directly associating with subunits of the COG tethering complex. In particular I focused on associations with the lobe A subunits (Cog1 to Cog4) under basal conditions which were selected based on their requirement for autophagy (Yen *et al.*, 2010). I provided evidence that Tlg2 associates with Cog2 and Cog4 by pull down assay (Figure 3-19). I also demonstrated direct associations between Tlg1 and Cog1, Cog2 and Cog4 (Figure 3-21, Figure 3-23 and Figure 3-25). In addition I showed that the Tlg1 and Cog1 interaction is functionally important as Tlg1 levels are reduced in a *cog1* strain (Figure 3-22). Similarly, mammalian Syntaxin 6 has previously been shown to associate with Cog6 via its SNARE domain and Syntaxin 6 levels are selectively reduced in *cog6* (Laufman *et al.*, 2011). The authors from this study also demonstrated that the Golgi localisation and colocalisation of Syntaxin 6 and its partner SNARE proteins were impaired under these conditions. Thus, depletion of Cog 6 resulted in inefficient SNARE complex formation.

No direct interactions were observed between Vti1 or Snc2 and any of the COG complex subunits investigated (section 3.2.2). In contrast to my findings, an association between mammalian Cog4 and Vti1 has previously been detected by co-immunoprecipitation (Laufman *et al.*, 2013). Specifically, Myc-tagged Cog4 was over-expressed in HEK293 cells, co-immuoprecipitated and assessed for binding with endogenous SNAREs and SM proteins by immunoblot analysis. It may be that mammalian Cog4 gained additional functions as a result of evolutionary divergence. For example, yeast Vps45 is exclusively implicated in protein traffic between the TGN and endosomal system (Bryant *et al.*, 1998) whereas mVps45 has evolved to also play a role in the recycling of plasma membrane receptors (Gengyo-Ando *et al.*, 2007; Rahajeng *et al.*, 2010). Alternatively, Cog4 shares sequence and structural homology with the MUN domain of Munc13, which has previously been shown, using nuclear magnetic resonance spectroscopy, to bind weakly to the SNARE domain of neuronal Syntaxin 1a (Ma *et al.*, 2011). The authors in this study mentioned that the Munc13 and Syntaxin 1a interaction was previously undetectable using standard techniques, including pull down assays. Thus, the discrepancy between homologous yeast and mammalian interaction systems may be the result of a weak interaction that exists between yeast Cog4 and Vti1. Thus, it is difficult to say that Tlg1 and Snc2 do not bind COG complex subunits and this area warrants further investigation with more powerful techniques. This contention may also explain my inconsistent and inconclusive

yeast two-hybrid interaction results obtained in chapter 3 (further discussed in section 3.2.1).

My pull down assay results presented in chapter 3 support a role for the Tlg2 SNARE domain in mediating interactions with Cog2 and Cog4 (Figure 3-19). This is consistent with other SNARE:COG interactions and supports an emerging role for the SNARE domain in mediating these interactions in both yeast and mammals (Shestakova *et al.*, 2007; Laufman *et al.*, 2011; Laufman *et al.*, 2013). Consistent with my results, mammalian Cog4 has been shown to bind the SNARE domain of Syntaxin 16, which is the orthologue of yeast Tlg2 (Laufman *et al.*, 2013). This interaction was demonstrated to be required for both the assembly and coordination of fusogenic SNARE complexes on the Golgi apparatus. It may be that this function is extended to the autophagic pathway where evidence supports a role for Tlg2 in conjunction with the COG complex.

Further studies are required to establish the composition of the Tlg2-containing SNARE complex involved in autophagosome formation and completion as the exocytic t-SNAREs Sso1 and Sec9 have also been implicated in anterograde trafficking of Atg9 to the PAS (Nair *et al.*, 2011). In support of a role for these exocytic t-SNAREs in autophagy, a Sso1-Sec9-Tlg2 complex was isolated by immunoprecipitation however this complex was unable to drive fusion *in vitro* (Nair *et al.*, 2011). Disruption of the Tlg2 partner SNARE proteins Tlg1, Vti1 and Snc2 may be utilised to investigate the localisation of Atg9-GFP under autophagy inducing conditions as was done for Tlg2 (Ohashi & Munro, 2010; Nair *et al.*, 2011). Defective Atg9 trafficking under these mutant conditions may provide further evidence in support of a role for the endosomal SNARE complex in autophagosome formation and completion.

Tlg2 has previously been shown to be required for homotypic TGN fusion reactions (Brickner *et al.*, 2001). Consistent with a role for Tlg2 in autophagy, homotypic fusion reactions between autophagosome precursor membranes are required to form mature autophagosomes (Moreau *et al.*, 2011). It is likely, given the redistribution of Atg9 and defective autophagosome formation in both *tlg2* and *cog* mutant strains, that Tlg2 and the COG complex mediate homotypic fusion not only between Atg9-containing vesicles but also between opposing membranes of the isolation membrane in order to complete autophagosome formation.

Recruitment of the core Atg machinery to the PAS, which includes the Atg1-Atg13-Atg17 kinase complex (section 1.1.3) precedes the arrival of Atg9-cotaining vesicles (Suzuki *et al.*, 2007). It is likely that Atg9 is directed to the PAS via direct association with Atg11 and/or Atg17 (He *et al.*, 2006; Sekito *et al.*, 2009). Atg11, which interacts with Atg1 and thereby direct its PAS localisation (Yorimitsu & Klionsky, 2005a), has recently been identified as a long coiled-coil tethering factor that is implicated in the anterograde trafficking of Atg9 to the PAS (He *et al.*, 2006; Lipatova *et al.*, 2012). A model by which coiled-coil proteins mediate long-range tethering followed by close-range recognition via multisubunit tethering factors and SNARE proteins has previously been proposed (Sztul & Lupashin, 2009). It is tempting to speculate a similar mechanism for the efficient anterograde trafficking of Atg9-containing vesicles to the PAS. More specifically, Atg9-containing vesicles, which originate from the Golgi endosomal system and supply proteins required for subsequent membrane expansion, may be directed to the PAS via direct association with Atg11, which mediates its long-range tethering to the isolation membrane possibly via a direct association with Atg19 (Yorimitsu & Klionsky, 2005a). In turn, Atg19 associates with Atg8, which is conjugated to the lipid phosphatidylethanolamine (PE) via an Atg4-dependent reaction to both the inner and outer isolation membranes (Kirisako *et al.*, 1999; Kirisako *et al.*, 2000). Dual interactions between Atg19-Atg11 and Atg19-Atg8 pairs may target Atg9-containing vesicles to the PAS in a manner analogous to that described for pre-aminopeptidase I-containing vesicles (Chang & Huang, 2007). Subsequent association between subunits of the COG complex and endosomal SNARE proteins could mediate close-range recognition. As a result, homotypic fusion reactions at the PAS can proceed and thereby allow elongation of the isolation membrane and completion of the autophagosome.

Collectively, the data presented in chapter 3 contributes to the increasing body of evidence supporting a role for multivalent interactions [reviewed in (Brocker *et al.*, 2010)], and in particular the endosomal SNARE and COG complexes, in specifying and coordinating fusion events.

7.2 Regulation of Tlg2 steady-state levels

Our group has previously demonstrated a role for both the proteasome and vacuole in mediating the regulation of Tlg2 steady-state levels (Bryant & James, 2001; Struthers, 2009). In chapter 4, I have extended this investigation and demonstrated a role for the autophagic pathway in regulating Tlg2 levels under wild type conditions (Figure 4-7). Tlg1, the partner SNARE protein of Tlg2, is protected from ubiquitination by palmitoylation (Valdez-Taubas & Pelham, 2005), which in turn can direct proteins for selective degradation by autophagy (Pankiv *et al.*, 2007). I therefore hypothesised that Tlg2, which regulates autophagy in yeast, is directed to the vacuole via selective autophagy and that its incorporation into this pathway is regulated by palmitoylation. In chapter 4 I confirmed a role for palmitoylation in regulating Tlg2 levels and acyl resin-assisted capture of endogenous Tlg2 to demonstrate that the palmitoyltransferase Swf1 mediates Tlg2 palmitoylation (Figure 4-8, Figure 4-9, Figure 4-11 and Figure 4-12).

To further address the specificity of Swf1 in Tlg2 palmitoylation, the *in vivo* steady-state levels and palmitoylation status of Tlg2 in mutant strains of the remaining six palmitoyltransferases in yeast could be assessed. The acyl resin-assisted capture approach employed in this study would be suitable for investigating palmitoylation of Tlg2 under these conditions (section 2.8.2) and could also be adapted to mass spectroscopy techniques in future experiments for identifying the residues involved in Tlg2 palmitoylation (Valdez-Taubas & Pelham, 2005; Forrester *et al.*, 2011).

Tlg2 can be degraded via both the proteasome and vacuole under wild type conditions (Bryant & James, 2001). The vacuolar contribution to Tlg2 degradation could be further assessed by investigating the steady-state levels of Tlg2 in *pep4-3* and *swf*1Δ double mutant strains. Further experiments could also address ubiquitination of Tlg2 in order to identify the lysine residue(s) mediating this modification. Marion Struthers in our laboratory previously demonstrated that Tlg2 is ubiquitinated in both wild type and *vps45* strains (Struthers, 2009). She subsequently performed a Tlg2 lysine residue substitution screen in order to identify the residues mediating this modification however none of the residues mutated prevented the degradation of Tlg2 (Struthers, 2009). The lysine residue at position 317, which lies adjacent to one of the two cysteine residue thought to mediate palmitoylation, was not investigated in Marion's screen. Instead, lysine

residues conserved between Syntaxin 16 and Tlg2 contained in the region between the SNARE domain and the TMD were selected for substitution. Previously it has been observed that the absence of palmitoylation could lead to ubiquitination of a nearby lysine residue (Valdez-Taubas & Pelham, 2005; Abrami *et al.*, 2006). Thus, mutation of this particular lysine residue at position 317 may be a potential site for ubiquitination and thereby a good target for future investigations. Furthermore, the manner by which ubiquitin is attached to its substrate protein determines its route of degradation or non-proteolytic function (Hershko & Ciechanover, 1998; Haglund & Dikic, 2005). As mentioned previously, Tlg2 can be degraded via both the proteasome and vacuole and ubiquitination signals directing substrates to the proteasome or vacuole are distinct. Lysine 63 (K63) poly-ubiquitinated chains have previously been demonstrated to target substrate proteins for degradation via autophagy (Tan *et al.*, 2008) , which terminates in the vacuole, whereas K48 poly-ubiquitination generally direct proteins for proteasome mediated degradation (Weissman, 2001). Tlg2 ubiquitination experiments could be followed up by investigating the nature of the ubiquitination involved, i.e. is Tlg2 mono- or poly-ubiquitinated? Also, if Tlg2 is poly-ubiquitinated, which lysine residues of ubiquitin mediate polypeptide chain formation? The latter could be assessed by employing immunoblot analysis using linkage-specific antibodies that recognise poly-ubiquitin chains joined through K63 or K48 (Newton *et al.*, 2008).

7.3 The T238N mutation in yeast Vps45

In chapter 5 I investigated the effects of the yeast T238N mutation on Vps45 function. This mutation is analogous to human Vps45 T224N, which has recently been associated with congenital neutropenia (Stepensky *et al.*, 2013; Vilboux *et al.*, 2013).

The threonine at position 224 and 238 in human and yeast Vps45, respectively, is evolutionarily conserved. A multiple amino acid sequence alignment of human and yeast Vps45 with yeast Vps33, which is evolutionarily related to Vps45 and whose crystal structure has been solved (Baker *et al.*, 2013), revealed that the T224N and T238N mutations in human and yeast Vps45, respectively, localises to domain 3a (Figure 5-3) (refer to section 1.3.1 for SM protein structure). The Munc18a tyrosine (Y) at position 337 also localises to domain 3a. Over-expression of the

Y337L (leucine) Munc18a mutant inhibits the release kinetics of exocytosis events, possibly due to its inability to bind the assembled neuronal SNARE complex via mode 3 binding (Boyd *et al.*, 2008). Similarly, the yeast Vps45 tryptophan (W) at position 244 to arginine (R) mutation (W224R) also localises to domain 3a however, unlike Munc18a Y337L, this dominant-negative mutant SM protein is capable of binding preassembled SNARE complexes (Carpp *et al.*, 2006). The continued ability of Munc18a Y337L and Vps45 W244R to associate with their respective cognate syntaxins via modes 1 and 2 binding, respectively, supports a role for domain 3a in regulating vesicle docking as opposed to SNARE complex assembly. Given the discrepancy between the mode 3 binding abilities of the Munc18a Y337L and Vps45 W244R mutant proteins, it is likely that the affected SM proteins' ability to mediate fusion events is affected in both these mutants. The functional significance of domain 3a described here is consistent with observations made for the yeast Vps45 T238N mutation in chapter 5. Structural alterations induced by this mutation may render Vps45 unstable, as was demonstrated in Figure 5-4 and Figure 5-5. As a consequence, Tlg2 levels were also reduced, which reflects the role for Vps45 in regulating Tlg2 levels and thereby membrane traffic through the endosomal system (Nichols *et al.*, 1998; Bryant & James, 2001). The diffuse cytoplasmic localisation of human Vps45 T224N observed by Vilboux and colleagues indicates that in addition to being unstable, Vps45's ability to attach to membranes through its interaction with Syntaxin 16 was also compromised (Vilboux *et al.*, 2013). This likely reflects defective mode 3 binding as described for the domain 3a mutation in Munc18a (Boyd *et al.*, 2008). Subsequently, an overall decrease and dispersed localisation in key Golgi endosomal fusion machinery components likely resulted in inefficient trafficking along this pathway. However, disruption of binding between Vps45 and Tlg2 does not necessarily impair SM protein function in membrane trafficking. For instance, the Vps45 leucine (L) to arginine (R) mutation at position 117 (L117R) disrupts binding with Tlg2 however its ability to restore CPY sorting in *vps45*Δ cells is comparable to that of wild type Vps45 (Carpp *et al.*, 2006). Similarly, CPY sorting remained intact in yeast cells harboring Vps45 T238N (Figure 5-6), however future experiments could assess the extent of CPY-containing vesicle accumulation and intracellular location in support of a role for defective endosomal trafficking under these conditions. Collectively, these perturbed Vps45 functions could inundate the earlier secretory pathway and result in ER stress. ER stress is a common inducer of cell apoptosis across species and is consistent with increased apoptosis

observed in yeast and human cells harboring Vps45 T238N (Figure 5-8) and T224N mutations, respectively (Stepensky *et al.*, 2013; Vilboux *et al.*, 2013). The association between increased cell apoptosis and a role for Vps45 is unrelated to phenotypes previously described for *vps* mutants which missort vacuolar resident enzymes, including CPY (Raymond *et al.*, 1992). This newly defined role for Vps45 may be related its chaperone function in promoting vesicle fusion via mode 3 binding which in turn is likely mediated by domain 3a. Collectively these results assign a novel functional role for Vps45 that is not associated with other class D *vps* mutants (Figure 5-9). Additionally, these results support a role for SM proteins at multiple steps during membrane fusion. The precise mechanisms underlying the phenotypes described for yeast Vps45 T238N will require further investigation.

7.4 Autophagy and endosomal trafficking in *C.elegans* development

Chapter 6 details an investigation into the role for autophagy and endosomal trafficking in *C.elegans* post-embryonic development. In particular, I was interested to investigate the role of these two pathways in the clearance of the cyclical pre-moult increase in intracellular membranes and vesicles associated with cuticle synthesis (section 1.5.2). *C.elegans unc-51* and *vps-45* mutants, which are the orthologs of yeast *atg1* and *vps45*, respectively, have previously been described (Brenner, 1974; Ogura *et al.*, 1994; Gengyo-Ando *et al.*, 2007); however their role in regulating the clearance of excess intracellular components at the end of each moult has not been investigated previously. In chapter 6 I characterised the phenotypes of *unc-51* and *vps-45* with the collagen *dpy-10(sc48*) glycine substitution or *dpy-10(e128)* null double mutant strains (section 6.2.3). Double mutants containing the *dpy-10(e128)* null allele produced synthetically sick strains in both the *unc-51(e369)* and *vps-45(tm246)* mutant backgrounds and their phenotypes were severely compounded when compared to either of the single mutant strains. This indicates that both *unc-51(e369)* and *vps-45(tm246)* alleles are functionally related to the *dpy-10(sc48)* and *dpy-10(e128)* alleles by a mechanism yet to be identified. A likely role for these genes in regulating the clearance of the pre-moult increase in intracellular components associated with cuticle synthesis was most evident in the *vps-45(tm246); dpy-10(sc48)* double mutant strain which contained an increased abundance of the collagen DPY-7

within the cuticle (Figure 6-15). The presence of soluble DPY-7, which was used as an indirect marker of retained intracellular components, in the *vps-45(tm246); dpy-10(sc48)* strain was also greater in abundance when compared with the respective single mutant and wild type strains (Figure 6-16). Collectively, given that loss of VPS-45 function results in an increased abundance of soluble and cuticular glycine substitution DPY-7 mutant collagen protein, VPS-45 is implicated in the turnover of DPY-7. This is consistent with a model whereby the increased persistence of the mutant collagen protein within the ER results in more DPY-7 being detected intracellularly (Figure 6-16) as well as within the cuticle (Figure 6-15).

The *unc-51(e369)* double mutant strains were severely paralysed and affected in their development and ability to lay eggs (section 6.2.4). Many genes, including *UNC-51*, exhibit pleiotropic effects *in vivo* (Ogura *et al.*, 1994; Ogura & Goshima, 2006; Aladzsity *et al.*, 2007). The dominant phenotype, which in this case is severe paralysis, can mask other informative phenotypes, including a possible role for autophagy in the clearance of the pre-moult increase in intracellular components. The Dpy phenotype exhibited by *unc-51(e369)* mutant nematodes is consistent with a role in cuticle formation. However, the masking effect of the dominant phenotype was evident in my study, as the severe paralysis and egg-laying deficiency of the *unc-51(e369)* single and double mutant strains interfered with sample preparation and phenotypic and behavioural characterisation and thereby subsequent investigations. Employing RNA-mediated interference [reviewed in (Mocellin & Provenzano, 2004)] to specifically inactivate expression of the *unc-51* allele in the *dpy-10(sc48)* glycine substitution and *dpy-10(e128)* null mutant backgrounds may circumvent these challenges. This method involves experimentally manipulating gene expression in *C.elegans* by feeding animals *E.coli* that expresses double-stranded RNA that is homologous to the gene of interest (Kamath *et al.*, 2001). Double-stranded RNA has the ability to specifically inactivate the corresponding gene via degradation of endogenous messenger RNA (Fire *et al.*, 1998; Timmons & Fire, 1998). Phenotypes induced by RNA-mediated interference can be titrated by altering the concentration of IPTG, which in turn is used to induce expression of double-stranded RNA (Kamath *et al.*, 2001). Residual *unc-51* gene expression may be sufficient to improve the phenotypes of *unc-51* containing double mutant strains described in chapter 6 and may elicit previously masked phenotypes.

Vps45 function is best described in the vacuolar protein sorting pathway where it directly associates with Tlg2 to ensure efficient delivery of proteins from the TGN into the endosomal system (Cowles *et al.*, 1994; Piper *et al.*, 1994; Nichols *et al.*, 1998; Bryant & James, 2001). In yeast, *vps45*Δ is defective in vacuolar protein sorting and growth (Rothman & Stevens, 1986; Robinson *et al.*, 1988) and exhibit accelerated rates of apoptosis (Stepensky *et al.*, 2013). However, the precise mechanism of Vps45 action is not known. Employing single and multicellular model systems to further study different aspects of Vps45 function will facilitate our understanding of SM protein function and thereby assist in the formulation of a unifying hypothesis of SM protein function.

References

Abeliovich H, Darsow T & Emr SD (1999) Cytoplasm to vacuole trafficking of aminopeptidase I requires a t-SNARE-Sec1p complex composed of Tlg2p and Vps45p. *EMBO J* **18**, 6005-6016.

Abeliovich H, Grote E, Novick P & Ferro-Novick S (1998) Tlg2p, a yeast syntaxin homolog that resides on the Golgi and endocytic structures. *J Biol Chem* **273**, 11719-11727.

Abrami L, Leppla SH & van der Goot FG (2006) Receptor palmitoylation and ubiquitination regulate anthrax toxin endocytosis. *J Cell Biol* **172**, 309-320.

Advani RJ, Bae HR, Bock JB, Chao DS, Doung YC, Prekeris R, Yoo JS & Scheller RH (1998) Seven novel mammalian SNARE proteins localize to distinct membrane compartments. *J Biol Chem* **273**, 10317-10324.

Aladzsity I, Toth ML, Sigmond T, Szabo E, Bicsak B, Barna J, Regos A, Orosz L, Kovacs AL & Vellai T (2007) Autophagy genes unc-51 and bec-1 are required for normal cell size in Caenorhabditis elegans. *Genetics* **177**, 655-660.

Antonin W, Fasshauer D, Becker S, Jahn R & Schneider TR (2002) Crystal structure of the endosomal SNARE complex reveals common structural principles of all SNAREs. *Nat Struct Biol* **9**, 107-111.

Aran V, Brandie FM, Boyd AR, Kantidakis T, Rideout EJ, Kelly SM, Gould GW & Bryant NJ (2009) Characterization of two distinct binding modes between syntaxin 4 and Munc18c. *Biochem J* **419**, 655-660.

Ashford TP & Porter KR (1962) Cytoplasmic components in hepatic cell lysosomes. *J Cell Biol* **12**, 198-202.

Augustin I, Rosenmund C, Sudhof TC & Brose N (1999) Munc13-1 is essential for fusion competence of glutamatergic synaptic vesicles. *Nature* **400**, 457-461.

Axe EL, Walker SA, Manifava M, Chandra P, Roderick HL, Habermann A, Griffiths G & Ktistakis NT (2008) Autophagosome formation from membrane compartments enriched in phosphatidylinositol 3-phosphate and dynamically connected to the endoplasmic reticulum. *J Cell Biol* **182**, 685-701.

Baba M, Osumi M & Ohsumi Y (1995) Analysis of the membrane structures involved in autophagy in yeast by freeze-replica method. *Cell Struct Funct* **20**, 465-471.

Baba M, Osumi M, Scott SV, Klionsky DJ & Ohsumi Y (1997) Two distinct pathways for targeting proteins from the cytoplasm to the vacuole/lysosome. *J Cell Biol* **139**, 1687-1695.

Baba M, Takeshige K, Baba N & Ohsumi Y (1994) Ultrastructural analysis of the autophagic process in yeast: detection of autophagosomes and their characterization. *J Cell Biol* **124**, 903-913.

Baker RW, Jeffrey PD & Hughson FM (2013) Crystal Structures of the Sec1/Munc18 (SM) Protein Vps33, Alone and Bound to the Homotypic Fusion and Vacuolar Protein Sorting (HOPS) Subunit Vps16*. *PLoS One* **8**, e67409.

Bartel P, Chien CT, Sternglanz R & Fields S (1993) Elimination of false positives that arise in using the two-hybrid system. *Biotechniques* **14**, 920-924.

Basu J, Shen N, Dulubova I, Lu J, Guan R, Guryev O, Grishin NV, Rosenmund C & Rizo J (2005) A minimal domain responsible for Munc13 activity. *Nat Struct Mol Biol* **12**, 1017-1018.

Bennett MK, Calakos N & Scheller RH (1992) Syntaxin: a synaptic protein implicated in docking of synaptic vesicles at presynaptic active zones. *Science* **257**, 255-259.

Birnboim HC & Doly J (1979) A rapid alkaline extraction procedure for screening recombinant plasmid DNA. *Nucleic Acids Res* **7**, 1513-1523.

Bjorkoy G, Lamark T, Brech A, Outzen H, Perander M, Overvatn A, Stenmark H & Johansen T (2005) p62/SQSTM1 forms protein aggregates degraded by autophagy and has a protective effect on huntingtin-induced cell death. *J Cell Biol* **171**, 603-614.

Bock JB, Matern HT, Peden AA & Scheller RH (2001) A genomic perspective on membrane compartment organization. *Nature* **409**, 839-841.

Bogdanovic A, Bennett N, Kieffer S, Louwagie M, Morio T, Garin J, Satre M & Bruckert F (2002) Syntaxin 7, syntaxin 8, Vti1 and VAMP7 (vesicle-associated membrane protein 7) form an active SNARE complex for early macropinocytic compartment fusion in Dictyostelium discoideum. *Biochem J* **368**, 29-39.

Boyd A, Ciufo LF, Barclay JW, Graham ME, Haynes LP, Doherty MK, Riesen M, Burgoyne RD & Morgan A (2008) A random mutagenesis approach to isolate dominant-negative yeast sec1 mutants reveals a functional role for domain 3a in yeast and mammalian Sec1/Munc18 proteins. *Genetics* **180**, 165-178.

Boztug K, Appaswamy G, Ashikov A, Schaffer AA, Salzer U, Diestelhorst J, Germeshausen M, Brandes G, Lee-Gossler J, Noyan F, Gatzke AK, Minkov M, Greil J, Kratz C, Petropoulou T, Pellier I, Bellanne-Chantelot C, Rezaei N, Monkemoller K, Irani-Hakimeh N, Bakker H, Gerardy-Schahn R, Zeidler C, Grimbacher B, Welte K & Klein C (2009) A syndrome with congenital neutropenia and mutations in G6PC3. *N Engl J Med* **360**, 32-43.

Bracher A, Perrakis A, Dresbach T, Betz H & Weissenhorn W (2000) The X-ray crystal structure of neuronal Sec1 from squid sheds new light on the role of this protein in exocytosis. *Structure* **8**, 685-694.

Bracher A & Weissenhorn W (2002) Structural basis for the Golgi membrane recruitment of Sly1p by Sed5p. *EMBO J* **21**, 6114-6124.

Bradford MM (1976) A rapid and sensitive method for the quantitation of microgram quantities of protein utilizing the principle of protein-dye binding. *Anal Biochem* **72**, 248-254.

Brenner S (1974) The genetics of Caenorhabditis elegans. *Genetics* **77**, 71-94.

Brickner JH, Blanchette JM, Sipos G & Fuller RS (2001) The Tlg SNARE complex is required for TGN homotypic fusion. *J Cell Biol* **155**, 969-978.

Brocker C, Engelbrecht-Vandre S & Ungermann C (2010) Multisubunit tethering complexes and their role in membrane fusion. *Curr Biol* **20**, R943-952.

Bruinsma P, Spelbrink RG & Nothwehr SF (2004) Retrograde transport of the mannosyltransferase Och1p to the early Golgi requires a component of the COG transport complex. *J Biol Chem* **279**, 39814-39823.

Bryant NJ & James DE (2001) Vps45p stabilizes the syntaxin homologue Tlg2p and positively regulates SNARE complex formation. *EMBO J* **20**, 3380-3388.

Bryant NJ & James DE (2003) The Sec1p/Munc18 (SM) protein, Vps45p, cycles on and off membranes during vesicle transport. *J Cell Biol* **161**, 691-696.

Bryant NJ, Piper RC, Gerrard SR & Stevens TH (1998) Traffic into the prevacuolar/endosomal compartment of Saccharomyces cerevisiae: a VPS45-dependent intracellular route and a VPS45-independent, endocytic route. *Eur J Cell Biol* **76**, 43-52.

Burkhardt P, Hattendorf DA, Weis WI & Fasshauer D (2008) Munc18a controls SNARE assembly through its interaction with the syntaxin N-peptide. *EMBO J* **27**, 923-933.
Carpp LN, Ciufo LF, Shanks SG, Boyd A & Bryant NJ (2006) The Sec1p/Munc18 protein Vps45p binds its cognate SNARE proteins via two distinct modes. *J Cell Biol* **173**, 927-936.
Carr CM, Grote E, Munson M, Hughson FM & Novick PJ (1999) Sec1p binds to SNARE complexes and concentrates at sites of secretion. *J Cell Biol* **146**, 333-344.
Chamberlain LH & Burgoyne RD (1998) The cysteine-string domain of the secretory vesicle cysteine-string protein is required for membrane targeting. *Biochem J* **335 (Pt 2)**, 205-209.
Chang CY & Huang WP (2007) Atg19 mediates a dual interaction cargo sorting mechanism in selective autophagy. *Mol Biol Cell* **18**, 919-929.
Chasseaud LF (1979) The role of glutathione and glutathione S-transferases in the metabolism of chemical carcinogens and other electrophilic agents. *Adv Cancer Res* **29**, 175-274.
Choi AM, Ryter SW & Levine B (2013) Autophagy in human health and disease. *N Engl J Med* **368**, 651-662.
Ciechanover A, Heller H, Elias S, Haas AL & Hershko A (1980) ATP-dependent conjugation of reticulocyte proteins with the polypeptide required for protein degradation. *Proc Natl Acad Sci U S A* **77**, 1365-1368.
Clark SL, Jr. (1957) Cellular differentiation in the kidneys of newborn mice studies with the electron microscope. *J Biophys Biochem Cytol* **3**, 349-362.
Coe JG, Lim AC, Xu J & Hong W (1999) A role for Tlg1p in the transport of proteins within the Golgi apparatus of Saccharomyces cerevisiae. *Mol Biol Cell* **10**, 2407-2423.
Conibear E & Stevens TH (1998) Multiple sorting pathways between the late Golgi and the vacuole in yeast. *Biochim Biophys Acta* **1404**, 211-230.
Costa M, Draper BW & Priess JR (1997) The role of actin filaments in patterning the Caenorhabditis elegans cuticle. *Dev Biol* **184**, 373-384.
Couve A, Protopopov V & Gerst JE (1995) Yeast synaptobrevin homologs are modified posttranslationally by the addition of palmitate. *Proc Natl Acad Sci U S A* **92**, 5987-5991.
Cowles CR, Emr SD & Horazdovsky BF (1994) Mutations in the VPS45 gene, a SEC1 homologue, result in vacuolar protein sorting defects and accumulation of membrane vesicles. *J Cell Sci* **107 (Pt 12)**, 3449-3459.
Cox GN, Kusch M, DeNevi K & Edgar RS (1981a) Temporal regulation of cuticle synthesis during development of Caenorhabditis elegans. *Dev Biol* **84**, 277-285.
Cox GN, Kusch M & Edgar RS (1981b) Cuticle of Caenorhabditis elegans: its isolation and partial characterization. *J Cell Biol* **90**, 7-17.
Dale DC, Person RE, Bolyard AA, Aprikyan AG, Bos C, Bonilla MA, Boxer LA, Kannourakis G, Zeidler C, Welte K, Benson KF & Horwitz M (2000) Mutations in the gene encoding neutrophil elastase in congenital and cyclic neutropenia. *Blood* **96**, 2317-2322.
De Duve C (1963) Ciba Foundation Symposium: Lysosomes. *Symposium on Lysosomes*, 446.
De Duve C & Wattiaux R (1966) Functions of lysosomes. *Annu Rev Physiol* **28**, 435-492.
Del Roso A, Vittorini S, Cavallini G, Donati A, Gori Z, Masini M, Pollera M & Bergamini E (2003) Ageing-related changes in the in vivo function of rat liver macroautophagy and proteolysis. *Exp Gerontol* **38**, 519-527.

Dell'Angelica EC, Shotelersuk V, Aguilar RC, Gahl WA & Bonifacino JS (1999) Altered trafficking of lysosomal proteins in Hermansky-Pudlak syndrome due to mutations in the beta 3A subunit of the AP-3 adaptor. *Mol Cell* **3**, 11-21.

Deter RL & De Duve C (1967) Influence of glucagon, an inducer of cellular autophagy, on some physical properties of rat liver lysosomes. *J Cell Biol* **33**, 437-449.

Donati A, Cavallini G, Paradiso C, Vittorini S, Pollera M, Gori Z & Bergamini E (2001) Age-related changes in the regulation of autophagic proteolysis in rat isolated hepatocytes. *J Gerontol A Biol Sci Med Sci* **56**, B288-293.

Drisdel RC, Alexander JK, Sayeed A & Green WN (2006) Assays of protein palmitoylation. *Methods* **40**, 127-134.

Dulubova I, Khvotchev M, Liu S, Huryeva I, Sudhof TC & Rizo J (2007) Munc18-1 binds directly to the neuronal SNARE complex. *Proc Natl Acad Sci U S A* **104**, 2697-2702.

Dulubova I, Sugita S, Hill S, Hosaka M, Fernandez I, Sudhof TC & Rizo J (1999) A conformational switch in syntaxin during exocytosis: role of munc18. *EMBO J* **18**, 4372-4382.

Dulubova I, Yamaguchi T, Gao Y, Min SW, Huryeva I, Sudhof TC & Rizo J (2002) How Tlg2p/syntaxin 16 'snares' Vps45. *EMBO J* **21**, 3620-3631.

Dulubova I, Yamaguchi T, Wang Y, Sudhof TC & Rizo J (2001) Vam3p structure reveals conserved and divergent properties of syntaxins. *Nat Struct Biol* **8**, 258-264.

Durfee T, Becherer K, Chen PL, Yeh SH, Yang Y, Kilburn AE, Lee WH & Elledge SJ (1993) The retinoblastoma protein associates with the protein phosphatase type 1 catalytic subunit. *Genes Dev* **7**, 555-569.

Edinger AL & Thompson CB (2003) Defective autophagy leads to cancer. *Cancer Cell* **4**, 422-424.

Fasshauer D, Sutton RB, Brunger AT & Jahn R (1998) Conserved structural features of the synaptic fusion complex: SNARE proteins reclassified as Q- and R-SNAREs. *Proc Natl Acad Sci U S A* **95**, 15781-15786.

Fernandez I, Ubach J, Dulubova I, Zhang X, Sudhof TC & Rizo J (1998) Three-dimensional structure of an evolutionarily conserved N-terminal domain of syntaxin 1A. *Cell* **94**, 841-849.

Fields S & Song O (1989) A novel genetic system to detect protein-protein interactions. *Nature* **340**, 245-246.

Fire A, Xu S, Montgomery MK, Kostas SA, Driver SE & Mello CC (1998) Potent and specific genetic interference by double-stranded RNA in Caenorhabditis elegans. *Nature* **391**, 806-811.

Forrester MT, Hess DT, Thompson JW, Hultman R, Moseley MA, Stamler JS & Casey PJ (2011) Site-specific analysis of protein S-acylation by resin-assisted capture. *J Lipid Res* **52**, 393-398.

Fotso P, Koryakina Y, Pavliv O, Tsiomenko AB & Lupashin VV (2005) Cog1p plays a central role in the organization of the yeast conserved oligomeric Golgi complex. *J Biol Chem* **280**, 27613-27623.

Frohlich KU & Madeo F (2001) Apoptosis in yeast: a new model for aging research. *Exp Gerontol* **37**, 27-31.

Furgason ML, MacDonald C, Shanks SG, Ryder SP, Bryant NJ & Munson M (2009) The N-terminal peptide of the syntaxin Tlg2p modulates binding of its closed conformation to Vps45p. *Proc Natl Acad Sci U S A* **106**, 14303-14308.

Geng J & Klionsky DJ (2010) The Golgi as a potential membrane source for autophagy. *Autophagy* **6**, 950-951.

Gengyo-Ando K, Kamiya Y, Yamakawa A, Kodaira K, Nishiwaki K, Miwa J, Hori I & Hosono R (1993) The C. elegans unc-18 gene encodes a protein expressed in motor neurons. *Neuron* **11**, 703-711.
Gengyo-Ando K, Kuroyanagi H, Kobayashi T, Murate M, Fujimoto K, Okabe S & Mitani S (2007) The SM protein VPS-45 is required for RAB-5-dependent endocytic transport in Caenorhabditis elegans. *EMBO Rep* **8**, 152-157.
Gerber SH, Rah JC, Min SW, Liu X, de Wit H, Dulubova I, Meyer AC, Rizo J, Arancillo M, Hammer RE, Verhage M, Rosenmund C & Sudhof TC (2008) Conformational switch of syntaxin-1 controls synaptic vesicle fusion. *Science* **321**, 1507-1510.
Gietz RD & Woods RA (2002) Transformation of yeast by lithium acetate/single-stranded carrier DNA/polyethylene glycol method. *Methods Enzymol* **350**, 87-96.
Glickman MH & Ciechanover A (2002) The ubiquitin-proteasome proteolytic pathway: destruction for the sake of construction. *Physiol Rev* **82**, 373-428.
Goldberg J, Nairn AC & Kuriyan J (1996) Structural basis for the autoinhibition of calcium/calmodulin-dependent protein kinase I. *Cell* **84**, 875-887.
Goldstein G, Scheid M, Hammerling U, Schlesinger DH, Niall HD & Boyse EA (1975) Isolation of a polypeptide that has lymphocyte-differentiating properties and is probably represented universally in living cells. *Proc Natl Acad Sci U S A* **72**, 11-15.
Gonzalez LC, Jr., Weis WI & Scheller RH (2001) A novel snare N-terminal domain revealed by the crystal structure of Sec22b. *J Biol Chem* **276**, 24203-24211.
Gonzalez Montoro A, Quiroga R, Maccioni HJ & Valdez Taubas J (2009) A novel motif at the C-terminus of palmitoyltransferases is essential for Swf1 and Pfa3 function in vivo. *Biochem J* **419**, 301-308.
Gourlay CW & Ayscough KR (2005) Identification of an upstream regulatory pathway controlling actin-mediated apoptosis in yeast. *J Cell Sci* **118**, 2119-2132.
Gregory RC, Taniguchi T & D'Andrea AD (2003) Regulation of the Fanconi anemia pathway by monoubiquitination. *Semin Cancer Biol* **13**, 77-82.
Grenda DS, Murakami M, Ghatak J, Xia J, Boxer LA, Dale D, Dinauer MC & Link DC (2007) Mutations of the ELA2 gene found in patients with severe congenital neutropenia induce the unfolded protein response and cellular apoptosis. *Blood* **110**, 4179-4187.
Guan R, Dai H & Rizo J (2008) Binding of the Munc13-1 MUN domain to membrane-anchored SNARE complexes. *Biochemistry* **47**, 1474-1481.
Gurunathan S, Chapman-Shimshoni D, Trajkovic S & Gerst JE (2000) Yeast exocytic v-SNAREs confer endocytosis. *Mol Biol Cell* **11**, 3629-3643.
Haglund K & Dikic I (2005) Ubiquitylation and cell signaling. *EMBO J* **24**, 3353-3359.
Hailey DW, Rambold AS, Satpute-Krishnan P, Mitra K, Sougrat R, Kim PK & Lippincott-Schwartz J (2010) Mitochondria supply membranes for autophagosome biogenesis during starvation. *Cell* **141**, 656-667.
Halachmi N & Lev Z (1996) The Sec1 family: a novel family of proteins involved in synaptic transmission and general secretion. *J Neurochem* **66**, 889-897.
Hanada T, Noda NN, Satomi Y, Ichimura Y, Fujioka Y, Takao T, Inagaki F & Ohsumi Y (2007) The Atg12-Atg5 conjugate has a novel E3-like activity for protein lipidation in autophagy. *J Biol Chem* **282**, 37298-37302.
Hanson PI, Otto H, Barton N & Jahn R (1995) The N-ethylmaleimide-sensitive fusion protein and alpha-SNAP induce a conformational change in syntaxin. *J Biol Chem* **270**, 16955-16961.

Hanson PI, Roth R, Morisaki H, Jahn R & Heuser JE (1997) Structure and conformational changes in NSF and its membrane receptor complexes visualized by quick-freeze/deep-etch electron microscopy. *Cell* **90**, 523-535.
Harding TM, Hefner-Gravink A, Thumm M & Klionsky DJ (1996) Genetic and phenotypic overlap between autophagy and the cytoplasm to vacuole protein targeting pathway. *J Biol Chem* **271**, 17621-17624.
Harding TM, Morano KA, Scott SV & Klionsky DJ (1995) Isolation and characterization of yeast mutants in the cytoplasm to vacuole protein targeting pathway. *J Cell Biol* **131**, 591-602.
Harju S, Fedosyuk H & Peterson KR (2004) Rapid isolation of yeast genomic DNA: Bust n' Grab. *BMC Biotechnol* **4**, 8.
Harrison SD, Broadie K, van de Goor J & Rubin GM (1994) Mutations in the Drosophila Rop gene suggest a function in general secretion and synaptic transmission. *Neuron* **13**, 555-566.
Hashizume K, Cheng YS, Hutton JL, Chiu CH & Carr CM (2009) Yeast Sec1p functions before and after vesicle docking. *Mol Biol Cell* **20**, 4673-4685.
He C, Song H, Yorimitsu T, Monastyrska I, Yen WL, Legakis JE & Klionsky DJ (2006) Recruitment of Atg9 to the preautophagosomal structure by Atg11 is essential for selective autophagy in budding yeast. *J Cell Biol* **175**, 925-935.
He Y & Linder ME (2009) Differential palmitoylation of the endosomal SNAREs syntaxin 7 and syntaxin 8. *J Lipid Res* **50**, 398-404.
Hedgecock EM, Culotti JG, Thomson JN & Perkins LA (1985) Axonal guidance mutants of Caenorhabditis elegans identified by filling sensory neurons with fluorescein dyes. *Dev Biol* **111**, 158-170.
Hernandez PA, Gorlin RJ, Lukens JN, Taniuchi S, Bohinjec J, Francois F, Klotman ME & Diaz GA (2003) Mutations in the chemokine receptor gene CXCR4 are associated with WHIM syndrome, a combined immunodeficiency disease. *Nat Genet* **34**, 70-74.
Hershko A & Ciechanover A (1998) The ubiquitin system. *Annu Rev Biochem* **67**, 425-479.
Hill JE, Myers AM, Koerner TJ & Tzagoloff A (1986) Yeast/E. coli shuttle vectors with multiple unique restriction sites. *Yeast* **2**, 163-167.
Hoffman CS & Winston F (1987) A ten-minute DNA preparation from yeast efficiently releases autonomous plasmids for transformation of Escherichia coli. *Gene* **57**, 267-272.
Holm C, Meeks-Wagner DW, Fangman WL & Botstein D (1986) A rapid, efficient method for isolating DNA from yeast. *Gene* **42**, 169-173.
Holthuis JC, Nichols BJ, Dhruvakumar S & Pelham HR (1998a) Two syntaxin homologues in the TGN/endosomal system of yeast. *EMBO J* **17**, 113-126.
Holthuis JC, Nichols BJ & Pelham HR (1998b) The syntaxin Tlg1p mediates trafficking of chitin synthase III to polarized growth sites in yeast. *Mol Biol Cell* **9**, 3383-3397.
Hosokawa N, Hara T, Kaizuka T, Kishi C, Takamura A, Miura Y, Iemura S, Natsume T, Takehana K, Yamada N, Guan JL, Oshiro N & Mizushima N (2009) Nutrient-dependent mTORC1 association with the ULK1-Atg13-FIP200 complex required for autophagy. *Mol Biol Cell* **20**, 1981-1991.
Hutchins MU & Klionsky DJ (2001) Vacuolar localization of oligomeric alpha-mannosidase requires the cytoplasm to vacuole targeting and autophagy pathway components in Saccharomyces cerevisiae. *J Biol Chem* **276**, 20491-20498.
Isogai S, Morimoto D, Arita K, Unzai S, Tenno T, Hasegawa J, Sou YS, Komatsu M, Tanaka K, Shirakawa M & Tochio H (2011) Crystal structure of the

ubiquitin-associated (UBA) domain of p62 and its interaction with ubiquitin. *J Biol Chem* **286**, 31864-31874.
Itakura E, Kishi-Itakura C & Mizushima N (2012) The hairpin-type tail-anchored SNARE syntaxin 17 targets to autophagosomes for fusion with endosomes/lysosomes. *Cell* **151**, 1256-1269.
Itakura E & Mizushima N (2010) Characterization of autophagosome formation site by a hierarchical analysis of mammalian Atg proteins. *Autophagy* **6**, 764-776.
Iwabuchi K, Li B, Bartel P & Fields S (1993) Use of the two-hybrid system to identify the domain of p53 involved in oligomerization. *Oncogene* **8**, 1693-1696.
Jahn R (2000) Sec1/Munc18 proteins: mediators of membrane fusion moving to center stage. *Neuron* **27**, 201-204.
Jahn R & Scheller RH (2006) SNAREs--engines for membrane fusion. *Nat Rev Mol Cell Biol* **7**, 631-643.
Jahn R & Sudhof TC (1999) Membrane fusion and exocytosis. *Annu Rev Biochem* **68**, 863-911.
James P, Halladay J & Craig EA (1996) Genomic libraries and a host strain designed for highly efficient two-hybrid selection in yeast. *Genetics* **144**, 1425-1436.
Jao CC, Ragusa MJ, Stanley RE & Hurley JH (2013) A HORMA domain in Atg13 mediates PI 3-kinase recruitment in autophagy. *Proc Natl Acad Sci U S A* **110**, 5486-5491.
Johnson LN, Noble ME & Owen DJ (1996) Active and inactive protein kinases: structural basis for regulation. *Cell* **85**, 149-158.
Johnston M (1987) A model fungal gene regulatory mechanism: the GAL genes of Saccharomyces cerevisiae. *Microbiol Rev* **51**, 458-476.
Johnstone IL (2000) Cuticle collagen genes. Expression in Caenorhabditis elegans. *Trends Genet* **16**, 21-27.
Johnstone IL & Barry JD (1996) Temporal reiteration of a precise gene expression pattern during nematode development. *EMBO J* **15**, 3633-3639.
Kabeya Y, Kamada Y, Baba M, Takikawa H, Sasaki M & Ohsumi Y (2005) Atg17 functions in cooperation with Atg1 and Atg13 in yeast autophagy. *Mol Biol Cell* **16**, 2544-2553.
Kabeya Y, Kawamata T, Suzuki K & Ohsumi Y (2007) Cis1/Atg31 is required for autophagosome formation in Saccharomyces cerevisiae. *Biochem Biophys Res Commun* **356**, 405-410.
Kabeya Y, Noda NN, Fujioka Y, Suzuki K, Inagaki F & Ohsumi Y (2009) Characterization of the Atg17-Atg29-Atg31 complex specifically required for starvation-induced autophagy in Saccharomyces cerevisiae. *Biochem Biophys Res Commun* **389**, 612-615.
Kamada Y, Funakoshi T, Shintani T, Nagano K, Ohsumi M & Ohsumi Y (2000) Tor-mediated induction of autophagy via an Apg1 protein kinase complex. *J Cell Biol* **150**, 1507-1513.
Kamath RS, Martinez-Campos M, Zipperlen P, Fraser AG & Ahringer J (2001) Effectiveness of specific RNA-mediated interference through ingested double-stranded RNA in Caenorhabditis elegans. *Genome Biol* **2**, RESEARCH0002.
Kang C, You YJ & Avery L (2007) Dual roles of autophagy in the survival of Caenorhabditis elegans during starvation. *Genes Dev* **21**, 2161-2171.
Kanki T, Wang K, Baba M, Bartholomew CR, Lynch-Day MA, Du Z, Geng J, Mao K, Yang Z, Yen WL & Klionsky DJ (2009) A genomic screen for yeast

mutants defective in selective mitochondria autophagy. *Mol Biol Cell* **20**, 4730-4738.
Katzmann DJ, Odorizzi G & Emr SD (2002) Receptor downregulation and multivesicular-body sorting. *Nat Rev Mol Cell Biol* **3**, 893-905.
Kawamata T, Kamada Y, Kabeya Y, Sekito T & Ohsumi Y (2008) Organization of the pre-autophagosomal structure responsible for autophagosome formation. *Mol Biol Cell* **19**, 2039-2050.
Keegan L, Gill G & Ptashne M (1986) Separation of DNA binding from the transcription-activating function of a eukaryotic regulatory protein. *Science* **231**, 699-704.
Kihara A, Noda T, Ishihara N & Ohsumi Y (2001) Two distinct Vps34 phosphatidylinositol 3-kinase complexes function in autophagy and carboxypeptidase Y sorting in Saccharomyces cerevisiae. *J Cell Biol* **152**, 519-530.
Kijanska M, Dohnal I, Reiter W, Kaspar S, Stoffel I, Ammerer G, Kraft C & Peter M (2010) Activation of Atg1 kinase in autophagy by regulated phosphorylation. *Autophagy* **6**, 1168-1178.
Kim DW, Massey T, Sacher M, Pypaert M & Ferro-Novick S (2001) Sgf1p, a new component of the Sec34p/Sec35p complex. *Traffic* **2**, 820-830.
Kim J, Huang WP, Stromhaug PE & Klionsky DJ (2002) Convergence of multiple autophagy and cytoplasm to vacuole targeting components to a perivacuolar membrane compartment prior to de novo vesicle formation. *J Biol Chem* **277**, 763-773.
Kirisako T, Baba M, Ishihara N, Miyazawa K, Ohsumi M, Yoshimori T, Noda T & Ohsumi Y (1999) Formation process of autophagosome is traced with Apg8/Aut7p in yeast. *J Cell Biol* **147**, 435-446.
Kirisako T, Ichimura Y, Okada H, Kabeya Y, Mizushima N, Yoshimori T, Ohsumi M, Takao T, Noda T & Ohsumi Y (2000) The reversible modification regulates the membrane-binding state of Apg8/Aut7 essential for autophagy and the cytoplasm to vacuole targeting pathway. *J Cell Biol* **151**, 263-276.
Kirkin V, Lamark T, Sou YS, Bjorkoy G, Nunn JL, Bruun JA, Shvets E, McEwan DG, Clausen TH, Wild P, Bilusic I, Theurillat JP, Overvatn A, Ishii T, Elazar Z, Komatsu M, Dikic I & Johansen T (2009) A role for NBR1 in autophagosomal degradation of ubiquitinated substrates. *Mol Cell* **33**, 505-516.
Kishore GM & Shah DM (1988) Amino acid biosynthesis inhibitors as herbicides. *Annu Rev Biochem* **57**, 627-663.
Klein C (2009) Congenital neutropenia. *Hematology Am Soc Hematol Educ Program*, 344-350.
Klionsky DJ (2005) The molecular machinery of autophagy: unanswered questions. *J Cell Sci* **118**, 7-18.
Klionsky DJ, Cueva R & Yaver DS (1992) Aminopeptidase I of Saccharomyces cerevisiae is localized to the vacuole independent of the secretory pathway. *J Cell Biol* **119**, 287-299.
Komatsu M, Waguri S, Koike M, Sou YS, Ueno T, Hara T, Mizushima N, Iwata J, Ezaki J, Murata S, Hamazaki J, Nishito Y, Iemura S, Natsume T, Yanagawa T, Uwayama J, Warabi E, Yoshida H, Ishii T, Kobayashi A, Yamamoto M, Yue Z, Uchiyama Y, Kominami E & Tanaka K (2007) Homeostatic levels of p62 control cytoplasmic inclusion body formation in autophagy-deficient mice. *Cell* **131**, 1149-1163.
Kov AL, Vellai T & Fritz M (2000) *Madame Curie Bioscience Database*. Austin, Texas: Landes Bioscience.

Kovacs AL & Zhang H (2010) Role of autophagy in Caenorhabditis elegans. *FEBS Lett* **584**, 1335-1341.
Kramer JM, Cox GN & Hirsh D (1982) Comparisons of the complete sequences of two collagen genes from Caenorhabditis elegans. *Cell* **30**, 599-606.
Kramer JM, French RP, Park EC & Johnson JJ (1990) The Caenorhabditis elegans rol-6 gene, which interacts with the sqt-1 collagen gene to determine organismal morphology, encodes a collagen. *Mol Cell Biol* **10**, 2081-2089.
Kuma A, Hatano M, Matsui M, Yamamoto A, Nakaya H, Yoshimori T, Ohsumi Y, Tokuhisa T & Mizushima N (2004) The role of autophagy during the early neonatal starvation period. *Nature* **432**, 1032-1036.
Lacks S & Greenberg B (1975) A deoxyribonuclease of Diplococcus pneumoniae specific for methylated DNA. *J Biol Chem* **250**, 4060-4066.
Laemmli UK (1970) Cleavage of structural proteins during the assembly of the head of bacteriophage T4. *Nature* **227**, 680-685.
Lane DP & Crawford LV (1979) T antigen is bound to a host protein in SV40-transformed cells. *Nature* **278**, 261-263.
Langone JJ (1982) Protein A of Staphylococcus aureus and related immunoglobulin receptors produced by streptococci and pneumonococci. *Adv Immunol* **32**, 157-252.
Latham CF, Lopez JA, Hu SH, Gee CL, Westbury E, Blair DH, Armishaw CJ, Alewood PF, Bryant NJ, James DE & Martin JL (2006) Molecular dissection of the Munc18c/syntaxin4 interaction: implications for regulation of membrane trafficking. *Traffic* **7**, 1408-1419.
Laufman O, Hong W & Lev S (2011) The COG complex interacts directly with Syntaxin 6 and positively regulates endosome-to-TGN retrograde transport. *J Cell Biol* **194**, 459-472.
Laufman O, Hong W & Lev S (2013) The COG complex interacts with multiple Golgi SNAREs and enhances fusogenic assembly of SNARE complexes. *J Cell Sci* **126**, 1506-1516.
Laufman O, Kedan A, Hong W & Lev S (2009) Direct interaction between the COG complex and the SM protein, Sly1, is required for Golgi SNARE pairing. *EMBO J* **28**, 2006-2017.
Lees JA, Yip CK, Walz T & Hughson FM (2010) Molecular organization of the COG vesicle tethering complex. *Nat Struct Mol Biol* **17**, 1292-1297.
Levy AD, Yang J & Kramer JM (1993) Molecular and genetic analyses of the Caenorhabditis elegans dpy-2 and dpy-10 collagen genes: a variety of molecular alterations affect organismal morphology. *Mol Biol Cell* **4**, 803-817.
Lewis MJ, Nichols BJ, Prescianotto-Baschong C, Riezman H & Pelham HR (2000) Specific retrieval of the exocytic SNARE Snc1p from early yeast endosomes. *Mol Biol Cell* **11**, 23-38.
Li W, Ma C, Guan R, Xu Y, Tomchick DR & Rizo J (2011) The crystal structure of a Munc13 C-terminal module exhibits a remarkable similarity to vesicle tethering factors. *Structure* **19**, 1443-1455.
Lian JP, Stone S, Jiang Y, Lyons P & Ferro-Novick S (1994) Ypt1p implicated in v-SNARE activation. *Nature* **372**, 698-701.
Liang XH, Jackson S, Seaman M, Brown K, Kempkes B, Hibshoosh H & Levine B (1999) Induction of autophagy and inhibition of tumorigenesis by beclin 1. *Nature* **402**, 672-676.
Lin RC & Scheller RH (2000) Mechanisms of synaptic vesicle exocytosis. *Annu Rev Cell Dev Biol* **16**, 19-49.

Linder ME & Deschenes RJ (2004) Model organisms lead the way to protein palmitoyltransferases. *J Cell Sci* **117**, 521-526.
Lipatova Z, Belogortseva N, Zhang XQ, Kim J, Taussig D & Segev N (2012) Regulation of selective autophagy onset by a Ypt/Rab GTPase module. *Proc Natl Acad Sci U S A* **109**, 6981-6986.
Lobo S, Greentree WK, Linder ME & Deschenes RJ (2002) Identification of a Ras palmitoyltransferase in Saccharomyces cerevisiae. *J Biol Chem* **277**, 41268-41273.
Longatti A & Tooze SA (2012) Recycling endosomes contribute to autophagosome formation. *Autophagy* **8**, 1682-1683.
Longtine MS, McKenzie A, 3rd, Demarini DJ, Shah NG, Wach A, Brachat A, Philippsen P & Pringle JR (1998) Additional modules for versatile and economical PCR-based gene deletion and modification in Saccharomyces cerevisiae. *Yeast* **14**, 953-961.
Ma C, Li W, Xu Y & Rizo J (2011) Munc13 mediates the transition from the closed syntaxin-Munc18 complex to the SNARE complex. *Nat Struct Mol Biol* **18**, 542-549.
Ma J & Ptashne M (1987) Deletion analysis of GAL4 defines two transcriptional activating segments. *Cell* **48**, 847-853.
MacDonald C (2009) Regulation of membrane fusion my Tlg2 and Vps45 through the endosomal system of Saccharomyces cerevisiae, University of Glasgow.
Madeo F, Frohlich E, Ligr M, Grey M, Sigrist SJ, Wolf DH & Frohlich KU (1999) Oxygen stress: a regulator of apoptosis in yeast. *J Cell Biol* **145**, 757-767.
Mannervik B (1985) The isoenzymes of glutathione transferase. *Adv Enzymol Relat Areas Mol Biol* **57**, 357-417.
Mao K, Chew LH, Inoue-Aono Y, Cheong H, Nair U, Popelka H, Yip CK & Klionsky DJ (2013) Atg29 phosphorylation regulates coordination of the Atg17-Atg31-Atg29 complex with the Atg11 scaffold during autophagy initiation. *Proc Natl Acad Sci U S A* **110**, E2875-2884.
Mari M, Griffith J, Rieter E, Krishnappa L, Klionsky DJ & Reggiori F (2010) An Atg9-containing compartment that functions in the early steps of autophagosome biogenesis. *J Cell Biol* **190**, 1005-1022.
Martinez-Vicente M, Sovak G & Cuervo AM (2005) Protein degradation and aging. *Exp Gerontol* **40**, 622-633.
Matsuura A, Tsukada M, Wada Y & Ohsumi Y (1997) Apg1p, a novel protein kinase required for the autophagic process in Saccharomyces cerevisiae. *Gene* **192**, 245-250.
Matyash V, Entchev EV, Mende F, Wilsch-Brauninger M, Thiele C, Schmidt AW, Knolker HJ, Ward S & Kurzchalia TV (2004) Sterol-derived hormone(s) controls entry into diapause in Caenorhabditis elegans by consecutive activation of DAF-12 and DAF-16. *PLoS Biol* **2**, e280.
Matyash V, Geier C, Henske A, Mukherjee S, Hirsh D, Thiele C, Grant B, Maxfield FR & Kurzchalia TV (2001) Distribution and transport of cholesterol in Caenorhabditis elegans. *Mol Biol Cell* **12**, 1725-1736.
McMahon L, Muriel JM, Roberts B, Quinn M & Johnstone IL (2003) Two sets of interacting collagens form functionally distinct substructures within a Caenorhabditis elegans extracellular matrix. *Mol Biol Cell* **14**, 1366-1378.
Melendez A, Talloczy Z, Seaman M, Eskelinen EL, Hall DH & Levine B (2003) Autophagy genes are essential for dauer development and life-span extension in C. elegans. *Science* **301**, 1387-1391.
Misura KM, Scheller RH & Weis WI (2000) Three-dimensional structure of the neuronal-Sec1-syntaxin 1a complex. *Nature* **404**, 355-362.

Mitchell DA, Vasudevan A, Linder ME & Deschenes RJ (2006) Protein palmitoylation by a family of DHHC protein S-acyltransferases. *J Lipid Res* **47**, 1118-1127.
Mizushima N (2005) The pleiotropic role of autophagy: from protein metabolism to bactericide. *Cell Death Differ* **12 Suppl 2**, 1535-1541.
Mizushima N (2007) Autophagy: process and function. *Genes Dev* **21**, 2861-2873.
Mizushima N & Levine B (2010) Autophagy in mammalian development and differentiation. *Nat Cell Biol* **12**, 823-830.
Mizushima N, Levine B, Cuervo AM & Klionsky DJ (2008) Autophagy fights disease through cellular self-digestion. *Nature* **451**, 1069-1075.
Mizushima N, Noda T & Ohsumi Y (1999) Apg16p is required for the function of the Apg12p-Apg5p conjugate in the yeast autophagy pathway. *EMBO J* **18**, 3888-3896.
Mizushima N, Sugita H, Yoshimori T & Ohsumi Y (1998) A new protein conjugation system in human. The counterpart of the yeast Apg12p conjugation system essential for autophagy. *J Biol Chem* **273**, 33889-33892.
Mizushima N, Yamamoto A, Hatano M, Kobayashi Y, Kabeya Y, Suzuki K, Tokuhisa T, Ohsumi Y & Yoshimori T (2001) Dissection of autophagosome formation using Apg5-deficient mouse embryonic stem cells. *J Cell Biol* **152**, 657-668.
Mocellin S & Provenzano M (2004) RNA interference: learning gene knock-down from cell physiology. *J Transl Med* **2**, 39.
Moreau K, Ravikumar B, Renna M, Puri C & Rubinsztein DC (2011) Autophagosome precursor maturation requires homotypic fusion. *Cell* **146**, 303-317.
Muratani M & Tansey WP (2003) How the ubiquitin-proteasome system controls transcription. *Nat Rev Mol Cell Biol* **4**, 192-201.
Nagle DL, Karim MA, Woolf EA, Holmgren L, Bork P, Misumi DJ, McGrail SH, Dussault BJ, Jr., Perou CM, Boissy RE, Duyk GM, Spritz RA & Moore KJ (1996) Identification and mutation analysis of the complete gene for Chediak-Higashi syndrome. *Nat Genet* **14**, 307-311.
Nair U, Jotwani A, Geng J, Gammoh N, Richerson D, Yen WL, Griffith J, Nag S, Wang K, Moss T, Baba M, McNew JA, Jiang X, Reggiori F, Melia TJ & Klionsky DJ (2011) SNARE proteins are required for macroautophagy. *Cell* **146**, 290-302.
Nakatogawa H, Ichimura Y & Ohsumi Y (2007) Atg8, a ubiquitin-like protein required for autophagosome formation, mediates membrane tethering and hemifusion. *Cell* **130**, 165-178.
Nakatogawa H, Ohbayashi S, Sakoh-Nakatogawa M, Kakuta S, Suzuki SW, Kirisako H, Kondo-Kakuta C, Noda NN, Yamamoto H & Ohsumi Y (2012) The autophagy-related protein kinase Atg1 interacts with the ubiquitin-like protein Atg8 via the Atg8 family interacting motif to facilitate autophagosome formation. *J Biol Chem* **287**, 28503-28507.
Nakatogawa H, Suzuki K, Kamada Y & Ohsumi Y (2009) Dynamics and diversity in autophagy mechanisms: lessons from yeast. *Nat Rev Mol Cell Biol* **10**, 458-467.
Newton K, Matsumoto ML, Wertz IE, Kirkpatrick DS, Lill JR, Tan J, Dugger D, Gordon N, Sidhu SS, Fellouse FA, Komuves L, French DM, Ferrando RE, Lam C, Compaan D, Yu C, Bosanac I, Hymowitz SG, Kelley RF & Dixit VM (2008) Ubiquitin chain editing revealed by polyubiquitin linkage-specific antibodies. *Cell* **134**, 668-678.

Nichols BJ, Holthuis JC & Pelham HR (1998) The Sec1p homologue Vps45p binds to the syntaxin Tlg2p. *Eur J Cell Biol* **77**, 263-268.
Nicholson KL, Munson M, Miller RB, Filip TJ, Fairman R & Hughson FM (1998) Regulation of SNARE complex assembly by an N-terminal domain of the t-SNARE Sso1p. *Nat Struct Biol* **5**, 793-802.
Nielsen E, Christoforidis S, Uttenweiler-Joseph S, Miaczynska M, Dewitte F, Wilm M, Hoflack B & Zerial M (2000) Rabenosyn-5, a novel Rab5 effector, is complexed with hVPS45 and recruited to endosomes through a FYVE finger domain. *J Cell Biol* **151**, 601-612.
Noda NN, Kumeta H, Nakatogawa H, Satoo K, Adachi W, Ishii J, Fujioka Y, Ohsumi Y & Inagaki F (2008) Structural basis of target recognition by Atg8/LC3 during selective autophagy. *Genes Cells* **13**, 1211-1218.
Noda T, Kim J, Huang WP, Baba M, Tokunaga C, Ohsumi Y & Klionsky DJ (2000) Apg9p/Cvt7p is an integral membrane protein required for transport vesicle formation in the Cvt and autophagy pathways. *J Cell Biol* **148**, 465-480.
Noda T, Matsuura A, Wada Y & Ohsumi Y (1995) Novel system for monitoring autophagy in the yeast Saccharomyces cerevisiae. *Biochem Biophys Res Commun* **210**, 126-132.
Noda T & Ohsumi Y (1998) Tor, a phosphatidylinositol kinase homologue, controls autophagy in yeast. *J Biol Chem* **273**, 3963-3966.
Novick P, Field C & Schekman R (1980) Identification of 23 complementation groups required for post-translational events in the yeast secretory pathway. *Cell* **21**, 205-215.
Novikoff AB, Essner E & Quintana N (1964) Golgi Apparatus and Lysosomes. *Fed Proc* **23**, 1010-1022.
Obara K, Sekito T, Niimi K & Ohsumi Y (2008) The Atg18-Atg2 complex is recruited to autophagic membranes via phosphatidylinositol 3-phosphate and exerts an essential function. *J Biol Chem* **283**, 23972-23980.
Ogura K & Goshima Y (2006) The autophagy-related kinase UNC-51 and its binding partner UNC-14 regulate the subcellular localization of the Netrin receptor UNC-5 in Caenorhabditis elegans. *Development* **133**, 3441-3450.
Ogura K, Wicky C, Magnenat L, Tobler H, Mori I, Muller F & Ohshima Y (1994) Caenorhabditis elegans unc-51 gene required for axonal elongation encodes a novel serine/threonine kinase. *Genes Dev* **8**, 2389-2400.
Ohashi Y & Munro S (2010) Membrane delivery to the yeast autophagosome from the Golgi-endosomal system. *Mol Biol Cell* **21**, 3998-4008.
Ohsumi Y (2001) Molecular dissection of autophagy: two ubiquitin-like systems. *Nat Rev Mol Cell Biol* **2**, 211-216.
Oka T, Ungar D, Hughson FM & Krieger M (2004) The COG and COPI complexes interact to control the abundance of GEARs, a subset of Golgi integral membrane proteins. *Mol Biol Cell* **15**, 2423-2435.
Oka T, Vasile E, Penman M, Novina CD, Dykxhoorn DM, Ungar D, Hughson FM & Krieger M (2005) Genetic analysis of the subunit organization and function of the conserved oligomeric golgi (COG) complex: studies of COG5- and COG7-deficient mammalian cells. *J Biol Chem* **280**, 32736-32745.
Okamoto K, Kondo-Okamoto N & Ohsumi Y (2009) Mitochondria-anchored receptor Atg32 mediates degradation of mitochondria via selective autophagy. *Dev Cell* **17**, 87-97.
Page AP & Johnstone IL (2007) The cuticle. *WormBook*, 1-15.
Pankiv S, Clausen TH, Lamark T, Brech A, Bruun JA, Outzen H, Overvatn A, Bjorkoy G & Johansen T (2007) p62/SQSTM1 binds directly to Atg8/LC3 to facilitate degradation of ubiquitinated protein aggregates by autophagy. *J Biol Chem* **282**, 24131-24145.

Paumet F, Brugger B, Parlati F, McNew JA, Sollner TH & Rothman JE (2001) A t-SNARE of the endocytic pathway must be activated for fusion. *J Cell Biol* **155**, 961-968.

Peanne R, Legrand D, Duvet S, Mir AM, Matthijs G, Rohrer J & Foulquier F (2011) Differential effects of lobe A and lobe B of the Conserved Oligomeric Golgi complex on the stability of {beta}1,4-galactosyltransferase 1 and {alpha}2,6-sialyltransferase 1. *Glycobiology* **21**, 864-876.

Pei J, Ma C, Rizo J & Grishin NV (2009) Remote homology between Munc13 MUN domain and vesicle tethering complexes. *J Mol Biol* **391**, 509-517.

Pelham HR (2001) SNAREs and the specificity of membrane fusion. *Trends Cell Biol* **11**, 99-101.

Perez-Victoria FJ & Bonifacino JS (2009) Dual roles of the mammalian GARP complex in tethering and SNARE complex assembly at the trans-golgi network. *Mol Cell Biol* **29**, 5251-5263.

Person RE, Li FQ, Duan Z, Benson KF, Wechsler J, Papadaki HA, Eliopoulos G, Kaufman C, Bertolone SJ, Nakamoto B, Papayannopoulou T, Grimes HL & Horwitz M (2003) Mutations in proto-oncogene GFI1 cause human neutropenia and target ELA2. *Nat Genet* **34**, 308-312.

Petiot A, Ogier-Denis E, Blommaart EF, Meijer AJ & Codogno P (2000) Distinct classes of phosphatidylinositol 3'-kinases are involved in signaling pathways that control macroautophagy in HT-29 cells. *J Biol Chem* **275**, 992-998.

Pevsner J, Hsu SC, Braun JE, Calakos N, Ting AE, Bennett MK & Scheller RH (1994) Specificity and regulation of a synaptic vesicle docking complex. *Neuron* **13**, 353-361.

Pfeffer SR (1999) Transport-vesicle targeting: tethers before SNAREs. *Nat Cell Biol* **1**, E17-22.

Pickart CM (2001) Mechanisms underlying ubiquitination. *Annu Rev Biochem* **70**, 503-533.

Pieren M, Schmidt A & Mayer A (2010) The SM protein Vps33 and the t-SNARE H(abc) domain promote fusion pore opening. *Nat Struct Mol Biol* **17**, 710-717.

Piper RC, Cooper AA, Yang H & Stevens TH (1995) VPS27 controls vacuolar and endocytic traffic through a prevacuolar compartment in Saccharomyces cerevisiae. *J Cell Biol* **131**, 603-617.

Piper RC, Whitters EA & Stevens TH (1994) Yeast Vps45p is a Sec1p-like protein required for the consumption of vacuole-targeted, post-Golgi transport vesicles. *Eur J Cell Biol* **65**, 305-318.

Podos SD, Reddy P, Ashkenas J & Krieger M (1994) LDLC encodes a brefeldin A-sensitive, peripheral Golgi protein required for normal Golgi function. *J Cell Biol* **127**, 679-691.

Qu X, Yu J, Bhagat G, Furuya N, Hibshoosh H, Troxel A, Rosen J, Eskelinen EL, Mizushima N, Ohsumi Y, Cattoretti G & Levine B (2003) Promotion of tumorigenesis by heterozygous disruption of the beclin 1 autophagy gene. *J Clin Invest* **112**, 1809-1820.

Quental R, Azevedo L, Matthiesen R & Amorim A (2010) Comparative analyses of the Conserved Oligomeric Golgi (COG) complex in vertebrates. *BMC Evol Biol* **10**, 212.

Rahajeng J, Caplan S & Naslavsky N (2010) Common and distinct roles for the binding partners Rabenosyn-5 and Vps45 in the regulation of endocytic trafficking in mammalian cells. *Exp Cell Res* **316**, 859-874.

Ravikumar B, Moreau K, Jahreiss L, Puri C & Rubinsztein DC (2010) Plasma membrane contributes to the formation of pre-autophagosomal structures. *Nat Cell Biol* **12**, 747-757.

Ravikumar B, Vacher C, Berger Z, Davies JE, Luo S, Oroz LG, Scaravilli F, Easton DF, Duden R, O'Kane CJ & Rubinsztein DC (2004) Inhibition of mTOR induces autophagy and reduces toxicity of polyglutamine expansions in fly and mouse models of Huntington disease. *Nat Genet* **36**, 585-595.

Raymond CK, Howald-Stevenson I, Vater CA & Stevens TH (1992) Morphological classification of the yeast vacuolar protein sorting mutants: evidence for a prevacuolar compartment in class E vps mutants. *Mol Biol Cell* **3**, 1389-1402.

Reddi HV & Kumar V (2004) Self-association of the hepatitis B virus X protein in the yeast two-hybrid system. *Biochem Biophys Res Commun* **317**, 1017-1022.

Reggiori F & Klionsky DJ (2002) Autophagy in the eukaryotic cell. *Eukaryot Cell* **1**, 11-21.

Reggiori F & Pelham HR (2001) Sorting of proteins into multivesicular bodies: ubiquitin-dependent and -independent targeting. *EMBO J* **20**, 5176-5186.

Reggiori F & Pelham HR (2002) A transmembrane ubiquitin ligase required to sort membrane proteins into multivesicular bodies. *Nat Cell Biol* **4**, 117-123.

Reggiori F, Tucker KA, Stromhaug PE & Klionsky DJ (2004) The Atg1-Atg13 complex regulates Atg9 and Atg23 retrieval transport from the pre-autophagosomal structure. *Dev Cell* **6**, 79-90.

Robinson JS, Klionsky DJ, Banta LM & Emr SD (1988) Protein sorting in Saccharomyces cerevisiae: isolation of mutants defective in the delivery and processing of multiple vacuolar hydrolases. *Mol Cell Biol* **8**, 4936-4948.

Roth AF, Feng Y, Chen L & Davis NG (2002) The yeast DHHC cysteine-rich domain protein Akr1p is a palmitoyl transferase. *J Cell Biol* **159**, 23-28.

Roth AF, Wan J, Bailey AO, Sun B, Kuchar JA, Green WN, Phinney BS, Yates JR, 3rd & Davis NG (2006) Global analysis of protein palmitoylation in yeast. *Cell* **125**, 1003-1013.

Rothman JH, Howald I & Stevens TH (1989) Characterization of genes required for protein sorting and vacuolar function in the yeast Saccharomyces cerevisiae. *EMBO J* **8**, 2057-2065.

Rothman JH & Stevens TH (1986) Protein sorting in yeast: mutants defective in vacuole biogenesis mislocalize vacuolar proteins into the late secretory pathway. *Cell* **47**, 1041-1051.

Saitoh T, Fujita N, Hayashi T, Takahara K, Satoh T, Lee H, Matsunaga K, Kageyama S, Omori H, Noda T, Yamamoto N, Kawai T, Ishii K, Takeuchi O, Yoshimori T & Akira S (2009) Atg9a controls dsDNA-driven dynamic translocation of STING and the innate immune response. *Proc Natl Acad Sci U S A* **106**, 20842-20846.

Salaun C, Greaves J & Chamberlain LH (2010) The intracellular dynamic of protein palmitoylation. *J Cell Biol* **191**, 1229-1238.

Sato M & Sato K (2013) Dynamic regulation of autophagy and endocytosis for cell remodeling during early development. *Traffic* **14**, 479-486.

Schulze KL, Littleton JT, Salzberg A, Halachmi N, Stern M, Lev Z & Bellen HJ (1994) rop, a Drosophila homolog of yeast Sec1 and vertebrate n-Sec1/Munc-18 proteins, is a negative regulator of neurotransmitter release in vivo. *Neuron* **13**, 1099-1108.

Scott RC, Schuldiner O & Neufeld TP (2004) Role and regulation of starvation-induced autophagy in the Drosophila fat body. *Dev Cell* **7**, 167-178.

Scott SV, Hefner-Gravink A, Morano KA, Noda T, Ohsumi Y & Klionsky DJ (1996) Cytoplasm-to-vacuole targeting and autophagy employ the same machinery to deliver proteins to the yeast vacuole. *Proc Natl Acad Sci U S A* **93**, 12304-12308.

Scott SV, Nice DC, 3rd, Nau JJ, Weisman LS, Kamada Y, Keizer-Gunnink I, Funakoshi T, Veenhuis M, Ohsumi Y & Klionsky DJ (2000) Apg13p and Vac8p are part of a complex of phosphoproteins that are required for cytoplasm to vacuole targeting. *J Biol Chem* **275**, 25840-25849.

Sekito T, Kawamata T, Ichikawa R, Suzuki K & Ohsumi Y (2009) Atg17 recruits Atg9 to organize the pre-autophagosomal structure. *Genes Cells* **14**, 525-538.

Seron K, Tieaho V, Prescianotto-Baschong C, Aust T, Blondel MO, Guillaud P, Devilliers G, Rossanese OW, Glick BS, Riezman H, Keranen S & Haguenauer-Tsapis R (1998) A yeast t-SNARE involved in endocytosis. *Mol Biol Cell* **9**, 2873-2889.

Shanks SG, Carpp LN, Struthers MS, McCann RK & Bryant NJ (2012) The Sec1/Munc18 protein Vps45 regulates cellular levels of its SNARE binding partners Tlg2 and Snc2 in Saccharomyces cerevisiae. *PLoS One* **7**, e49628.

Sherman F (1997) An introduction to the genetics and molecular biology of the yeast saccharomyces cerevisiae. In *The encyclopedia of molecular cell biology and molecular medicine*, pp. 302-325 [RA Meyers, editor]. Weinheim, Germany: VCH Publisher.

Shestakova A, Suvorova E, Pavliv O, Khaidakova G & Lupashin V (2007) Interaction of the conserved oligomeric Golgi complex with t-SNARE Syntaxin5a/Sed5 enhances intra-Golgi SNARE complex stability. *J Cell Biol* **179**, 1179-1192.

Shestakova A, Zolov S & Lupashin V (2006) COG complex-mediated recycling of Golgi glycosyltransferases is essential for normal protein glycosylation. *Traffic* **7**, 191-204.

Shoulders MD & Raines RT (2009) Collagen structure and stability. *Annu Rev Biochem* **78**, 929-958.

Siddiqui SS, Aamodt E, Rastinejad F & Culotti J (1989) Anti-tubulin monoclonal antibodies that bind to specific neurons in Caenorhabditis elegans. *J Neurosci* **9**, 2963-2972.

Simonsen A, Bremnes B, Ronning E, Aasland R & Stenmark H (1998) Syntaxin-16, a putative Golgi t-SNARE. *Eur J Cell Biol* **75**, 223-231.

Singh RH & Sulston JE (1978) Some observations on moulting in Caenorhabditis elegans. *Nematologica* **24**, 63-71.

Smith RD & Lupashin VV (2008) Role of the conserved oligomeric Golgi (COG) complex in protein glycosylation. *Carbohydr Res* **343**, 2024-2031.

Sogaard M, Tani K, Ye RR, Geromanos S, Tempst P, Kirchhausen T, Rothman JE & Sollner T (1994) A rab protein is required for the assembly of SNARE complexes in the docking of transport vesicles. *Cell* **78**, 937-948.

Sollner T, Bennett MK, Whiteheart SW, Scheller RH & Rothman JE (1993a) A protein assembly-disassembly pathway in vitro that may correspond to sequential steps of synaptic vesicle docking, activation, and fusion. *Cell* **75**, 409-418.

Sollner T, Whiteheart SW, Brunner M, Erdjument-Bromage H, Geromanos S, Tempst P & Rothman JE (1993b) SNAP receptors implicated in vesicle targeting and fusion. *Nature* **362**, 318-324.

Stellberger T, Hauser R, Baiker A, Pothineni VR, Haas J & Uetz P (2010) Improving the yeast two-hybrid system with permutated fusions proteins: the Varicella Zoster Virus interactome. *Proteome Sci* **8**, 8.

Stepensky P, Saada A, Cowan M, Tabib A, Fischer U, Berkun Y, Saleh H, Simanovsky N, Kogot-Levin A, Weintraub M, Ganaiem H, Shaag A, Zenvirt S, Borkhardt A, Elpeleg O, Bryant NJ & Mevorach D (2013) The Thr224Asn mutation in the VPS45 gene is associated with the congenital neutropenia and primary myelofibrosis of infancy. *Blood* **121**, 5078-5087.

Stevens T, Esmon B & Schekman R (1982) Early stages in the yeast secretory pathway are required for transport of carboxypeptidase Y to the vacuole. *Cell* **30**, 439-448.

Struhl K & Davis RW (1977) Production of a functional eukaryotic enzyme in Escherichia coli: cloning and expression of the yeast structural gene for imidazole-glycerolphosphate dehydratase (his3). *Proc Natl Acad Sci U S A* **74**, 5255-5259.

Struthers MS (2009) An evolutionarily conserved regulatory mechanism for endosomal membrane trafficking, University of Glasgow.

Struthers MS, Shanks SG, MacDonald C, Carpp LN, Drozdowska AM, Kioumourtzoglou D, Furgason ML, Munson M & Bryant NJ (2009) Functional homology of mammalian syntaxin 16 and yeast Tlg2p reveals a conserved regulatory mechanism. *J Cell Sci* **122**, 2292-2299.

Sulston JE, Schierenberg E, White JG & Thomson JN (1983) The embryonic cell lineage of the nematode Caenorhabditis elegans. *Dev Biol* **100**, 64-119.

Sutton RB, Fasshauer D, Jahn R & Brunger AT (1998) Crystal structure of a SNARE complex involved in synaptic exocytosis at 2.4 A resolution. *Nature* **395**, 347-353.

Suvorova ES, Duden R & Lupashin VV (2002) The Sec34/Sec35p complex, a Ypt1p effector required for retrograde intra-Golgi trafficking, interacts with Golgi SNAREs and COPI vesicle coat proteins. *J Cell Biol* **157**, 631-643.

Suvorova ES, Kurten RC & Lupashin VV (2001) Identification of a human orthologue of Sec34p as a component of the cis-Golgi vesicle tethering machinery. *J Biol Chem* **276**, 22810-22818.

Suzuki K, Kirisako T, Kamada Y, Mizushima N, Noda T & Ohsumi Y (2001) The pre-autophagosomal structure organized by concerted functions of APG genes is essential for autophagosome formation. *EMBO J* **20**, 5971-5981.

Suzuki K, Kubota Y, Sekito T & Ohsumi Y (2007) Hierarchy of Atg proteins in pre-autophagosomal structure organization. *Genes Cells* **12**, 209-218.

Suzuki K & Ohsumi Y (2010) Current knowledge of the pre-autophagosomal structure (PAS). *FEBS Lett* **584**, 1280-1286.

Sztul E & Lupashin V (2009) Role of vesicle tethering factors in the ER-Golgi membrane traffic. *FEBS Lett* **583**, 3770-3783.

Takeshige K, Baba M, Tsuboi S, Noda T & Ohsumi Y (1992) Autophagy in yeast demonstrated with proteinase-deficient mutants and conditions for its induction. *J Cell Biol* **119**, 301-311.

Tan JM, Wong ES, Kirkpatrick DS, Pletnikova O, Ko HS, Tay SP, Ho MW, Troncoso J, Gygi SP, Lee MK, Dawson VL, Dawson TM & Lim KL (2008) Lysine 63-linked ubiquitination promotes the formation and autophagic clearance of protein inclusions associated with neurodegenerative diseases. *Hum Mol Genet* **17**, 431-439.

Tang BL, Low DY, Lee SS, Tan AE & Hong W (1998) Molecular cloning and localization of human syntaxin 16, a member of the syntaxin family of SNARE proteins. *Biochem Biophys Res Commun* **242**, 673-679.

Tellam JT, James DE, Stevens TH & Piper RC (1997) Identification of a mammalian Golgi Sec1p-like protein, mVps45. *J Biol Chem* **272**, 6187-6193.
Terman A, Dalen H & Brunk UT (1999) Ceroid/lipofuscin-loaded human fibroblasts show decreased survival time and diminished autophagocytosis during amino acid starvation. *Exp Gerontol* **34**, 943-957.
Terman A, Gustafsson B & Brunk UT (2007) Autophagy, organelles and ageing. *J Pathol* **211**, 134-143.
Thumm M, Egner R, Koch B, Schlumpberger M, Straub M, Veenhuis M & Wolf DH (1994) Isolation of autophagocytosis mutants of Saccharomyces cerevisiae. *FEBS Lett* **349**, 275-280.
Timmons L & Fire A (1998) Specific interference by ingested dsRNA. *Nature* **395**, 854.
Toonen RF, de Vries KJ, Zalm R, Sudhof TC & Verhage M (2005) Munc18-1 stabilizes syntaxin 1, but is not essential for syntaxin 1 targeting and SNARE complex formation. *J Neurochem* **93**, 1393-1400.
Tooze SA & Yoshimori T (2010) The origin of the autophagosomal membrane. *Nat Cell Biol* **12**, 831-835.
Ungar D & Hughson FM (2003) SNARE protein structure and function. *Annu Rev Cell Dev Biol* **19**, 493-517.
Ungar D, Oka T, Brittle EE, Vasile E, Lupashin VV, Chatterton JE, Heuser JE, Krieger M & Waters MG (2002) Characterization of a mammalian Golgi-localized protein complex, COG, that is required for normal Golgi morphology and function. *J Cell Biol* **157**, 405-415.
Ungar D, Oka T, Vasile E, Krieger M & Hughson FM (2005) Subunit architecture of the conserved oligomeric Golgi complex. *J Biol Chem* **280**, 32729-32735.
Valdez-Taubas J & Pelham H (2005) Swf1-dependent palmitoylation of the SNARE Tlg1 prevents its ubiquitination and degradation. *EMBO J* **24**, 2524-2532.
Valls LA, Hunter CP, Rothman JH & Stevens TH (1987) Protein sorting in yeast: the localization determinant of yeast vacuolar carboxypeptidase Y resides in the propeptide. *Cell* **48**, 887-897.
van der Vaart A & Reggiori F (2010) The Golgi complex as a source for yeast autophagosomal membranes. *Autophagy* **6**, 800-801.
VanRheenen SM, Cao X, Lupashin VV, Barlowe C & Waters MG (1998) Sec35p, a novel peripheral membrane protein, is required for ER to Golgi vesicle docking. *J Cell Biol* **141**, 1107-1119.
VanRheenen SM, Cao X, Sapperstein SK, Chiang EC, Lupashin VV, Barlowe C & Waters MG (1999) Sec34p, a protein required for vesicle tethering to the yeast Golgi apparatus, is in a complex with Sec35p. *J Cell Biol* **147**, 729-742.
Vanrheenen SM, Reilly BA, Chamberlain SJ & Waters MG (2001) Dsl1p, an essential protein required for membrane traffic at the endoplasmic reticulum/Golgi interface in yeast. *Traffic* **2**, 212-231.
Veit M, Sollner TH & Rothman JE (1996) Multiple palmitoylation of synaptotagmin and the t-SNARE SNAP-25. *FEBS Lett* **385**, 119-123.
Verhage M, Maia AS, Plomp JJ, Brussaard AB, Heeroma JH, Vermeer H, Toonen RF, Hammer RE, van den Berg TK, Missler M, Geuze HJ & Sudhof TC (2000) Synaptic assembly of the brain in the absence of neurotransmitter secretion. *Science* **287**, 864-869.
Vilboux T, Lev A, Malicdan MC, Simon AJ, Jarvinen P, Racek T, Puchalka J, Sood R, Carrington B, Bishop K, Mullikin J, Huizing M, Garty BZ, Eyal E, Wolach B, Gavrieli R, Toren A, Soudack M, Atawneh OM, Babushkin T, Schiby G,

Cullinane A, Avivi C, Polak-Charcon S, Barshack I, Amariglio N, Rechavi G, van der Werff ten Bosch J, Anikster Y, Klein C, Gahl WA & Somech R (2013) A congenital neutrophil defect syndrome associated with mutations in VPS45. *N Engl J Med* **369**, 54-65.

Vogel K & Roche PA (1999) SNAP-23 and SNAP-25 are palmitoylated in vivo. *Biochem Biophys Res Commun* **258**, 407-410.

Wach A, Brachat A, Pohlmann R & Philippsen P (1994) New heterologous modules for classical or PCR-based gene disruptions in Saccharomyces cerevisiae. *Yeast* **10**, 1793-1808.

Walter DM, Paul KS & Waters MG (1998) Purification and characterization of a novel 13 S hetero-oligomeric protein complex that stimulates in vitro Golgi transport. *J Biol Chem* **273**, 29565-29576.

Weimbs T, Low SH, Chapin SJ, Mostov KE, Bucher P & Hofmann K (1997) A conserved domain is present in different families of vesicular fusion proteins: a new superfamily. *Proc Natl Acad Sci U S A* **94**, 3046-3051.

Weimer RM & Richmond JE (2005) Synaptic vesicle docking: a putative role for the Munc18/Sec1 protein family. *Curr Top Dev Biol* **65**, 83-113.

Weissman AM (2001) Themes and variations on ubiquitylation. *Nat Rev Mol Cell Biol* **2**, 169-178.

Whyte JR & Munro S (2001) The Sec34/35 Golgi transport complex is related to the exocyst, defining a family of complexes involved in multiple steps of membrane traffic. *Dev Cell* **1**, 527-537.

Whyte JR & Munro S (2002) Vesicle tethering complexes in membrane traffic. *J Cell Sci* **115**, 2627-2637.

Willett R, Kudlyk T, Pokrovskaya I, Schonherr R, Ungar D, Duden R & Lupashin V (2013) COG complexes form spatial landmarks for distinct SNARE complexes. *Nat Commun* **4**, 1553.

Winston F, Chumley F & Fink GR (1983) Eviction and transplacement of mutant genes in yeast. *Methods Enzymol* **101**, 211-228.

Wood WB (1988) *The Nematode Caenorhabitis Elegans*: Cold Spring Harbor Laboratory Press.

Woolford CA, Daniels LB, Park FJ, Jones EW, Van Arsdell JN & Innis MA (1986) The PEP4 gene encodes an aspartyl protease implicated in the posttranslational regulation of Saccharomyces cerevisiae vacuolar hydrolases. *Mol Cell Biol* **6**, 2500-2510.

Wuestehube LJ, Duden R, Eun A, Hamamoto S, Korn P, Ram R & Schekman R (1996) New mutants of Saccharomyces cerevisiae affected in the transport of proteins from the endoplasmic reticulum to the Golgi complex. *Genetics* **142**, 393-406.

Xie Z & Klionsky DJ (2007) Autophagosome formation: core machinery and adaptations. *Nat Cell Biol* **9**, 1102-1109.

Xie Z, Nair U & Klionsky DJ (2008) Atg8 controls phagophore expansion during autophagosome formation. *Mol Biol Cell* **19**, 3290-3298.

Xu H, Jun Y, Thompson J, Yates J & Wickner W (2010) HOPS prevents the disassembly of trans-SNARE complexes by Sec17p/Sec18p during membrane fusion. *EMBO J* **29**, 1948-1960.

Yamaguchi T, Dulubova I, Min SW, Chen X, Rizo J & Sudhof TC (2002) Sly1 binds to Golgi and ER syntaxins via a conserved N-terminal peptide motif. *Dev Cell* **2**, 295-305.

Yang Z & Klionsky DJ (2010) Eaten alive: a history of macroautophagy. *Nat Cell Biol* **12**, 814-822.

Yen WL, Shintani T, Nair U, Cao Y, Richardson BC, Li Z, Hughson FM, Baba M & Klionsky DJ (2010) The conserved oligomeric Golgi complex is involved in

double-membrane vesicle formation during autophagy. *J Cell Biol* **188**, 101-114.

Yik JH & Weigel PH (2002) The position of cysteine relative to the transmembrane domain is critical for palmitoylation of H1, the major subunit of the human asialoglycoprotein receptor. *J Biol Chem* **277**, 47305-47312.

Yla-Anttila P, Vihinen H, Jokitalo E & Eskelinen EL (2009) 3D tomography reveals connections between the phagophore and endoplasmic reticulum. *Autophagy* **5**, 1180-1185.

Yochem J, Tuck S, Greenwald I & Han M (1999) A gp330/megalin-related protein is required in the major epidermis of Caenorhabditis elegans for completion of molting. *Development* **126**, 597-606.

Yorimitsu T & Klionsky DJ (2005a) Atg11 links cargo to the vesicle-forming machinery in the cytoplasm to vacuole targeting pathway. *Mol Biol Cell* **16**, 1593-1605.

Yorimitsu T & Klionsky DJ (2005b) Autophagy: molecular machinery for self-eating. *Cell Death Differ* **12 Suppl 2**, 1542-1552.

Yoshihisa T & Anraku Y (1990) A novel pathway of import of alpha-mannosidase, a marker enzyme of vacuolar membrane, in Saccharomyces cerevisiae. *J Biol Chem* **265**, 22418-22425.

Young AR, Chan EY, Hu XW, Kochl R, Crawshaw SG, High S, Hailey DW, Lippincott-Schwartz J & Tooze SA (2006) Starvation and ULK1-dependent cycling of mammalian Atg9 between the TGN and endosomes. *J Cell Sci* **119**, 3888-3900.

Yue Z, Jin S, Yang C, Levine AJ & Heintz N (2003) Beclin 1, an autophagy gene essential for early embryonic development, is a haploinsufficient tumor suppressor. *Proc Natl Acad Sci U S A* **100**, 15077-15082.

Zeevaert R, Foulquier F, Jaeken J & Matthijs G (2008) Deficiencies in subunits of the Conserved Oligomeric Golgi (COG) complex define a novel group of Congenital Disorders of Glycosylation. *Mol Genet Metab* **93**, 15-21.

Zhang Y, Yan L, Zhou Z, Yang P, Tian E, Zhang K, Zhao Y, Li Z, Song B, Han J, Miao L & Zhang H (2009) SEPA-1 mediates the specific recognition and degradation of P granule components by autophagy in C. elegans. *Cell* **136**, 308-321.

Zhao J, Brault JJ, Schild A, Cao P, Sandri M, Schiaffino S, Lecker SH & Goldberg AL (2007) FoxO3 coordinately activates protein degradation by the autophagic/lysosomal and proteasomal pathways in atrophying muscle cells. *Cell Metab* **6**, 472-483.

Zink S, Wenzel D, Wurm CA & Schmitt HD (2009) A link between ER tethering and COP-I vesicle uncoating. *Dev Cell* **17**, 403-416.

Zolov SN & Lupashin VV (2005) Cog3p depletion blocks vesicle-mediated Golgi retrograde trafficking in HeLa cells. *J Cell Biol* **168**, 747-759.

Publications

Stepensky P, Saada A, Cowan M, Tabib A, Fischer U, Berkun Y, Saleh H, Simanovsky N, Kogot-Levin A, Weintraub M, Ganaiem H, Shaag A, Zenvirt S, Borkhardt A, Elpeleg O, Bryant NJ & Mevorach D (2013) The Thr224Asn mutation in the VPS45 gene is associated with the congenital neutropenia and primary myelofibrosis of infancy. *Blood* **121**, 5078-5087.